Universität Bayreuth
Forschungsstelle Atmosphärische Chemie

Experimental and theoretical examination of the chemical kinetics of a pollutant coating on porous particles

Dissertationsschrift von
Diplom-Ingenieur Radostin Gavrilov

Vorgelegt der Fakultät für Biologie, Chemie und Geowissenschaften,
Universität Bayreuth

1. Introduction

Pesticides are widely used in agriculture in order to improve the efficiency of food production. About 5 million tons of pesticides are used world-wide annually (OECD, 2003). A disadvantage of the large pesticide use is its potential impact on the environment by toxic effects. Therefore, the interest in the distribution in the environment and the chemical reactions increases constantly. The pesticides are semivolatile compounds. They are aerosol-borne in the troposphere to a major portion. The variety of phase-transfer processes (such as absorption and adsorption) has a big influence on chemical and biological transformation and on the dispersion of the pesticides. Each process must be quantified individually in order to understand the relevant processes for the degradation of a certain pesticide. The most important degradation path of the pesticides is the chemical reaction with OH-radicals in the atmosphere. Therefore, the reaction with OH-radicals is an important process with respect to the regulations of the authorities on persistence in the environment.

There are various substances which are highly toxic and harmful for the human health and for the environment, and 12 most harmful substances were included in the Stockholm convention on persistent organic pollutants (POPs): Aldrin, Chlordane, dichlorodiphenyltrichloroethane (DDT), Dieldrin, Endrin, Heptachlor, Mirex, Toxaphene, polychlorobiphenyls (PCBs), hexachlorobenzene, dioxins and furans (EU, 2004). Aldrin was chosen for the experiments of the present work. The degradation in the atmosphere and its products have been investigated actively in the 70s of the past century. The aim of this work is to investigate Aldrin with a novel experimental and mathematical approach.

It turned out in the present study that the smog chamber method for examining the kinetics of the experiments needs to be interpreted in a new way. Agglomerated particles of fused silica (Aerosil 380, DEGUSSA) served as model particles, were coated with the test substance, exposed to OH radicals in the chamber and analyzed for the test substance. It now appears that migration of the pesticides within the particles has to be taken into account after an improved understanding of the transport processes in the porous particles.

This work attempts to explain the observations. The diffusion equation, coupled with chemical reaction, was used to simulate the degradation behavior of the substance by the reaction with OH-radicals.

This work delivers:

- structure parameters of the agglomerates
- degradation experiments of Aldrin

- degradation products
- develops a diffusion model with chemical reaction
- fits the experimental results and obtains the rate constant

The chapters of this work are given as follows:

In chapter 2, previous work on photochemical experiments on Aldrin will be described, and the role of the aerosols in the atmosphere will be explained.

In chapter 3, the experimental facility is introduced. The smog chamber was constructed to fit into a refrigerated laboratory. The powder coating, production of the agglomerates, sampling and analysis technology are explained in this chapter. Measurements of temperature gradients in the chamber will be explained in detail.

In chapter 4 the production and measurement of OH radicals will be explained. A gas chromatograph with a preconcentration device for gas samples and an ozone analyzer were connected with the chamber and were used for analysis of the gas phase. Four reference hydrocarbons were used to calculate the OH exposure from their degradation rate.

In chapter 5, the analysis of Aldrin and its reaction products will be explained. The aerosol density was measured and interpolated for the aerosol sample used for the concentration analysis.

In chapter 6 the theoretical basis of the diffusion model is introduced. The diffusion processes are briefly explained. The influence of the particle structure is also given. The individual parts of the model are explained in connection with the physical processes.

In chapter 7, some relationships will be presented for the calculation of the OH rate constant, the lifetime and the long-range transport of substances occurring in the atmosphere.

The results of this research are presented in the following chapters and will be divided into two sections – experimental and theoretical results.

In chapter 8, the temperature gradients in the chamber, the concentration of the aerosol and the concentration of the substance on the aerosol will be presented. On the basis of

experiments, a coating of the powder by the substance with a defined surface coverage is given.
The agglomerates were characterized by diameter and inner structure. The diameter was measured by an electrostatic particle sizer. The structure was examined by ion etching and scanning electron microscopy (SEM). The experiments and the strategy of product identification are introduced.

In chapter 9 the theoretical results, obtained from the fitting procedure, are presented. The relations between the fitted values will be explained. The lifetime was calculated by fitting an appropriate function to the experimental points. The OH rate constant was then calculated from known OH concentrations.

The reactivity of Aldrin with ozone was investigated in chapter 10. The time profiles of Aldrin and Dieldrin were compared at different concentrations of ozone.

In chapter 11, the reaction products are identified. For this purpose, separate experiments with Aldrin-coated microballoons were made, and the products were analyzed by GC-MS.

In chapter 12, the experimental and theoretical results will be discussed.

In chapter 13, some conclusions will be given.

2. Relation to previous work on the examination of degradation kinetics

2.1. Aim of the work

This work investigates one of the substances (Aldrin) included in the Stockholm Convention. The Stockholm Convention forms the main structure for the limitation of the pollution by persistent organic pollution (POPs). The Convention includes 12 substances that are harmful to human health and environment and it stops their production and use. There are certainly more substances which might be included in the convention if their degradation rates would have been studied.

Persistent organic pollutants are chemical substances that possess certain toxic properties and, unlike other pollutants, resist degradation, which make them particularly harmful for human health and the environment. POPs accumulate in the living organisms, are transported by air, water and migratory species and accumulate in the terrestrial and aquatic ecosystems.

The group of the POPs are presented pesticides, industrial chemicals and unintentional chemical by-products.

There are four properties of the POP chemicals for the evaluation of their risk level.

1) They are highly toxic;
2) they are persistent, lasting for years or even decades before degrading into less dangerous forms;
3) they evaporate and travel long distances through the air and through water; and
4) they accumulate in fatty tissue (UNEP, 2005).

A toxic substance has the potential to generate adverse human health or environmental effects at specific exposures. The intrinsic toxicity of a substance can be identified by standard laboratory tests. For the environment, these properties include short-term (acute) or long-term (chronic) effects. For human health, the properties include toxicity through breathing or swallowing the substance, and effects such as cancer, reproductive and neurological effects.

A persistent substance resists physical, biological and chemical degradation. A measure of a substance's persistence can be determined from laboratory tests and from measurements in the environment (Euro Chlor, 2003).

The transport of the POPs depends on the temperature. They evaporate from the warm places, absorb on the particular matter and transport by the wind. They reach cold places where these chemicals settling on the plants and the earth. So they could be transported over long ranges.

These chemicals are still in use or storage in East Europe, Asia and Africa. Their persistence allows the transport from the places of use or the storage even to the Arctic and Antarctica (UNEP, 2005).

A bioaccumulative substance builds up in tissues of living organisms as a result of direct exposure to polluted water, air or soil, or through consumption of contaminated food. A measure of the ability to bioaccumulate is expressed as a ratio of the substance's concentration in the organism and the medium to which it is exposed.

The criteria to the chemicals determined in the POPs Protocol are:

1) Half-life in water > 2 months or in sediment > 6 months or in soil > 6 months;
2) Vapour pressure < 1000 Pa *and* half-life in air > 2 days *or* monitoring data in remote area;
3) Bio-accumulation : log K_{ow} > 5 (log K_{ow} value is the relative solubility of the substance in octanol (representing fat) compared to water);
4) The possible toxic effect to the human health and/or environment .

Aldrin is an organochlorine pesticide. It was produced commercially since 1950. It was widely used up to 1970s as an insecticide for the treatment of seed and for the control of many soil pests. The global production of Aldrin was estimated to be 13000 t/year in 1972. In the early 1970s the use of the pesticide was restricted or banned in a number of industrial countries. Because of its persistence in the environment, toxicity and high bio-accumulation in the fatty tissue, the production and the use was restricted. The production decreased to less than 2500 t/year in 1984. Remaining amount of the pesticide was produced in Asia and Africa or stored in Eastern Europe.

Aldrin is practically insoluble in water. The substance is soluble in organic solvents (hexane, ketones and alcohols). The vapour pressure of Aldrin is 6.5 x 10^{-5} mmHg at 25 °C (Burin et al., 1989). Aldrin metabolizes readily to Dieldrin in plants and animals. In this work it was observed, that the transformation of Aldrin in the atmosphere by the chemical reaction with hydroxyl radicals leads to Dieldrin as well. Dieldrin was found more frequently in the atmosphere, water and soil than Aldrin. Therefore, national and international regulatory bodies have considered these two closely related insecticides together. The practicability of considering them jointly is further emphasized by the lack of a significant difference in their acute and chronic toxicity and by their common mode of action.

Aldrin and Dieldrin were detected in the atmospheric environment in the vapor phase, adsorbed on dust particles, or in rainwater in concentrations dependent on the sampling area.

In general they were detected in agricultural areas. The mean concentration in the air was approx. 1-2 ng/m^3 and maximum concentrations were about 40 ng/m^3. In the rainwater the

concentration was app. 10-20 ng/litre and on occasion higher (see Marlow et al., 1982; Marlow & Wallace, 1983 in Burin et al., 1989).

Much higher concentrations in the air were measured in houses treated for the control of termites. They were in the range of 0.4-7 $\mu g/m^3$. The measured concentrations were dependent on the time of sampling or days after treatment and type of house. The concentrations decreased rapidly within the first 8 weeks. Aldrin and Dieldrin migrated into the food from the treated laminated timber and plywood, by direct contact and/or sorption from the atmosphere (see Dobbs & Williams, 1983 in Burin et al., 1989).

Aldrin was found seldom in the food. Dieldrin was found more often in diary products, meat products, fish, oil and fats, potatoes and other vegetables. Concentrations in the range from 0.02 to 0.2 mg/kg product have been recommended as maximum residue limits (MRLs) by the FAO/ WHO Joint Meetings on Pesticide Residues (see FAO/WHO, 1964, 1965a,b, 1967a,b, 1968a,b, 1969a,b, 1970a,b, 1971a,b, 1975a,b, 1976a,b, 1978a,b in Burin et al., 1989).

Dieldrin was detected in adipose tissue, organs, blood or other tissue of the population. Mean values of 0.1 – 0.4 mg/kg were reported in adipose tissue over the last 25 years (see Quinby (1963), Hoffman et al. (1965), Morgan and Roan (1970), Warnick (1972), Kutz et al. (1979), Holt et al. (1986) in Burin et al., 1989). A decreasing trend was determined in the last decades.

Aldrin and Dieldrin are highly toxic for the human organism. The lowest fatal dose has been estimated to be 10 mg/kg body weight for humans. On the other hand, survivors of acute or subacute intoxications recovered completely.

The transport and distribution of both pesticides between soil, water and air is caused by the low water solubility, hydrophobic character and strong adsorption on soil.

The experimental and theoretical research of the OH-reactivity of the semivolatile substances should help to assess the persistence and the long range transport of pesticides through the air in the future in the implementation of the plant protection products law and the possible burden of nature in remote areas (Ramesh et al., 1990; Wittlinger and Ballschmiter, 1990). The influence of the aerosol on the pollutant lifetime must also be examined.

The main degradation products of Aldrin exposure were Photoaldrin and Dieldrin. Dieldrin was converted to Photodieldrin and other unidentified products. Furthermore, CO_2 and HCl were formed from the degradation of the compounds. The irradiation time by a high-pressure mercury lamp (Philips, HPK 125 W), their emission begins at 230 nm, was 6 days respectively 2 day (Gäb et al., 1974b). However, the presence of hydroxyl radicals was not taken into account in those early days of atmospheric photochemistry, and the degradation behavior was explained by a photolysis of the compounds instead.

The degradation of Photodieldrin leads to the formation of Photoaldrinchlorohydrin and Photoaldrinketones. The UV-spectrum of Photodieldrin was measured adsorbed on silica gel. The absorption maximum of Photodieldrin in n – hexane shifted from λ_{max}= 193 nm to λ_{max}= 264 nm (adsorbed on silica gel). The UV-spectrum of silica gel was not shown in the work of Gäb et al., (1974a).

The overview of Korte and co-workers gives information about the photoreactions of chlorinated cyclodiene insecticides (Parlar and Korte, 1977). According to the authors Aldrin could undergo intramolecular photoisomerisation reactions. Intramolecular bridges are formed during the reaction using different sensitizers. Aldrin undergoes isomerisation to Photoaldrin using solutions of acetophenone and benzophenone as photosensitizers. Another possibility is a dechlorination resulting mainly from the unsensitized reactions. The dechlorinated products were formed by photoreactions or reactions with other hydrocarbons using various solvents by the detachment of chlorine atoms from the double bond.

The reaction of the Dieldrin with O (^{3}P) atoms from photolysis of NO_2 in carbon tetrachloride (λ > 230 nm) is another reaction pathway. Hydroxy-, chloro- and nitro derivates were detected and identified.

The cyclodiene insecticides could react with O (^{3}P) formed by 1) electric discharge, 2) N_2O photolysis with a mercury lamp and 3) NO_2 photolysis to convert Aldrin to Dieldrin and Photodieldrin. Another possibility is the parallel formation of Photoaldrin from Aldrin, where Photoaldrin reacts further with O (^{3}P) to form Photodiedrin.

The main product, a dihydrochlorocarboxylic acid from the degradation of Aldrin respectively Dieldrin, was detected in soil especially in pesticide treated soil. Dechlorination was observed after irradiation with UV – light (λ < 300 nm). Photoisomerisation of dihydrochlorocarboxylic acid was observed by the irradiation (λ > 300 nm) (Gäb et al., 1975).

Besides the OH-reactivity the degradation products should also be analyzed. The products of the photodecomposition were analyzed by Crosby and Moilanen (1974). The detected products were Dieldrin, Photoaldrin and Photodieldrin. The experiments were made in the gas phase in a special apparatus where the Aldrin vapor was irradiated. Draper and Crosby (1984) investigated the degradation of Aldrin in water and used dilute hydrogen peroxide as OH precursor.

The semivolatile substances have a low volatility at room temperature. This fact makes it difficult to characterize and handle the vapors. The analysis of such substances is more appropriate in the aerosol-borne state. A high-purity fused silica (SiO_2) was chosen as inert carrier. The industrial product Aerosil 380 from DEGUSSA has a high specific surface of 380 m^2/g. The inert behaviour of Aerosol is well known from earlier research projects (Palm et al.

(1998), Behnke et al.(1987); Zetzsch, 1991a). The primary particles have a mean diameter of 7 nm, and Aerosil has a bulk density of 30 g/l and a tampered density of 50 g/l and a high porosity (98.6 %) according to the specifications of the manufacturer, see also www.aerosil.com.

3. Materials and methods

3.1. Aerosol smog chamber experiments

An aerosol smog chamber, dismantled at the Fraunhofer-;Institute at Hannover, was reinstalled at the University of Bayreuth in the new refrigerator laboratory, coolable down to -28°C. The smog chamber was made of glass (Duran, Schott) with 1 m inner diameter and 4 m height, consisting of 4 parts and corresponding to a volume of 3200 L. Teflon film (FEP 200A, 0.05 mm) was used as seals between the 4 parts of the chamber. Both ends (top and bottom) were also closed by Teflon film.

The cooling of the chamber should decrease the evaporation of substance from the surface of the particles, (Behnke et al., 1987a; b), and the experiments could be made at environmentally relevant temperature of the troposphere, for example at the middle, global tropospheric temperature or simulate even the arctic climate.

The size of the smog chamber should increase the residence time of the agglomerates.

This leads to high aerosol concentrations at longer durations of the experiment. The smog chamber with the measurement equipment is schematically shown in fig. 3.1. The solar simulator is placed below the chamber. 16 fluorescent lamps (Osram Eversun Super, 80 W) are used to simulate the sunshine. A photograph of the chamber is shown in fig. 3.2.

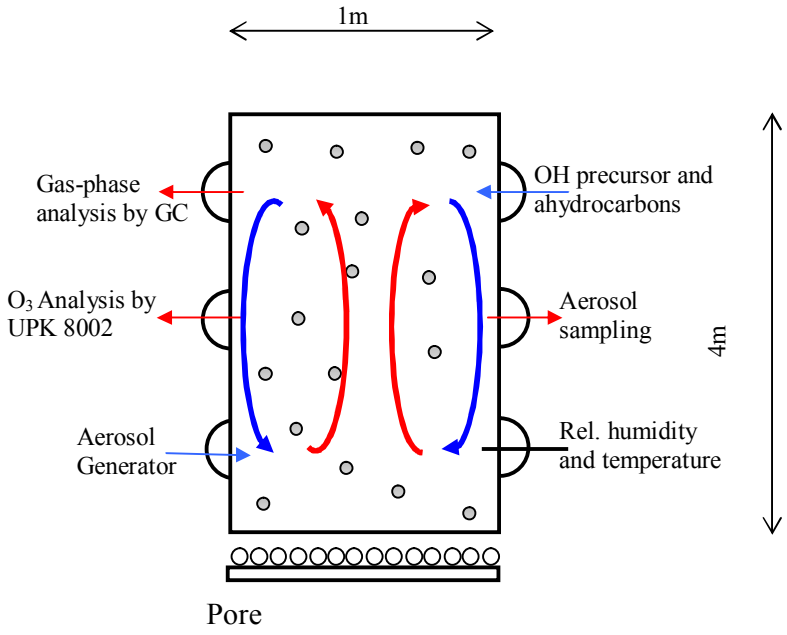

Fig. 3.1 Scheme of the aerosol smog chamber. The chamber simulates atmospheric relevant, photochemical reactions and direct photolysis.

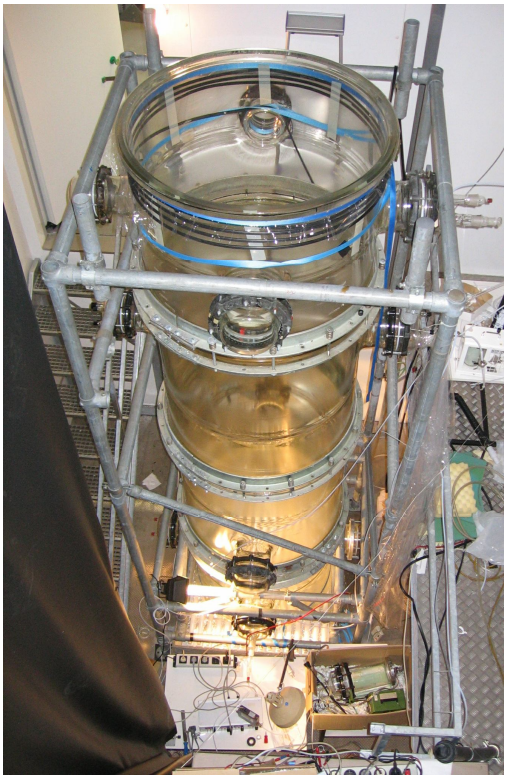

Fig. 3.2 A photograph of the smog chamber. The aerosol feeding device can be seen in the lower part of the photograph in front and also the sun simulator below the chamber.

The position of the solar simulator below the chamber causes a vertical temperature gradient and facilitates a mixing of the chamber aerosol. Temperature and relative humidity were measured by a hygrometer/digital transmitter (Steinecker Elektronik GmbH), and the ozone concentration was monitored by an ozone analyzer, Bendix/UPK 8002. The aerosol agglomerates were produced by an aerosol generator, which is directly connected to the smog chamber. Devices for aerosol sampling, analysis of trace gases and dosage of OH precursor are also connected to the chamber.

3.2. Characterization of aerosol mass, size distribution and lifetime

The aerosol concentration is a very important quantity for the evaluation of the results of an experiment.

A total number of 10 aerosol samples are taken on Teflon filters during each experiment, where 6 of those serve for the concentration measurement of Aldrin and 4 for the determination of the mass concentration of the aerosol. For a desirable determination with a precision of 1%, the sample weight m_f should be at least 50 µg, and the volume for aerosol sampling is adjusted accordingly. The samples are first discharged electrostatically for approx. 24 h and then

weighed with a microbalance (Sartorius SC2). It takes about 5 min each to reach the equilibrium on the microbalance during the measurements. The aerosol concentration, C_{Ae} , is calculated from the filter weight and the taken air volume,

$$C_{Ae} = m_f / V_f. \quad \textbf{(3.1)}$$

C_{Ae} is the aerosol concentration, m_f the weight of the aerosol agglomerates collected on the filter for the aerosol-mass calculation, and V_f is the air volume taken for the sampling.

Since the aerosol concentration decreases exponentially, the analysis samples, which are taken between the aerosol concentration samples, can be interpolated to obtain the aerosol mass for the other filter samples. The intercept ($C_{Ae\ 0}$) and the slope (b) are taken from the aerosol concentration decrease for each experiment by linear regression of semilogarithmic plots.

The aerosol concentrations C_{Ae} for time t are calculated from the two parameters for every experiment.

$$C_{Ae} = C_{Ae\ 0}\ exp(-b*t) \quad \textbf{(3.2)}$$

Fig. 3.3 shows such measurements; the residence time is up to 45 hours.

Some factors could affect the aerosol concentration in the smog chamber. According to table 8.7 the maximum relative humidity could be used as a measure for the aerosol concentration. The aerosol particles were produced by spraying the suspension into the smog chamber. The drops dry out to become agglomerated aerosol particles. The high relative humidity is correlated with high aerosol concentration. The total residence time of the aerosol depends on the size distribution of the particles that depends on the nozzle adjustment for a constant air flow and a constant suspension flow. It was required to clean the nozzle and the experimental set up for aerosol production regularly, every 4 experiments. The adjustment of the nozzle was then slightly different afterwards, and that could affect, as we see in fig 3.3, the aerosol concentration. The remaining experiments are pictured in the appendix with their residence time.

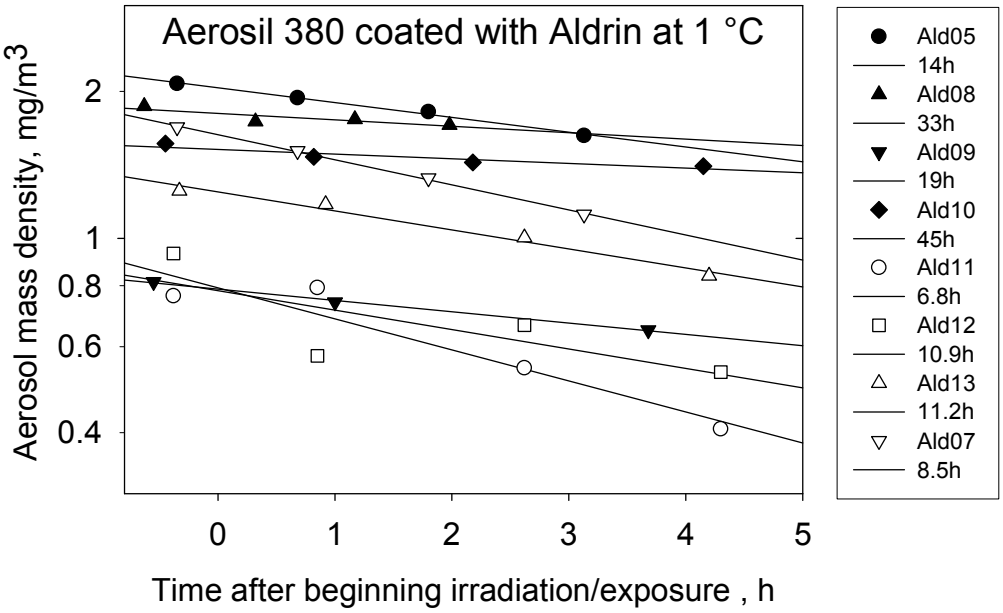

Fig. 3.3 : Decrease of the aerosol mass density after the dosage of aerosol particles of Aerosil 380 coated with Aldrin into the chamber at approximately 1°C. The experiment numbers, AldXX, and mean residence times are given in the legend.

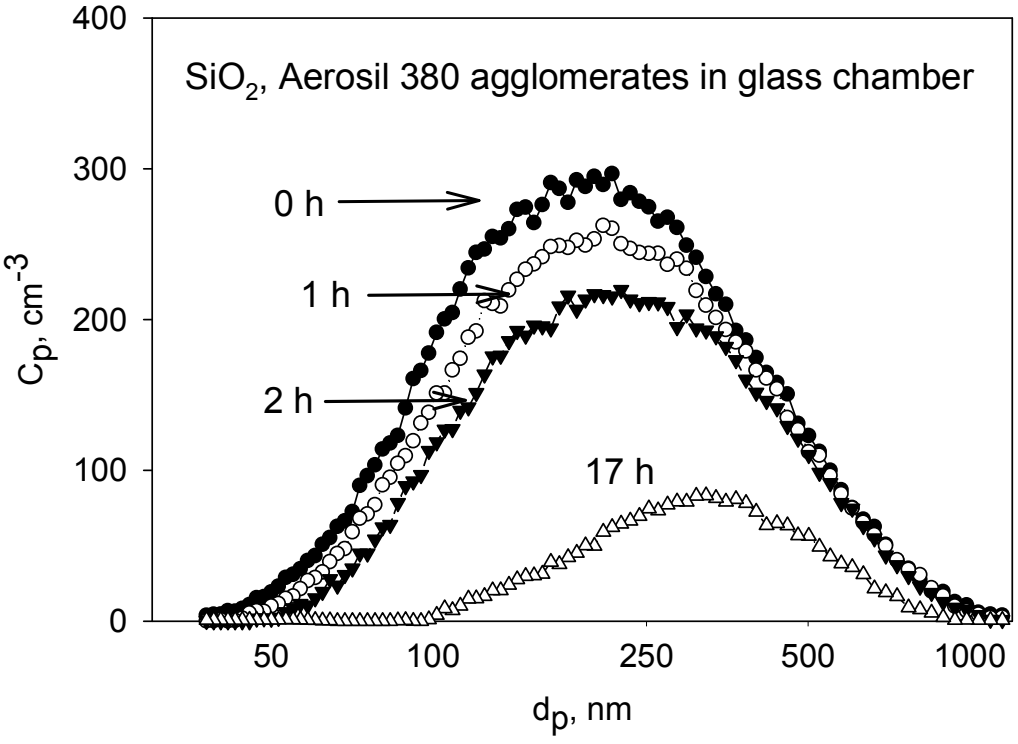

Fig. 3.4 The number distribution c_p is shown for some time points during one experiment.

The size distribution of agglomerates in the chamber is represented in fig. 3.4. The bigger particles undergo sedimentation in the chamber and accordingly the residence time is shorter. Forming the third power of this distribution, one gets the volume distribution that has its maximum at a larger diameter and is decisive for the fate of the test substance that should be evenly distributed on the primary particles (fig 3.5). The maximum of the volume distribution shifts to agglomerates with diameter 600 – 700 nm. The agglomerate diameter was measured up to 1050 nm. The mass distribution corresponds to the volume distribution and is shifted to the particles with bigger diameter.

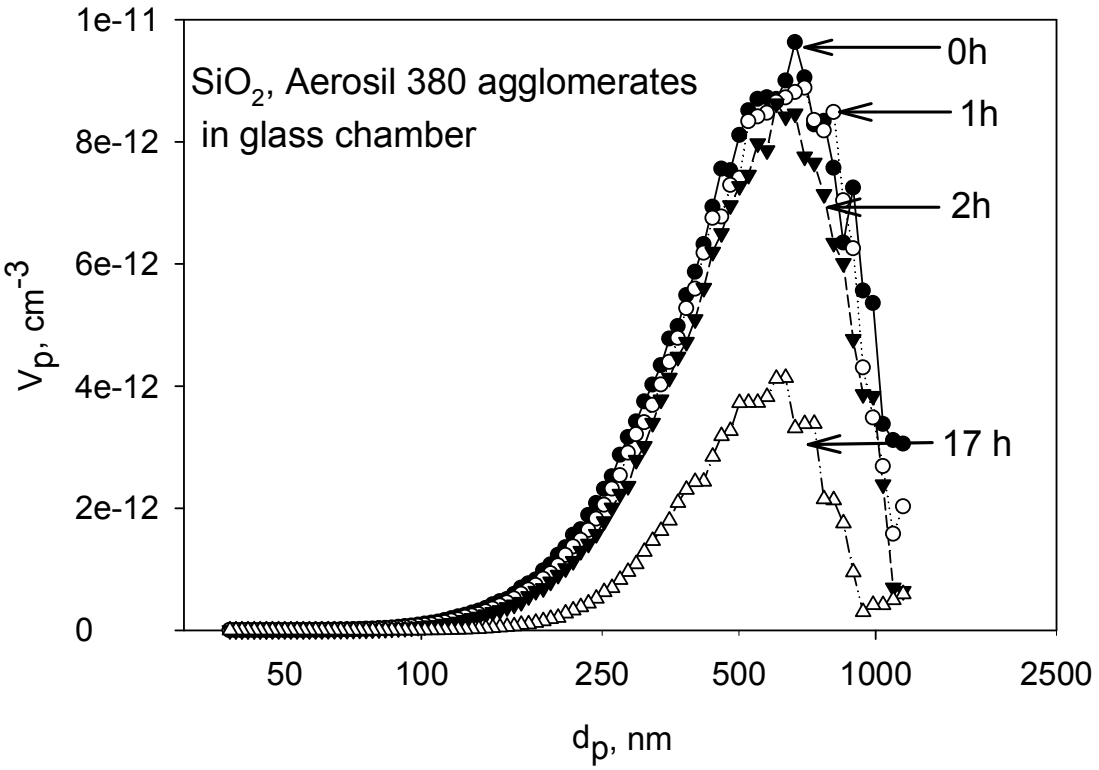

Fig. 3.5 The volume distribution V_p is shown for some time points during one experiment.

The agglomerate residence time can be plotted vs. the aerodynamic diameter, fig. 3.6. The small agglomerates are lost by diffusion and coagulation.

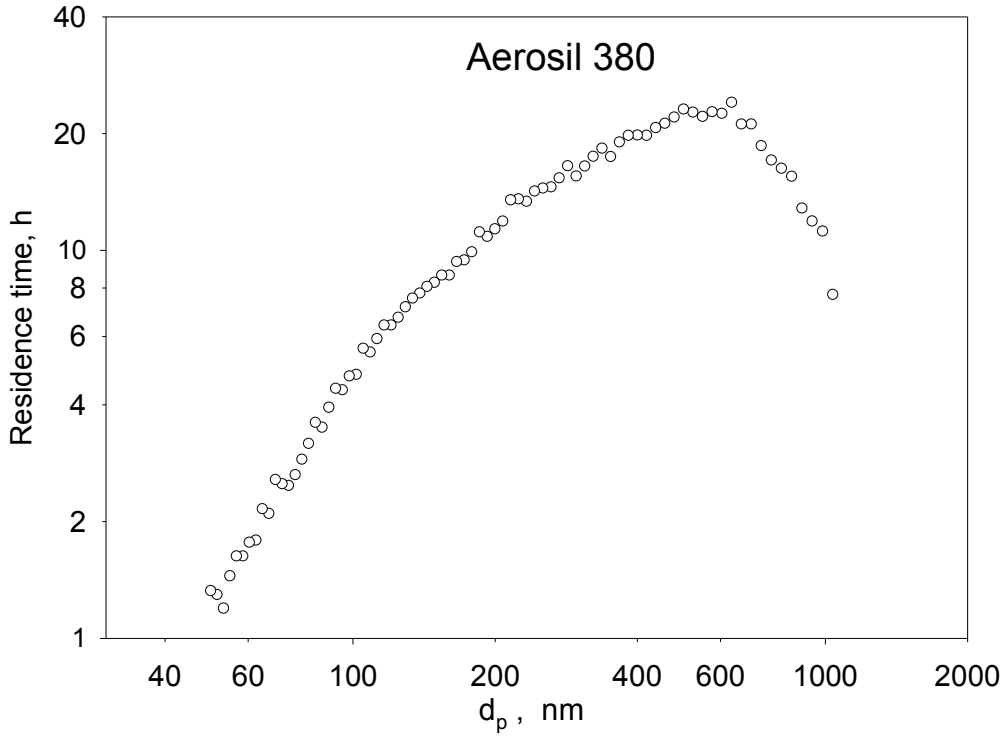

Fig. 3.6 Residence time as a function of the aerodynamic diameter. A residence time of 20 hours is exceeded in the diameter range of 400 to 800 nm. At long times the deposition process diffusion/coagulation and sedimentation will generate a maximum of the abundance of the particles at 600 nm.

3.3. Sampling, solar simulator, Aerosil coating and aerosol feeding devices

The size of the chamber, the size of the agglomerates sprayed into the chamber and the physico-chemical properties of the test substance require specific devices and methods for investigating the kinetics of such substances. Below the devices used for the coating of the test substance on the carrier will be shown and also the devices for the sampling of the spayed agglomerates. Fluorescent lamps were used as a solar simulator.

3.3.1. Aerosil coating and aerosol production

The aerosol carrier, Aerosil 380, Degussa, was mixed with the test substance in dichloromethane and was dried in a rotary evaporator, fig. 3.7. The quantity of test substance is about 1% w/w of the Aerosil mass.

Fig. 3.7 Rotary evaporator. The coated powder can be seen in the bulb.

The equipment for the aerosol production is shown in fig.3.8. The powder is suspended in distilled water by a high-speed blender (Ultra-Turrax) to obtain 0.01 % w/w. The aerosol suspension was filled into a motor-driven syringe and was sprayed by a preheated airflow through a nozzle. The suspension flow was 19 ml/h and the air flow was 20 L/h. The aerosol droplets dry in the subsequent glass-cylinder of the aerosol generator to form solid porous agglomerates. A cooling hose is installed on the glass tube between the aerosol generator and the smog chamber. The moisture condenses in the cooled zone. The relative humidity decreases, and higher aerosol concentrations were achieved. The aerosol reaches the aerosol smog chamber, where the humidity is measured continuously. The optimum aerosol concentration (approx. 1 $\mu g/m^3$) was observed at approx. 50 % relative humidity.

The suspension was dispersed by a two phase nozzle (Schlick, S6). The OH precursor was injected by an air stream. Then OH radicals were produced by different techniques, with or without light source. The aerosol sample was taken on a Teflon filter using a vacuum pump. The test substance was extracted by n-hexane from the aerosol and analyzed by gas chromatography.

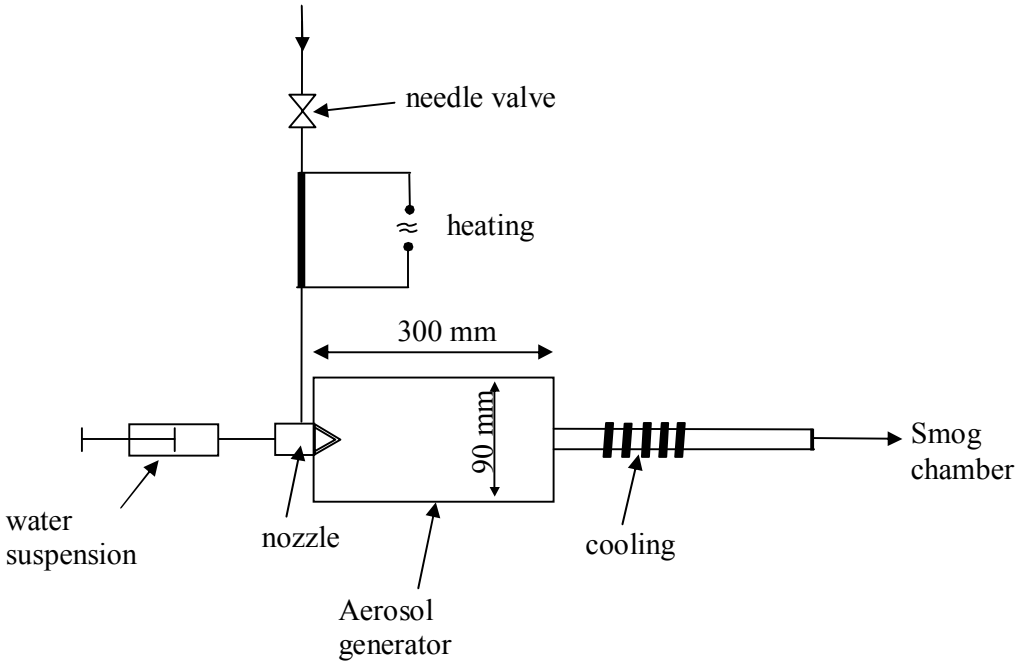

Fig. 3.8 Experimental set up for aerosol production. The aqueous suspension is sprayed into the glass cylinder and fed into the chamber.

3.3.2. Sampling device

The components of the sampling train (fig. 3.9) are a stainless steel tube (L = 925 mm, d_i = 7 mm), a filter holder (d_a = 40 mm) (fig. 3.10) and a vacuum pump. The steel tube, the filter holder and the vacuum pump are connected by Teflon tube. The air flow was measured by a gas meter.

Teflon filters, (Sartorius d = 38 mm, PTFE-Filter, pore-size: 0.2 µm), were used for sampling. The high resistance against all solvents and the good mechanical stability was selected as advantage for the filter material. The Teflon filter was put into a stainless steel filter holder. Then the Teflon tubing from the steel tube to the vacuum pump was connected and the aerosol agglomerates were sampled on the filter by the vacuum pump.

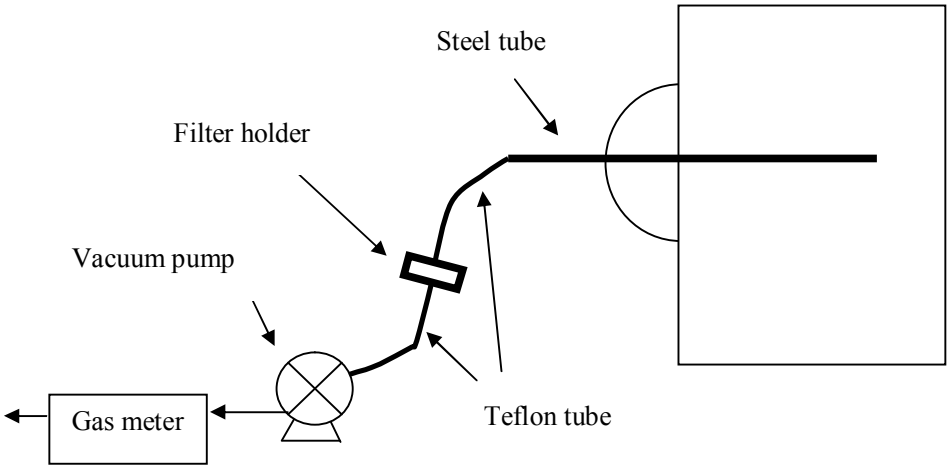

Fig. 3.9 Sampling train. A stainless steel tube was connected to the chamber. The tube and the filter holder were connected by Teflon tubing. The agglomerates were sucked in by a vacuum pump from the chamber. The air flow was measured by a gas meter.

After the sampling the filter is taken out from the holder and is placed into a vial. The test substance was extracted from the agglomerates with 1 µl solution of n-hexane using Mirex (pesticide) as internal standard. The concentration of Mirex in the standard solution was 20 µg/l. The sample is then extracted for 3 min in an ultrasonic bath and centrifuged for 5 min before GC analysis.

Fig. 3.10 Photograph of the filter holder. The Teflon filter can be seen in the filter holder.

3.3.3. Solar simulator

Fig. 3.11 shows the spectrum of the solar simulator in comparison with the sun spectrum in Europe. In the spectrum, the usual mercury lines of fluorescent lamps could be observed (313, 334, 366, 408 and 436 nm) which can serve for calibration of the wavelength scale of the monochromator, agreeing within 1 nm with the readings. Their intensities are not negligible in

comparison with the emission spectrum of the fluorescence dye in form of a Gaussian function, and they must be taken into account in quantitative evaluations of the photolysis of specific molecules by comparison with the UV spectrum of the absorbers in some cases. The mercury lines could influence the photolysis of the OH precursors, especially by hydrogen peroxide.

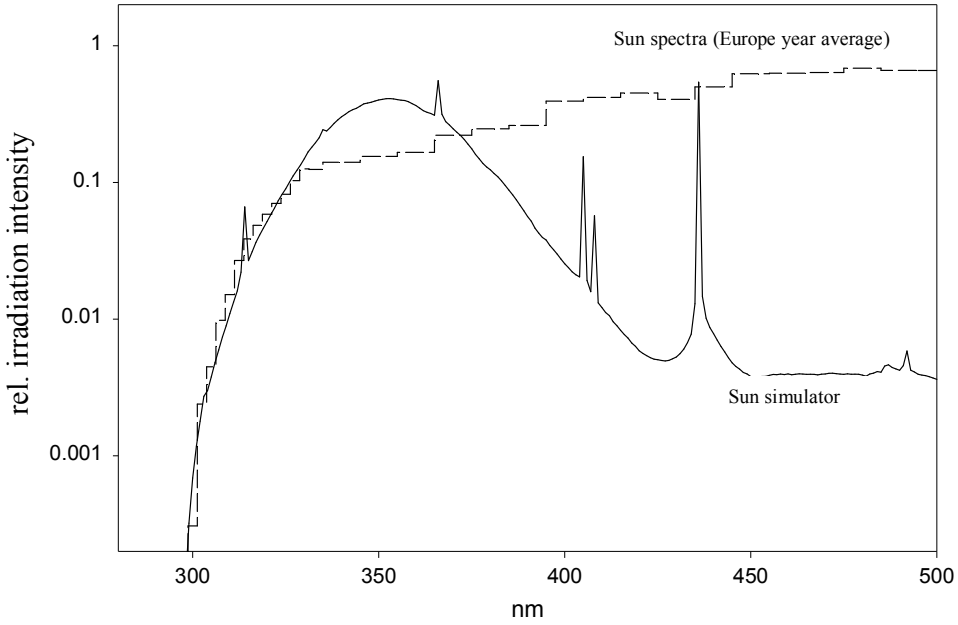

Fig. 3.11 Spectrum of the sun simulator, consisting of 16 fluorescence lamps Osram Eversun Super in comparison with the sun spectrum.

The carrier material should not absorb in the spectrum of the sun simulator, and Aerosil was chosen as a carrier that does not absorb in this range (Krüger et al., 2001).

The usual OH precursors of the atmosphere: ozone, H_2O_2, HONO and CH_3ONO (used in the chamber experiments) have largely continuous spectra, and their overlap with the sun and/or sun simulator can be calculated.

The solar spectrum and the solar simulator spectrum overlap very well in the actinic area between 310 and 330 nm, and the solar simulator spectrum is somewhat stronger in comparison with the sun spectrum in the subsequent range up to 370 nm. The intensity of the solar simulator decreases in the visible range (where photolysis is hardly expected) opposite to the sun spectrum which does not disturb the photolysis rates because the molecules are anyway transparent there (note, that the logarithmic diagram of fig. 3.11 does not give absolute values and that the absolute intensity of the solar simulator is much weaker than the sun). By mounting aluminum foil as reflector, the radiation intensity of the solar simulator was

increased by about 40%. The solar simulator is suitable consequently also to persistence tests with respect to direct photolysis.

3.4. Measurement of the temperature gradients in the smog chamber

The temperature gradient ensures the mixing of the air in the chamber. The air movement mixes the aerosol with the OH precursor and the hydrocarbons, which indicate the OH concentration. It is well-known that the temperature difference between the bottom and the top of the chamber causes the mixing in the chamber. Further temperature gradients exist between the wall and the middle of the chamber. So the OH precursor and the hydrocarbons are uniformly distributed in the whole chamber. They can react with the aerosol agglomerates not only in some zones but also in the whole volume of the chamber (although the irradiation of the chamber by the solar simulator is slightly inhomogeneous, decreasing approximately in a linear fashion with distance from the lamps by a factor of 2.

The temperature measurements were made by a thermistor with a negative temperature coefficient (NTC).

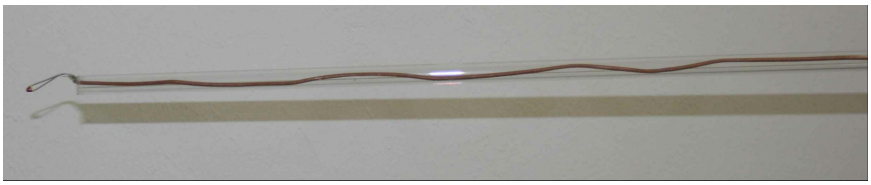

Fig. 3.12 Photograph of the NTC sensor

The sensor was connected with an extension wire that was placed in a glass tube (L = 93 cm) as shown in fig. 3.12. For measurements of the temperature in the center of the chamber the sensor was placed into a glass neck 35 cm from the chamber top and 70 cm from the chamber bottom. The sensor was placed on the wall 20 cm from the bottom and then 20 cm from the top of the chamber. The sensor was used without a radiation protection.

The electrical resistance of the thermistor is temperature dependent. The excellent sensitivity of the thermistor makes the instrument very suitable for measurements of small temperature gradients. The NTC sensor has very good long time stability, and it can be calibrated absolutely. The electrical resistance of the thermistor was measured by a Keithley digital ohmmeter 195A. The data recording was made by a suitable program written in Rocky Mountain Basic licensed by HP (Krüger, 2005).

The measurement sequence was chosen to minimize the influence of the air warming in the chamber during the measurements. At the beginning, a stable temperature was achieved in the chamber. Then the temperature was measured without light source. The temperature was measured at the top and at the bottom. The light source was turned on, and (after achieving a stable temperature) the measurement was repeated. The delay of the signal by the heat capacity of the thermistor must be also taken into account. The calibration was made comparing the measured temperature with the ice melting point. It was assumed, that the influence of switching the solar simulator off has two stages of impact on the cooling curve. In the first stage the thermistor cools itself after irradiation. Then the air temperature in the chamber cools down in the second stage. If the time is plotted vs. time, then the temperature curve can be extrapolated to the temperature axes. The extrapolated temperature is an approximation of the air temperature.

Both stages could be fitted to a double exponential function in the form $T = T_0 + a e^{-bx} + c e^{-dx}$, where the second exponential function deals with the chamber cooling.

4. Production of OH-radicals in the smog chamber

The techniques of OH production will be described below. OH radicals were produced by appropriate chemical reactions in the presence or in the absence of a light source. The reactions mechanism will also be presented.

Four hydrocarbons were used as reference substance to calculate the OH exposure. The dilution of the chamber was also taken into consideration by an inert standard. The analysis of the hydrocarbons and the calculation of the OH exposure will be presented.

4.1. Precursors of OH radicals

An extremely efficient OH production method is the photolysis and consecutive photochemistry of methyl nitrite and formaldehyde:

$CH_3ONO + h\nu \rightarrow CH_3O + NO$

$CH_3O + O_2 \rightarrow HO_2 + CH_2O$

$CH_2O + h\nu \rightarrow CHO + H$

$H + O_2 + M \rightarrow HO_2 + M$

$CHO + O_2 \rightarrow HO_2 + CO$

$HO_2 + NO \rightarrow OH + NO_2$

$CH_2O + OH \rightarrow H_2O + CHO$ ….

Ozone can be formed by methyl-nitrite photolysis through photolysis of NO_2 from the reaction $HO_2 + NO \rightarrow NO_2 + OH$ (by the well-known reactions of the Leighton-cycle: $NO_2 + h\nu \rightarrow NO + O$, $O + O_2 + M \rightarrow O_3 + M$). Ozone can finally build up to a few ppm. The degradation intermediates of the hydrocarbons are peroxides (at low NO_x concentration), aldehydes, ketones and unsaturated carbonyl compounds which are degraded by OH radicals and photolysis, producing further radicals.

The final inorganic product of the photodegradation of methyl nitrite is nitric acid that may modify compounds by protonation. This can be avoided by employing H_2O_2 as photolytic precursor of OH radicals:

$H_2O_2 + h\nu \rightarrow 2\ OH,$

where the reaction of OH with the precursor

$OH + H_2O_2 \rightarrow H_2O + O_2$

limits the level of OH radicals that can be reached.

The spectra of ozone, hydrogen peroxide and methyl nitrite were compared with the sun simulator spectrum in fig. 4.1 (Ackerman, 1971), (DeMore et al., 1997), (Molina and Molina, 1981; Nicovich and Wine, 1988; Vaghjiani and Ravishankara, 1989).

The photolysis rate constant k can be calculated by the following equation

$$k_{ph} = I/\tau = \int I(\lambda,z)\cdot\sigma(\lambda)\cdot Q\, d\lambda\,, \qquad \textbf{(4.1)}$$

integrating the product of the solar flux intensity I at the zenith angle z, the photoabsorption cross-section σ in this range of wavelengths and the quantum yield Q of photodegradation over the absorbing wavelength λ of the pollutant (Güsten, 1986). The photolysis rate constants of hydrogen peroxide, ozone and methylnitrite are calculated assuming the quantum yield Q is equal to 1 (or every absorbed photon leading to reactant consumption during the photochemical reaction).

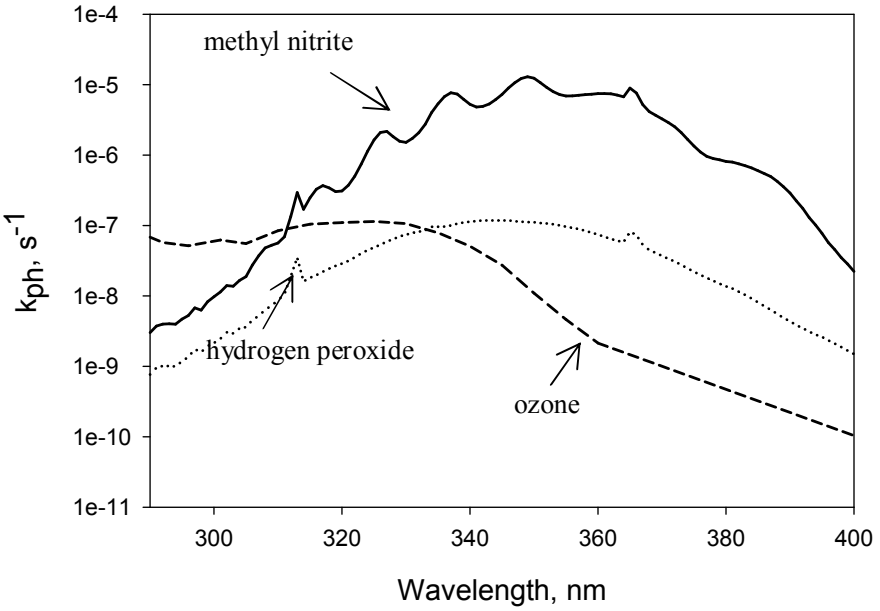

Fig. 4.1 Overlap of the sun simulator spectrum with the spectra of hydrogen peroxide (the dotted line), ozone (the dashed line) and methyl nitrite(the solid line).

The small overlap of the hydrogen peroxide and sun simulator spectra does not cause a significant photolysis of hydrogen peroxide and there is no production of OH radicals. The same is valid for ozone. The experiments have verified this calculation.

The photolysis rates of methylnitrite, ozone and hydrogen peroxide were calculated from eq. 4.1. The photolysis rate constant is k (metylnitrite) = $1.5\cdot10^{-2}$ s^{-1}, that of ozone - k (O_3) =

$1.27 \cdot 10^{-4}$ s^{-1}, that of hydrogen peroxide - k (H_2O_2) = $2.6 \cdot 10^{-4}$ s^{-1}. The calculations of the photolysis rate constants correlate with the measured spectra. The used sun simulator does not cause the photolysis of ozone and hydrogen peroxide. Methylnitrite in contrast to the both substances is a very good precursor of OH radicals.

The photolysis rate of hydrogen peroxide will increase because of the influence of the irradiation emission of the mercury (see fig. 3.11) at 313 nm and 366 nm with $1.5 \cdot 10^{-7}$ s^{-1} respectively with $5.7 \cdot 10^{-7}$ s^{-1}.

The photolysis of ozone can be used as another OH-precursor under formation of electronically excited O atoms (Takahashi et al., 2005), which react further with H_2O to form OH:

$O_3 + h\nu\ (\lambda \leq 310\ nm) \rightarrow O(^1D) + O_2\ (a^1\Delta)$

$O(^1D) + H_2O \rightarrow 2\ OH.$

The sun simulator irradiate from 290 nm to the infrared spectra. The overlapping zone is from 290 nm to 310 nm. The concentration of ozone was measured during the experiments also. Its concentration was some ppb. The reaction may take place by the formation of the hydroxyl radicals.

OH-radicals can be produced in the absence of light, for example by the reaction of ozone with olefins or hydrazine (used in these experiments) (Tuazon et al., 1983). The reaction of O_3 with N_2H_4 is rapid. The reaction proceeds in the air via a chain mechanism with N_2H_3, N_2H_2 and OH radicals as the chain carriers (Pitts et al., 1980; Tuazon et al., 1982; Tuazon et al., 1981).

Initiation:

$H_2NNH_2 + O_3 \rightarrow H_2NNH + OH + O_2$

Propagation:

$H_2NNH_2 + OH \rightarrow H_2NNH + H_2O$

$H_2NNH + O_2 \rightarrow NH{=}NH + HO_2$

$NH{=}NH + O_3 \rightarrow NH{=}N + OH + O_2$

Termination:

$NH{=}NH + OH \rightarrow NH{=}N + H_2O$

Product formation:

$NH{=}N + O_2 \rightarrow N_2 + HO_2$

$HO_2 + HO_2 \rightarrow H_2O_2 + O_2$

Such dark-sources of OH are used if one wants to exclude the photolysis as loss-pathway.

Another OH precursor could be photolysis of water vapour (Ung, 1974). Hydroxyl radicals could be formed according to the reaction:

$H_2O + h\nu\ (\lambda \leq 242\ nm) \rightarrow \quad H\ (1^2S) + OH\ (X^2\Pi)$.

The lamps do not irratiate in this part of the spectra. There are no conditions for the produsing of hydroxyl radicals (fig. 3.11).

4.2. OH production

OH radicals were generated in the chamber by photolysis of H_2O_2 by the irradiation from the solar simulator (although we now understand that the efficiency of the solar simulator is quite low). The OH radicals react with the hydrocarbons and other substances. Possible leaks of the chamber or analytical fluctuations, caused by variable sampling, are detected by measurement of the inert substance perfluorohexane.

Higher OH-concentrations can be reached by photolysis of methyl nitrite, because this molecule absorbs up to larger wavelengths and uses the light of the solar simulator consequently better, so that the OH radical concentration can reach levels up to $5 \cdot 10^7$ cm^{-3}. Methyl nitrite was synthesized by esterification of nitrous acid with methanol (by acidifying a mixture of methanol and $NaNO_2$ with 50 % sulphuric acids at -18°C). The methyl nitrite production is described in detail in the appendix. Methyl nitrite is thermally unstable and is therefore stored in the freezer.

A known volume of gaseous methylnitrite was injected by a syringe into one or two gas-collection tubes and then was slowly flushed by an air stream into the chamber. Under irradiation, OH radicals were produced. One gas-collection tube is sufficient if the experiment is short (for example 2 hours). The precursor concentration is high at the beginning und low at the end. Two gas-collection tubes are more suitable for experiments with a longer duration (for example 5 or more hours). Two gas collecting tubes facilitate to obtain a constant dose rate of methyl nitrite and a constant OH-concentration during the experiment. The concentration of methyl nitrite in both gas-collection tubes is calculated for the used air flow. The required OH concentration can be adjusted by the air flow and by the injected methylnitrite concentration. Calculated time profiles of methyl nitrite are shown in fig. 4.2.

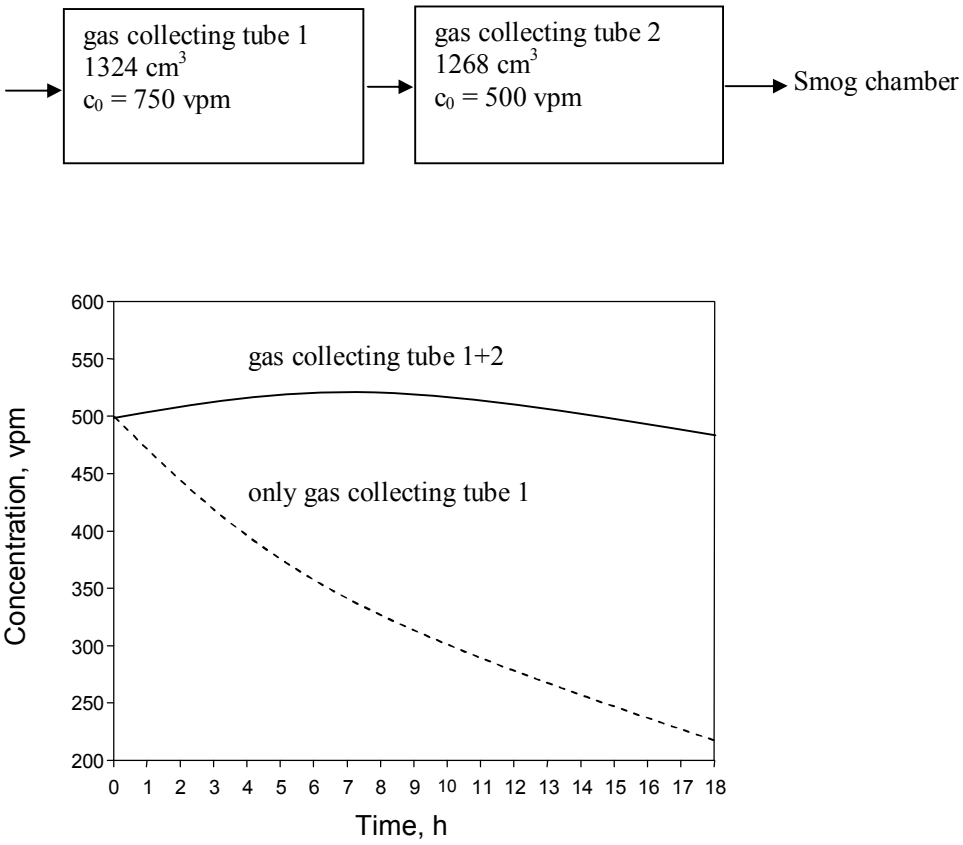

Fig. 4.2: Dosage of methylnitrite into the smog chamber, using 2 gas-collection tubes with different initial concentrations. This method warrants a fairly constant production of OH.

Higher OH concentrations can be obtained by methyl nitrite and lower ones by H_2O_2. High OH concentrations could be obtained with hydrazine/ozone, too. The UV spectrum of methyl nitrite overlaps with the spectrum of the solar simulator in a larger interval than the spectrum of H_2O_2.

Also completely without light, OH radicals can be produced by the reaction of ozone with olefins or with hydrazine (used for the experiments in this work). Ozone is generated by photolysis of O_2 at 185 nm, using 3 Hg low-pressure lamps (Penray) in a constant air flow. Ozone was also produced by an electric discharge in a commercial ozone generator Sorbios GSG 001.2. The ozone concentration is measured in the chamber by an ozone analyzer (UPK, measurement method by chemiluminescence). The addition of hydrazine (Roth, water-free, purum) is controlled by an air flow through an impinger. Hydrazine and ozone were mixed in the chamber, and OH radicals were produced by their reactions.

4.3. Analytics the gas phase and characterization of the exposure atmosphere

The concentration of OH-radicals cannot be measured directly by spectroscopic techniques in our chamber. A measurement technique employed in other laboratories is laser induced fluorescence (LIF) at low pressure, also called fluorescence assay by gas expansion (FAGE) (Schlosser et al., 2006). An additional technique, differential optical absorption spectroscopy (DOAS) was established.

Both instruments are complex and expensive laser instruments for the detection of OH under atmospheric conditions, which were developed as field instruments and then adapted to the SAPHIR chamber in Jülich. The laser-DOAS (Differential Optical Absorption Spectroscopy) instrument measures absorber densities based on the Beer-Lambert law. Long path absorption is achieved by 112 travels through a 20 m base length mirror system inside the SAPHIR chamber. Its sensitivity is limited to $8.6 \cdot 10^5$ cm^{-3} (for 200 s integration time) (Brandenburger et al., 1998). On the other hand, it needs no calibration, since its accuracy (6.5%) is based solely on physical data of the OH radical (Dorn et al., 1995), where the line broadening parameters have been determined by Leonard (1989).

The LIF FAGE (Fluorescence Assay Gas Expansion) instrument detects the laser-induced flouorescence of OH radical at low pressure. LIF has a lower detection limit down to $1.4 \cdot 10^5$ cm^{-3} (signal to noise ratio = 2,30 s integration time) and a higher precision compared to DOAS (Heard and Pilling, 2003) . On the other hand, it needs laborious calibrations with a radical source and requires a sample volume of several standard liters per minute.

The main requirements of both instruments are met by the SAPHIR chamber: long base length (20 m) and room enough for the DOAS mirror system, and a big total volume (270 m^3) compared to the probe volume of the LIF instrument even if diurnal cycles are measured. Both techniques are highly demanding and are thus not applicable for our smog chamber.

The concentration was therefore measured indirectly by using reference substances. Hydrocarbons with well-known rate constants (including a well-known dependence on temperature) were selected as reference substances. There are also additional requirements for the reference substances: They must have similar and short retention times in the gas chromatograph. The concentration of the reference substances must be low, but measurable. If the concentration of hydrocarbons is high, their reactions would reduce the OH concentration.

Furthermore, the hydrolysis of NO_2 molecules on the wall could produce OH radicals.

$2\ NO_2 + H_2O \rightarrow HNO_2 + HNO_3$

The photolysis of HNO_3 is not effective. More effective is the photolysis of HNO_2.

$HNO_2 \rightarrow OH + NO$

One reference substance is used to consider the leakages and the dilution of the chamber contents by the sampling. This substance must not react with OH radicals. In this way one can separate OH reactivity from dilution.

Up to four of the following hydrocarbons are used as reference substances: n-octane, n-hexane, n-butane, 2,2,3-trimethylbutane and 2,2-dimethylbutane. Perfluorohexane is used as inert dilution standard. A mixture of three of the hydrocarbons, perfluorohexane and air was prepared in a gas-collection tube. A volume of 50 ml of this mixture was injected into the chamber to obtain concentrations of 60 ppb for the hydrocarbons each and 120 ppb for perfluorohexene.

The hydrocarbons were measured by gas chromatography using an FID detector and a modified coldtrap injector, where the principle has been described by Nolting et al. (1988).

The hydrocarbons are measured before the beginning of the OH production and then at temporal intervals of 15 - 30 minutes, according to demand. For a time period of 3 minutes each, a sample of 20 ml was cryofocussed in a glass-coated steel capillary at -110°C (using liquid nitrogen and a magnetic valve to control the flow). The temperature is chosen so that the oxygen from the air does not condense but all hydrocarbons (besides methane) quantitatively. A constant flow during the sampling was ensured with a micro orifice in the pipeline of the vacuum pump. The preconcentrator device can be seen in fig. 4.3 (gas chromatograph Siemens Sichromat 2). Sudden heating of the stainless steel capillary injects the cryofocussed hydrocarbons into the gas chromatograph, where they are separated by a 50m Chrompack AL – PLOT column (d_i = 0.32 mm, film thickness: 5 µm, temperature program: constant 150°C)

Fig. 4.3: Photograph of the GC with the modified cold trap injector for the analysis of the hydrocarbons.

Typical chromatograms are presented in fig. 4.4. The four peaks correspond to perfluorohexane, 2,2-dimethylbutane, n-hexane and 2,2,3-trimethylbutane.

The area was evaluated by a PC-based laboratory data system (HP ChemStation), and this area is proportional to the concentration of the reference compounds.

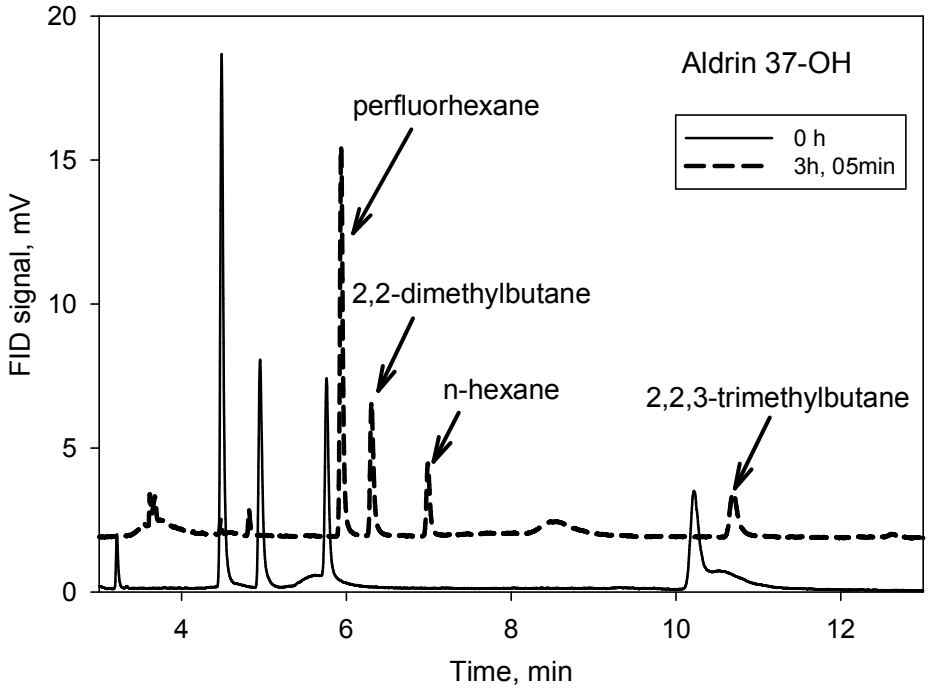

Fig. 4.4: Chromatograms of the hydrocarbons at the beginning of the experiment and 3h 05min later during the experiment.

The calculation method is introduced below. The freezing out of the sample continues for 3 minutes. The start time *t* must be corrected by half of the freezing out – time. The next step is the standardization of perfluorohexane and the other hydrocarbons.

$$[HC]^{j}_{norm,i} = [HC]^{j}_{i} \cdot [PHF]_0 / [PHF]_i \qquad \textbf{(4.2)}$$

Here $[HC]^{j}_{norm}$ is the normalized peak area or also concentration of a hydrocarbon *j* with time *i*, $[HC]^{j}_{i}$ is the measured peak area with the time *i*, $[PFH]_0$ – the initial peak area of PFH, $[PHF]_i$– the peak area of PFH with time *i*.

The time step is given by

$$\Delta t = t_i - t_{i-1} \qquad \textbf{(4.3)}$$

The disappearance of a single hydrocarbon could be described by first order kinetic equation.

$$\frac{d \ln[HC]}{dt} = -k_{OH}[OH] \qquad \textbf{(4.4)}$$

Where [HC] is the peak area of the hydrocarbon after time t, k_{OH} – the rate constant, [OH] – concentration of hydroxyl radicals. From this equation the concentration of the hydroxyl radicals could be calculated. The peak area is evaluated from the chromatographic measurements. The temperature dependencies of the rate constant k_{OH}, of the hydrocarbons are given in Table 4.1 (Atkinson, 1994).

Eq. (4.5) is obtained after integration of eq. (4.4).

$$\ln \{ [HC]_0^j / [HC]_t^j \} = k_{OH}^j \int [OH]\, dt \qquad (4.5)$$

From equation (4.5), the concentration of OH radicals can be calculated for hydrocarbon, *j*.

$$[OH]_i^j = ln([HC]_{norm,i-1}^j / [HC]_{norm,i}^j) / (k_{OH}^j \cdot \Delta t) \qquad (4.6)$$

Table 4.1: The rate constants of the reference substances were calculated for a temperature of 2ºC from the corresponding Arrhenius equations, the error estimates refer to the recommendations by Atkinson at 298 K

Compound	Rate constant, k_{OH} ($cm^3 s^{-1}$), at 275 K , error estimate	Temperature dependence of k_{OH} ($cm^3 s^{-1}$) (Arrhenius expression)
2,2-Dimethylbutane	$1.87 \cdot 10^{-12}$ ± 30 %	$2.84 \cdot 10^{-11}$ exp(-747 K/ T)
n – Hexane	$5.20 \cdot 10^{-12}$ ± 25 %	$1.35 \cdot 10^{-11}$ exp(-262 K/ T)
n – Octane	$7.82 \cdot 10^{-12}$ ± 20 %	$3.12 \cdot 10^{-11}$ exp(-380 K/ T)
Perfluorohexane	Completely unreactive	
2,2,3,3-Tetramethylbutane	$9.02 \cdot 10^{-12}$ ± 20 %	$1.63 \cdot 10^{-17}$ T^2 exp(- 86 K/ T)
2,2,3-Trimethylbutane	$4.13 \cdot 10^{-12}$ ± 30%	$9.04 \cdot 10^{-18}$ T^2 exp(495 K/ T)

The peak area in the chromatograms can fluctuate strongly, and therefore the decay is smoothed by integration, using equation (4.7).

$$\int [OH]_i^j \cdot dt = \sum ([OH]_{i-1}^j + [OH]_i^j) \Delta t \qquad (4.7)$$

Three hydrocarbons were used in the experiments in order to determine the OH concentration by averaging. The mean OH exposure is calculated from equation (4.7).

$$\overline{\int [OH]\, dt} = \frac{\sum_1^j \int [OH]\, dt}{\sum_1^j j} \qquad (4.8)$$

Fig. 4.5 shows the decrease of perfluorohexane by dilution (filled circles) and its normalized area for t=0 (hollow circles). Then the decrease of dilution-corrected concentrations of n-hexane, 2,2-dimethylbutane and 2,2,3-trimethylbutane (the hollow symbols) is caused by reaction with OH.

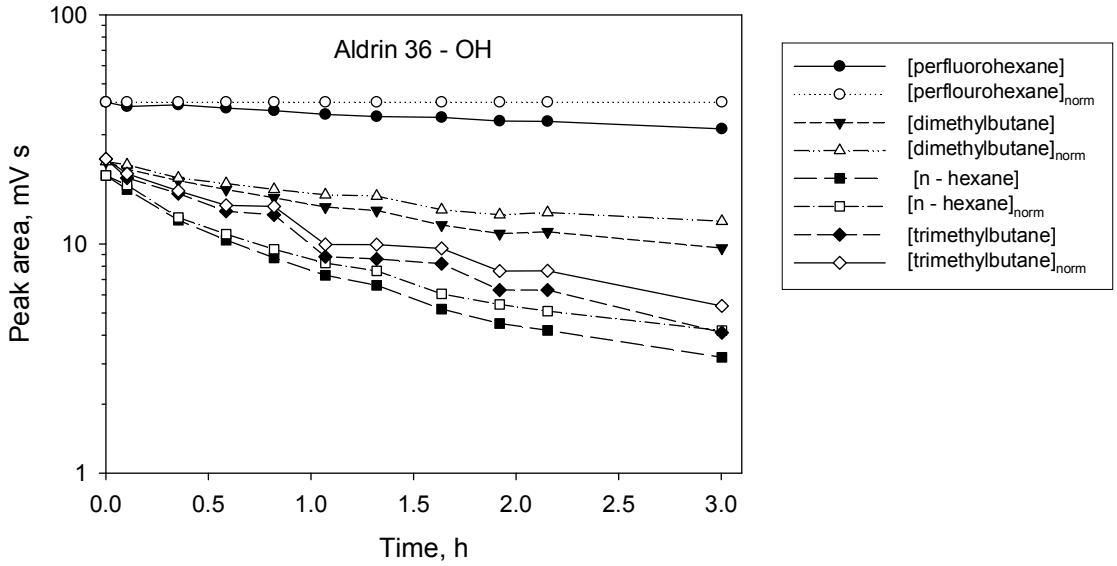

Fig. 4.5 The raw data of peak areas for the three hydrocarbons and perfluorohexane during one experiment Aldrin 36 (filled symbols) are indicated by the filled symbols. The normalized peak areas (using perfluorohexane as reference) are shown as hollow symbols.

The calculation method is introduced in three further illustrations. As example, an experiment is shown where methyl nitrite was the OH precursor. The temperature was 2°C. The chromatograms (fig. 4.4) are integrated. The values of the peak areas are shown in fig. 4.5 (hollow symbols). The values were normalized (eq. 4.1), and the effect of the normalization can be observed as increased and slightly smoothed values.

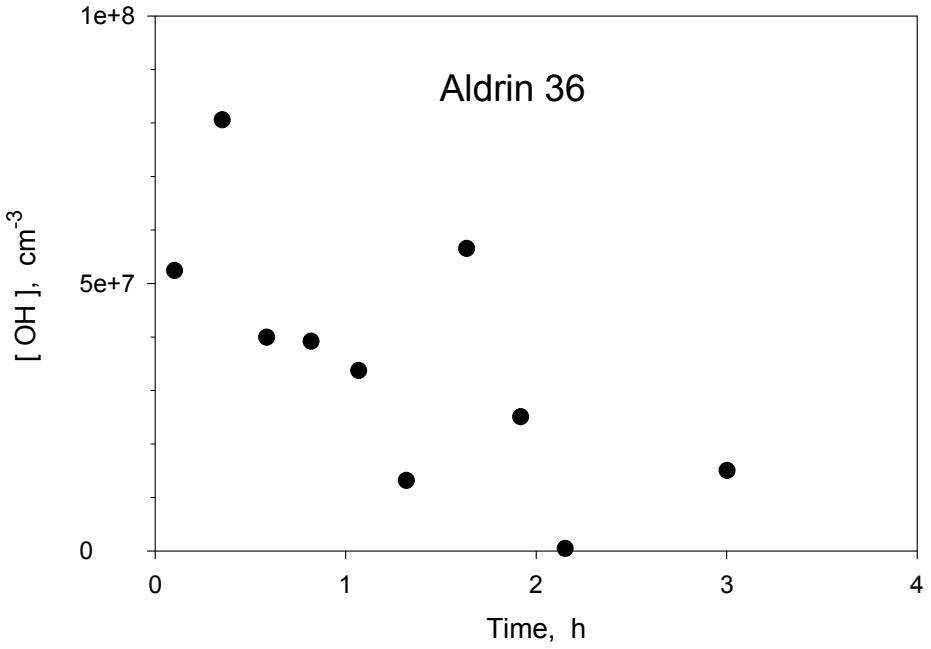

Fig. 4.6 The concentrations of OH calculated from the difference of two successive hydrocarbon peak areas show a large scatter.

The OH-concentration was calculated by eq. 4.4 and is displayed in fig. 4.6, illustrating the role of the area fluctuations. The area fluctuations are due to the evaluation of two successive measurements. These fluctuations cause strong fluctuations of the calculated OH concentration. The integration of the chromatograms could be another source for error. This error depends on the OH concentration. If the OH concentration is high, hydrocarbon degradation is more rapid and the peak area differences are higher. In this case the error of the peak area evaluation has less influence on the calculation of the OH concentration. On other hand, lower OH concentrations deals with low hydrocarbon degradations and smaller differences between the peaks areas of two successively measurements. In this case a low error of the peak evaluation could lead to high deviations of the calculated OH concentration.

The concentration profile of OH can be compared with the integrated OH values (fig. 4.7). The smoothing effect of the method makes it easier to imagine the OH profile and to evaluate the experiment. The ozone concentration profile is also shown in the figure. The comparison between the time integral of OH and the ozone concentration profile serves for the purpose of evaluating the measurement quality.

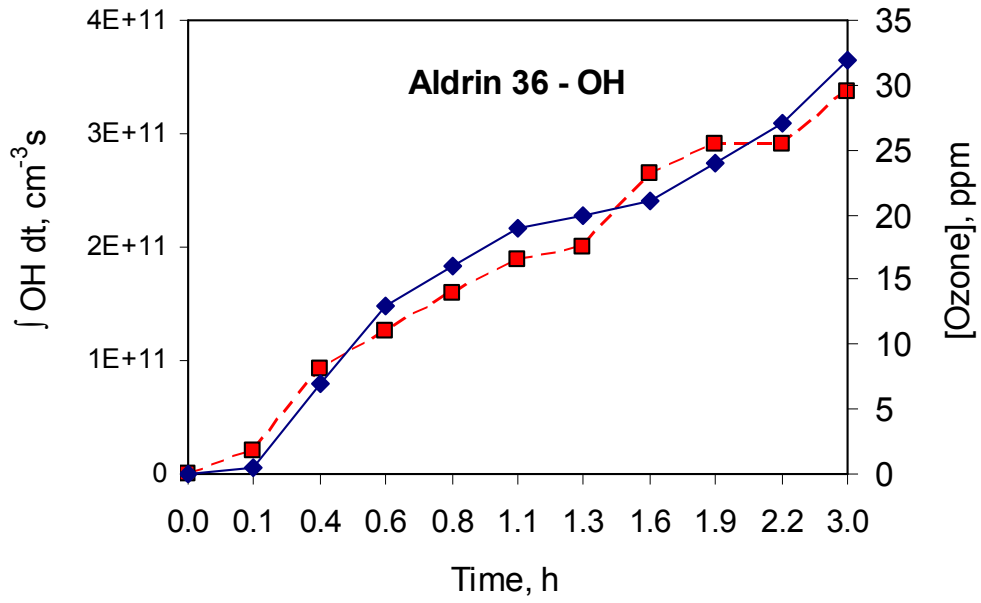

Fig. 4.7: Temporal course of the time integral of the OH concentration (squares). The concentration of ozone is shown also (diamonds).

Stated uncertainties of the rate constant ratios represent 95% confidence limits.

Stated uncertainties of the experimental rate constants reflect the estimated overall uncertainty recommended for the reference rate constants: n-hexane ±25%, 2,2-dimethylbutane ±30%, 2,2,3-trimethylbutane ±30%.

A possible systematic uncertainty could add additional 10-15 % to the values of the calculated OH concentration, considering the errors in the rate constants for the four reference hydrocarbons (Chen et al., 2006).

5. Analysis of the test compound and the products

After the description of the experimental devices, the analysis of the test compound, Aldrin, will be described. Six filter samples were taken from the chamber and placed into 3 ml sample vials. The substance was dissolved by adding 1 ml of n-hexane, containing Mirex (15µg/L) as internal standard. Then it was extracted form the filter samples by treating the vials in an ultra-sonic bath for a period of 3 min and then centrifuging the mixture of aerosol and extract for a period of 3 min at 8000 rpm. The extract with the test substance was analysed by gas chromatography, using an ECD (electron capture detector). Each sample was analysed twice at least. The concentration depends on the air volume taken from the chamber. The dilution factor must be taken into account for every sample. The dilution factor was calculated from the chamber volume and the air volume taken during the sampling.

$$a_v = exp\ (V_{dil} / 3200\ L) \quad \textbf{(5.1)}$$

a_v is the dilution factor, V_{dil} the dilution volume, because of the sampling, 3200 L the chamber volume.

$$m'_f = C_{Ae} \cdot V_f \quad \textbf{(5.2)}$$

m'_f is the interpolated filter weight, C_{Ae} is the interpolated aerosol concentration, V_f is the air volume taken during the sampling. These variables are calculated from the data in the previous chapter (see chapter 3.2).

With known filter weight and air volume taken for the sampling from the chamber, the average aerosol concentration C'_{Ae} can be calculated for the sample. The time point of sampling is calculated as average between the sampling beginning and the sampling end.

$$C'_{ae} = m'_f \cdot V_f \quad \textbf{(5.3)}$$

With the calculation, all required data describing the aerosol are available. The next step is the analysis of the test compound concentration. The aerosol mass densities obtained from the filters used for the aerosol concentration measurement are shown in fig. 5.1 (○). From the decreasing curve the aerosol concentration of the filter samples taken for chemical analysis was interpolated (□).

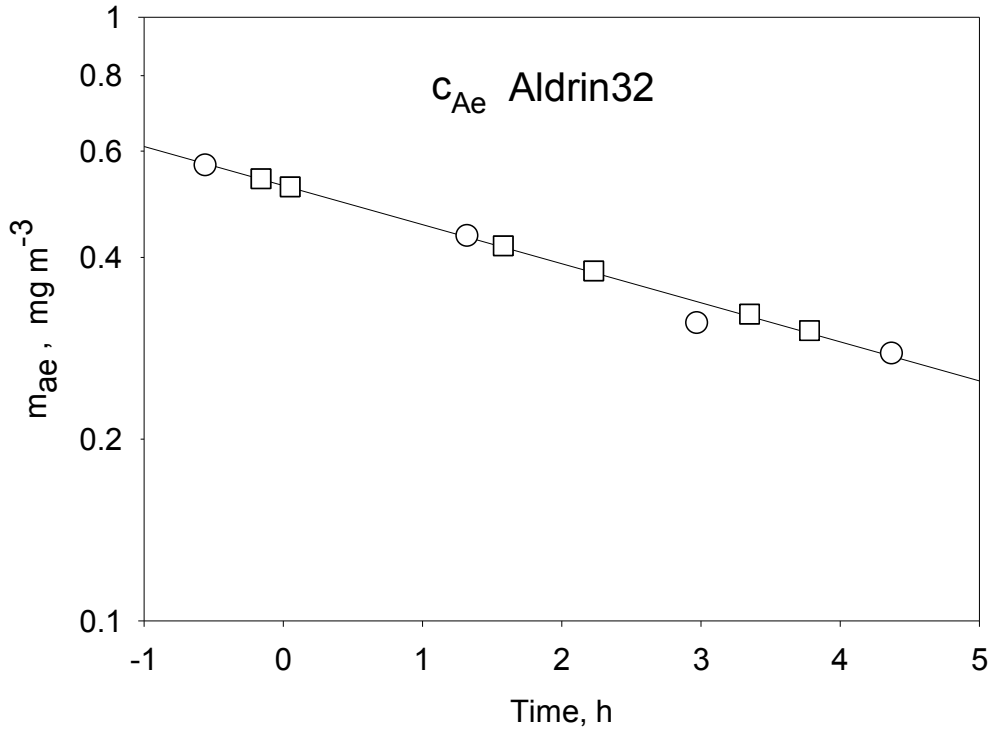

Fig. 5.1 The aerosol mass density was determined (○), and the aerosol concentration for the filters analysed (□) was interpolated.

The chromatograms were evaluated by manual integration. The peak area of the test compound is normalized by the peak area of the internal standard. The peak area of the standard fluctuates for every measurement. The fluctuations are mainly caused by the manual injection. So one of the standard peak concentrations was chosen for basis concentration, and the other measurements are based on this standard concentration in order to minimize the error of the manual injection.

$$C_{p,norm}(\mathrm{t}) = C_p(\mathrm{t}) \cdot (C'_{st} / C_{st}(\mathrm{t})) \qquad \textbf{(5.4)}$$

$C_{p,norm}(\mathrm{t})$ denotes the normalized peak area/concentration and C_p (t) the measured peak area, C'_{st} – a constant basis standard concentration, $C_{st}(\mathrm{t})$ – the standard concentration.

The compound is theoretically regularly distributed on the carrier, i.e. the higher aerosol concentration contains a higher compound concentration. The next expression considers the aerosol concentration.

$$C_{p,ae}(\mathrm{t}) = C_{p,norm}(\mathrm{t}) / m_{ae}(\mathrm{t}) \qquad \textbf{(5.5)}$$

The concentration profile is usually plotted vs. time or time integral of OH concentration.

The products of the reaction can be analyzed directly from the sample extract. Another possibility is separate experiments with larger initial levels of Aldrin for this type of analysis.
The first method has the advantage to save time and materials for separate experiments. But the main disadvantage is the low concentration of the products in the extract solution. High product concentrations can be employed in simpler, separate experiments, avoiding the aerosol phase.
The rotary evaporator was used in this work to obtain high concentrations of products. The samples were analyzed by GC – MS.

6. Transport through porous agglomerates

In this chapter, the transport processes and the influence of the particle structure on the transport processes will be explained. The transport processes depend very strongly on the structure and properties of the compound in the particle. The theoretical calculation of the diffusion coefficient will be explained in detail. The model structure and parts of the model will also be presented. Every part of the model corresponds to the definite physical background. The dependence between OH concentration and chemical reactions will be explained and connected with the knowledge of the structure of the porous particles. Two transport phenomena play an important role for the investigation of the rate constant. These are evaporation of the substance from the particle surface and the diffusion. This is, as we see, affected by the OH concentration. The behavior of the system is shown by the variation of the different variables. The capability of the model to describe the experimental results is represented in some theoretical calculations.
The results were fitted by the commercial program "EASY FIT" (Schittkowski, 2002). The mathematical model was adjusted to the experiments and programmed, the experimental results are added and the unknown parameters were fitted. The fitting parameters are dependent on the experimental conditions.

6.1. General comments

The processes in porous media are more complex and involve more steps than typical homogeneous reactions in the liquid or gas phase. For homogeneous reactions, rates are characterized by the temperature or by the frequency of the molecular collisions, which is proportional to the concentration of each of the reacting species. In the gas phase, concentration is directly proportional to the partial pressure for each species. The chemical reactions in the porous media and physical processes may also affect the overall reaction or process. A heterogeneous process can be broken down into the following steps.

1. Diffusional transport of the OH radicals across the boundary layer between the gas and solid phases.
2. Collision of the OH radicals with the wall or with adsorbed molecules.
3. Reaction between OH radicals and the adsorbed substance.

Any of these steps may be rate determining under the right conditions.

The larger number of steps in the heterogeneous processes increases the number of variables. Only temperature and pressure affect the rate of homogeneous reactions, but heterogeneous processes are affected by mass transfer, both within the gas phase and across the boundary regions between the gas and solid phases and by the effective size of the solid phase participating in the reaction. These two factors introduce the following additional parameters that may affect the overall rate of heterogeneous processes

- Physical properties of the OH radicals, including
  - Diffusion coefficient
  - Lifetime
- Physical and chemical properties of the solid phase, including
  - Geometric surface area
  - Surface roughness
  - Surface area to volume ratio
  - Porosity or void volume
  - Pore diameter
  - Pore length
  - Pore tortuosity
  - Particle size
  - Morphology
  - Bulk density
  - Impurity content.

Many of the parameters describing the properties of the solid phase are not independent. For example, the bulk density is dependent on porosity, pore properties, particle size, and morphology.

Because of the multitude of variables, it is difficult to ensure that experiments isolate the effects of the experimental variables and obtain results that apply to fundamental processes involved in the overall heterogeneous process (Propp, 1998)

6.2. Knudsen diffusion

For the pores with radius smaller than 100 nm the molecules collide more often with the walls of the porous particle than with other molecules. The mean free path of the molecules is longer than the pore radius.

The free mean path, λ, of a molecule can be calculated by the equation

$$\lambda = \frac{RT}{\sqrt{2}\,\pi\, d^2 N_A P} \qquad \textbf{(6.1)}$$

where R is the gas constant, T – temperature, d – molecule diameter, N_A – Avogadro's number, P – pressure.

The molecule then flies through the pore with a series of "random flights". Such a situation is shown in fig. 6.1. The highly reactive molecules (OH radicals) collide with the porous agglomerate or with the adsorbed molecules of the test compound. When OH radicals collide with a test compound, the molecule may react to form product molecules or the OH radicals may travel deeper into the pore. The possible phenomena of these transport processes will be described later. Here will be described only the transport mechanism that becomes important for the considered problem. It is important to keep in mind that the adsorbed molecules can also diffuse. This diffusion must be taken into account by the process description. There are many possibilities for the calculation of the diffusion coefficient. A very famous expression (Jonson and Stewart, 1965) is

$$D_k = \frac{2r}{3}\sqrt{\frac{8k_B T}{\pi m}} = \frac{2r}{3}\bar{\upsilon} \qquad \textbf{(6.2)}$$

Here is D_k the diffusion constant in air, k_B - Boltzmann constant, T – temperature, m – molecule mass, r – molecule radius, $\bar{\upsilon}$ - mean molecular speed.

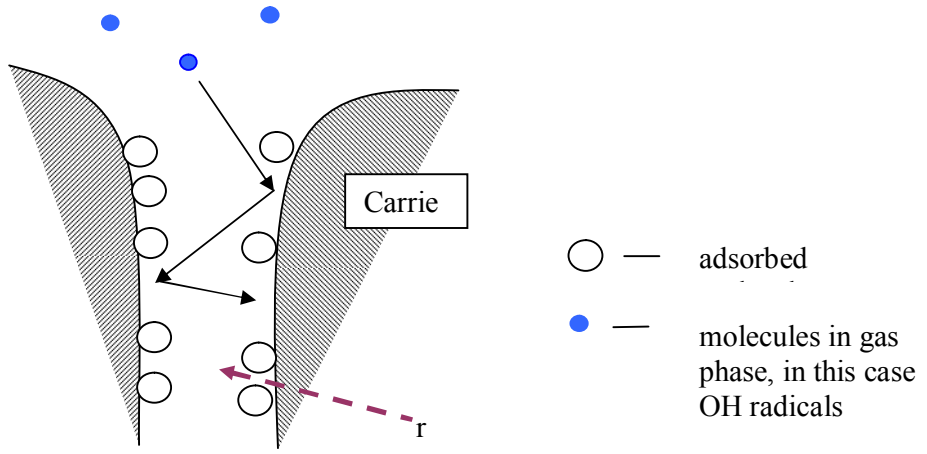

Fig. 6.1 Reaction in a single pore. The surface of the carrier is partly loaded with adsorbed molecules. The molecules in the gas phase can react with the adsorbed molecules or can travel down into the pore. The traveling down requires many collisions with the pore wall.

6.3. Surface diffusion

Another relevant transport process in porous media is surface diffusion. The mechanism of surface flow is usually activated diffusion, and its magnitude depends on the extent of

adsorption, the strength of the adsorption, the surface mobility, the morphology and the particle size of the solid phase. The nature of the surface diffusion can be very complicated if the surface is energetically heterogeneous (Sircar and Rao, 1990).

The activated diffusion deals with the occupation of the energetically favorable sites and the probability to jump to other more favorable places (Georgievskii and Pollak, 1994).

The surface diffusion may become important because of a low vapor pressure of the investigated test substance. That means that the main portion of the compound is adsorbed on the carrier surface and that the concentration of the molecules in the gas phase is low. A concentration gradient may cause the molecules to even it out by diffusion on the surface.

6.4. Calculation of effective diffusion coefficient

There is a small number of semivolatile substances with known diffusion coefficients. The coefficient can be calculated by the equation (Knox and McLaren, 1964):

$$D_{eff} = \frac{D_{air}}{\tau \cdot R_f} . \qquad \textbf{(6.3)}$$

Here D_{air} is the molecular diffusivity, τ the tortuosity of the pores in the agglomerate, and R_f the retardation factor. The diffusivity D_{air} was calculated by the FSG method of Fuller, Schettler and Giddings (Fuller et al., 1966), see also (Fuller et al., 1969; Fuller and Giddings, 1965; Fuller et al., 1966; Lyman, 1990). The absolute average error of the method is 7.6 %.

The pores are not cylindrical. They are tortuous. The tortuous pores hinder the mass transport, lead to slower diffusion and to a lower diffusion coefficient.

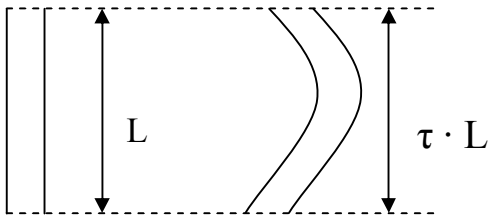

Fig. 6.2 Illustration of the concept for the ideal and tortuous pore.

A comparison between an ideal and a tortuous pore is shown in fig. 6.2. The tortuosity factor $\boldsymbol{\tau}$ takes into consideration that the real pores are tortuous. The tortuosity is assumed to be 3.

The retardation factor R_f can be calculated by

$$R_f = 1 + \frac{\rho_{bulk} \cdot K^{ads}}{\varepsilon} \quad \textbf{(6.4)}$$

The carrier density is ρ_{bulk} , ε is the porosity of the agglomerates, K^{ads} is the solid/air partition constant for the compound. The calculation of K^{ads} is described in (Goss and Schwarzenbach, 2002). The program "Absolv" was used for the prediction of H-bonding acidity parameter and H-bonding basicity parameters required for the calculation of the solid/air partion constant (Algorithms, 2005).

The structure of the agglomerates can affect the exchange of organic compounds and radical species between the gas and particulate phases in the atmosphere. Thus we need to characterise the structure with respect to particle size distribution, pore size distribution, porosity and other parameters. The structure parameters are important for realizing the model definition (Wheeler, 1950).

There are various methods for investigating the structure of porous materials. The most often used are the BET method and mercury porosimetry. The powder or material amount required for the measurements are ca. 1 g. High mercury pressure is required during a measurement by mercury porosimetry. The pressure may destroy the Aerosil agglomerates, insofar the mechanical properties of the agglomerates are unknown. The sample preparation for both methods requires techniques that might destroy the agglomerates.

Ion beam etching and field emission scanning electron microscopy (FESEM) were used as appropriate method to investigate the inner structure of the particles. The samples were stabilized by an epoxy resin (Höhn and Obenaus, 2004). This method yields access to the structure of a single particle by a non-destructive observation and has been used for characterising ceramic powders and materials.

Filter samples loaded with agglomerates were investigated in the Fraunhofer-IKTS at Dresden by ion beam etching. The aerosol loading on the filter was 231 µg. The images were evaluated in the present thesis, using the program "Lince" (dos Santos e Lucato, 2000). The images were evaluated for porosity, particle size and pore size. This evaluation leads to the formulation of the mathematical model.

6.5. Defining the mathematical model

After structure investigation of the agglomerates a mathematical model was defined to calculate the observed substance loss by the photochemical reaction. The model was employed by Balmer et al. (2000) for the description of photolysis of chemicals in soil and is adjusted to the spherical agglomerates of the present study.

At the beginning of the experiment the OH radical attacks the aerosol agglomerates. OH radicals may be adsorbed on the carrier surface for a very short time and then re-evaporate from the surface. But there is no evidence for this phenomenon. On other hand, the surface of the carrier is partially loaded with adsorbed molecules, and the molecules can also diffuse into the direction of lower concentration. The OH radicals diffuse into the pore, either they collide with an adsorbed substance molecule and react, or they travel down into the pore and react further with other molecules. Concentration gradients form in the agglomerate, and this leads to a diffusion of the substance from the agglomerate core to the periphery. So the OH radicals can penetrate only a few nm into the agglomerate. The first order rate constant alters with the changing OH concentration. The process is shown schematically in fig.6.3 The penetration depth, R_0, can not be determined experimentally but will be calculated by the fitting procedure.

The substance molecules either react with the OH molecules or they leave the surface and evaporate into the gas phase. When the OH concentration is high, all substance molecules react. In this case their evaporation is negligibly small.

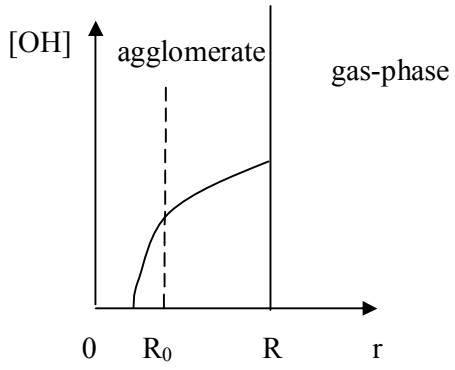

Fig. 6.3 Scheme of the theoretical concept describing degradation of the test compound adsorbed on the carrier.

On the other hand, the agglomerates were dissolved in solvent and analyzed. So only the total amount of the compound was measured and not the concentration gradient in the agglomerate. Therefore the reaction zone can not be experimentally measured.

The concept for the processes is shown schematically in fig. 6.4.

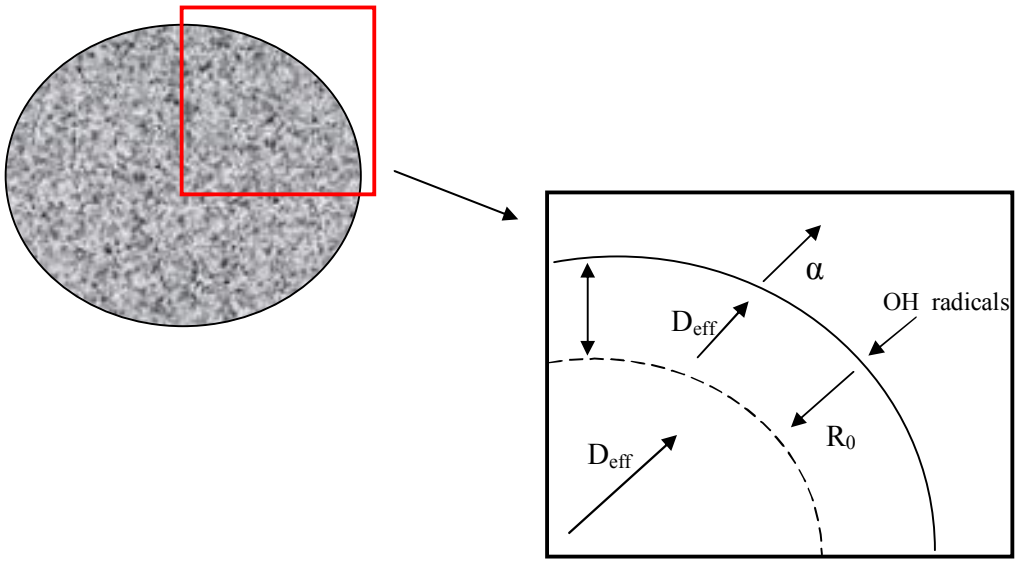

Fig. 6.4 Diffusion, chemical reaction and evaporation are the three loss mechanisms in the porous agglomerate. The OH radicals penetrate into the particle and react with the test substance.

The OH radicals penetrate only a few nm into the agglomerate, and the bigger agglomerates contain more substance than the smaller agglomerates. When the sample is analyzed, the bigger agglomerates contribute larger amounts than the smaller ones. It is therefore practical for the model to take only the big agglomerates into consideration. For the agglomerates a diameter of 1 μm was taken as representative.

The diffusion model coupled with chemical reaction was used to describe the substance loss during the experiment.

$$\frac{\partial C}{\partial t} = D_{eff}\left(\frac{\partial^2 C}{\partial r^2} + \frac{2}{r}\cdot\frac{\partial C}{\partial r}\right) - \tau^{-1}\cdot C\cdot exp(-r/(R_0/ln\,2)) \qquad \textbf{(6.5)}$$

where C is the substance concentration, t – time, r – radial distance, D_{eff} – effective diffusion coefficient, τ^{-1} – the lifetime, R_0 – the OH profile in the agglomerate.

The following boundary conditions could be defined

$$\left.\frac{\partial C}{\partial r}\right|_{r=0} = 0 \qquad \textbf{(6.6)}$$

in the center of the particle. This is a symmetry boundary condition. And

$$\left.\frac{\partial C}{\partial r}\right|_{r=R} = h\cdot C \qquad \textbf{(6.7)}$$

at the surface of the particle. This boundary condition defines the evaporation constant, h, of the compound from the agglomerate surface.

Equation (6.7) is a Neumann type boundary condition. The boundary condition is deduced from the general form in (Crank, 1975).

$$-D_{eff}\frac{\partial C}{\partial n} = \alpha (C_0 - C_s) \qquad \textbf{(6.8)}$$

The equation usually means that the material flux across unit area of the surface is proportional to the difference between the surface concentration C_s and the concentration C_0 of the outside medium, i.e. is given by $\alpha\ (C_s - C_0)$. But the rate of substance loss from the unit area of the surface is $-D_{eff}\,\partial C / \partial n$ in the direction of the normal n, measured away from the surface. If we assume that the concentration of the outside medium C_0 is equal to zero and

$h = \alpha / D_{eff}$, we obtain equation (6.7).

If the surface is perpendicular to the r – direction (these are polar coordinates), then the gradient $\partial C / \partial n$ is equal to $\partial C / \partial r$, if n is along the direction of increasing x.

The evaporation can be neglected if the OH concentration is high. All of the test substance reacts with the OH radicals and no molecules are going lost. Then at the agglomerate edge the Neumann boundary condition is defined in the form

$$\left.\frac{\partial C}{\partial r}\right|_{r=R} = 0 \qquad \textbf{(6.9)}$$

The advantage of the boundary condition is the reduction of the relevant variables (here: neglecting the evaporation). That allows the fitting of the effective diffusion coefficient and a comparison with the theoretical diffusion coefficient.

Below the influence of the different variables will be described and thus the adequateness of the mathematical model. Here the influence of the OH-radical concentration is indirectly shown. Low concentrations of OH correspond to long lifetime and via versa, according to the equation $\tau^{-1} = k_{OH}\,[OH]$.

The influence of the lifetime is shown in fig. 6.5. The lifetime is the most important parameter to be fitted. The mathematical model must be sensitive for its alteration.

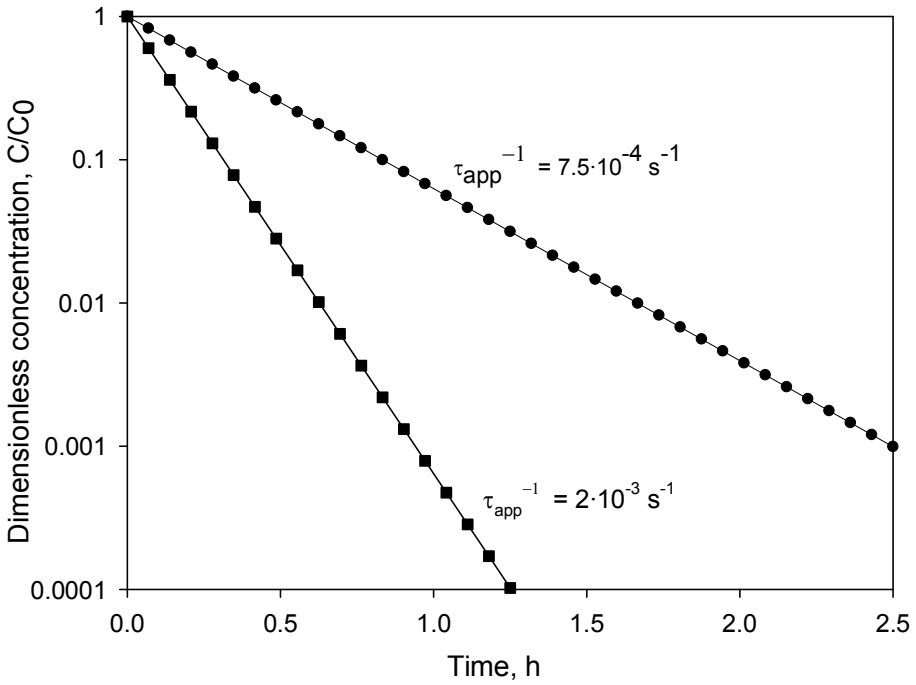

Fig. 6.5 The influence of the lifetime conditions: agglomerate diameter D_p = 1 μm, diffusivity $D_{eff} = 10^{-11}$ cm^2s^{-1}, OH profile in the agglomerate R_0 = 100 nm, evaporation constant h = 10^{-8} cm^{-1}, reaction rate $\tau^{-1} = 10^{-3}$ s^{-1} (■), reaction rate $\tau^{-1} = 10^{-6}$ s^{-1} (●)

Two simulations were made with lifetime corresponding to $\tau^{-1} = 10^{-3}$ s^{-1} and $\tau^{-1} = 10^{-6}$ s^{-1}. The conditions correspond to an experiment with high concentration of OH radicals in fig. 6.5 (say, [OH] = 10^8 cm^{-3} at $k_{OH} = 10^{-11}$ cm^3s^{-1}) and to an experiment with low OH concentration (say, [OH] = 10^5 cm^{-3} at the same k_{OH}). The apparent reaction rates are shown in the figure at the calculated curves. Both values differ from the real value of the reaction rate. For a fast reaction ($\tau^{-1} = 10^{-3}$ s^{-1}) the apparent reaction rate is two times lower than the real value. In the second case the apparent reaction rate is 750 times higher than the input value ($\tau^{-1} = 10^{-6}$ s^{-1}).

The influence of the penetration depth is shown in fig. 6.6. The reaction zone is reduced 10 times, from 100 nm to 1 nm. In this case the OH radicals penetrate into a small depth and the substance loss is also smaller. This case deals with denser agglomerates caused by the suspension density, compound to carrier ratio or other experimental conditions during the aerosol spaying. Then the OH radicals can not penetrate deeply into the agglomerate. The input reaction rate was not changed but the apparent reaction rates differ by factors of 2 and 5, respectively.

The model calculates well the faster and slower diffusion. The effect can be observed when the diffusion coefficient is changed from 10^{-11} cm^2/s to 10^{-14} cm^2/s (fig.6.7). The substance is transported more slowly to the reaction zone; on other hand, the OH radicals penetrate

only 100 nm into the agglomerate. It was shown that the influence is very significant when the coefficient was modified within 4 decades.

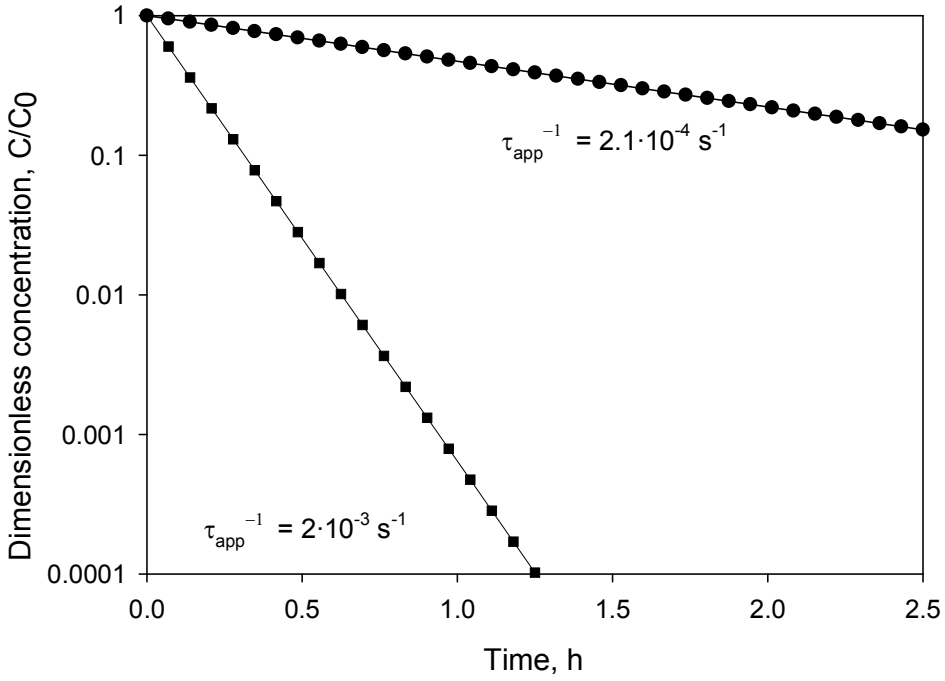

Fig. 6.6 The influence of the penetration depth. Conditions: agglomerate diameter D_p = 1 µm, diffusivity $D_{eff} = 10^{-11}$ cm^2s^{-1}, reaction rate $\tau^{-1} = 10^{-3}$ s^{-1}, evaporation constant h = 10^{-8} cm^{-1}, OH profile in the agglomerate R_0 = 1 nm (●), OH profile in the agglomerate R_0 = 100 nm (■)

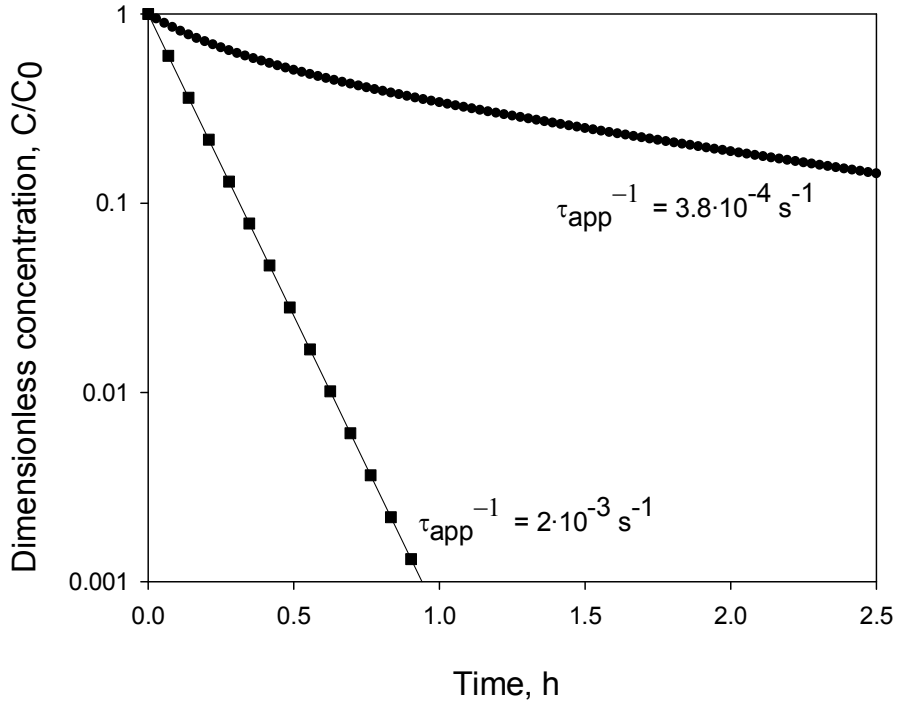

Fig. 6.7 The influence of effective diffusion coefficient. Conditions: agglomerate diameter D_p = 1 µm, OH profile in the agglomerate R_0 = 100 nm, reaction rate $\tau^{-1} = 10^{-3}$ s^{-1}, evaporation constant h = 10^{-8} cm^{-1}, diffusivity $D_{eff} = 10^{-14}$ cm^2s^{-1} (●), diffusivity $D_{eff} = 10^{-11}$ cm^2s^{-1} (■)

The concentration decay at the start of the experiment can be observed in the real experiments. The calculation shows that this decay is due to diffusion.

The decrease of the evaporation delays the substance loss from the agglomerates (fig. 6.8). The effect is more distinct if the OH concentration is low and consequently the lifetime is longer.

Calculations with a variable evaporation coefficient were made to show the behavior when the compound lifetime is short. The situation corresponds to high OH concentration. The influence decreases with the decrease of the evaporation coefficient. The calculation corroborates the assumption that the evaporation is negligible in comparison to the other loss processes. This calculation also corroborates the boundary condition defined by eq. 3.6.

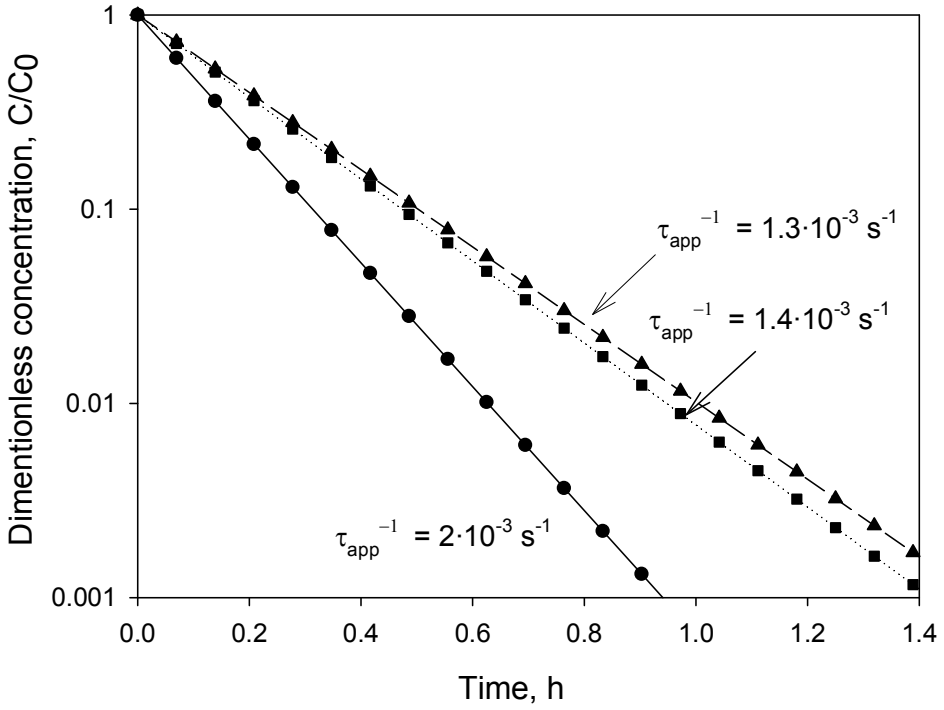

Fig. 6.8 Conditions: agglomerate diameter D_p = 1 µm, diffusivity $D_{eff} = 10^{-11}$ cm^{2}s^{-1}, OH profile in the agglomerate R_0 = 100 nm, inverse lifetime $\tau^{-1} = 10^{-3}$ s^{-1}, evaporation rate $h_1 = 10^{-8}$ cm^{-1} (●), $H_2 = 10^{-9}$ cm^{-1} (■), $h_3 = 10^{-11}$ cm^{-1} (▲)

The influence of evaporation is much bigger for slow reaction. The same values of the evaporation coefficient are used for the calculation of the concentration profile shown in fig. 6.9. The temperature in the chamber plays an important role for reducing the evaporated portion of the molecules.

Comparing the degradation curves when the evaporation rate is high ($h_1 = 10^{-8}$ cm^{-1}) in fig. 6.8 and 6.9, similarity of the curves could be defined. This similarity can increase the uncertainties when the parameters from the experiment are fitted.

All of the variables depend on the morphology of the agglomerate. The spray production, the conditions of spray drying and solid concentration in the suspension can influence the agglomerate structure and/or their size. Finally the behavior of the system is less or more different.

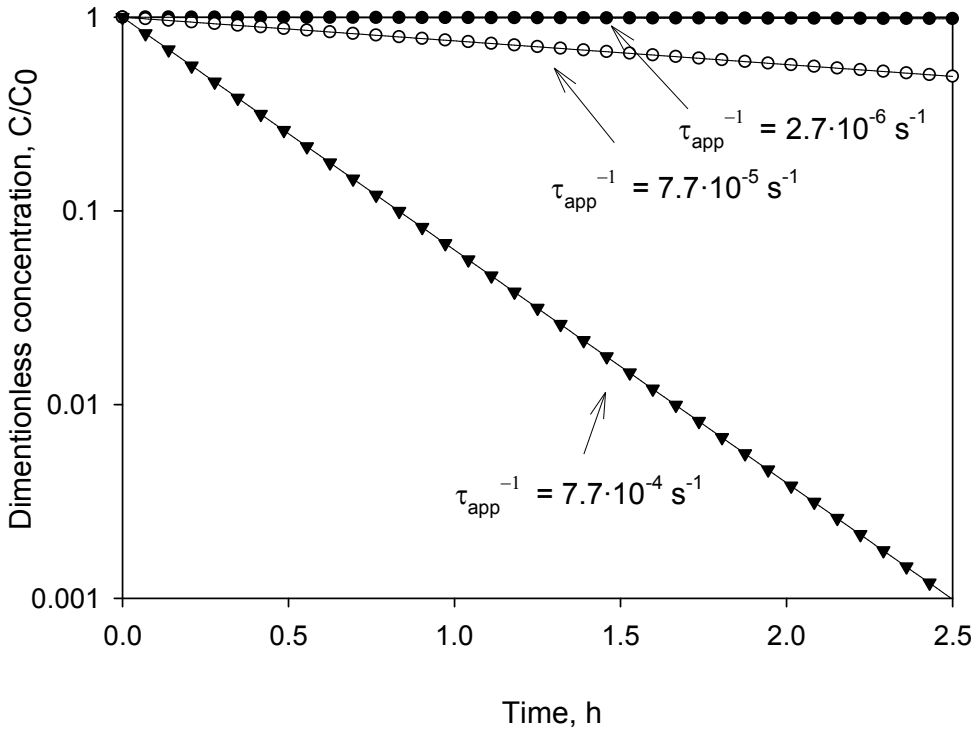

Fig. 6.9 Conditions: agglomerate diameter D_p = 1 µm, diffusivity $D_{eff} = 10^{-11}$ cm^{2}s^{-1}, OH profile in the agglomerate R_0 = 100 nm, inverse lifetime $\tau^{-1} = 10^{-6}$ s^{-1}, evaporation rate $h_1 = 10^{-8}$ cm^{-1} (●), $h_2 = 10^{-9}$ cm^{-1} (○), $h_3 = 10^{-11}$ cm^{-1} (▲)

6.6. Fitting procedure of the parameter

In the previous chapter a theoretical calculation was shown. The parameter values were not real (like the experiment), but realistic (in a typical range for experiments).

After the experimental work the proper method for the parameter estimation procedure must be chosen. A commercial program "Easy Fit" was used for the parameter estimation. The program uses a quasi – Newton method for the evaluation procedure. The calculation algorithm is described in (Schittkowski, 2002). The method of lines was used for the solution of the partial differential equation. The background idea of the method is the transformation of the partial differential equation into a system of ordinary differential equations by discretizing the model function with respect to the spatial variable *x*. More details are given in (Schiesser, 1991).

Every fitting calculation begins with the input of the starting value. The starting value must be near to the expected parameter value. Then the experimental results are imported into the program. After the calculation the obtained function parameters can be compared with the experimental results. An improved possibility to estimate the goodness of the calculation is the residual graph. The residuals are the differences between the experiment results and the mathematical model. It may occur that more than one combination of parameters value approximates well the experimental results. Then a reasonable solution must be chosen.

7. Calculation of the apparent rate constant from the degradation curve of the test compound

The test substance concentration decreases exponentially with time, assuming a rate constant of 1. order:

$$C = C_0 \cdot exp(- k \cdot t) \quad \textbf{(7.1)}$$

Here k refers to a first-order rate constant, that can be calculated for every experiment, and k_{OH} is the bimolecular second-order OH-rate constant, according to:

$$k = k_{OH} \cdot [OH]. \quad \textbf{(7.2)}$$

k_{OH} is independent of the OH concentration. The lifetime of the substance can be calculated for any OH concentration.

$$\tau = \frac{1}{k} \quad \textbf{(7.3)}$$

The reciprocal value τ is useful for the calculation of the half-life.

$$t_{1/2} = ln(2) \cdot \tau \quad \textbf{(7.4)}$$

The lifetime is directly proportional to the half-life.

The rate constant is an important parameter for the evaluation of the distribution of contaminants in the environment.

The degradation experiments can be evaluated by eq. (7.1) and eq. (7.2). If the degradation curves from chapter 6 would be evaluated by eq. (7.1) and (7.2), then different rate constants would result for every case although the reaction rate is the same. Of course the elimination of diffusivity and the elimination or the minimization of evaporation allows the use of eq. (7.1) and (7.2). This would require the usage of new materials or other devices to produce agglomerates.

The influence of the OH radicals can be evaluated in a naïve manner. If the reaction rate would be constant for different OH levels, the reaction rate decreased. A comparison and specific values will be shown in the results section.

8. Experimental results

In this chapter the experimental results will be presented. The temperature gradient of the air in the smog chamber was measured in order to check the mixing of the chamber content. The air and aerosol mixing could be evaluated from the measurements. A rapid mixing in the chamber ensures the production of OH radicals in the whole chamber volume and their reaction with aerosol agglomerates.

The concentration of the test substance was measured after the coating procedure. There were no losses of test substance during the coating. Some Aldrin was detected on the foil on the bottom of the chamber. The foil was used for 10 experiments each. The measurements of the extracted Aldrin before the start of the experiment showed a contamination of the powder with Dieldrin. The measurements did not show ageing of the coated Aerosil. The structure of the agglomerates was investigated. Ion beam etching was used for the preparation of samples, and the images of the structures were taken by FESEM. The agglomerates and pore size distribution was evaluated from the images using the program “Lince”.

The substance evaporation from the agglomerate surface was reduced by a decrease of the temperature. The experiments did not show any degradation of Aldrin by photolysis. The product formation was high when the OH concentration was high. Two products were detected: Dieldrin and Photoaldrin.

8.1. Measurement of the temperature gradient in the smog chamber

The experiments were performed at about 2°C and -10°C. The temperature gradient was measured at these two temperatures. The measuring places are shown in fig. 8.1.

The temperature in the room was 2°C, and the measurements in the central axis of the cylindrical glass chamber are shown in fig. 8.2 and fig. 8.3.

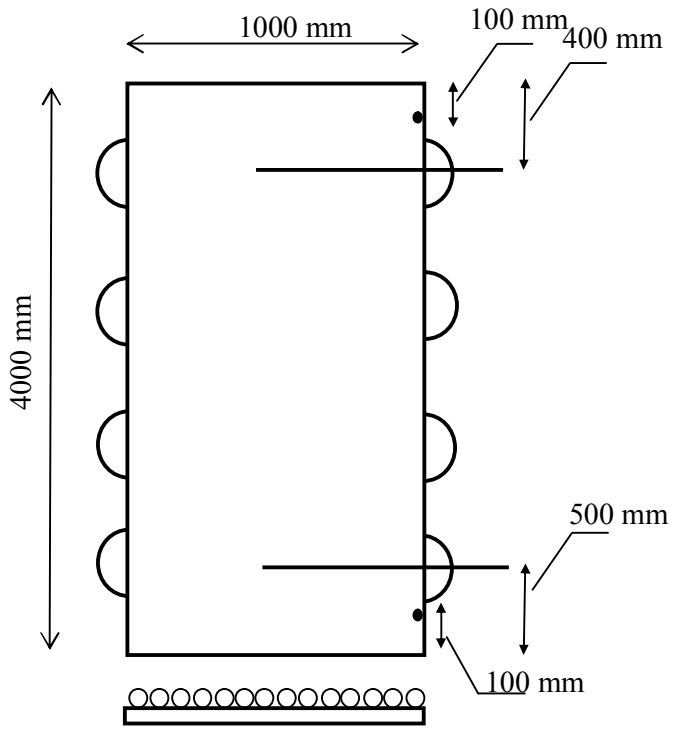

Fig. 8.1 The temperature was measured on the wall and in the middle of the chamber and also on the bottom and on the top. The distance between measurement place on the wall and the chaber top/bottom was 100 mm. The distance between the measurement place in the chamber middle and the top/bottom was 400 respectively 500 mm.

A double exponential function was extrapolated to give an initial value of the irradiated chamber of 3.42°C and a final value of 3.1 °C in the dark chamber. The corresponding equation is $T = 3.135 + 0.042 \cdot \exp(-0.0135 \cdot t) + 0.3 \cdot \exp(-0.004 \cdot t)$ (fig. 8.2).

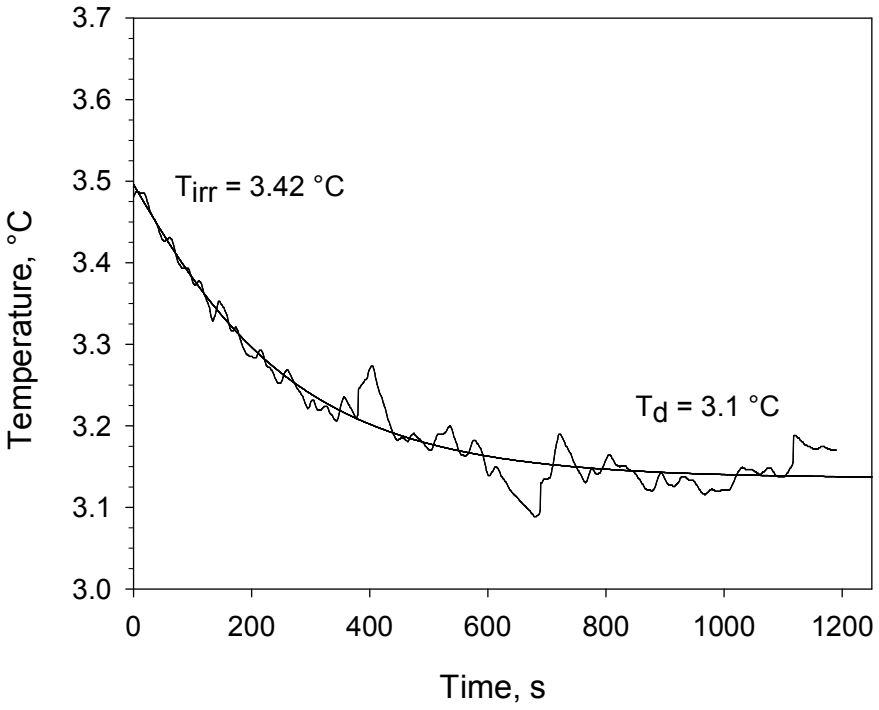

Fig. 8.2 Extrapolation of the temperature curve on the top and in the middle of the chamber. The first stage is the cooling of the thermistor, and in the second stage the cooling of the air was measured. The temperature in the cooled room is 2°C.

The cooling curve at the bottom was fitted to a double exponential function, considering the time constant of the sensor, determined in fig. 8.3 and delivered a temperature at the bottom middle (close to the axis of the glass cylinder) of 4.4°C in the irradiated chamber (see fig. 8.3) and a final temperature of 3.4 °C in the dark chamber. The related equation is

$T = 3.4 + 0.4 \cdot \exp(-0.0078 \cdot t) + 1.08 \cdot \exp(-0.00051 \cdot t)$.

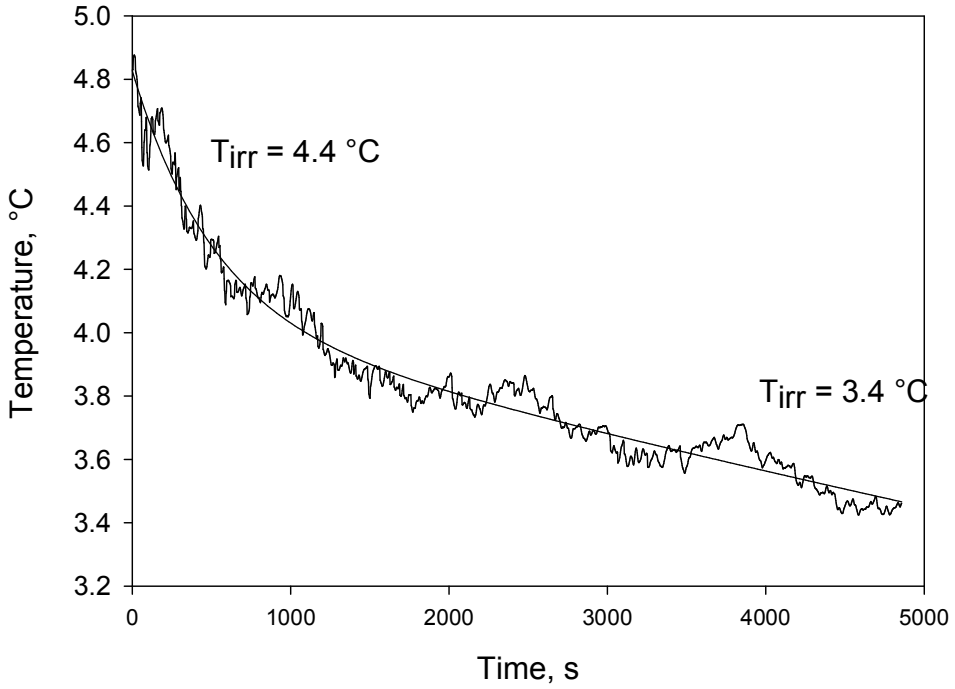

Fig. 8.3 The extrapolated temperature at the bottom and in the middle of the chamber. The temperature in the cooled room is 2°C.

The temperature in the chamber without light source was also determined from the curves. The temperature was measured before turning the solar simulator on. The temperature gradient can be read off from both of the graphics.

The temperature on the wall was measured in the same manner. Fig. 8.4 shows the temperature curve. The lamps were turned on, and the air and the glass walls were warmed to a constant temperature. Then the lamps were turned off, and the sensor and the wall were cooled. The cooling curve was extrapolated to the beginning of the cooling. Considering the second part of the curve, the temperature on the wall was 7.1°C in the irradiated chamber (fig.8.4). The corresponding equation is $T = 2.8 + 0.63 \cdot exp(-0.0078 \cdot t) + 4.33 \cdot exp(-0.00026 \cdot t)$.

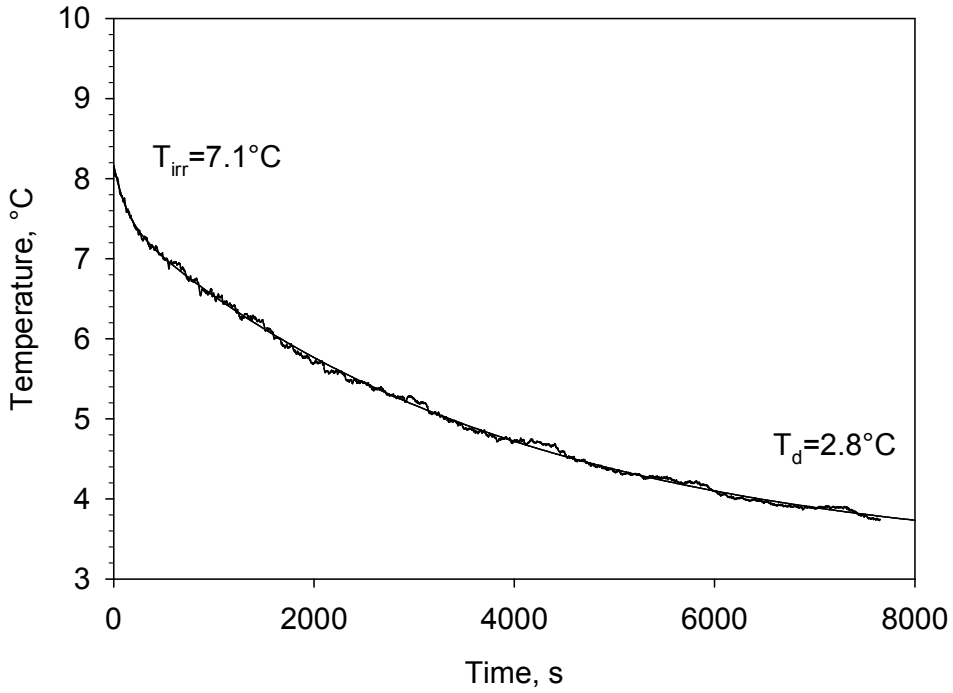

Fig. 8.4 The temperature on the wall was extrapolated to 7.1°C.

The temperature on the wall in the dark chamber is shown in fig. 8.5. The difference between both temperatures is small 2.1°C – on the bottom and 2.3°C – on the top. The fluctuations are caused by the periodical work of the fans from air-conditioning system. The room temperature varies in a range of approx. 2°C degrees. The temperature in the chamber varies by approx. 0.2°C.

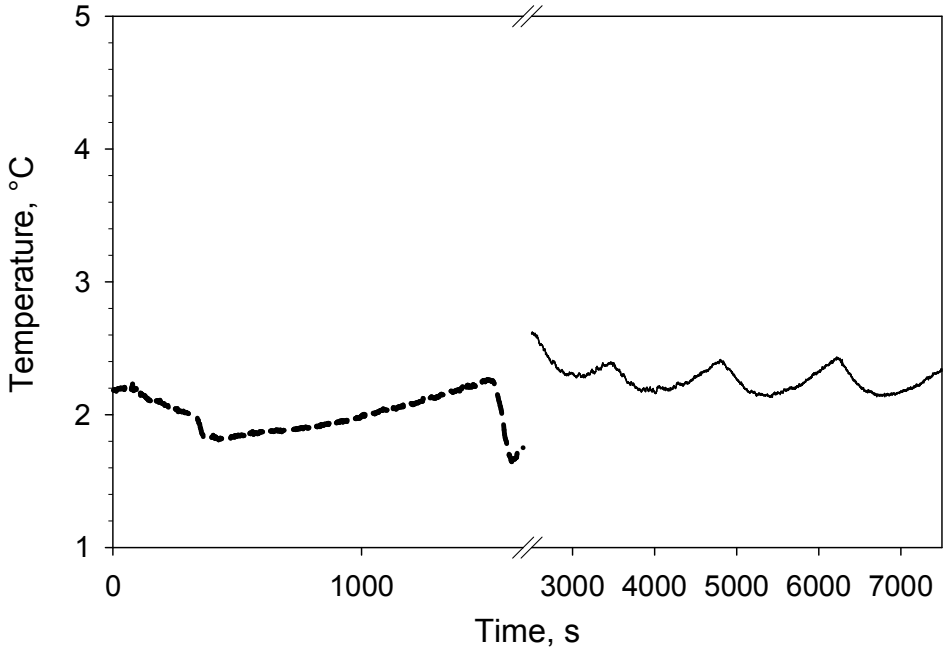

Fig. 8.5 The wall temperature was measured on the bottom (dashed line) and on the top (solid line).

The results are summarized in table 8.1.

Table 8.1 Measured temperatures and temperature differences in the chamber with and without light source at 2°C room temperature.

	Temperature bottom/middle, °C	Temperature bottom/wall, °C	Δt, °C	Temperature top/middle, °C	Temperature top/wall, °C	Δt, °C
with irradiation	4.4	7.1	2.7	3.4	2.3	1.1
without irradiation	3.4	2.1	1.3	3.1	2.3	0.8

The temperature gradient decreases with increasing height. The mixing rate is faster in the lower part of the chamber and decreases in the upper part. The temperature gradient and respectively the mixing in the chamber are lower in absence of the light source.

The temperature gradient was measured at the temperature -10°C in the room. The evaluated temperature at the bottom was -6.8ºC (fig.8.6) according to the equation

$T = -8.6 + 0.46 \cdot exp(-0.0078 \cdot t) + 1.24 \cdot exp(-0.00033 \cdot t)$.

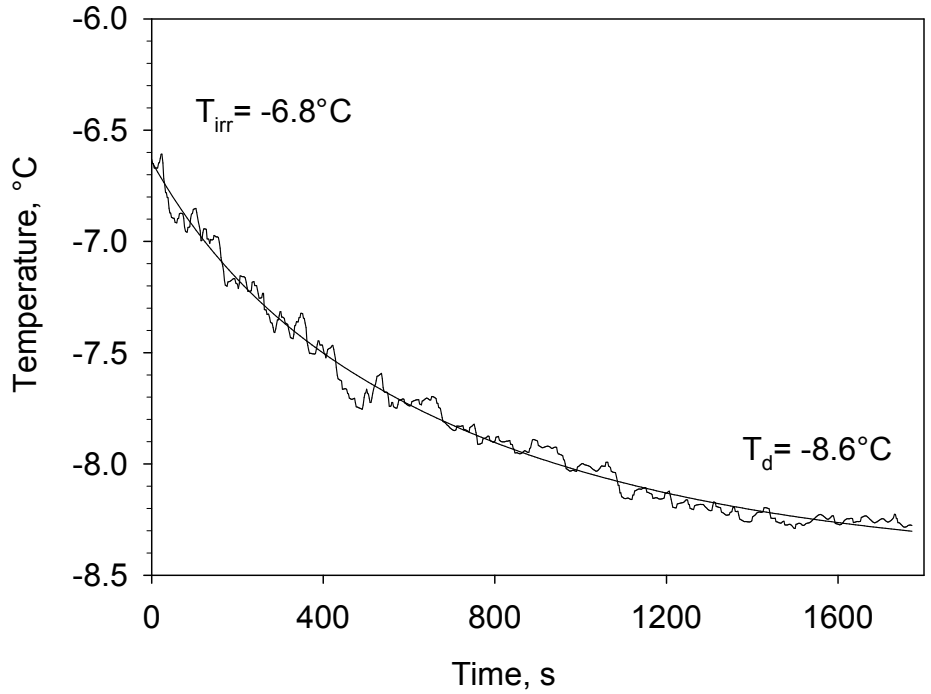

Fig. 8.6 The temperature of the bottom of the chamber is circa -7.0°C. The temperature in the cooled room is -10°C.

The evaluated temperature at the top was -7.2ºC (fig. 8.7) according to the equation

$T = -8.4 + 0.17 \cdot exp(-0.0078 \cdot t) + 1.65 \cdot exp(-0.0014 \cdot t)$.

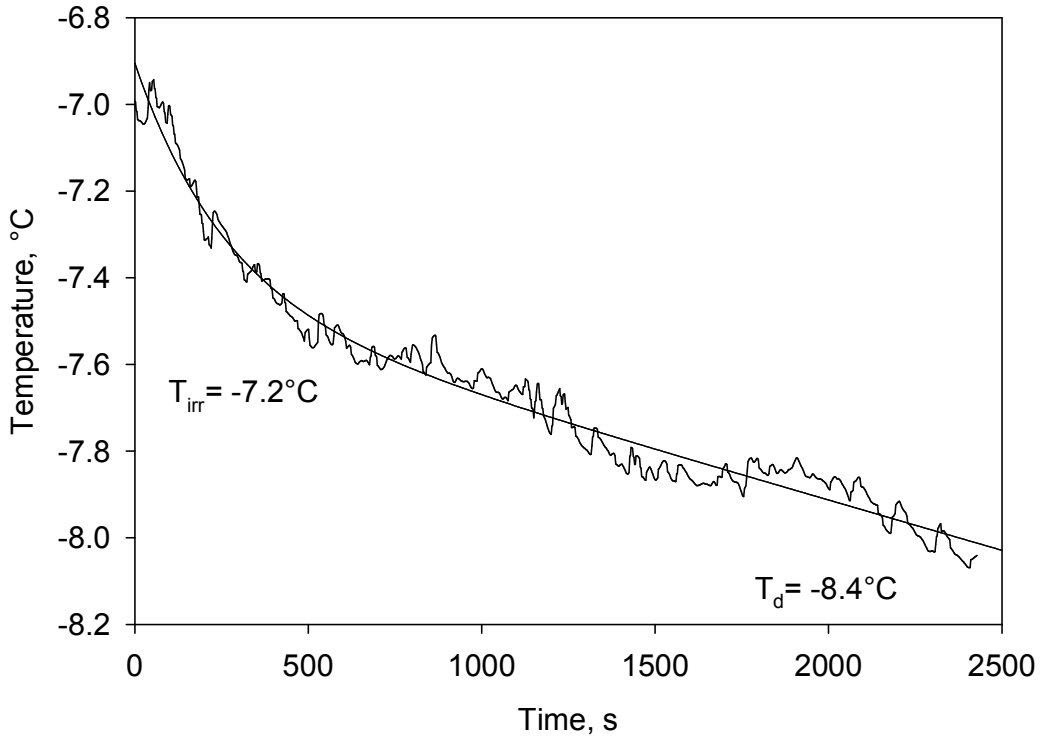

Fig. 8.7 The temperature of the top of the chamber is circa -7.2°C. The temperature in the cooled room is -10°C.

The temperature in the chamber and on the wall could be calculated using the temperature difference measured at 2°C. The results are summarized in table 8.2.

Table 8.2 Measured temperatures and temperature differences in the chamber with and without light source at -10°C room temperature.

	Temperature bottom/middle, °C	Temperature bottom/wall, °C	Δt, °C	Temperature top/middle, °C	Temperature top/wall, °C	Δt, °C
with irradiation	-6.8	-4.1	2.7	-7.2	-8.3	1.1
without irradiation	-8.6	-9.9	1.3	-8.4	-9.2	0.8

The temperature gradient was higher when the chamber was irradiated than the gradient in the dark chamber.

The temperature gradient between smog chamber wall and center was higher when the smog chamber was irradiated. The mixing intensity in the low part is high and slows to the

chamber top. Calculation of the temperature and velocity distribution in the chamber could be helpful for the evaluation of the air mixing.

8.2. Analysis of the lost substance during the coating procedure

The coating procedure was explained in chapter 3.3.3. The substance amount adhering to the Aerosil particles was measured after the coating procedure. The expected concentration was 15 µg/L. A fixed amount of coated powder was taken for the measurement, weighed by the electronic balance and dissolved in n-hexane, containing Mirex as inert standard. The solution was diluted to appropriate concentrations for the measurements by GC-ECD. A calibration curve was determined (see appendix), and the amount of the test substance was calculated from the observed peak area. The amount of compound was compared before and after the coating procedure.

Table 8.3: The calculated Aldrin loss amount by carrier – Aerosil

Aldrin peak area, mV·s	Mirex peak area, mV·s	Norm. Aldrin peak area, mV·s	[Aldrin], µg/L	Recovered amount, %
1278.8	1385	1278.8	17.8 ± 0.5	118
1422	1640.4	1194.5	16.6 ± 0.5	110

The Aldrin concentration for the second measurement is normalized by the Mirex peak area from the first measurement. The difference between first and second measurement without normalizing is 10 %. If the peak area is normalized with the standard peak area of Mirex, then the difference is about 5 %. The concentration of Aldrin in the solution is calculated with standard curve. The standard deviation of the measurements was 2.8 %.

The expected concentration in the solution is 15 µg/L. The recovered amount is 118% and 110%. The values are thus larger than expected, though within the accuracy of the sample preparation and coating process: During the coating process of Aerosil by Aldrin no loss was detected.

The same procedure was performed with Aldrin on microballoons (SiO_2 GeFa Verbund-werkstoffe). There are three measurements. The carrier was solved only in n-hexane without Mirex as internal standard. The surface of the microballoons is about 0.08 m^2/g (estimated value), compared to the surface of Aerosil – 380 m^2/g which is much larger than the mircoballoons surface. The Aldrin coating is more than a monomolecular layer on the carrier. The number of the layers could be calculated according to the molecule volume and the used

substance amount (1 % Aldrin, typical amount is 0.01 g). This amount could form about 100 layers on the glass balloons. The molecules adhere weaker to the material.

Table 8.4: The calculated Aldrin loss amount by carrier – glass microballoons

Aldrin peak area, mV·s	[Aldrin], µg/L	Recovered amount, %
844.8	11.6 ± 0.4	44
1845	25.6 ± 0.8	97.3
1520	21 ± 0.8	79.7

The coating of the material is more inhomogeneous than the coating on Aerosil and on average about 74 % of the compound adheres to the carrier.

8.3. Analysing the FEP foil at the bottom of the chamber

The main loss process of aerosol during an experiment is sedimentation of the coarse agglomerates on the chamber bottom, further to the sampling. The foil was changed every 10 experiments (after about 5 months), and the vertical chamber walls were flushed with an 0.1 M aqueous solution of NaOH. NaOH was used to neutralize the HONO on the wall during the production of OH radicals from methyl nitrite. Then the bottom foil was washed with n-hexane (100 mL) and analyzed by GC-ECD. Aldrin (the peak at 8.1 min in fig. 8.8) was found in the extract. The Aldrin concentration was 29 µg/L. Dieldrin and Photoaldrin were not detected in the solution.

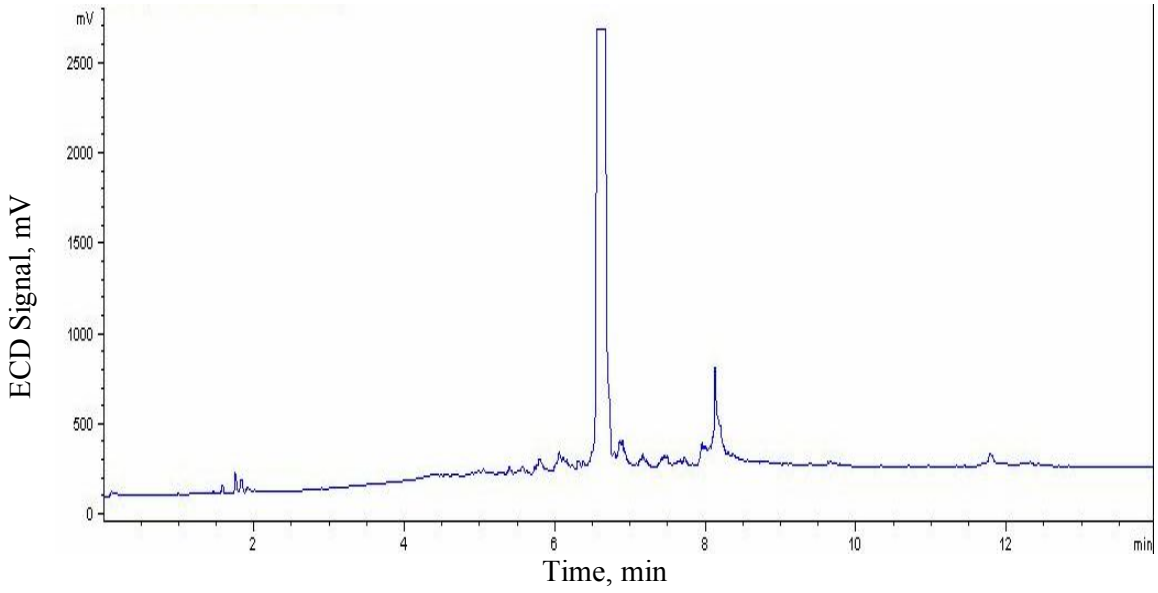

Fig. 8.8 Chromatogram of the extract from the bottom foil of the chamber. There is a contamination peak at 6.5 min, and the aldrin peak is at 8.1 min.

As mentioned above, the coating of Aldrin on Aerosil was carried out without significant losses. The amount of Aldrin found deposited on the foil was 3 μg. This amount corresponds to about 300 μg of Aerosil that are deposited on the foil from the 10 experiments. The sedimented amount is half of the sprayed Aerosil amount into the chamber. The other peaks may be contaminants, penetrating through the foil and adsorbed on the carrier (a plasticizer may be present from the PVC cage of the other chamber). Although the Aldrin molecules were possibly trapped in the structure of the agglomerates, they can diffuse out of them slowly, the evaporation is expected to increase when the light source is turned on and the foil warms up. The evaporated Aldrin molecules might affect the experiment, and such an influence can be prevented when the chamber is clean. Therefore the chamber was washed every 10 experiments.

8.4. Ageing of the coated powder

The powder was stored in a volumetric flask. It was wrapped in aluminum foil to prevent light penetration. The ratio between the start peak areas of Aldrin and Dieldrin was used to calculate the ageing. The peak area before the experiment start was used to calculate the ratio $[Dieldrin]_0 / [Aldrin]_0$. Dieldrin was chosen as stable product from the degradation of Aldrin.

The ratio of 18 experiments was calculated. There were blank experiments, with light source and without OH precursor and also experiments with light source and OH precursor. The experiments are shown in the sequence of their realization (the table with the experiments is shown below). The ratio is found to be independent of the experiment number. A small amount of Dieldrin is present in the Aldrin as byproduct of Aldrin solution. The Dieldrin concentration was about 1% of the Aldrin concentration. There is no ageing of the coated Aerosil during the storage.

8.5. Structure evaluation of the agglomerates

The structure of the agglomerates might be investigated by Hg porosimetry or BET analysis. Both methods require big amounts of powder. On other hand, a typical sample weighs about 50 μg. The agglomerates deposited on the Teflon filters can complexly reshuffle in other vessels without destruction of the agglomerates structure. These methods are not useful in this case.

The ion beam etching is a new method used for studies of the structure of porous media. The method is much more expensive than the other classical methods.

A sample from a dark chamber run has been used for the present work. The deposit has been analyzed by S. Höhn at the Fraunhofer-Institute for Ceramic Materials: stabilized by epoxy resin, cut and treated by ion-beam etching (Höhn and Obenaus, 2004). The field emission scanning electron micrographs (FESEM) were evaluated at Bayreuth, using the program "Lince" (dos Santos e Lucato, 2000). It employs the line-intercept method developed for grain size analysis. The image is crossed with lines or circles, and the interceptions of the lines with the interfaces are marked by the user. The program calculates, as porosity, the fraction of the total line length traversing pores. Absolute length measurements are also supported by the program. It performs the scaling (pixel to nm), lists the lengths of individual line intervals and calculates a mean and variance.

Several FESEM images like fig. 8.9 have been taken. Images spanning almost the whole thickness of the deposit on the filter are appropriate for determining the agglomerate diameter.

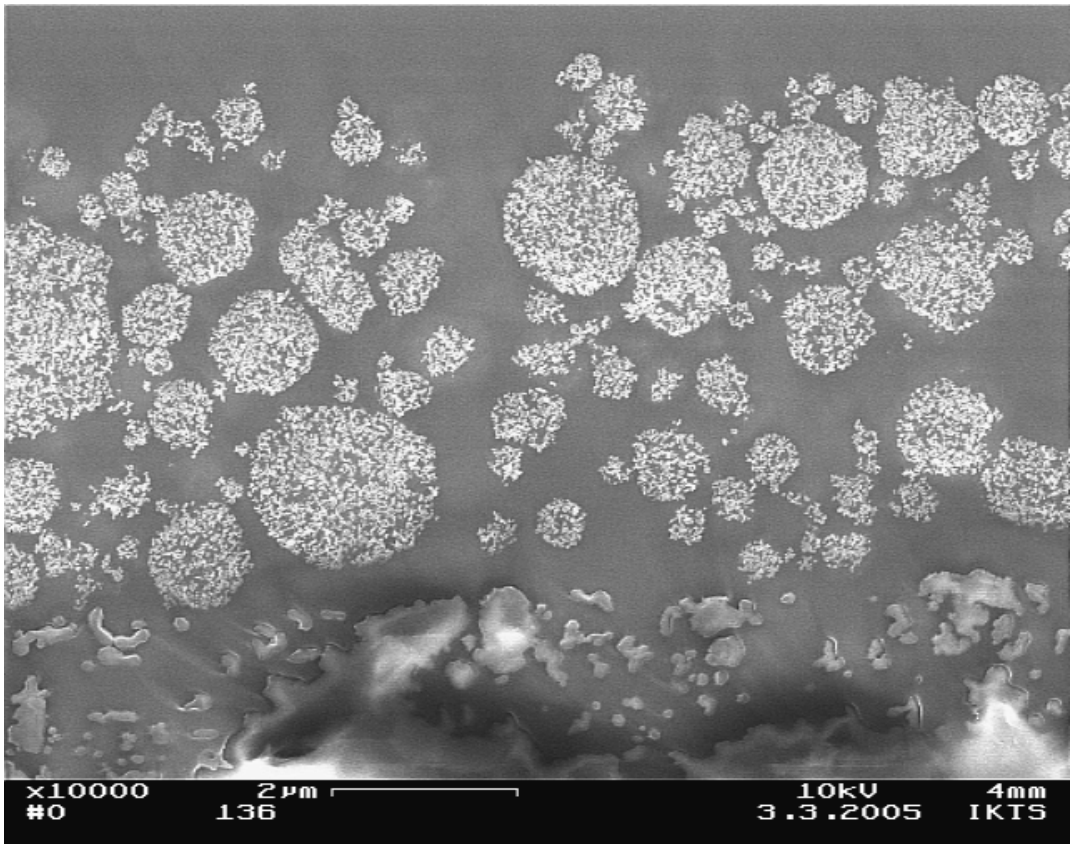

Fig. 8.9 Section though the filter sample. The agglomerates are visible lying on the Teflon filter in the lower part of the imagine.

The size profile of the agglomerate sample is shown in fig. 8.10.

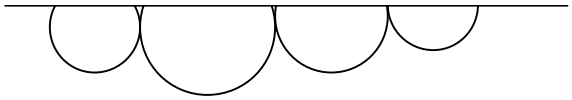

Fig. 8.10 Scheme of the agglomerate sample after ion beam etching. The surfaces imagine was taken in perpendicular direction by FESEM.

The overall shape observed in fig. 8.9 is spherical as expected for drying droplets. The droplets have obviously been of different size. The agglomerates on the filter are not destroyed by their impact with the filter material. The distribution of 115 agglomerate diameters from two images is shown in fig. 8.11.

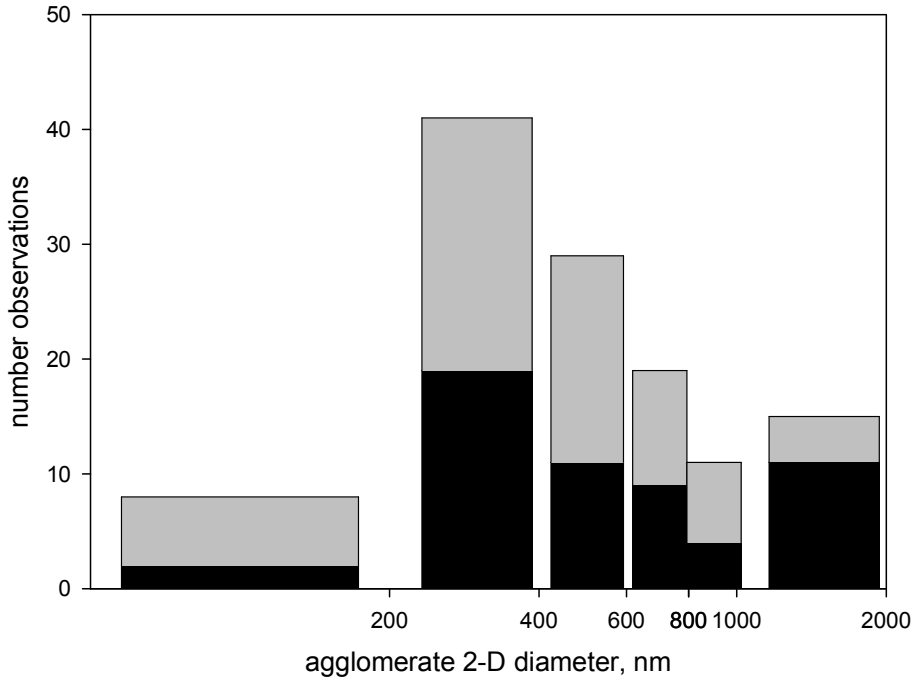

Fig. 8.11 Distribution of 2D-diameters. A correction for off-centre cuts would shift the peak to almost 400 nm. The individual measurement sets are shown in different color.

The contact points are too small (point contact) to be visible in the images. The measured porosity of the agglomerates lying on the Teflon filter from the two images was about 50 %. This porosity value is typical for the fixed bed. We can assume that the ion beam etching did not influence the structure of the layer and the structure of the agglomerates.

The agglomerate size distribution was evaluated from the cross section images. The real size of the agglomerates is bigger than the observed size in the images (fig. 8.10). The FESEM method can not show the topography of the etched filter sample. The observed agglomerate

diameter would shift the peak of the agglomerate distribution to 400 nm. The distribution of diameters found on the images has its peak well above the 200 nm observed with the differential mobility analyser (DMA) during filter sampling (fig. 8.12). The porosity of about 50 % – not containing the space between primary particles in close contact – is somewhat lower than the 75 % estimated from DMA data and mass of aerosol drawn on filters.

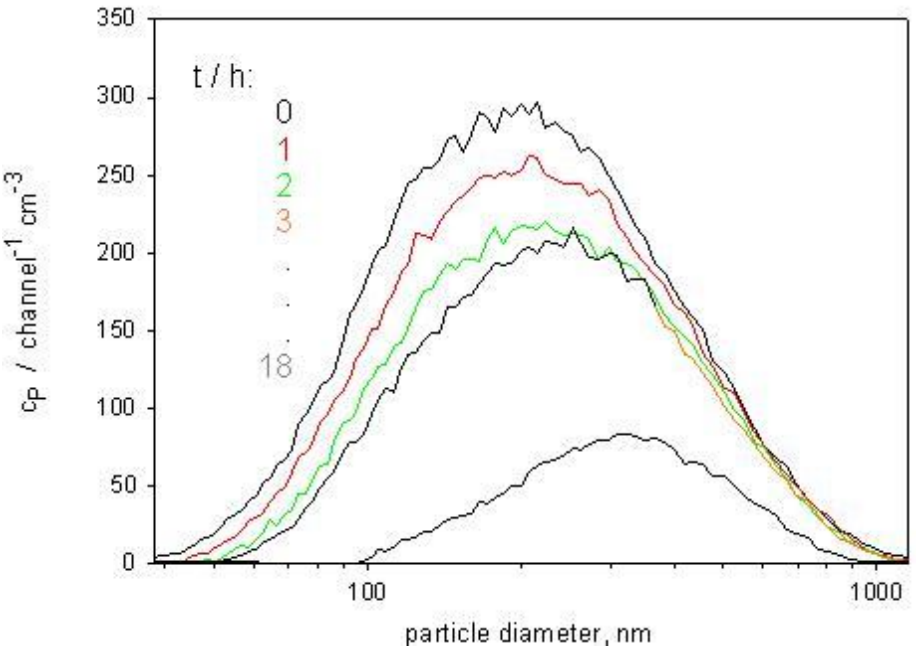

Fig. 8.12 Agglomerate size distribution determined by a differential mobility analyser (DMA).

The agglomerates in both images are split into 6 classes: 0-200 nm, 200 – 400, 400 – 600, 800 – 1000, 1000 – 2000. Most particles (72.4%) have diameters between 200 and 1000 nm. The small particles (<200 nm) are 6.4 % of all particles. The coarse particles (>1000nm) constitute 12.3% and they are more abundant than the small particles. The sample was taken at the start of the experiment, and the presence of such particles on the filter is possible.

Higher resolved images were used for the evaluation of the porosity. The inner structure appears to be independent of size and fairly constant between centre and rim. What may be mistaken as the primary particles (7 nm), are compact but irregularly shaped clusters of several of them. Thus, only the space between those clusters could be marked as pores, as shown in fig. 8.13.

Table 8.5: Agglomerate size distribution

Class, nm	0-200		200-400		400-600		600-800		800-1000		1000-2000	
	Obs.	%	Obs.	%	Obs.	%	Obs.	%	Obs.	%	Obs.	%
Measurement 1	2	1.5	19	15.3	11	9.0	9	7.3	4	3.3	11	9.0
Measurement 2	6	4.9	22	17.9	18	14.5	10	8.0	7	5.7	4	3.3
Total	8	6.4	33	33.2	29	23.5	19	15.3	11	9.0	15	12.3

Lines through 223 pores of 4 agglomerates yield a porosity of about 50 %.

Contacts between the clusters appear to be so numerous that those semivolatile compounds which are mobile on SiO_2 would find short migration paths to the outside of the agglomerates.

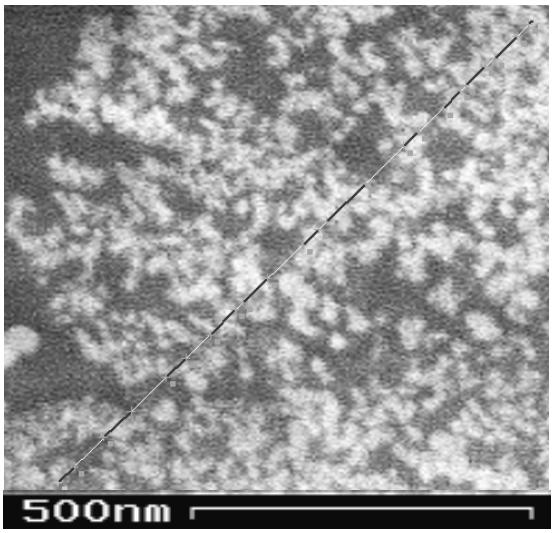

Fig. 8.13 Example of an evaluated image of a particle, using the program "Lince".

The same evaluation of the images was made for the agglomerates pore network. The peak of the pore distribution would then shift to 30 nm (fig. 8.14).

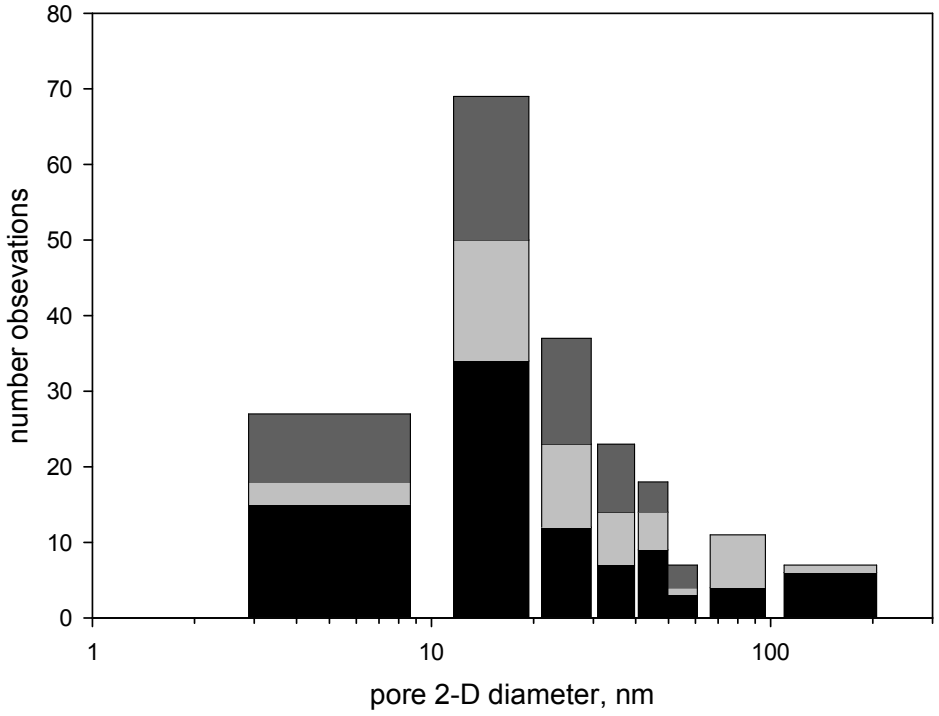

Fig. 8.14 Distribution of 2-D pore diameter. The distribution would shift the peak to 30 nm. The three measurement sets are shown in different colour.

Pores with diameters smaller than 1 nm are called micropores, those with diameters between 1 and 50 nm are called mesopores and those with diameters bigger than 50 nm are called macropores. (Gregg and Sing, 1982), (Hugo and Koch, 1979). According to this system, the agglomerates of Aerosil 380 are characterized as mesoporous, since 86.5 % of the pores have diameters between 1 and 50 nm (table 8.4).

Table 8.6: Pore size distribution

Class, nm	Mean diam., nm	Measurement 1		Measurement 2		Measurement 3		Total	
		Obs.	%	Obs.	%	Obs.	%	Obs.	%
1 – 10	5	15	7.4	3	1.5	9	4.4	27	13.3
10 – 20	15	34	17.1	16	8.0	19	9.4	69	34.5
20 – 30	25	12	6.0	11	5.6	14	7.0	37	18.6
40 – 50	45	9	4.4	5	2.5	4	2.0	18	8.9
50 – 60	55	3	1.5	1	0.5	3	1.5	7	3.5
60 – 100	80	4	2.0	7	3.4	0	0	11	5.4
100 - 200	150	6	3.0	1	0.5	0	0	7	3.5

The small pore diameter influences the transport processes in porous media very strongly. The small pores hinder the transport of OH radicals into the agglomerates. On the other hand, the slow diffusion coefficient of the test compound may be limiting for the chemical reaction in the agglomerate. Both of these conditions can influence the evaluation process and impose the use of a more complex model than the theory of the chemical kinetics.

8.6. Experiments with Aerosil in the smog chamber

The experiments were performed in the glass smog-chamber at 2°C and -10°C. A total of 36 experiments with Aerosil were made at two different temperatures and falling into three groups. The first group was the experiments that investigate the evaporation rate of Aldrin from the agglomerates. The second group of experiments were made with light source and without OH precursor. The absence or presences of photolysis of Aldrin can be distinguished in this way. The third group of experiments was made to measure the degradation rate of Aldrin coatings on Aerosil.

Table 8.7 Summary of the experiments made in the smog chamber at 2°C (*), at -10°C (**) and at 10°C(***)

Experiment	Light source	OH-precursor	$[OH]/10^6$ cm^{-3}	$\int[OH]dt/10^{10}$ $cm^{-3}s$	k_{app} / 10^{-10} cm^3s^{-1}	τ_{app}^{-1} h^{-1}	max. humidity	comments
Aldr 01	Dark							
Adr 02	Light							
Aldr 03	Light					1.9		
Aldr 04	Light					1.2		
Aldr 05*	Light	methylnitrite	18	16	-	-	58.3	
Aldr 06*	Light	methylnitrite	3.6	3.8	-	-	63.6	
Aldr 07*	Dark	methylnitrite	0	0	-	-	58.3	
Aldr 08*	Dark	N_2H_4/O_3 (300ppb)	930	12	-	-	60.2	
Aldr 09*	Dark	N_2H_4/O_3 (330ppb)	10	12	-		34.0	
Aldr 10*		N_2H_4/O_3 (max. 5.5 ppm)	28	38	0.13 ± 0.06	0.42	63.0	
Aldr 11*	Light	without OH - precursor	1.4	2	3.4 ± 0.43	1.54	49.5	
Aldr 12*	Light	H_2O_2	1.0	1.8	5.6 ± 0.39	1.40	49.7	
Aldr 13*	Light	without OH - precursor	1.3	1.8	2.6 ± 0.31	0.48	50.0	

Aldr 14**	Light	without OH - precursor	2.3	3.8	0.87 ± 0.08	0.37	52.0	
Aldr 15**	Dark	without OH - precursor	-	-	-		66.0	
Aldr 16**	Dark	O_3 (max 5.9 ppm)	-	-	-	-	53.2	
Aldr 17**	Dark	O_3 (max 20 ppm)	-	-	-	-	63.2	
Aldr 18**	Light	without OH - precursor	-	-	-	-	41.3	chamber cleaning
Aldr 19**	Light	without OH - precursor	0.0	-	-	-	55.3	
Aldr 20**	Light	H_2O_2	0.2	0.27	-	-	49.8	
Aldr 21**	Light	H_2O_2	0.5	0.49	3.1 ± 1.3	1.17	49.7	
Aldr 22**	Dark	O_3 (17.9 ppm)	-	-	-		58.0	
Aldr 23**	Light	H_2O_2	0.6	0.87	2.6 ± 0.06	0.98	49.7	
Aldr 24**								cancelled
Aldr 25**	Light	methylnitrite	2.8	2.7	1.2 ± 0.24	1.1	51.0	
Aldr 26**	Light	methylnitrite	3.6	4.9	0.7 ± 0.58	1.1	51.2	
Aldr 27**	Light	methylnitrite	3.4	5.9	0.59 ± 0.07	0.6	52.0	
Aldr 28**	Light	methylnitrite	1.5	2.9	2.4 ± 0.06	1.38	-	
Aldr 29*	Dark	without OH - precursor	-	-	-	-	-	cancelled
Aldr 30*	Dark	without OH - precursor	-	-	-	-	49.7	
Aldr 31*	Light	without OH - precursor	0.0	0	0	-	51.2	
Aldr 32*	Light	methylnitrite	18	25	0.11		61.3	
Aldr 33*	Dark	N_2H_4/O_3 (860 ppb)	18	19	-	-	59.0	
Aldr 34*	Dark	N_2H_4/O_3 (max 14.2 ppm)	72	55	0.002	0.5	68.5	
Aldr 35**								cancelled
Aldr 36*	Light	methylnitrite	20	18	-	-	-	
Aldr 37*	Light	methylnitrite	20	18.6	0.012	0.67	54.3	
Aldr 38*	Light	methylnitrite	30	25.6	0.014	1.56	46.0	
Aldr 40***	Dark	without OH -precursor	0	0	-	0.16	55	
Aldr 41*	Light	methylnitrite	23	33	0.078	1.35	49	

Except the experiments of the Aldrin degradation there are experiments after the chamber cleaning. The chamber was cleaned before Aldrin05, before Aldrin18 and before Aldrin29. The experiments prove the quality of the cleaning. It is well-known that the smog chamber

produces OH radicals. In the presence of contaminants on the chamber wall the production of OH radicals can be significant. The experiments Aldrin 11 and Aldrin 13 are examples for such phenomena. Other experiments were cancelled because of technical problems (there are about 10 technical devices and they must work flawlessly during the experiment). Experiments with ozone were also made with the aim to investigate the degradation due to chemical reaction but those experiments were not evaluated. An ozone generator was used to produce ozone. During the introduction of ozone an unknown contamination occurred. The contaminant reacted with the all organic compounds during the chamber feeding with ozone. After the stopping the ozone feeding, ozone was measured in ppm concentration but the reaction did not continue. This leads to the suspicion of an unknown contamination from the electric discharge of the ozonizer.

The experiments made by ozone feeding were also impossible to evaluate. The experiment procedure was taken under control after feeding the chamber with high ozone concentration and start of the aerosol feeding after the ozone production.

8.7. Analysis of the parameters and the gas-phase compounds

Aldrin was extracted from the Teflon filters after the sampling by n-hexane. The extract was analyzed by gas chromatography (Siemens Sichromat 2 with on-column injector and ECD detector). The capillary column was: 8 m Chrompack Cp – Sil 5 CB, d_i = 0.32 mm, film thickness 1.2 µm. The hydrocarbons in the gas phase were analyzed by another Siemens Sichromat 2 with cryofocusing and FID detector. The capillary column was 50 m Chrompack AL – PLOT, d_i = 0.32 mm, film thickness 5 µm.

Pressure in the chamber was 1 atm. There is a bypass always open to the atmosphere. Chamber relative humidity (r.h., %) and temperature (T, °C) were measured by a hygrometer digital transmitter (Steinecker Elektronik GmbH) for simultaneous measurement of temperature and relative humidity.

8.8. Evaporation of Aldrin from the agglomerate surface at different temperatures

The evaporation of Aldrin was tested in the first chamber runs at 2°C and -10°C. Other loss processes as photolysis were also verified by the experiment. The Aldrin on the carrier evaporates stronger at 2ºC than at -10ºC (fig. 8.15).

During the first hour of the experiment at 2ºC the concentration decreased strongly. A decreasing exponential function could be fitted. During the rest of the time the Aldrin

concentration was constant. The experimental points at 10 ºC could be fitted by linear regression.

It must be assumed that the Aldrin has evaporated completely and that the squares represent blank values of the analyses. The concentrations fluctuate stronger during the -10ºC experiment. The strong fluctuations may have been caused by the low degree of the mixing in the chamber (see chapter 7.1).

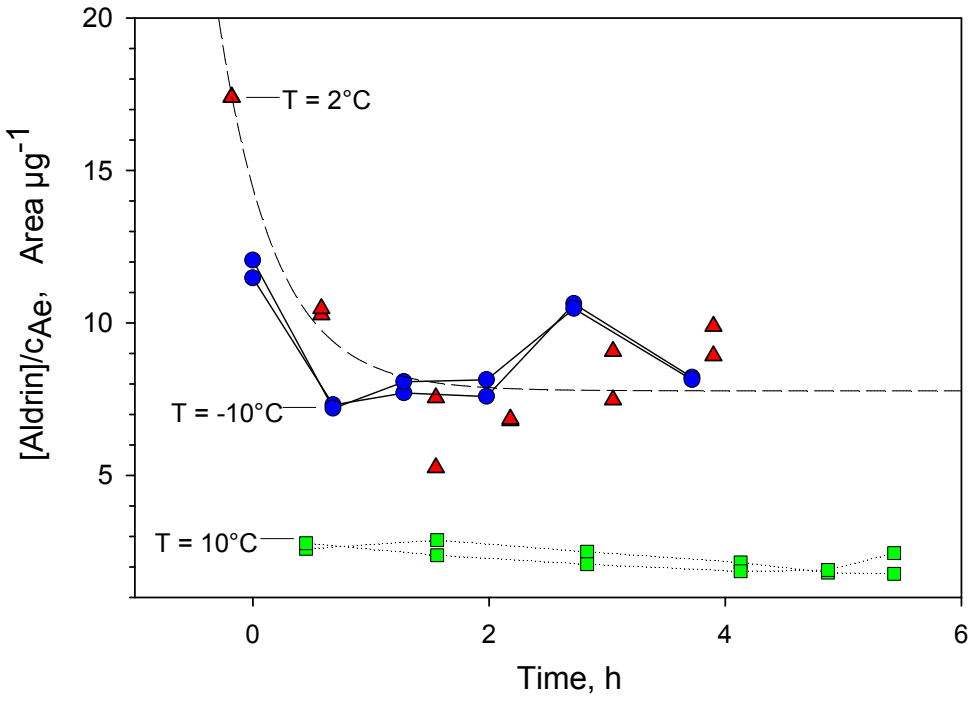

Fig. 8.15 Blank experiment at 2°C(dashed line and triangles, Aldrin 11), at -10ºC (straight line, points, Aldrin 15) and 10ºC (dotted line, squares, Aldrin 40). The experiment was made without light source, and no OH radicals were produced.

8.9. Photolysis of Aldrin

The possible photolysis of Aldrin was also investigated in the chamber. The UV spectrum of Aldrin is referred to and shown in fig. 8.16. The substance absorbs light in the UV range. It does not absorb light in the visible range. Photolysis is not expected.

Fig. 8.17 shows an experiment with light source in order to check any photolysis of Aldrin. The concentration of Aldrin did not decrease under irradiation of the aerosol in the chamber, although there is again a strong fluctuation of the concentration.

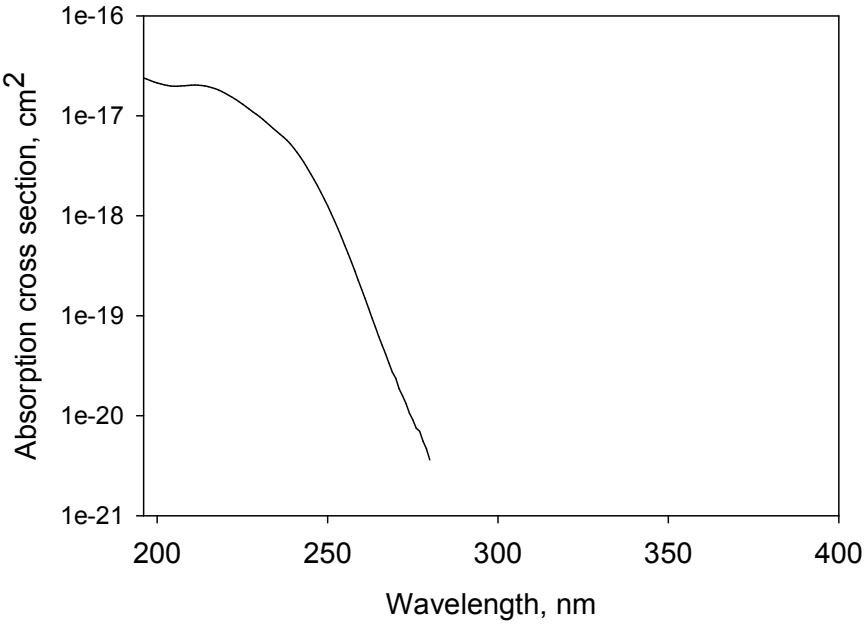

Fig. 8.16 UV spectrum of Aldrin in n-hexane.

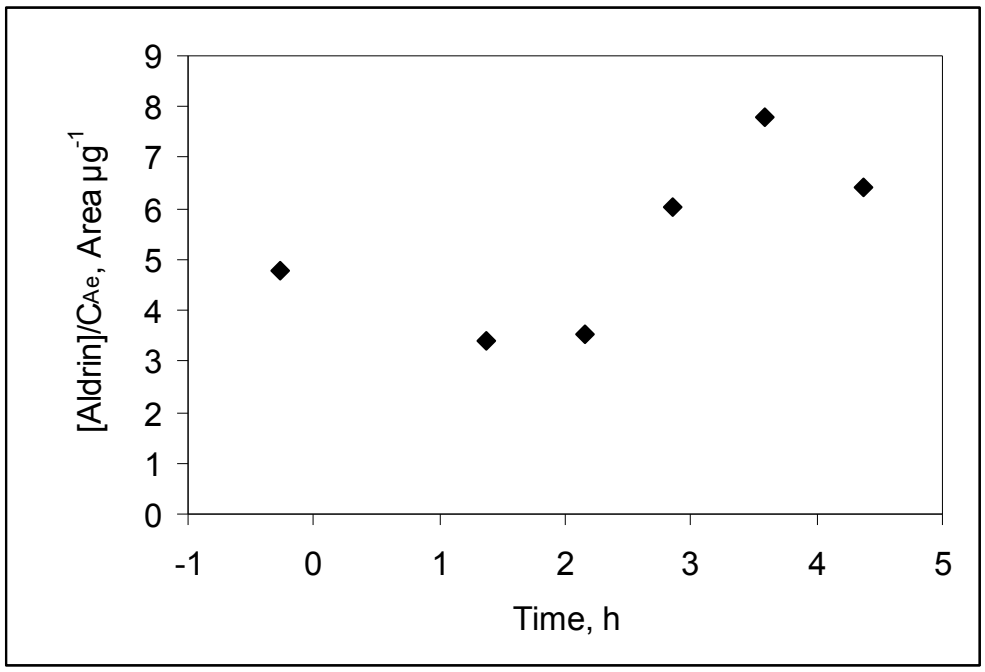

Fig. 8.17 Photolysis experiment (Aldrin 19).

The experiment does not differ from the blank experiments in the previous chapter.
Further photolysis experiments were made with glass balloons. These experiments do again not indicate any photolysis of Aldrin.

8.10. Degradation kinetics of Aldrin at different temperatures

The experiments was made with 60 mg coated Aerosil, suspended in 60 ml water. The suspension was mixed with an Ultra-Turrax stirrer for 1 min and sprayed into the chamber. The smog chamber was fed until 50 % relative humidity was reached. After stopping of the feeding, the relative humidity increases further by ca. 10 %. At the beginning of the experiment the bigger agglomerates sediment faster than the small particles. Then the remaining, smaller agglomerates have a longer airborne duration in the chamber. The temperature is relatively high due to the irradiation and the residual water evaporates from the agglomerates.

The initial relative humidity is about 60 %. The water vapour begins to condense at relative humidities of 90 % at 2ºC and 80% at -10ºC (Hyland, 1975; Sonntag, 1990). On other hand, high aerosol concentration is a requirement for a good reproducibility of the experiments. The higher aerosol concentration allows taking a heavier sample by a smaller air volume for a shorter time. That could improve the calculation of aerosol concentration.

The time dependent decrease of the Aldrin concentration is shown in fig. 8.18.

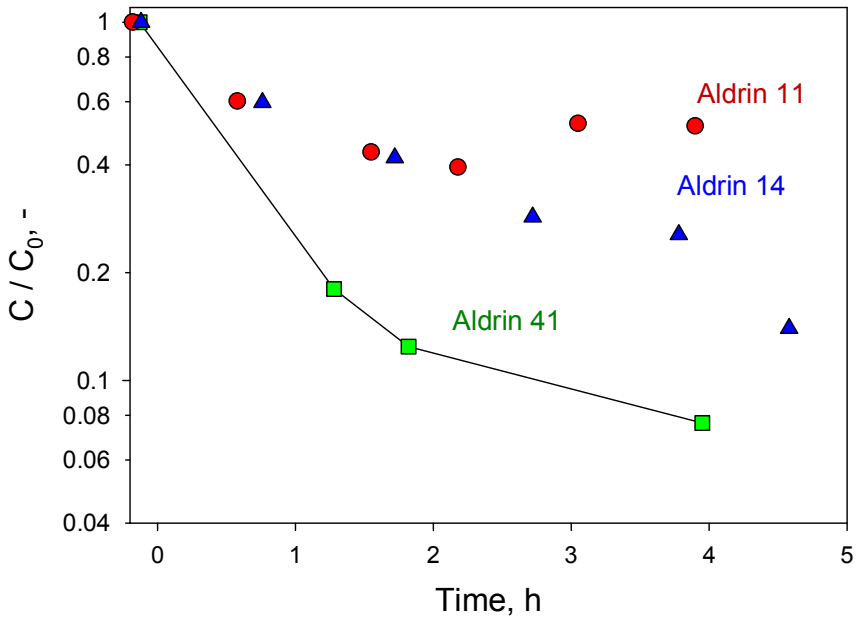

Fig. 8.18 The decrease of the Aldrin concentration is caused by the presence of OH radicals. Aldrin 11 is a "blank" experiment at 2°C in the absence of OH; the aerosol was exposed to a low OH concentration (Aldrin 14) and a high concentration (Aldrin 41).

The analysis technique allows measuring the concentration in a very large measurement range. The lifetime decreases with the increasing OH concentration. The "blank" experiment at 2°C is shown where the evaporation is higher. The low Aldrin concentration was measured less accurately than the higher values. The fluctuation of the baseline influences stronger the peak analysis, and the points fluctuate in the low concentration range.

The concentration profile of Aldrin can be presented as a function of OH exposure (fig. 8.19). The Aldrin decreases exponentially with exposure; where else the concentration scatter can be seen at the lower Aldrin concentrations.

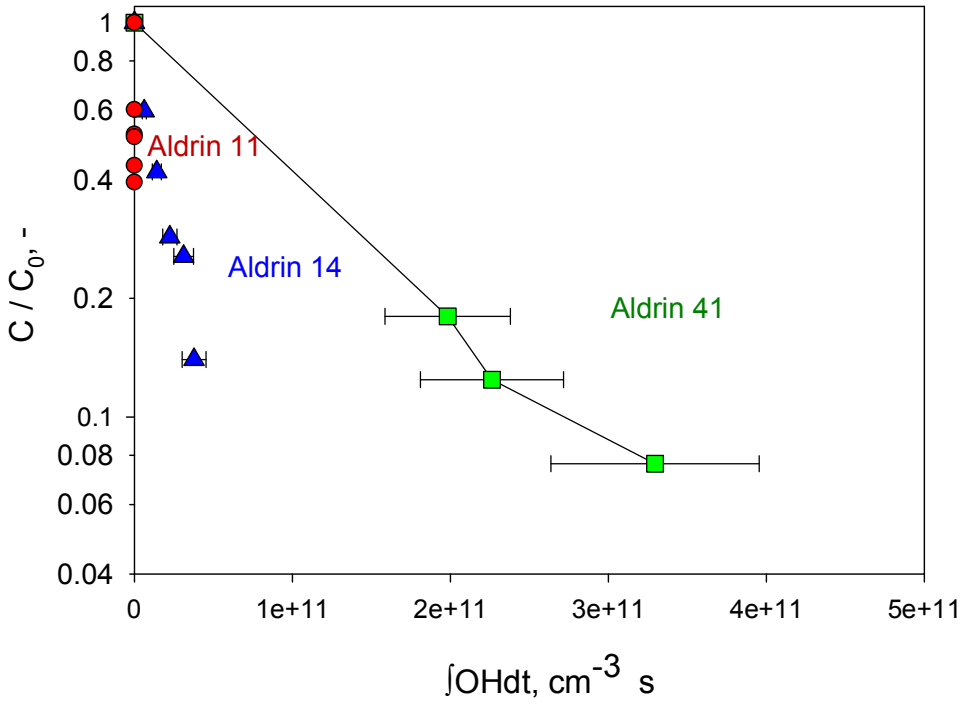

Fig. 8.19 Semilogarithmic diagram of the decreasing concentration vs. OH exposure.

Three experiments are shown in fig. 8.20 and fig. 8.21. The experimental conditions are nearly identical. The comparison is between two experiments at -10°C and one – at 2°C. The slope or the lifetime of Aldrin in fig. 8.20 is similar for the three experiments (see table 8.7). The OH exposure is different in the three cases. The temperature does not influence the degradation of Aldrin. This is an indication for the influence of the diffusion.

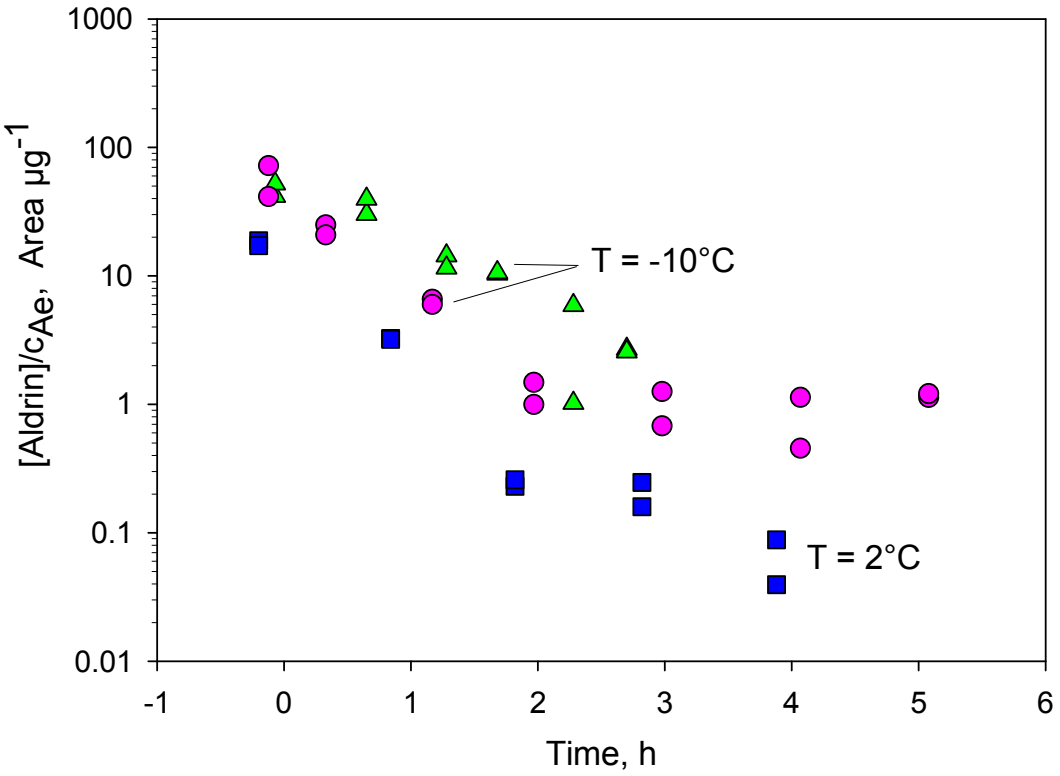

Fig. 8.20 Time – dependant plot of the experiments at different temperature. Aldrin 21 ▲, Aldrin 28 ●, Aldrin 12 ■.

Different experimental conditions and their fluctuations can add to the uncertainties. The three experiments proceed analogical in fig. 8.20 and fig. 8.21.

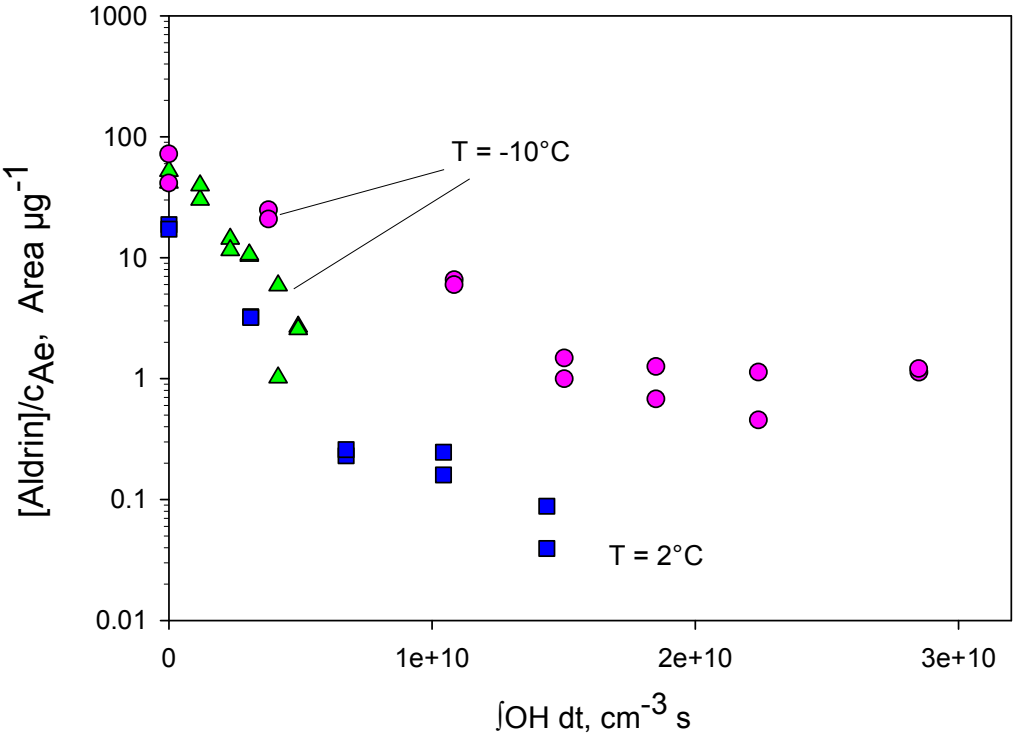

Fig. 8.21 Comparison between Aldrin 21 ▲, Aldrin 28 ●, Aldrin 12 ■.

The similar slope of the degradation curve corresponds to the degradation by OH radicals.

8.11. Reaction products and their behavior

Two products were detected from the chemical reaction of Aldrin with OH radicals. The first product is Dieldrin and it is a stable product from the chemical reaction. The second product is Photoaldrin. Photoaldrin is less stable than Dieldrin. Both products form simultaneously. Photoaldrin can not be detected in some experiments. We detected later that Photoaldrin decomposes rapidly and that the substance may decompose before the analysis.

The influence of the OH exposure is presented in fig.8.22. The aerosol in Aldrin 27 was exposed to higher OH – concentration than Aldrin 21. The concentration of the products is corresponding to the higher OH concentration, higher than the concentration of Aldrin 21. Photoaldrin was not detected in Aldrin 21.

Direct comparison between two experiments at 2ºC and -10ºC can be made in fig. 8.22 and fig. 8.23. The initial concentration at 2ºC is 4 times lower than the initial concentration at -10ºC. The OH exposure during experiment Aldrin 13 is twice as high as in Aldrin 21 but the product yield is not higher than the product yield in Aldrin 27.

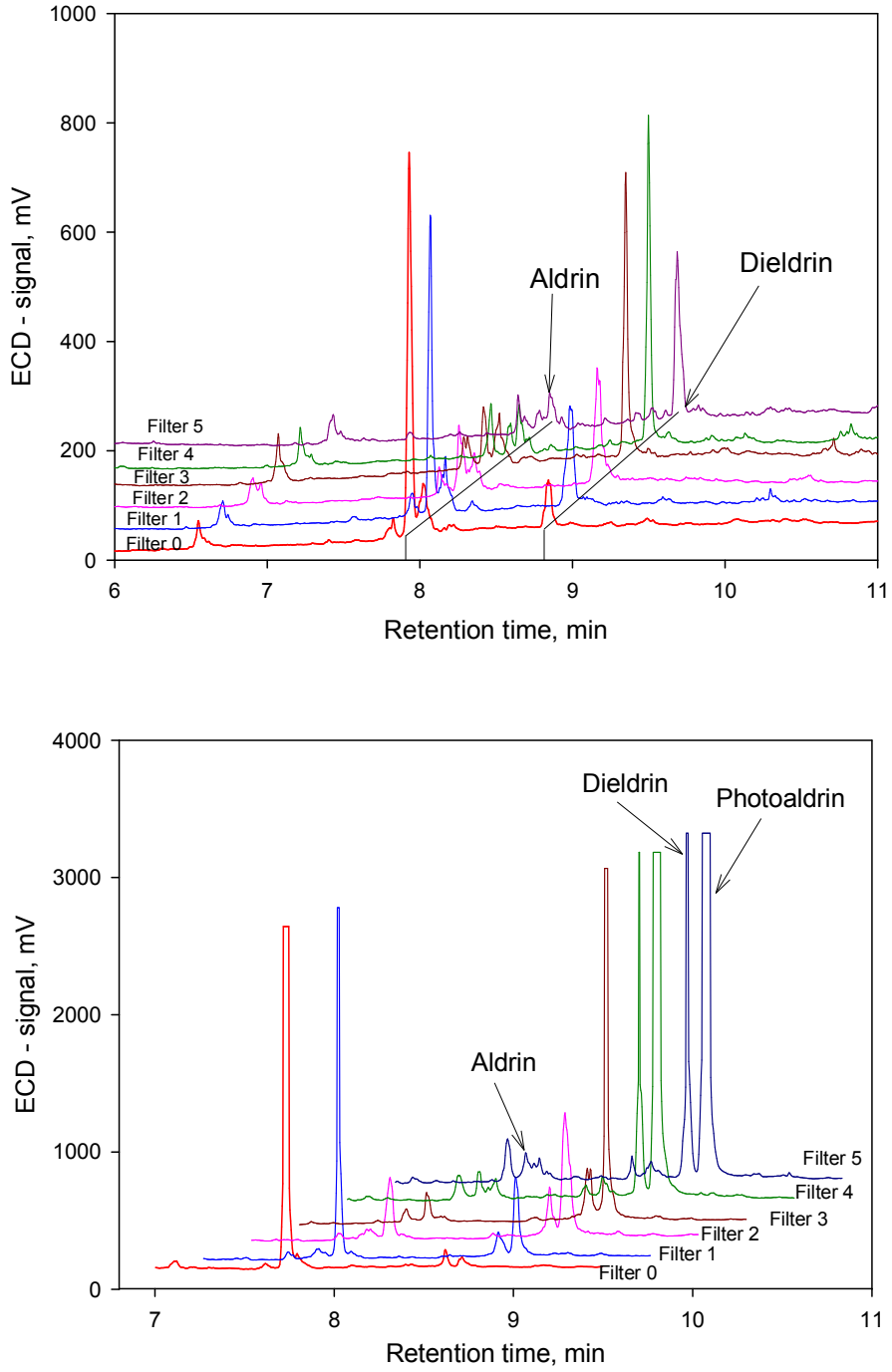

Fig. 8.22 Chromatograms from experiments Aldrin 21 (above) and Aldrin 27 (below). Aldrin21 (above) was made by OH - exposure = $4.9 \cdot 10^9$ $cm^{-3}s$, Aldrin 27 (below) was made by OH – exposure = $5.9 \cdot 10^{10}$ $cm^{-3}s$. The both experiments were made at -10°C.

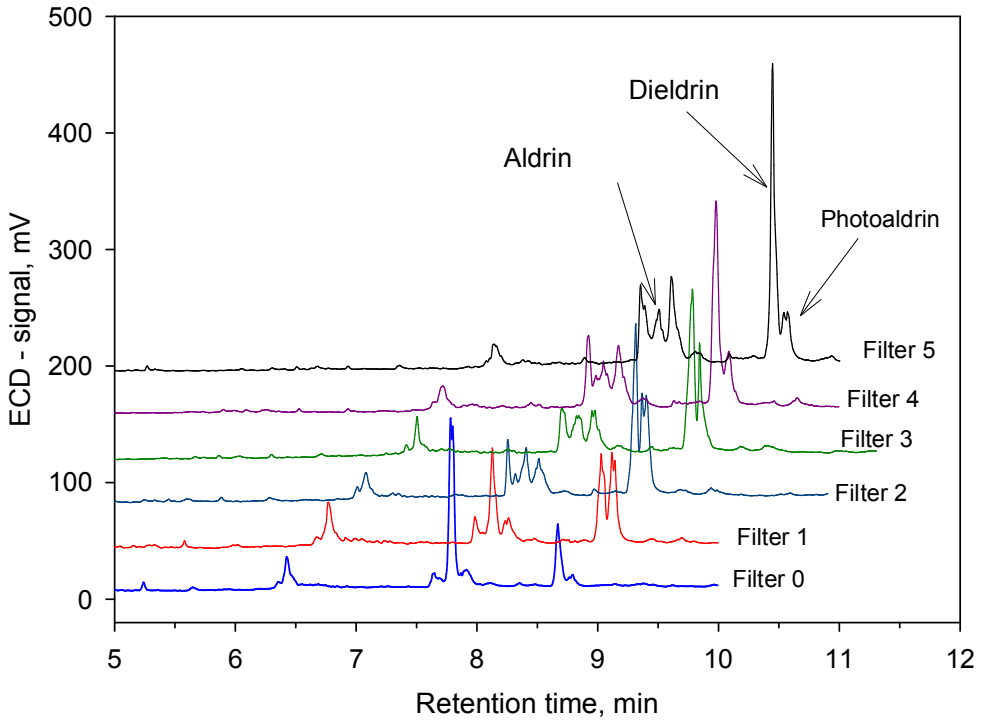

Fig. 8.23 Chromatograms from the experiment Aldrin 13, made at 2°C and OH – exposure = $1.8 \cdot 10^{10}$ $cm^{-3}s$.

Two experiments (Aldrin 13 and Aldrin 27) are compared with each other in fig. 8.24. The initial concentration in Aldrin 13 is lower than the initial concentration in Aldrin 27. The different initial values indicate the influence of the temperature in the chamber. Generally the products presented vs. time and vs. OH exposure have a similar behavior. Dieldrin and Photoaldrin are formed simultaneously.

The Dieldrin was formed slower than Photoaldrin and its concentration increases during the experiment. Dieldrin may react further with OH radicals. That indicates the lower formation of Dieldrin in Aldrin 27 where the OH exposure is generally higher than the exposure in Aldrin 13.

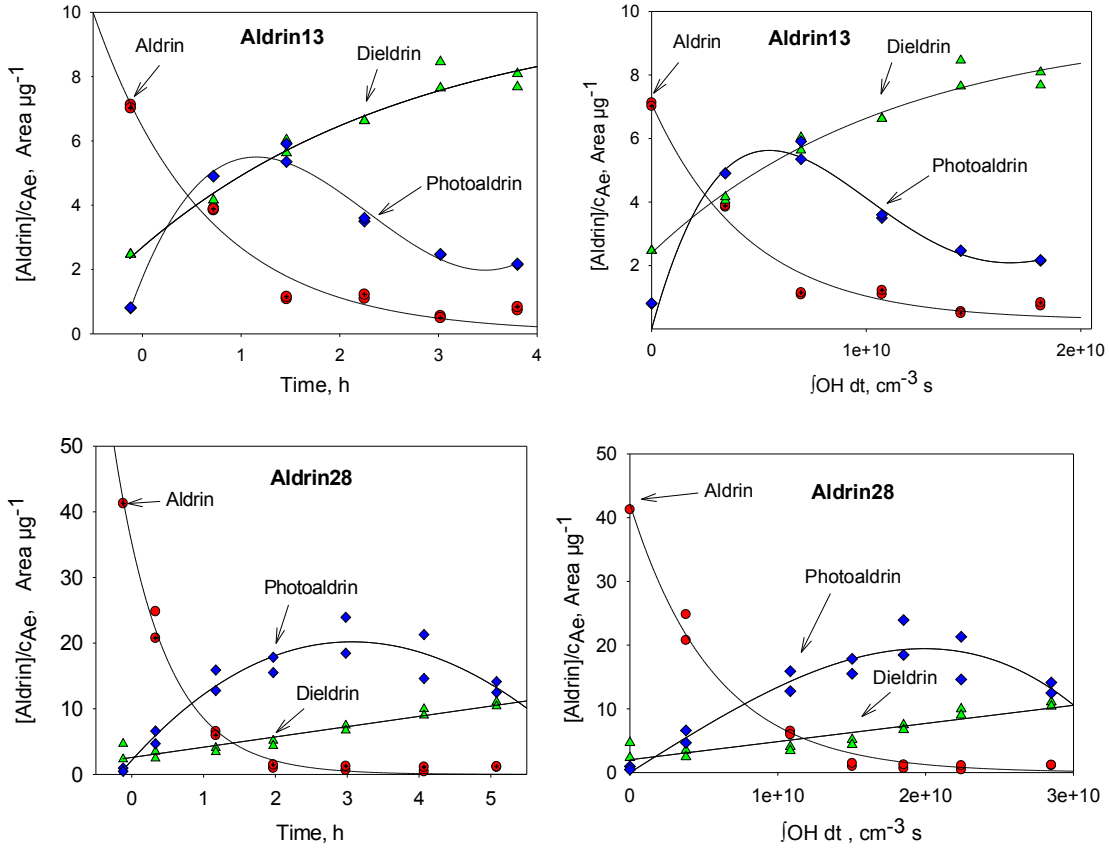

Fig. 8.24 Comparison of the behavior of Aldrin, Dieldrin and Photoaldrin vs. time and vs. OH – exposure in Aldrin 13 (above) and Aldrin 28 (below).

The Dieldrin behavior is similar in the rest of experiments exposed to high OH concentration. Photoaldrin was formed faster, reacts with OH radicals and then its concentration decreases. The compound is not detected in the initial sample.

8.12. Verification of the rate constants of the reference hydrocarbons

A verification of the rate constants (Atkinson, 1994) and degradation rates of the reference hydrocarbons was made to prove the quality of the hydrocarbon measurements. The rate constants of the reference substances have critical significance for the calculation of the OH – concentrations.

The following equation is used:

$$\frac{-dln[HC]^{j}_{norm,i}/dt}{k_{OH}} = [OH] \qquad \textbf{(8.1)}$$

The expression $-dln[HC]^{j}_{norm,i}/dt$ in the equation is the slope of the decay of the hydrocarbons in a semilogarithmic diagram. The main results are shown in table 8.8, where the individual constants for every hydrocarbon with index $[OH]_{Oct}$, $[OH]_{TMB}$, etc. are

presented. The mean value $\overline{[OH]}$ was calculated and the average of the absolute deviations of data points from their mean. The average deviation is a measure of the variability in a data set. The last column gives the deviation (%) from the mean value. The complete results are shown in the appendix. The recommended rate constants at the temperatures of the experiments are shown in tables 8.9 and 8.11.

The average deviation is in most cases below 10 %. Sometimes, only two hydrocarbons were used to measure the OH – concentration, and in those cases the uncertainties are higher than in the other cases. The uncertainty is clearly lower if three hydrocarbons are employed to determine OH from the average than if two hydrocarbons are used. If only one hydrocarbon is used, an uncertainty is not defined. The evaluation of the measurements quality shows the reliability of the method and the reliability of the calculated OH – concentration.

The rate constants of the reference hydrocarbons were updated during the experimental phase, since there are new recommendations for the rate constants of the reference hydrocarbons (Atkinson, 2003). Table 8.8 was recalculated with the updated rate constants and the results are presented in table 8.10.

Table 8.8 The calculated OH levels obtained from n-octane, 2,2,3-trimethylbutane, 2,2,3,3-tetramethylbutane, 2,2-dimethylbutane and n-hexane are shown in the first four columns. The mean value and the average deviation were calculated. The percentage value of the average deviation from the mean value was calculated in the last column

	$[OH]_{Oct}$	$[OH]_{TMB}$	$[OH]_{TeMB}$	$[OH]_{DMB}$	$[OH]_{Hex}$	$\overline{[OH]}$	Ave. dev.	%
Aldr 10	$9.9\cdot10^{6}$	-		$3.3\cdot10^{7}$	$2.7\cdot10^{7}$	$2.2\cdot10^{7}$	$8.9\cdot10^{6}$	38.3
Aldr 11	-	-		$2.9\cdot10^{6}$	$1.12\cdot10^{6}$	$2.1\cdot10^{6}$	$8.9\cdot10^{5}$	43.2
Aldr 12	-	-		$1.1\cdot10^{6}$	$8.2\cdot10^{5}$	$9.8\cdot10^{5}$	$1.6\cdot10^{5}$	16.6
Aldr 13	-	-		$1.2\cdot10^{6}$	$1.1\cdot10^{6}$	$1.2\cdot10^{6}$	$5.3\cdot10^{4}$	4.4
Aldr 14	-	-		$3.0\cdot10^{6}$	$1.23\cdot10^{6}$	$2.1\cdot10^{6}$	$8.7\cdot10^{5}$	40.3
Aldr 20	-	$1.8\cdot10^{5}$		$1.6\cdot10^{5}$	$3.5\cdot10^{5}$	$2.3\cdot10^{5}$	$8.0\cdot10^{4}$	34.8
Aldr 21	-	$5.5\cdot10^{5}$		$6.1\cdot10^{5}$	$4.9\cdot10^{5}$	$5.4\cdot10^{5}$	$4.3\cdot10^{4}$	7.7
Aldr 23	-	$1.3\cdot10^{5}$		$1.3\cdot10^{6}$	$6.7\cdot10^{5}$	$7.00\cdot10^{5}$	$4.0\cdot10^{5}$	57.7
Aldr 25	-	$3.1\cdot10^{6}$		$2.8\cdot10^{6}$	$2.8\cdot10^{6}$	$2.9\cdot10^{6}$	$1.4\cdot10^{5}$	4.7
Aldr 26	-	$3.9\cdot10^{6}$		$3.8\cdot10^{6}$	$3.7\cdot10^{6}$	$3.8\cdot10^{6}$	$9.9\cdot10^{4}$	2.6
Aldr 27	-	$2.4\cdot10^{6}$		$1.8\cdot10^{6}$	$2.00\cdot10^{6}$	$2.1\cdot10^{6}$	$2.0\cdot10^{5}$	9.7
Aldr 28	-	$1.6\cdot10^{6}$		$1.5\cdot10^{6}$	$1.5\cdot10^{6}$	$1.6\cdot10^{6}$	$3.1\cdot10^{4}$	2.0
Aldr 32	-	-		-	$2.2\cdot10^{6}$	$2.2\cdot10^{6}$	-	-
Aldr 34	-	$6.65\cdot10^{7}$		$7.4\cdot10^{7}$	$6.4\cdot10^{7}$	$6.8\cdot10^{7}$	$3.7\cdot10^{6}$	5.3
Aldr 36	-	$5.7\cdot10^{6}$		$1.43\cdot10^{7}$	-	$1.0\cdot10^{7}$	$4.3\cdot10^{6}$	
Aldr 37	-	$1.65\cdot10^{7}$		$1.8\cdot10^{7}$	$1.7\cdot10^{7}$	$1.6\cdot10^{7}$	$7.6\cdot10^{4}$	0.5
Aldr 38		-		$2.8\cdot10^{7}$	$2.7\cdot10^{7}$	$2.8\cdot10^{7}$	$4.1\cdot10^{5}$	1.5
Aldr 41			$1.3\cdot10^{7}$	$6.2\cdot10^{6}$	$1.07\cdot10^{7}$	$8.4\cdot10^{6}$	$2.2\cdot10^{6}$	26.5
Mean								19.5

Table 8.9 OH rate constants of the reference hydrocarbons at 263 K, 275 K and 298 K, calculated according to Atkinson (1994)

	k_{OH}, cm^3s^{-1}		
	T = 263 K	T = 275 K	T = 298 K
2,2-Dimethylbutane	$1.66 \cdot 10^{-12}$	$1.88 \cdot 10^{-12}$	$2.3 \cdot 10^{-12}$
n-Hexane	$5.0 \cdot 10^{-12}$	$5.2 \cdot 10^{-12}$	$5.6 \cdot 10^{-12}$
n-Octane	$7.4 \cdot 10^{-12}$	$7.8 \cdot 10^{-12}$	$8.7 \cdot 10^{-12}$
2,2,3,3-Tetramethylbutane	$8.1 \cdot 10^{-13}$	$9.02 \cdot 10^{-13}$	$1.07 \cdot 10^{-12}$
2,2,3-Trimethylbutane	$4.1 \cdot 10^{-12}$	$4.13 \cdot 10^{-12}$	$4.22 \cdot 10^{-12}$

The uncertainties are slightly smaller after the recalculation. Only one experiment exceeds the uncertainty limit of 30 %. Four other experiments are close to the limit. It is clear that the deviation of the rate constant of one hydrocarbon with some percent reduces or increases the total uncertainty.

Table 8.10 OH-levels calculated from n-octane, 2,2,3-trimethylbutane, 2,2,3,3-tetrametylbutane, 2,2-dimethylbutane and n-hexane are shown in the first four columns. The mean value and the average deviation were calculated. The percentage value of the average deviation from the mean value was calculated in the last column

	$[OH]_{Oct}$	$[OH]_{TMB}$	$[OH]_{TeMB}$	$[OH]_{DMB}$	$[OH]_{Hex}$	$\overline{[OH]}$	Ave. dev.	%
Aldr 10	$9.8 \cdot 10^6$			$3.5 \cdot 10^7$	$3.1 \cdot 10^7$	$3.3 \cdot 10^7$	$2.0 \cdot 10^6$	6.0
Aldr 11				$3.1 \cdot 10^6$	$1.4 \cdot 10^6$	$2.3 \cdot 10^6$	$8.7 \cdot 10^5$	38.3
Aldr 12				$1.2 \cdot 10^6$	$9.8 \cdot 10^5$	$1.1 \cdot 10^6$	$1.2 \cdot 10^5$	10.8
Aldr 13				$1.3 \cdot 10^6$	$1.3 \cdot 10^6$	$1.3 \cdot 10^6$	$1.8 \cdot 10^4$	1.2
Aldr 14				$3.2 \cdot 10^6$	$1.5 \cdot 10^6$	$2.4 \cdot 10^6$	$8.8 \cdot 10^5$	37.4
Aldr 20		$1.9 \cdot 10^5$		$1.8 \cdot 10^5$	$4.0 \cdot 10^5$	$2.6 \cdot 10^5$	$9.4 \cdot 10^4$	36.9
Aldr 21		$6.2 \cdot 10^5$		$6.4 \cdot 10^5$	$5.6 \cdot 10^5$	$6.2 \cdot 10^5$	$3.7 \cdot 10^4$	6.0
Aldr 23		$1.4 \cdot 10^5$		$1.4 \cdot 10^6$	$7.7 \cdot 10^5$	$7.7 \cdot 10^5$	$4.2 \cdot 10^5$	54.6
Aldr 25		$3.5 \cdot 10^6$		$3.1 \cdot 10^6$	$3.2 \cdot 10^6$	$3.3 \cdot 10^6$	$1.8 \cdot 10^5$	5.4
Aldr 26		$4.4 \cdot 10^6$		$4.1 \cdot 10^6$	$4.2 \cdot 10^6$	$4.3 \cdot 10^6$	$1.2 \cdot 10^5$	2.8
Aldr 27		$2.7 \cdot 10^6$		$1.9 \cdot 10^6$	$2.3 \cdot 10^6$	$2.3 \cdot 10^6$	$2.4 \cdot 10^5$	10.2
Aldr 28		$1.8 \cdot 10^6$		$1.7 \cdot 10^6$	$1.7 \cdot 10^6$	$1.7 \cdot 10^6$	$4.9 \cdot 10^4$	2.9
Aldr 32					$2.4 \cdot 10^6$	$2.4 \cdot 10^6$	-	-
Aldr 34		$7.4 \cdot 10^7$		$6.9 \cdot 10^7$	$6.9 \cdot 10^7$	$7.1 \cdot 10^7$	$2.2 \cdot 10^6$	3.1
Aldr 36		$6.5 \cdot 10^6$		$1.4 \cdot 10^7$		$1.0 \cdot 10^7$	$3.5 \cdot 10^6$	35.2
Aldr 37		$1.8 \cdot 10^7$		$1.6 \cdot 10^7$	$1.8 \cdot 10^7$	$1.8 \cdot 10^7$	$3.2 \cdot 10^5$	1.9
Aldr 38		-		$3.0 \cdot 10^7$	$3.1 \cdot 10^7$	$3.0 \cdot 10^7$	$3.6 \cdot 10^5$	5.0
Aldr 41			$1.5 \cdot 10^7$	$6.6 \cdot 10^6$	$1.2 \cdot 10^7$	$1.1 \cdot 10^7$	$3.0 \cdot 10^6$	27.1
Mean								18.0

Table 8.11 OH rate constants of the reference hydrocarbons at three temperatures, calculated according to the updated recommendation by Atkinson (2003)

	k_{OH}, cm^3s^{-1}		
	T = 263 K	T = 275 K	T = 298 K
2,2-Dimethylbutane	$1.6\cdot10^{-12}$	$1.8\cdot10^{-12}$	$2.1\cdot10^{-12}$
n-Hexane	$4.6\cdot10^{-12}$	$4.7\cdot10^{-12}$	$5.2\cdot10^{-12}$
n-Octane	$7.3\cdot10^{-12}$	$7.5\cdot10^{-12}$	$8.1\cdot10^{-12}$
2,2,3,3-Tetramethylbutane	$7.0\cdot10^{-13}$	$7.9\cdot10^{-13}$	$9.72\cdot10^{-13}$
2,2,3-Trimethylbutane	$3.5\cdot10^{-12}$	$3.7\cdot10^{-12}$	$3.8\cdot10^{-12}$

Here an example will be given to illustrate the statement. If, for example, the rate constant of hexane is increased by 30 % we obtain an increase of $k_{OH,hex} = 4.64\cdot10^{-12}$ $cm^{-3}s^{-1}$ by 30 % to $k_{OH,hex} = 6\cdot10^{-12}$ $cm^{-3}s^{-1}$. This rate constant was used to recalculate the constant of the experiments Aldrin 10 and Aldrin 37. The recalculated average deviation is 19 % for Aldrin 10 and 10.4 % for Aldrin 37. The uncertainty multiplies only by 30 % deviation of the hexane rate constant.

8.13. Calculation of the effective rate constant for the degradation of Aldrin

An apparent rate constant can be calculated for every experiment with Aldrin. The calculated apparent rate constants are plotted vs. the OH – concentration in a double logarithmic diagram (fig. 8.25). The figure contains 148 measurement points, and a regression line with a slope of 0.81±0.3 describes the data reasonably well.

The theoretical rate constants (dashed line in fig.8.25) were calculated according to the mathematical model described in chapter 6 eq. (6.4). The calculation was made with constant values for the evaporation constant **h**, for the penetration depth of the OH – radicals $\mathbf{R_0}$, the diffusivity $\mathbf{D_{eff}}$, the reaction rate, $\boldsymbol{\tau}^{-1}$, the duration, **t**, of the experiment and the diameter $\mathbf{D_p}$ of the agglomerates. Realistic parameter values are chosen for the calculation.

The apparent reaction rate was calculated from the concentration decrease curve as in fig. 6.5 to fig. 6.11

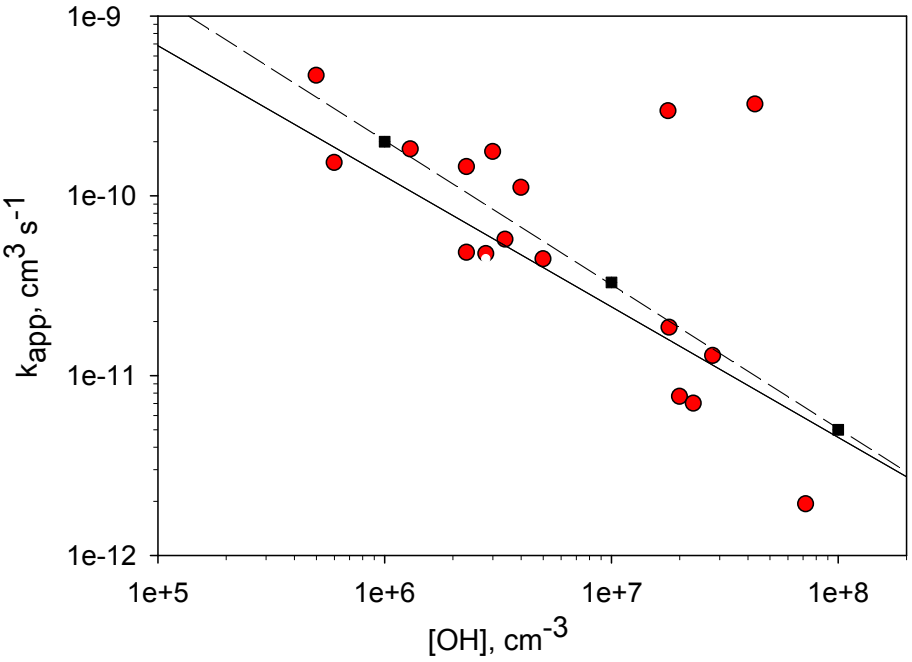

Fig. 8.25 The individual apparent rate constants are shown for every experiment. The squares are the calculated rate constants from the model according to eq. 6.4. For the calculations the following values were used: D_p = 1 µm, t = 2.7 h, $D_{eff} = 3.89 \cdot 10^{-11}$ $cm^2 s^{-1}$, $\tau^{-1} = 0.001$ s^{-1}, R_0 =20 nm, 60 nm and 100 nm and h= $1 \cdot 10^{-8}$ cm^{-1}.

The apparent reaction rate can be calculated from the degradation curve. Dividing the reaction rate by the OH – concentration, one obtains the apparent rate constant. The slope of the theoretical rate constant is *tan* $\alpha = 0.8$. The slope of the observed apparent rate constant differs from these of the theoretical rate constant and thought to be caused by different influence factors – chemical reaction, evaporation, penetration of the OH radicals into the agglomerate and diffusion as far as the diffusivity is a constant.

All of the experiments lie on a straight line in a double logarithmic diagram. The high rate constants of $1 \cdot 10^{-9}$ $cm^{-3} s^{-1}$ to $1 \cdot 10^{-10}$ $cm^{-3} s^{-1}$ at low levels of OH can be explained by the influence of the compound evaporation from the agglomerate surface and chemical reaction. The influence of the evaporation on the effective rate constants in the middle range from $1 \cdot 10^{-10}$ $cm^{-3} s^{-1}$ to $1 \cdot 10^{-11}$ $cm^{-3} s^{-1}$ is lower. In this range there is an influence of the chemical reaction and of diffusion of the substance to the reaction zone and weaker but not negligible influence of evaporation. The main processes defining the effective rate constant smaller than $1 \cdot 10^{-11}$ $cm^{-3} s^{-1}$ are the diffusion and the chemical reaction.

Some of the experiments are not used to fit the individual rate constant. These are the experiments with ozone. During those experiments the degradation rate of the reference hydrocarbons was not typical for the degradation by OH radicals and with ozone they can not

react. It was mentioned above that other radicals might have been produced by the synthesis of ozone in the electrical discharge of the ozone generator (Sorbios GSG 001.2).

The reaction rate of Aldrin is shown in fig. 8.26. The reaction rate calculated directly from the experiments does not increase with increasing OH concentration. Only the experiments made at the FhG institute at Hannover shorten the Aldrin lifetime (fig. 8.26 above). The experiments made at low OH concentration (fig. 8.26 below) fluctuate strongly. From the upper diagram it must be concluded that some of the experiments do not shorten the Aldrin life-time and some others do it. Absence of chemical reaction could be assumed for the do-not-shorten-life-time experiments, even if products were measured during the experiments. The experiments were interpreted by the mathematical model defined in chap. 6.

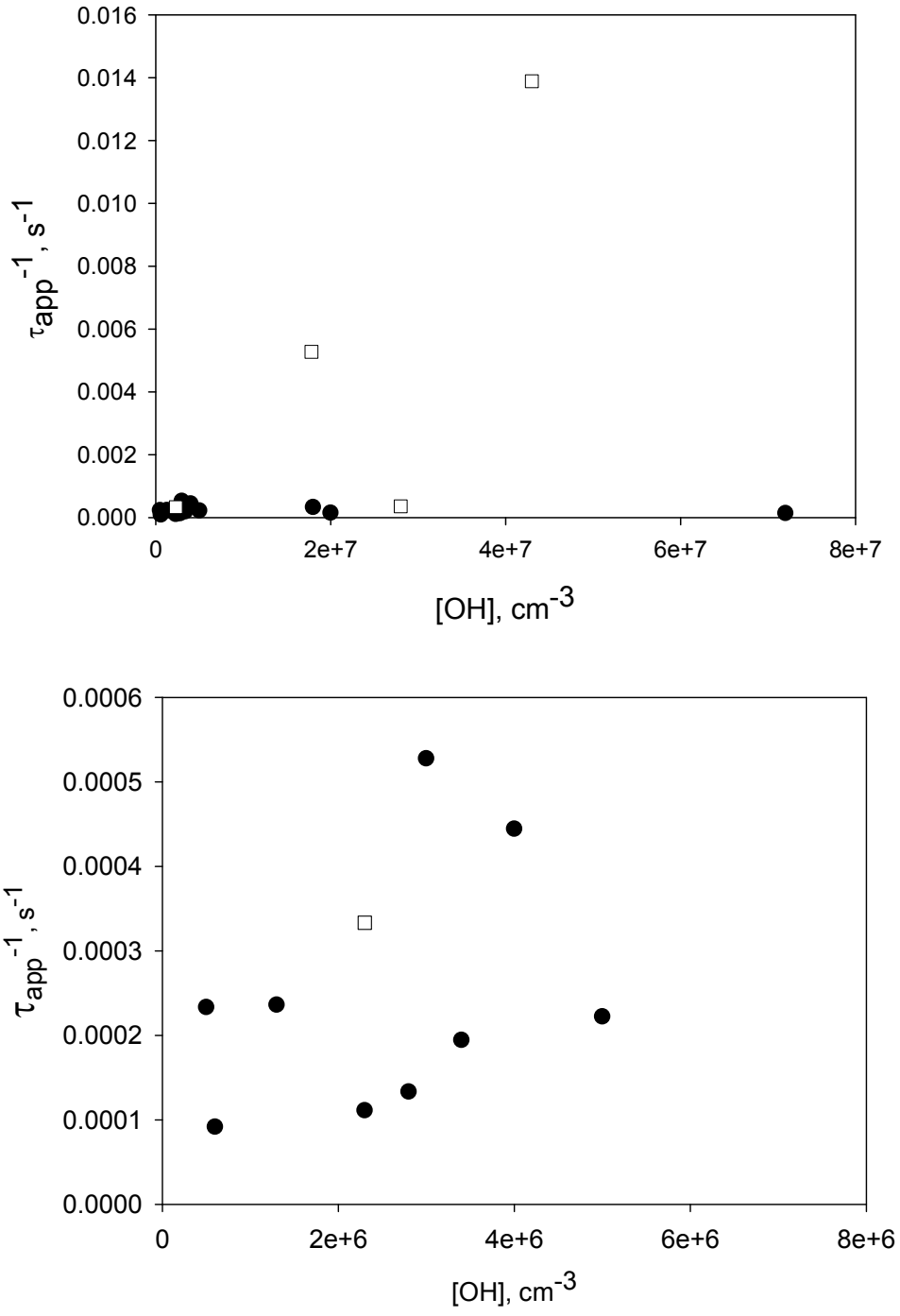

Fig. 8.26 The lifetime of Aldrin vs. the OH concentration. The lifetime was calculated for every experiment. The experiments marked with squares were made at the FhG at Hannover.

9. Results from the fitting procedure

In chapter 6 a mathematical procedure was defined which approximates the chemical reaction of a semivolatile substance with OH radicals penetrating into the porous, coated agglomerates.

In chapter 8.5 the structure of the agglomerates was evaluated.

In this chapter the estimated parameters will be presented. The relations between the estimated parameters will be explained. Beyond the related parameters there are physical processes, which may cause different effects during an experiment.

Lifetime, diffusivity, evaporation constant and penetration depth were fitted. The diffusivity, the lifetime and the penetration depth were estimated from the experiments at -10°C. The evaporation constant, the lifetime and the penetration depth were fitted from the experiments at 2°C. The evaporation was neglected for the experiments at -10°C. The estimated diffusivity was used for the fitting procedure of the 2°C experiments.

At the beginning a relation between the free mean path of the OH radicals and the pore structure of the agglomerates was calculated to explain the finite penetration depth of the OH radicals. The free mean path of the OH radical can be calculated assuming the diameter of an oxygen molecule. The calculated free mean path is $\lambda = 50\ nm$. The free mean path is two times longer than the mean pore diameter. The tortuosity level is high. The OH radical reacts with Aldrin molecules after some collisions with the walls. It is unrealistic to assume an infinite penetration depth in this case.

The mathematical model (eq. 6.4) was programmed in Easy Fit. The equation was solved by the method of the lines. The equation was solved with 51 lines. The solution of the equation for one of the experiments (Aldrin 34) is presented in fig. 9.1. The lines at constant radial distance are the solution of the equation by this method (fig. 9.1 above). The solution equation with the estimated parameters is compared with the experimental points (fig. 9.1 below).

The initial values of the unknown parameters were put into the model. Then the model parameters were specified. The description of the first and second derivatives was made by a five point formula, using an implicit method for solving the equation system. The numerical method for the fitting procedure is SQP – Newton – Gauss method. The other parameters: norm, iterations etc. were automatically chosen.

The program allows it to import the measurement points from an Excel file. The most important result is the linear increase of the reaction rate with increasing OH concentration (fig. 9.2). The inverse lifetime at low OH concentration tends to zero. Some of the fitted lifetimes at low OH concentrations fluctuate strongly.

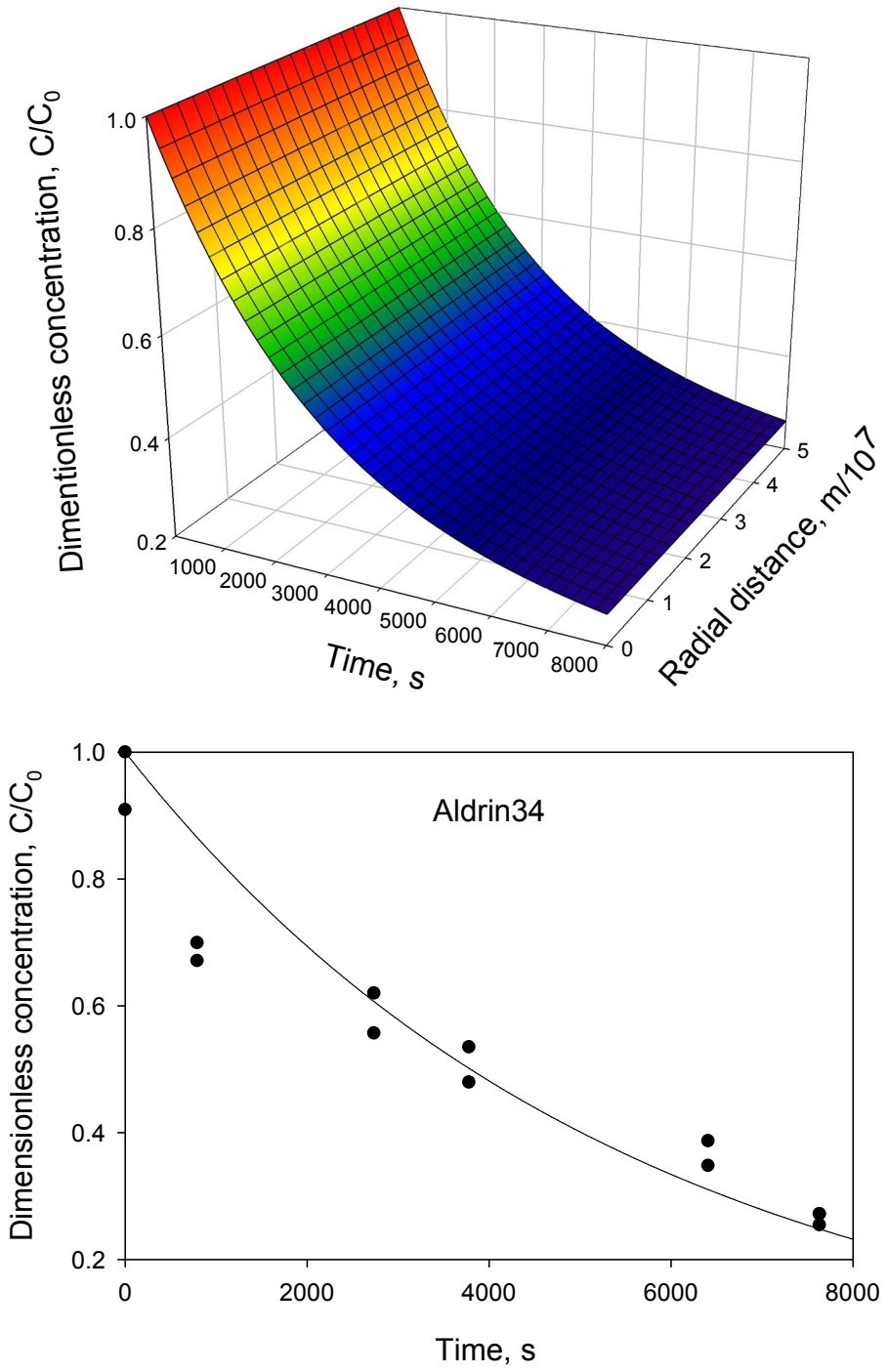

Fig. 9.1 Solution of the partial differential equation with the estimated parameters from experiment Aldrin 34 (above). Comparison of the solution with the experimental points (below).

In the figure the uncertainties of the OH measurement are shown as horizontal error bars. The uncertainty is calculated in chapter 8.13 and it is estimated to be19 %. The uncertainty sources are discussed on p. 26.

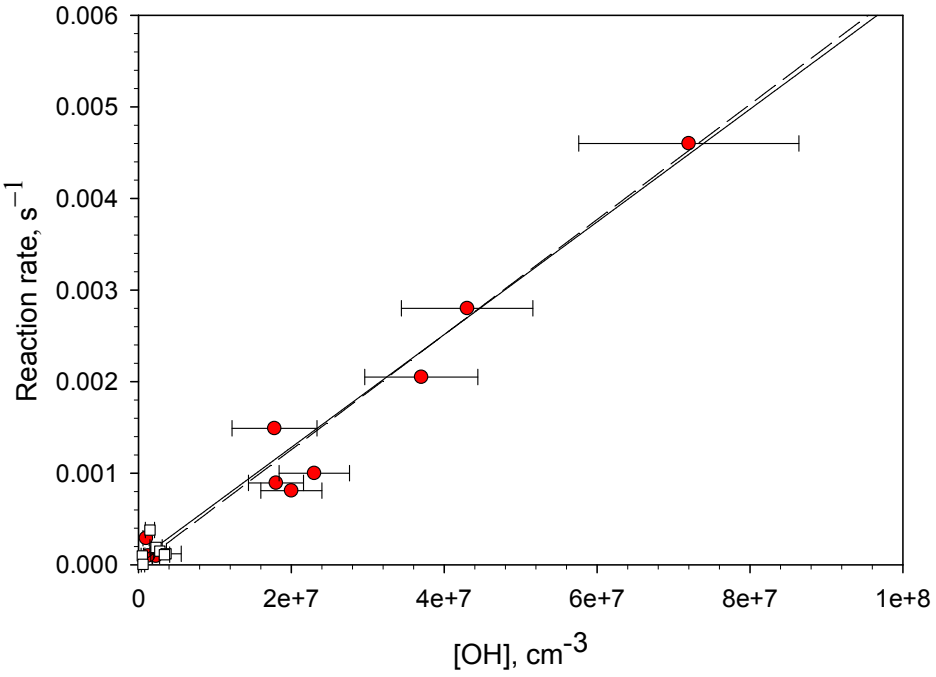

Fig. 9.2 Fitted inverse lifetime from the experiments increases linearly with increasing OH concentration. The horizontal error bar indicates the uncertainties caused by the OH evaluation.

There is other experimental problem. The test substance degrades as fast as the hydrocarbons. That means that the experiment takes about 1.3 h. During the experiment 4 filter samples for the calculation of the aerosol mass and 6 filter samples for the measurement of the concentration must be taken.

The weight of the filter for the calculation of the aerosol mass must be enough for a measurement with an electronic scale. So the sampling duration is longer. The test substance may fully degrade and only 3 or 4 samples for concentration measurement are available. Such an experiment is not useful and must be repeated.

In fig. 9.3 the penetration depth is shown vs. OH – concentration. The penetration depth increases exponentially to a maximum with increasing OH – concentration.

The OH radicals penetrate into the agglomerate and normally do not reach the centre. The penetration depth is very low at low OH – concentrations. The reaction zone is restricted to the first few nanometers in the agglomerates. The substance diffuses from the core to the reaction zone, and the OH radicals can not penetrate deeply into the agglomerate.

The evaporation constant was calculated for the experiments made at 2°C, omitting the experiments made at -10°C (fig. 9.4).

There may be two competing processes, the chemical reaction and the evaporation. The Aldrin molecules react with the OH radicals and can not leave the agglomerate surface. Therefore the evaporated portion decreases with increasing OH radicals. There are two ranges. The first range in from $2 \cdot 10^{-15}$ to $2 \cdot 10^{-12}$ cm s^{-1} includes the evaporation constants estimated from the experiments at 2°C, where are evaluated evaporation constants are sparse (circles in fig. 9.4). The second range from $2 \cdot 10^{-16}$ to $5 \cdot 10^{-16}$ cm s^{-1} includes the evaporation constants estimated from the experiments at minus 10°C. The evaporation constant decreases with the decreasing temperature (the squares in fig. 9.4).The evaluated evaporation constants are sparse. The estimated values are influenced by the others parameters.

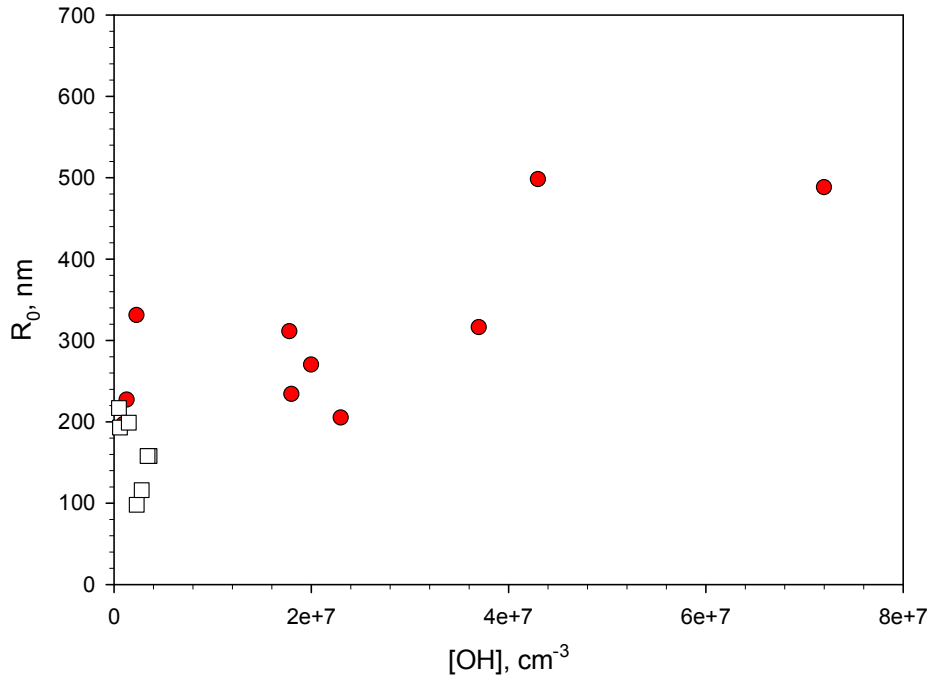

Fig. 9.3 The penetration depth of the OH radicals into the agglomerates was fitted for every experiment.

The goodness of the estimated parameters can be evaluated from a comparison of fig. 9.2, fig. 9.3 and fig. 9.4. At the low OH concentration the reaction rate is close to zero, i.e. the lifetime is long. The OH radicals penetrate only a few nanometers into the agglomerates. The Aldrin molecules evaporate from the surface. Conversely at high OH concentrations the lifetime is short, and the OH radicals penetrate deep into the agglomerate but not to the agglomerate centre, and the molecules react with OH radicals instead of evaporating.

The rate constant k_{OH} can be calculated by eq. 7.2. The calculated rate constants are shown in fig. 9.5.

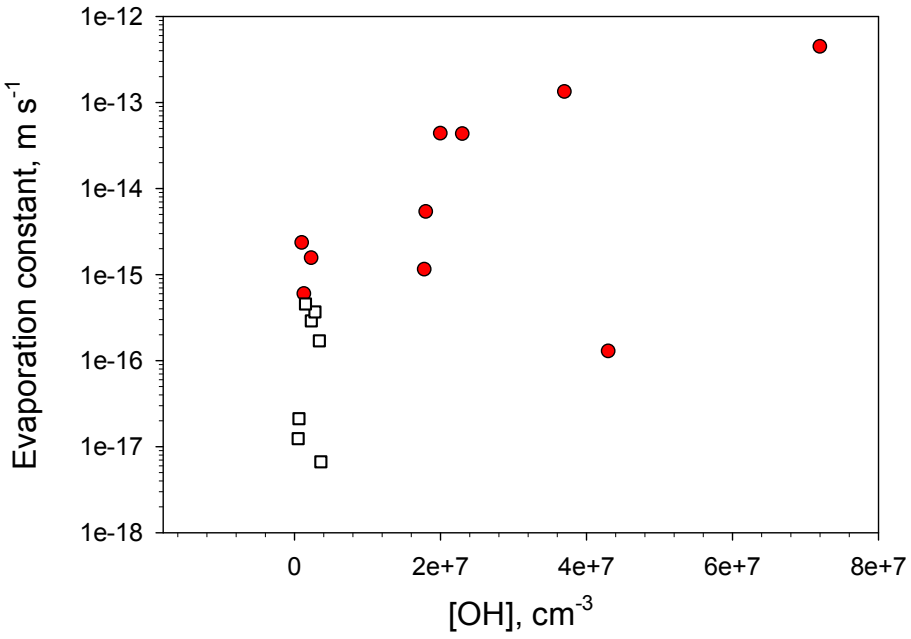

Fig. 9.4 The evaporation constant is plotted vs. the OH concentration.

It was not clear how to evaluate these results. This figure is actually derived from fig. 9.2. The estimated inverse lifetime can be described by a linear polynomial

$$\tau^{-1} = a + b \bullet [OH] \text{ , } s^{-1}. \quad \textbf{(9.1)}$$

On the other hand if [OH] → 0, then $\tau^{-1} \rightarrow 0$. The overall rate constant k_{OH} is calculated by

$$k_{OH} = \frac{\tau^{-1}}{[OH]} = \frac{a}{[OH]} + b, \; cm^{-3}s^{-1}. \quad \textbf{(9.2)}$$

The calculated individual rate constants can be approximated by an inverse first order polynomial.

In both equations we can assume that $a \approx 0$. Equation (9.1) and (9.2) transform in

$$\tau^{-1} = b \bullet [OH] \text{ and} \quad \textbf{(9.3)}$$

$$k_{OH} = b. \quad \textbf{(9.4)}$$

From this interpretation it can be concluded that in fig. 9.2 the overall rate constant k_{OH} is the slope of the curve and in fig. 9.5 is the constant b of the regression equation.

The estimated lifetime was evaluated by eq. 9.1 and 9.3. The resulting equations are

$$\tau^{-1} = (5.2 \pm 5) \cdot 10^{-5} + (\underline{6.2 \pm 1}) \cdot 10^{-11}) \bullet [OH] \quad R^2 = 0.98 \quad \textbf{(9.5)}$$

and

$$\tau^{-1} = 0 + (\underline{6.3 \pm 1.1)\cdot 10^{-11}}) \bullet [OH]. \quad R^2 = 0.97 \qquad \textbf{(9.6)}$$

In the both cases the estimated points were not weighted, employing the program SigmaPlot 8.0. The axes intercept is near zero according to eq. 9.1. The slope *b* is identical from calculation by eq. 9.1 or eq. 9.3. Both equations are shown in fig. 9.2. They overlap completely.

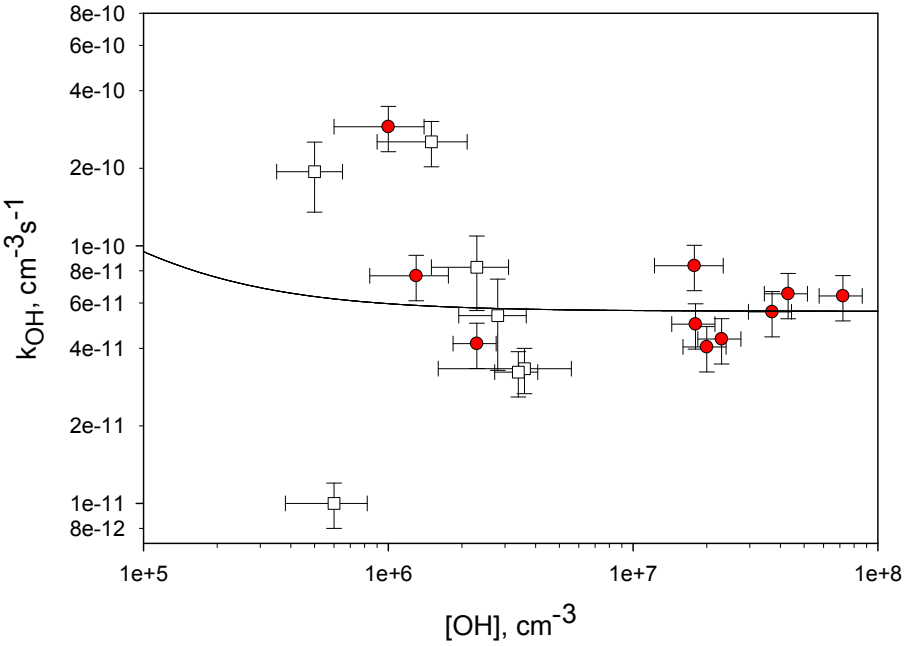

Fig. 9.5 The individual rate constants were fitted by a first order polynomial.

The individual rate constants were fitted (eq. 9.7) according to eq. 9.2.

$$k_{OH} = \underline{(5.1 \pm 1.0)\cdot 10^{-11}} + \left(\frac{1.3\cdot 10^{-5}}{[OH]}\right), \text{ cm}^{-3}\text{s}^{-1}. \qquad \textbf{(9.7)}$$

The calculated OH rate constants are sparser when the OH concentration is low. As we see in chapter 6.5, the observed OH rate constant and the true OH rate constant are close to each other when the OH concentration is high. This implies a fitting of the function with a statistical weight of $1/y^2$. As expected, the equation describes well the OH rate constants by the high OH concentration. The OH rate constant from eq. 9.2 agrees well with the OH rate constant calculated in eq.(9.5) and eq. (9.6). The evaluation of the OH rate constants by eq. (9.4) is not reliable because of the sparse OH rate constants at low OH concentration.

The diffusivity was estimated from the experiments at -10°C. The diffusivity can also be calculated by eq. 6.2. The Abraham solution parameters were estimated with the program ADME Boxes 3.0, Absolv (Pharma Algorithms, 2005).

The calculated diffusion coefficient is $D_{eff} = 3.71 \cdot 10^{-11}\ cm^2 s^{-1}$. The estimated diffusion coefficient is $D_{eff} = (4.6 \pm 2.2) \cdot 10^{-11}\ cm^2 s^{-1}$. Both diffusion coefficients are in good agreement.

Comparison will be made between the results before and after the fitting procedure, and the result of the fitting will be described.

At the first the reaction rate is compared in fig. 9.6

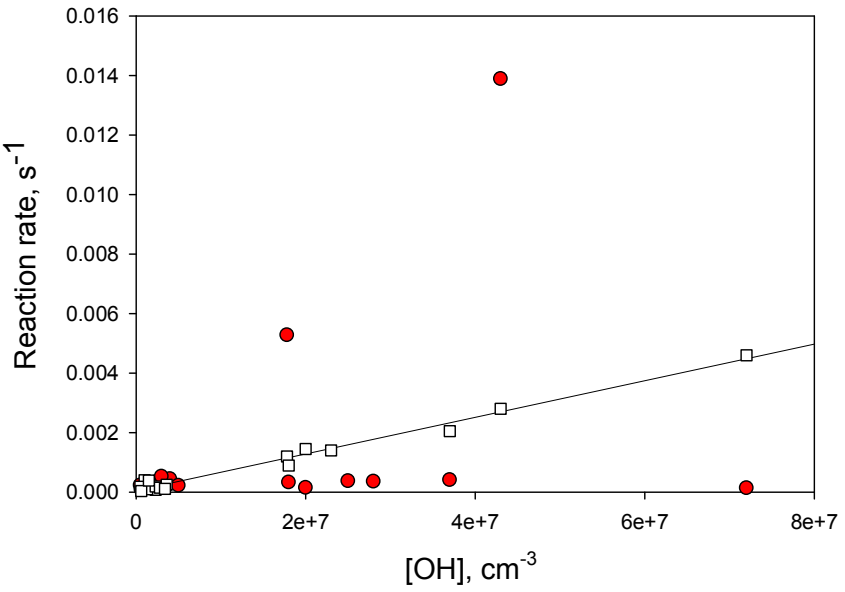

Fig. 9.6 Comparison between apparent reaction rate (●) and the evaluated reaction rate (□), delivering a slope of $6 \times 10^{-11} cm^3 s^{-1}$.

The uncorrected data are sparse. The data are corrected by the linear function from the OH concentration. The most important role plays the different penetration depth of the radicals as far as the evaporation constant is independent of the OH concentration.

In fig. 9.7 the apparent and OH rate constants are shown.

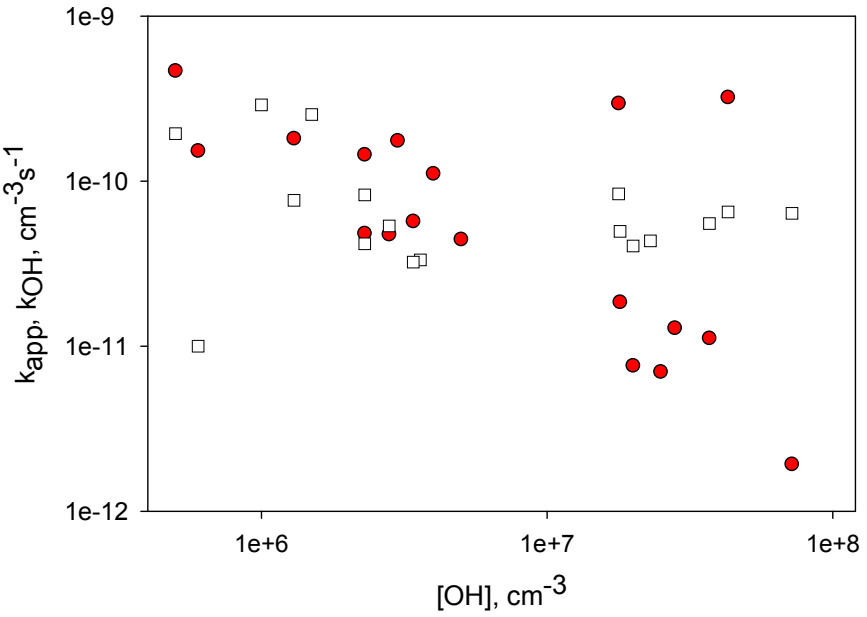

Fig. 9.7 Comparison between the apparent (●) and the OH rate constant (□), delivering a mean value of $9x10^{-11}cm^3s^{-1}$ for the OH rate constant. The discrepancy is only minor and is caused by the data at low OH.

The dependency of the rate constant on the OH concentration is corrected for the apparent rate constant at low OH concentration as well as the apparent constants at high OH concentration.

10. Reaction with Ozone

Three experiments were made to investigate the reactivity of ozone with Aldrin. Ozone was produced by a Sorbios GSG 001.2 ozonizer. The chamber was fed for different periods of time depending on the desired final ozone concentration. The ozone concentration varied during the experiments. The three experiments are compared in fig. 10.1.

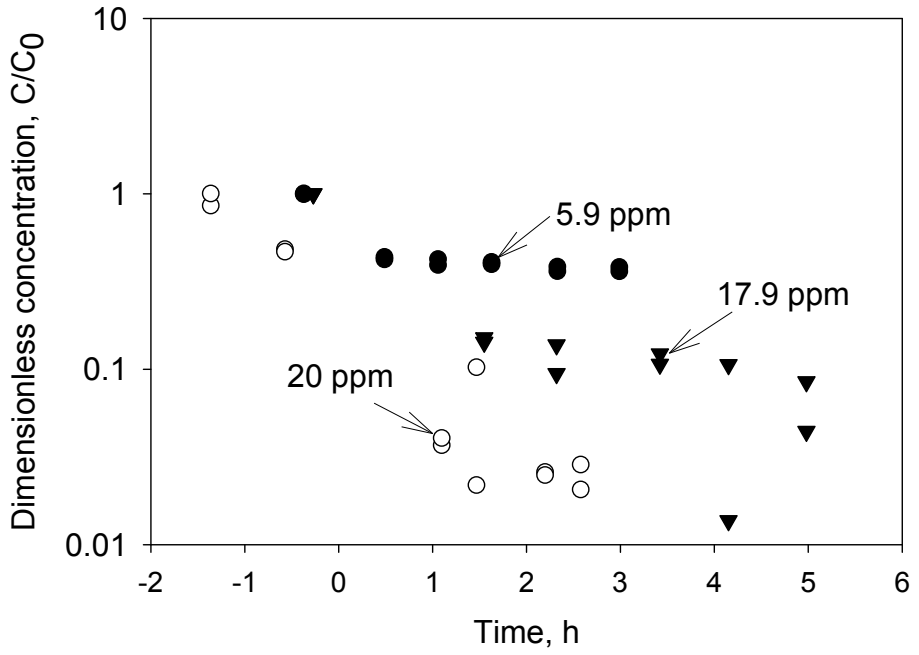

Fig. 10.1 Comparison between Aldrin 16 (●), Aldrin 22 (▼), Aldrin 17 (○). The smog chamber was fed with ozone for different time periods, shortest - Aldrin 16, where the maximum concentration is 5.9 ppm and longest - Aldrin 17, where the maximum concentration was 20 ppm.

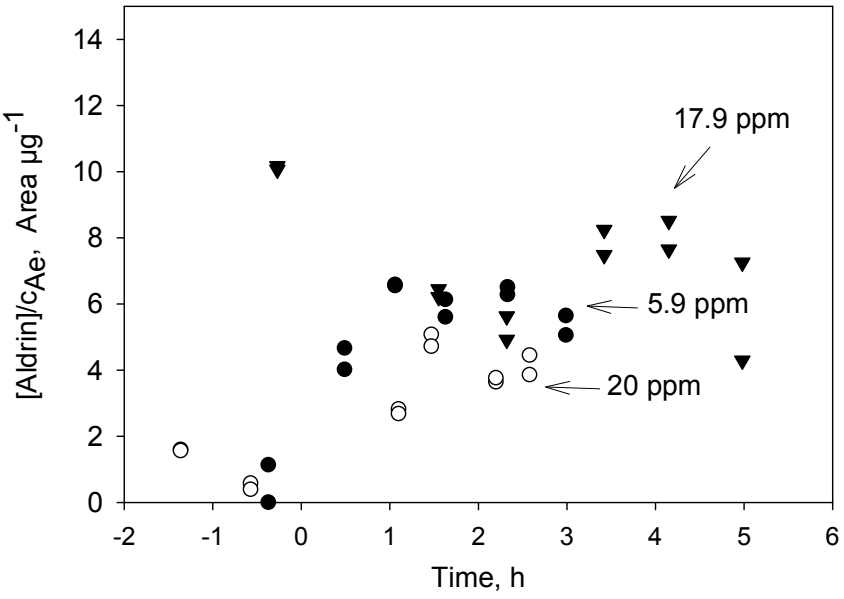

Fig. 10.2 Dieldrin concentration profile in Aldrin 16 (●), Aldrin 22 (▼), Aldrin 17 (○).

The shortest duration of the chamber feeding with ozone was in experiment Aldrin 16 and longest in Aldrin 17. The maximum ozone concentration during the experiments was 5.9, 17.9 and 20 ppm. The feeding duration influenced the Aldrin concentration. The substance and the reference hydrocarbons were degraded very quickly during the chamber feeding. When the feeding was stopped the concentration of Aldrin and reference hydrocarbons (with correction for the dilution) was constant.

The degreasing Aldrin concentration correlates with the formation of Dieldrin (fig. 10.2). There is not clear correlation between ozone concentration and Dieldrin formation/degradation. The Dieldrin concentration is constant after the feeding.

11. Analysis of the products from the chemical reaction

In this chapter the method used for the identification of the reaction products will be explained. The concentration of Aldrin and the products on the Aerosil sample taken from the smog chamber was too small to be analyzed by GC-MS. A rotary evaporator was used for carrying out the chemical reaction on larger quantities of sample. The samples were analyzed by GC-ECD at the first. The products were found to be identical with those measured in the smog chamber. Dieldrin and Photoaldrin were identified as reaction products. The substances were formed simultaneously.

11.1. Used material and facilities

The concentrations of the compounds in the aerosol samples were too small to identify them directly by GC-MS. The samples were produced in separate experiments and analyzed by a quadrupole GC – MS instrument (5890 Series II and MSD 5970, Hewlett Packard) with the following parameters: a 15 m column (DB-5HT, J&W scientific, 0.25 mm inner diameter, 0.1 µm film thickness, 1 µl injection volume, 300°C injector temperature, 340°C transfer line temperature, 1ml/min He as carrier gas, temperature program: start temperature: 50°C, temperature rate: 25.0 °C/min, final temperature: 250 °C, hold for 5.50 min, rate: 5.5 °C/min, final temperature: 300 °C, hold for 5.0 min.
Aerosil 380 and glass balloons (SiO_2 GeFa Verbundwerkstoffe) were used as carrier. The properties of Aerosil were discussed above. The size distribution of glass balloons is shown in the appendix. The maximum of the particle size distribution is at 75 µm. The particles are non-porous and have a very small surface area (approximately 0.15 m^2/ g assuming the bulk density of the material is 1 kg/m^3).
The glass balloons were coated by the same procedure as Aerosil. Methylnitrite was used as OH precursor. A quartz bulb (500 ml) was used for the experiments. The light source consisted of 4 fluorescent lamps (Philips TL29D16, 16 W each).

11.2. Carrying out the test

The coated powder (approx. 0.2 g) was weighed on an electronic scale. The powder was put into the quartz flask, that was sealed with paraffin foil. Gaseous methyl nitrite between 3 and 14 cm^3) was injected and the flask was sealed again. The rotary evaporator was turned on and then the lamps. Samples of 1 mg of the powder were taken for analysis

after 20 – 30 min reaction time. The powder was immersed in 6 ml of n-hexane. The sample was concentrated to 1 ml and extracted by treating it for 3 min in an ultrasonic bath and centrifuging 5 min before analysis. The extract was analyzed by GC-ECD and/or GC-MS.

11.3. Photolysis of Aldrin

The photolysis of Aldrin was investigated in the smog chamber at the beginning, but the experiments with the rotary evaporator allow to analyze bigger substance amounts and to detect smaller product amounts.

The coated microballoons powder was exposed for 18 hours to the irradiation and analyzed. The same sample was exposed to OH radicals and was analyzed again. ECD chromatograms are shown in fig. 10.1.

The first peak at a retention time of 8 min is Aldrin. There is no indication for photolysis of Aldrin, comparing of the solid line (the sample before irradiation) and the dashed line in fig. 10.1. The Dieldrin and Photoaldrin peaks were expected at 8.9 min and 9.1 min. There are two substances in very low concentration. The peak at 9.5 min is a contamination with constant concentration. A big powder sample was extracted to detect other substances except Aldrin (see fig. 10.2). The signal from the Aldrin is much stronger than the upper detection limit of ECD (500 mV).

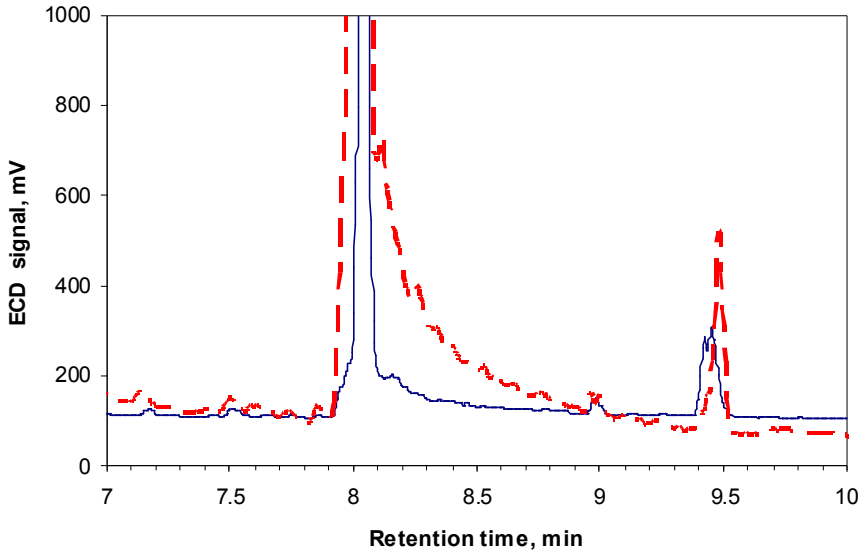

Fig. 11.1 Photolysis of Aldrin and chemical reaction with OH radicals. The Aldrin standard solution (solid line) is compared with the Aldrin extract after the irradiation (dashed line).

The powder amount in both measurements was large in order to detect any products. The powder amount can be observed from the Aldrin peak. It is very wide, and there was one small peak at 9 min. Dieldrin was detected in the non-irradiated and in the irradiated sample and also in the experiments in the smog chamber in the sample before the experiment start.

11.4. Products formation and instability

The Aldrin, Dieldrin and Photoaldrin peaks were identified by GC-MS. The first peak is Aldrin. The second peak at 7.4 min is Dieldrin. The third peak at 7.6 min is Photoaldrin.

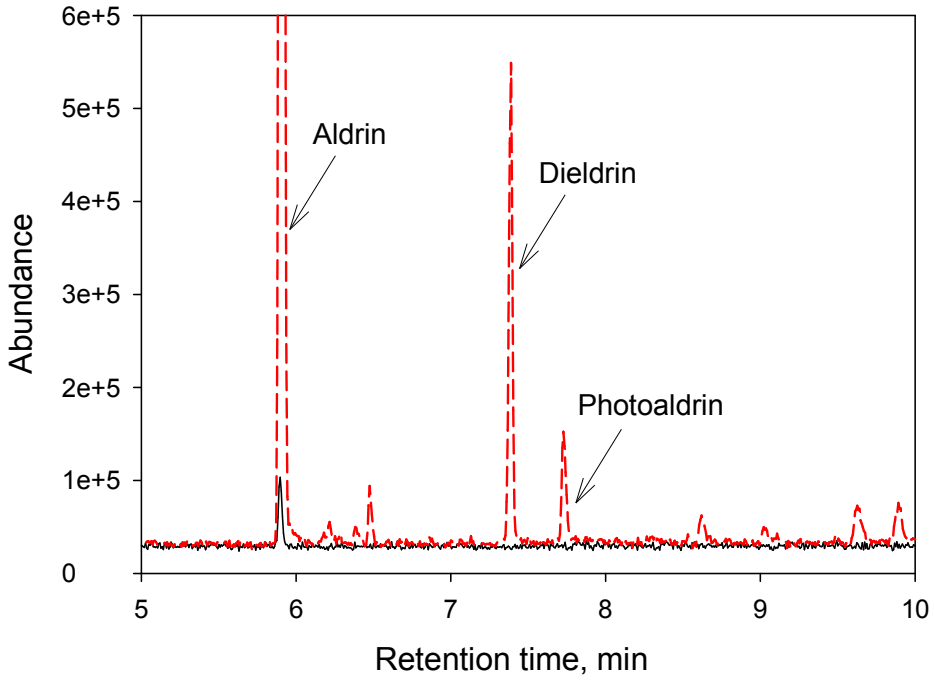

Fig. 11.2 Comparison of the chromatograms of the Aldrin standard solution (solid line) and extracted solution after chemical reaction (dashed line). The Aldrin peak is at 5.9 min, the Dieldrin peak is at 7.4 min and the Photoaldrin peak is at 7.8 min.

Two products, Dieldrin and Photoaldrin, were formed after the chemical reaction (dashed line in fig.11.2). The figure shows also the peak of the Aldrin standard (solid line). The GC-ECD and GC-MS measurements confirm that the same products were produced in the smog chamber and in the experiments with the rotary evaporator.

The mass spectrum of Aldrin is shown in fig. 11.3 and the mass spectrum of Dieldrin in fig. 11.4. Both mass spectra were found in the NIST library.

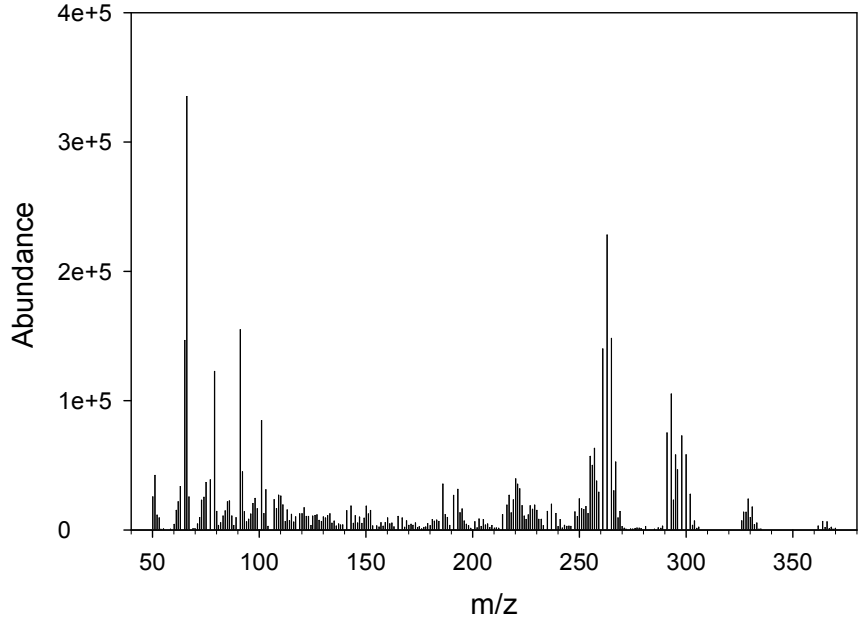

Fig. 11.3 Mass spectrum of Aldrin.

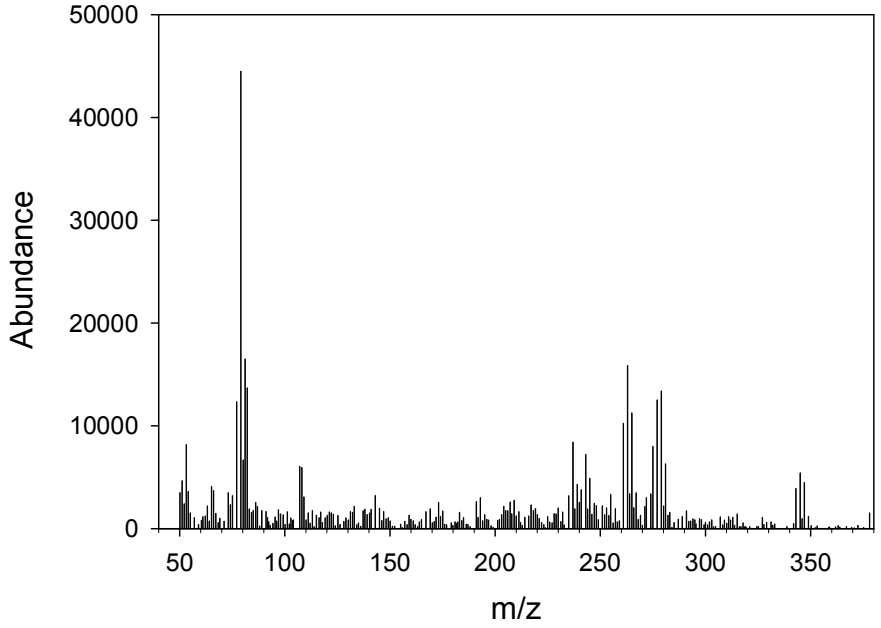

Fig. 11.4 Mass spectrum of Dieldrin.

A mass spectrum of Photoaldrin (Onuska and Comba, 1975) is shown in fig. 11.5., and the mass spectrum of the substance, that was identified as Photoaldrin, is shown in fig. 11.6. The structure of both spectra appears to be similar, besides the stronger noise in the Photoaldrin mass spectrum (fig. 11.6).

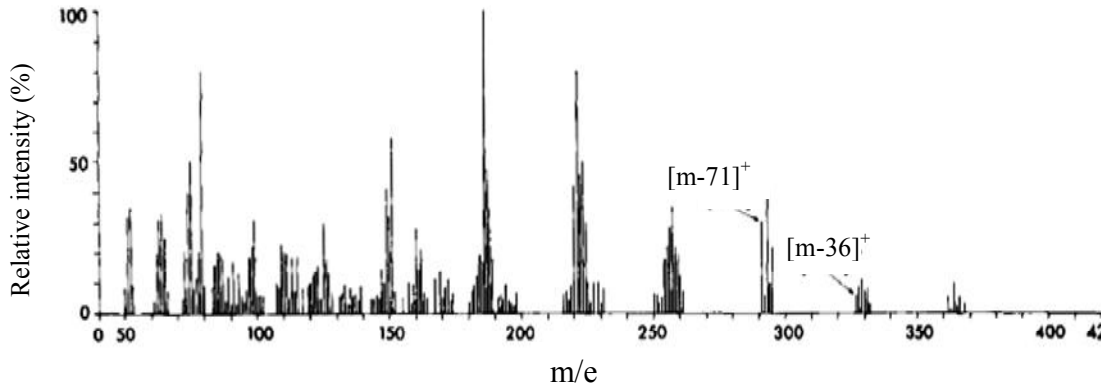

Fig. 11.5 Mass spectrum of Photoaldrin standard (mol. wt 362).

The problems with the analysis of Photoaldrin were connected with its instability. The sample was analyzed immediately after the degradation experiment and shown in fig 11.7. The sample was analyzed on the next day again and four days later.

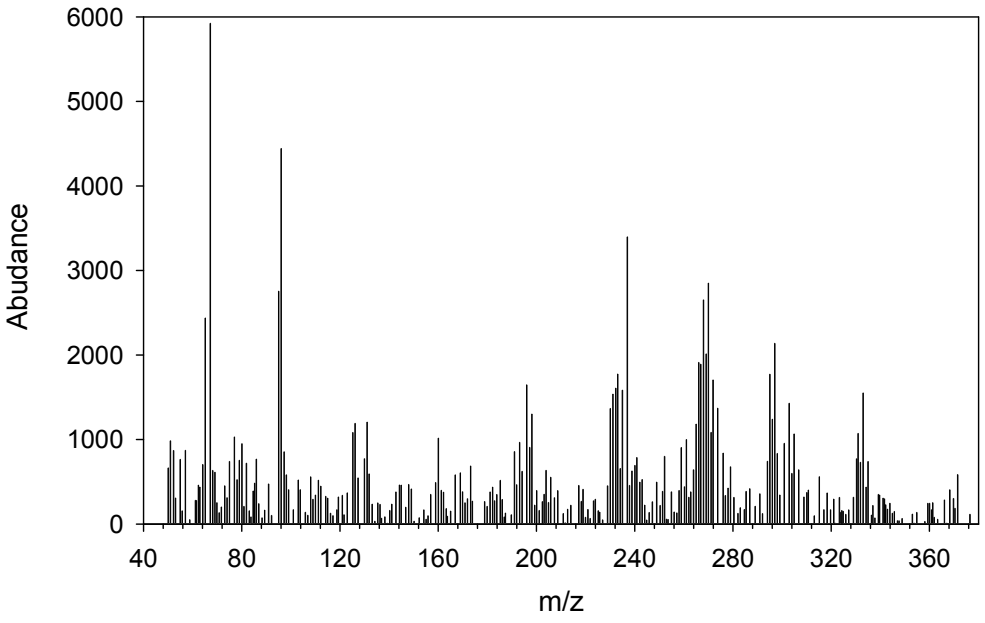

Fig. 11.6 Mass spectrum of the peak identified as Photoaldrin in this work.

The Photoaldrin concentration (at 9.1 min) is nearly constant in the first two measurements. The concentration of Photoaldrin is lower comparison to the Aldrin peak (8 min) and Dieldrin (9.2 min). Its instability makes it very difficult to identify it with the available devices.

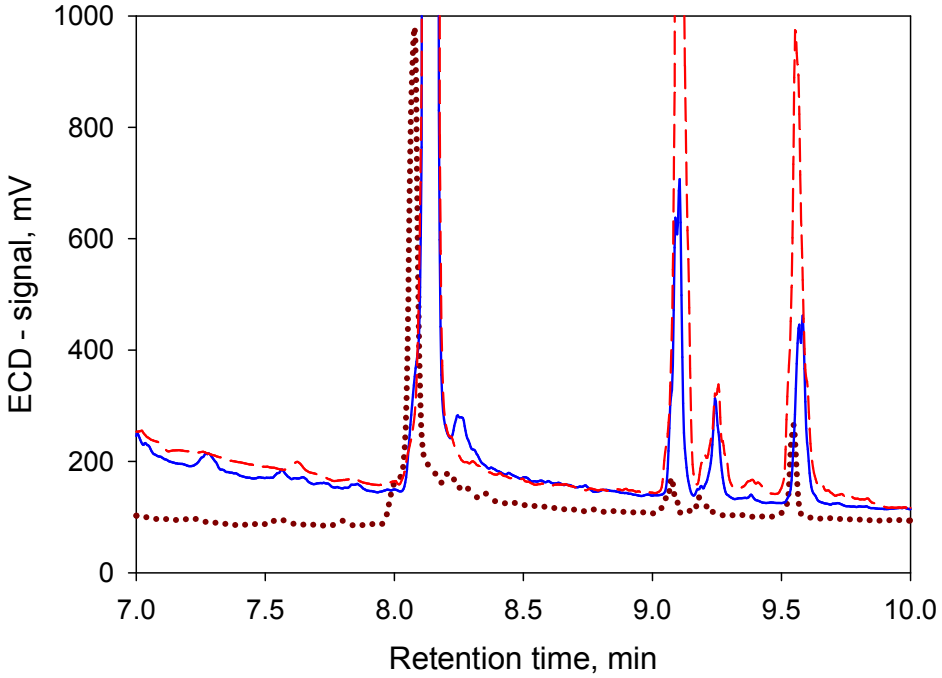

Fig. 11.7 The measurements present the instability of Photoaldrin. Measurement at the 01.02. – the dashed curve, measurement at the 02.02. – the solid curve, measurement at 06.02. – the dotted curve.

12. Discussion

In this chapter some conclusions are drawn concerning the chemical processes on porous media supporting the model developed and of results presented in this work. In the first part the degradation experiments, the product formation and dynamics and also the structure of the agglomerates are critically discussed. Then a procedure to study chemical degradation on porous media is proposed, which can provide a better understanding of the chemical processes.

The dimensions of the smog chamber require the availability of temperature gradients between the top and the bottom of the chamber and also between the wall and the chamber centre. The temperature gradient causes an intensive air mixing in the chamber. Operating the chamber at 2°C, the temperature was measured at four sites on the bottom centre and wall, then on the top centre and wall. The temperature difference was bigger (Δt = -2.7°C on the bottom and Δt = -1.1°C on the top) when the smog chamber was irradiated i.e. the mixing in the chamber was more intensive. The temperature gradient was lower (Δt = -1.3°C on the bottom and Δt = -0.8°C on the top) when the smog chamber was not irradiated i.e. the mixing in this case was slower. The same temperature gradients were measured at -10°C.

The substance loss during the coating procedure was measured. Aldrin was extracted from the carrier (Aerosil) and analyzed by GC-ECD. The measured concentration after the extraction was approx. 10 % higher than the input concentration. The solvent (n-hexane) may evaporate during the preparation procedures. The loss of the substance was measured when the carrier was glass micro balloons. The losses were 15 % because of the smaller surface of the microballoons.

After the experiments, the bottom foil of the chamber was washed with n-hexane. The solution was then analyzed to evaluate the sedimented agglomerates. About half of the agglomerate mass was deposited on the bottom foil during 10 experiments.

A small amount of Dieldrin was detected in the coating with Aldrin. The Dieldrin concentration was irregular in the powder analyzed before the experiment beginning and no aging was detected. The Dieldrin/Aldrin ratio was around 5%, scattering up to 20%. An inhomogeneous distribution of the compounds may have caused these ambiguous results.

The agglomerate structure was investigated from FESEM (Field Emission Scanning Electron Microscopy) images taken by the Fraunhofer-Institute IKTS at Dresden, where the agglomerate samples were prepared by immersion into epoxy resin and ion beam etching before field emission scanning. Samples were taken at the beginning of the experiment, when the agglomerate size distribution is representative for the experiment start. A portion of 57 % of the evaluated agglomerates were found to have diameters between 200 and 600 nm. This size

distribution shifts to larger agglomerates during the experiment. Measurements made with a differential mobility analyser at Bayreuth correlate well with the evaluation of the FESEM images.

The pore size distribution was also evaluated from the FESEM images, where 64 % of the evaluated pores were found to have diameters between 10 and 40 nm.

The pore size plays an important role in the penetration of the OH radicals into the agglomerates. The pore size is smaller than the mean free path of the OH radicals. The OH radicals collide often with the pore walls, which are coated with Aldrin and react to the products.

The evaporation of adsorbed compounds was reduced by lowering the temperature, and experiments were made at two different temperatures: 2°C and -10°C. One of the possible pathways of Aldrin is photolysis. Experiments without OH production were made in the smog chamber and in the rotating evaporator. No products are found, even after 18 h irradiation in the rotary evaporator. Some authors report for photolysis of Aldrin. The products, which were expected, are Photoaldrin, Dieldrin and Photodieldrin (Crosby and Moilanen, 1974; Draper and Crosby, 1984) The lamps used by these authors may have had high UV radiation. The described experimental conditions were possibly not environmentally relevant.

OH radicals were produced by the photolysis of methyl nitrite and by reaction of a mixture of ozone with hydrazine. OH radicals were also produced during the irradiation of the smog chamber. Hydrogen peroxide was not appropriate for the producing of OH radicals since the sun simulator spectrum overlaps only poorly with the spectrum of hydrogen peroxide.

The Aldrin degradation and respectively the product yield increase with increasing OH exposure. There is no influence of the temperature on the degradation rate.

Dieldrin and Photoaldrin were detected as reaction products. Both products were formed simultaneously. Photoaldrin is more reactive than Dieldin. Photoaldrin was formed faster and degraded faster than Dieldrin. Dieldrin was more stable than Photoaldrin. Both products were analyzed by GC-MS. Aldrin and Dieldrin were identified from the NIST library, where photoaldrin was not included. A reference spectrum was reported by Onuska and Comba (1975). Both mass spectra are quire similar. A simultaneous formation of Dieldrin and Photoaldrin was reported also by Onuska and Comba (1975).

These authors report also the simultaneous formation of the both products. Only the photolysis of Aldrin was investigated, and the spectrum of their lamps has a larger UV radiation. According to the data of NIST app. 40-48% of the total energy is in the ultraviolet portion of the spectrum, 40-43% in the visible, the balance in the infrared (NIST, 2007).

In the present study, the OH concentration was calculated from the degradation rate of three reference hydrocarbons, and their OH rate constants were used for the calculation. The uncertainty of the rate constants causes a corresponding uncertainty of the calculated OH concentration. The slope of the curve determined from the hydrocarbon peak areas and the recommended rate constant was used to evaluate the uncertainty of the calculated OH concentration individually for every experiment. The deviation from the mean value was calculated. In general, the uncertainty is low when three hydrocarbons are used in the experiment. The uncertainty is higher when only two hydrocarbons are used. The typical estimated uncertainty was 18 %.

The kinetics of Aldrin degradation could be estimated directly using a first order rate law. Comparing all experiments there is a dependence of the OH rate constant on the OH concentration although the OH rate constant of Aldrin should be independent of the OH concentration. Then the structure of the agglomerates was taken into account. The porosity of the agglomerate, the diffusivity of the compound, the adsorption of the compound on the solid surface, the evaporation of the substance from the agglomerate surface, the chemical reaction and the penetration of the OH radicals into the agglomerates were taken into account in a mathematical model to describe the concentration decrease of Aldrin.

The evaporation was neglectable for experiments made at -10°C. The solid/air partition constant influences the adsorption of Aldrin on the Aerosil (quartz glass) surface. In general, there is a strong decrease of the adsorption with increasing temperature. For volatile organic compounds the adsorption constant changes by a factor of 2-3 per 10°C (Goss, 2004). Aldrin is a semivolatile substance and the adsorption constant changes by a factor of 4-5 per 10°C.

The porosity was evaluated from FESEM images of the agglomerates. The porosity is approximately 50 %.

There were no experimental results before for Aldrin. The diffusivity, the lifetime, the evaporation and the OH penetration depth were estimated from the experiment.

The effective diffusivity was calculated to be $D_{eff,\,th} = 3.7 \cdot 10^{-11}\ cm^2 s^{-1}$ at T = 263 K and $D_{eff,\,th} = 4.0 \cdot 10^{-11}\ cm^2 s^{-1}$ at T = 275 K. These values correspond very well to the estimated diffusivity which is $D_{eff} = (4.6 \pm 2.2) \cdot 10^{-11}\ cm^2 s^{-1}$.

Both values agree well. The effective diffusivity of p-nitroanisole and trifluralin was calculated from experimental data for the adsorption constant (Balmer et al., 2000). The values are in the same range as the effective diffusion coefficient estimated in this work.

The reciprocal lifetime increases linearly with the OH concentration and the OH penetration depth increases with increasing OH concentration. The evaporation rate decreases with

increasing OH concentration. The estimated parameters are in agreement with the physical concept for the process. It was assumed that the OH rate constant is independent from the OH concentration. The second assumption is absence of reaction when no OH radicals are available. The assumption is fulfilled because of the absence of photolysis as a possible loss path. The value of the OH rate constant is $k_{OH} = (6.2 \pm 1.1) \cdot 10^{-11}\ cm^3 s^{-1}$. There are no other experimental data available in the literature for the degradation of Aldrin by OH. The OH rate constant at 298 K may also be calculated from structure/reactivity-relations using the computer program AOPWIN (EPISuite, 2000; Meylan and Howard, 1993). The theoretical value is calculated to be $k_{OH,\ th} = 6.3 \cdot 10^{-11}\ cm^3 s^{-1}$, in reasonable agreement with the experiment. It should be noted that the value is calculated for the gas-phase reaction and that it is based on addition of hydroxyl radicals to the double bond. The experimental value related to the heterogeneous reaction should be slower than the gas-phase reaction because of steric factors. The program has some further disadvantages since the intermolecular interactions can not be taken into account. The extrapolation of this method for compound classes not presented in the database used for its development is not recommended, as mentioned by Franklin et al. in the monograph of the SETAC (Klecka, 2000).

For the first time, experiments were performed in the cooled chamber with 4005 L volume at -10°C. The mathematical model was developed and used for the first time for the evaluation of experiments. Experiments with other substance are needed to validate the model and evaluation of the parameters.

13. Conclusions

A new cooled smog chamber with a volume of 3200 L.was installed at the University of Bayreuth. The temperature gradients were measured in the chamber, operating at a temperature of 2°C and -10°C. Mixing was provided by turbulence caused by the colder top and warmer bottom of the chamber: Operating the chamber at 2°C and -10°C, the temperature gradient between bottom centre and bottom wall was found to be Δt =-2.7°C in the irradiated chamber and Δt =-1.3°C without light source. The temperature gradient on the top between centre and wall was Δt =-1.1°C in the presence of irradiation and Δt =-0.8°C without irradiation.

Aldrin could be coated on highly disperse fused silica particles (Aerosil 380, Degussa) without losses. The foil of the chamber bottom was washed with n-hexane after 10 experiments. The solution was analyzed and Aldrin was detected. Approx. 50% of the sprayed Aldrin-coated particles in the chamber sediment on the bottom foil. Dieldrin traces were detected in the Aldrin powder. The concentration ratio between Aldrin and Dieldrin does not depend on the storage duration. The agglomerate structure was evaluated from images taken at the Fraunhofer-Institute IKTS at Dresden, where the agglomerate samples were prepared by immersion into epoxy resin and ion beam etching prior to taking images by FESEM (Field Emission Scanning Electron Microscopy). The maximum of the agglomerate size distribution was at a diameter of 300 nm. The porosity of the agglomerates is 50%. The maximum of the pore size distribution was at 20 nm.

Aldrin does not absorb light in the range of the sun simulator emission, and a photolysis of Aldrin is not possible with the used sun simulator. Degradation experiments of Aldrin with OH radicals were performed at 2°C and -10°C. Two transformation products were detected – Photoaldrin and Dieldrin. Additional experiments with coated microballoons produced sufficient amounts of both products for an identification by GC-MS.

The uncertainties of the OH radical calculation were evaluated from the experiments. The uncertainty of the calculations was about 19%.

The OH rate constant was fitted to the observations of the experiments, and a value of $k_{OH} = (6.2 \pm 1.1) \cdot 10^{-11}\ cm^3 s^{-1}$ was obtained. An effective diffusion coefficient was fitted to the experiments as well, leading to $D_{eff} = (4.6 \pm 2.2) \cdot 10^{-11}\ cm^2 s^{-1}$.

14. Summary

The persistence in the different compartments and in the atmospheric long-range transportation is important property of pesticides as representatives of the semivolatile substances. These compounds could be distributed dependent on the air pressure as well as the temperature - between gas and particle phase. In an aerosol smog chamber could be simulated the atmospheric degradation of airborne substances through hydroxyl radicals.

The smog-chamber was cooled on 2 and -10°C and the degradation kinetic of semivolatile substance (Aldrin) coated on fine quartz particles (Aerosil 380) was researched. The coated Aerosil was mixed with water in ration 1:1000 and the suspension was sprayed into the chamber. Fine agglomerates were formed during the spaying with mean diameter approximately 1 µm.

The precursors for the production of hydroxyl radicals were either reacting mixtures of hydrazine and ozone in absence of light source or photolysis of methylntrite. The concentration of hydroxyl radicals was varied over two powers of ten, from approximately $5 \cdot 10^5$ to $7 \cdot 10^7$ cm^{-3}. The concentration of that OH–radicals was calculated over the degradation rate of hydrocarbons (n-octane, n-hexane, 2,2,3-trimthylbutane, 2,2-dimethylbutane and 2,2,3,3-tetramethylbutane). The hydrocarbons were cryofocussed in a glass-coated steel capillary at -110°C (using liquid nitrogen and a magnetic valve to control the flow) and analyzed gas chromatographically.

Two products (Photoaldrin and Dieldrin) could be detected from the chemical reaction of Aldrin with hydroxyl radicals. A high concentration of the products were produced with additional experiments with coated Aerosil and glass balloons (d = 70 µm, unporous) and production of hydroxyl radicals from the methylnitrite photolysis in an irradiated rotating evaporator. The products were extracted from the carrier material and were identified with GC–MS. Photoaldrin was formed faster than Dieldrin and reacts also faster then Dieldrin.

The temperature gradient between the top and the bottom of the smog-chamber was measured. The temperature difference is important for the air mixing of the chamber content. In the presence of a light-source (the fluorescence lamps are under the the smog camber) the temperature difference is 1.0 °C and ensures a fast mixing in the chamber. This difference of the not irradiated chamber is about 0.3 °C and causes a insufficient mixing, that is noticeable through strong fluctuations of the aerosol density.

The structure of the aerosol agglomerates was imaged according to the ion etching method with FESEM (Field Emission Scanning Electron Microscopy) in the Fraunhofer-IKTS. The

imagines were evaluated in this work with the program “Lince”. A maximum of the agglomerate diameter was obtained by 0,5 µm. The pore size distribution has a maximum by approximately 20 nm diameter.

The life-time of Aldrin and respectively the rate constant of the reaction with hydroxyl radicals could be calculated directly from the experiments. The observed rate constant had a dependence on the OH–concentration in approaching form $3.5 \cdot 10^{-5} \cdot [OH]^{-0.88}$ (the function yields a straight in double logarithmic scale).

On the basis of the structure of the agglomerates, a mathematical model was applied from the literature in order to take the influence of the agglomerate structure into account. The observed concentration of Aldrin decreases because of the chemical reaction, the radial diffusion from the agglomerate center to the periphery and because of the evaporation of the substance from the agglomerate surface.

It is considered also in the model that the concentration of the hydroxyl radicals alters with the penetration in the agglomerate. The penetration depth can not be determined experimentally. This value, as well as the life-time and the diffusion coefficient could be estimated from the experiments. If the experiment is made by low temperature, the evaporation could be neglect. The evaporated part of Aldrin decreases with the increasing OH concentration.

The reciprocal life-time or the reaction rate of Aldrin increases linearly with the increase of the OH concentration. The rate constant of the reaction of Aldrin and OH radicals could be calculated from the reaction rate and the OH concentration. The OH rate constant was $k_{OH} = 6.2 \cdot 10^{-11} \pm 1.3 \cdot 10^{-11}$ $cm^{-3}s^{-1}$. The effective diffusion coefficient was calculated by -10°C and yielded a value of $D_{eff} = 4.6 \cdot 10^{-11} \pm 2.2 \cdot 10^{-11}$ cm^2s^{-1}.

15. Zusammenfassung

Die Persistenz in unterschiedlichen Kompartimenten und der atmosphärische Ferntransport sind wichtige Eigenschaften von Pestiziden als Vertreter der mittelflüchtigen Substanzen, die dabei – je nach Dampfdruck bzw. Temperatur - zwischen Gas – und Partikelphase verteilt werden können.

In einer Aerosol – Smogkammer kann man den atmosphärischen Abbau von partikelgebundenen Stoffen durch OH – Radikale simulieren.

Die Smogkammer wurde auf 2 und -10°C abgekühlt, und es wurden kinetische Untersuchungen eines mittelflüchtigen Stoffes (Aldrin) als dünne Belegung auf feinteiligem Quarzglas (Aerosil 380) durchgeführt. Das belegte Aerosil wurde als feine Aerosolpartikel in der Kammer versprüht und bildete dabei Agglomerate mit einem mittleren Durchmesser von ca. 1 µm.

Als Vorläufer für die Erzeugung von OH – Radikalen wurde entweder Methylntrit photolysiert oder es wurden reagierende Gemische von Hydrazin und Ozon bei Dunkelheit benutzt. Die Konzentration von OH – Radikalen wurde über zwei Zehnerpotenzen variiert, von ca. $5 \cdot 10^5$ bis $7 \cdot 10^7$ cm^{-3}. Die Konzentration der OH – Radikale wurde über die Abbaugeschwindigkeiten von Kohlenwasserstoffen (n-Octan, n-Hexan, 2,2,3-Trimethylbutan und 2,2-Dimethylbutan) bestimmt. Die Kohlenwasserstoffe wurden in einer glasbeschichteten Kapillare als Kühlfalle ausgefroren und gaschromatographisch analysiert.

Zwei Produkte (Photoaldrin und Dieldrin) der chemischen Reaktion von Aldrin mit OH – Radikalen konnten beobachtet werden. Für die Identifizierung wurden die Produkte mit zusätzlichen Experimenten mit belegtem Aerosil und Glaskugeln (d = 70 µm, unporös) und Erzeugung von OH – Radikalen aus Photolysierung von Methylnitrit in einem bestrahlten Rotationsverdampfer in größeren Konzentrationen erzeugt, aus dem Trägermaterial extrahiert und mit GC – MS nachgewiesen. Photoaldrin wurde schneller als Dieldrin gebildet und abgebaut.

Die Temperaturgefälle zwischen Boden und Deckel der Smogkammer, die maßgeblich für die Durchmischung des Kammerinhalts sind, wurden gemessen. Bei Anwesenheit einer Lichtquelle (die Leuchtstoffröhren befinden sich unter der Kammer) ist die Temperaturdifferenz 0.5 °C und sichert eine rasche Durchmischung in der Kammer. Die Temperaturdifferenz der unbelichteten Kammer ist kleiner als 0.1 °C und bewirkt eine mangelhafte Durchmischung der Kammer, die sich durch starke Schwankungen der Aerosoldichte bemerkbar macht.

Die Struktur der Aerosolagglomerate wurde nach Ionenstrahlätzen mit FESEM – (**F**ield **E**mission **S**canning **E**lectron **M**icroscopy) im Fraunhofer-IKTS abgebildet. Die Aufnahmen

wurden in dieser Arbeit mit dem Programm “Lince” ausgewertet. Ein Häufigkeitsmaximum der Agglomerate wurde bei 0,5 µm Durchmesser festgestellt. Die Porengrößenverteilung weist ein Maximum der Häufigkeit bei ca. 20 nm Durchmesser auf.

Die Lebensdauer von Aldrin bzw. die Geschwindigkeitskonstante der Reaktion mit OH - Radikalen konnte direkt aus den Experimenten bestimmt werden. Die so beobachtete Geschwindigkeitskonstante wies eine Abhängigkeit von der OH – Konzentration in annähernder Form $3{,}5 \cdot 10^{-5} \cdot [OH]^{-0{,}88}$ (die Funktion ergibt eine Gerade in doppellogarithmischer Darstellung) auf.

Aufgrund der Struktur der Agglomerate wurde ein mathematisches Modell aus der Literatur angewendet, um den Einfluss der Agglomeratstruktur zu berücksichtigen. Die beobachtete Konzentration von Aldrin nimmt wegen der chemischen Reaktion, der radialen Diffusion aus dem Zentrum der Agglomerate an die Peripherie und wegen der Verdampfung der Substanz von der Agglomeratoberfläche ab. Es ist auch im Modell berücksichtigt, dass sich die Konzentration der OH – Radikale mit dem Eindringen im Agglomerat ändert. Die Eindringtiefe kann nicht experimentell ermittelt werden. Dieser Wert, sowie auch die Lebensdauer und der Diffusionskoeffizient können angepasst werden. Wenn das Experiment bei tieferen Temperaturen durchgeführt wird, kann man die Verdampfung vernachlässigen. Der verdampfte Anteil von Aldrin nimmt mit zunehmender OH – Konzentration ab.

Die reziproke Lebensdauer oder die Reaktionsgeschwindigkeit von Aldrin nimmt linear mit der Zunahme der OH – Konzentration zu. Die Geschwindigkeitskonstante der Reaktion von Aldrin und OH – Radikalen lässt sich aus der Reaktionsgeschwindigkeit und der OH – Konzentration berechnen und beträgt $k_{OH} = (6.2 \pm 1.3) \cdot 10^{-11}$ $cm^{-3}s^{-1}$ festgelegt. Der effektive Diffusionskoeffizient wurde bei -10°C berechnet und ergab einen Wert von $D_{eff} = (4.6 \pm 2.2) \cdot 10^{-11}$ cm^2s^{-1}.

16. References

Ackerman, M. (1971). "UV-solar radiation related to mesospheric processes." *Mesospheric Models and Related Experiments*, G. Fiocco, ed., D. Reidel Publishing Company, Dordrecht, 149-159.

Atkinson, R. (1994). Gas-phase tropospheric chemistry of organic compounds, *M. N. J. Phys. Chem. Ref. Data*.

Atkinson, R. (2003). "Kinetics of the gas-phase reactions of OH radicals with alkanes and cycloalkanes." *Atmos. Chem. Phys.*, 3, 2233-2307.

Balmer, M., Goss, K.-U., and Schwarzenbach, R. (2000). "Photolytic transformation of organic pollutants on soil suface - an experimental approach." *Environ. Sci. Technol.*, 34, 1240 - 1245.

Behnke, W., Nolting, F., and Zetzsch, C. (1987). "The atmospheric fate of DI(2-ethylhexyl-)phthalate, adsorbed on various metal oxide model aerosols and on coal fly ash." *J. Aerosol Sci.*, 18, 849-852.

Behnke, W., Nolting, F., and Zetzsch, C. (1987a). "An aerosol smog chamber for testing abiotic degradation of compounds with low volatility." *Pesticide Science and Biotechnology*, 401-404.

Behnke, W., Nolting, F., and Zetzsch, C. (1987b). "A smog chamber study on the impact of aerosols on the photodegradation of chemicals in the atmosphere." *J. Aerosol Sci.*, 18, 65-71.

Brandenburger, U., Brauers, T., Dorn, H.-P., Hausmann, M., and Ehhalt, D. H. (1998). "In-situ measurement of tropospheric hydroxyl radicals by folded long-path laser absorption during the field campaign POPCORN in 1994." *J. Atmos. Chem.*, 31, 181-204.

Burin, G., Desi, I., Dobson, S., Goulding, R., Rahde, A. F., Kashyap, S. K., Takeda, M., and Raalte, H. G. S. V. (1989). Environmental health criteria 91, Aldrin and Dieldrin, *World Health Orgnization, Geneva*.

Chen, L., Mizukado, J., Kutsuna, S., Tokuhashi, K., and Sekiya, A. (2006). "Rate constants of gas-phase reactions of trans-cyc-$CF_2CF_2CHFCHF$- and cyc-$CF_2CF_2CH_2CHCl$- with OH radicals at 253-328 K." *Chemical Physics Letters*, 418, 519-523.

Crank, J. (1975). The Mathematics of Diffusion, *Oxford Science Publications*.

Crosby, D. G., and Moilanen, K. W. (1974). "Vapor-phase photodecomposition of aldrin

and dieldrin." *Archives of Environmental Contamination and Toxicology*, 2(1), 65-74.

DeMore, W. B., Sanders, S. P., Golden, D. M., Hampson, R. F., Kurylo, M. J., Howerd, C. J., Ravishankara, A. R., Kolb, C. E., and Molina, M. J. (1997). "Chemical kinetics and photochemical data for use in stratospheric modeling. Evaluating No.12." Jet Propulsion Laboratory, Rasadena, CA.

Dorn, H.-P., Neuroth, R., and Hofzumahaus, A. (1995). "Investigation of OH absorption cross sections of rotational trasition in the A^2S^+, u' = 0 <- X^2P, u" = 0 band under atmospheric conditions: implication for tropospheric long-path absorption measurements." *J. Geophys. Res.*, 100, 7397-7409.

dos Santos e Lucato, S. L. (2000). "Lence", TU Darmstadt, FB Materials Science, Ceramics Group.

Draper, W. M., and Grospy, D. G. (1984). "Solar photooxidation of pesticides in dilute hydrogen peroxide." *J. Agric Food Chem.*, 32, 231 - 237.

Euro Chlor (2003). “POPs & PBTs”. *Euro Chlor Press*

Fuller, E. N., and Giddings, J. C. (1965). "A Comparison of Methods for Predicting Gaseous Diffusion Coefficients." *J. Gas Chromatogr.*, 3, 222.

Fuller, E. N., Schettler, P. D., and Giddings, J. C. (1966). "New method for prediction of binary gas-phase diffusion coefficients." *Ind & Eng Chem*, 58, 18-27.

Fuller, E. N., Ensley, K., and Giddings, J. C. (1969). “Diffusion of halogenated hydrocarbons in helium. The effect of structure on collision cross sections.” *J. Phys. Chem.*, 73, 3679.

Gäb, S., Parlar, H., and Korte, F. (1974a). "Reactionen von Photodieldrin als Festkorper auf Glas und adsorbiert an Kiesel Gel Bei UV-Bestrahlung." *Chemosphere*, 5, 187-192.

Gäb, S., Parlar, H., Nitz, S., Hustert, K., and Korte, F. (1974b). "Photochemischer Abbau von Aldrin, Dieldrin und Photodiedrin als Festkorper im Sauerstoffstrom." *Chemosphere*, 5, 183-186.

Gäb, S., Saravanja, V., and Korte, F. (1975). "Contribution to the ecologic chemistzy. Pt. 73. Irradiation studies of aldrin and chlordene adsorbed on a silica gel surface." In: *Bull. Environ. Contam. Toxicol. ; Vol/Issue: 13:3*, United States, Pages: 301-306 306.

GeFa Verbundwerkstoffe, SiO_2 Glass balloons

Georgievskii, Y., and Pollak, E. (1994). "Semiclassical theory of activated diffusion." *Physical Review E*, 49(6), 5098 - 5102.

Goss, K.-U. (2004). "The air/surface adsorption equilibrium of organic compounds under ambient conditions." *Critical Reviews in Environmental Science and Technology*, 34, 339-389.

Goss, K.-U., and Schwarzenbach, R. P. (2002). "Adsorption of a diverse set of organic vapors on quartz, CaCO3 and α-Al2O3 at Different Relative Humidities." *Journal of Colloid and Interface Science*, 252, 31-41.

Gregg, S.J., and Sing K.S.W. (1982). "Adsorption, Surface Area and Porosity", 2nd ed., *Academic Press*

Grosby, D. G., and Moilanen, K. W. (1974). "Vapor-phase photodecomposition of aldrin and dieldrin." *Archives of Environmental Contamination and Toxilogy*, 2(1), 62-74.

Güsten, H. (1986). "Photocatalytic degradation of atmospheric pollutants on the surface of metal oxides." In: *Chemistry of Multiphase Atmospheric Systems*, W. Jaeschke, ed., Springer-Verlag.

Heard, D. E., and Pilling, M. J. (2003). "Measurement of OH and HO_2 in the troposhere." *Chem. Rev.*, 103, 5163-5198.

Höhn, S., and Obenaus, P. (2004). „Ionenpräparation von keramischen Pulvern und Grünkörpern für die hochauflösende Rasterelektronen –mikroskopie." *Prakt. Met. Sonderband*, 36, 299 - 303.

Holländer, W., Windt, H., and Bo, Y. (1995). "Reduced sticking upon brownian contact of submicrometer particles coated with an organic liquid." *Journal of Colloid and Interface Science*, 173, 478-485.

Hugo, P., and Koch H. (1979). "Production of porous alumina with defined bimodal pore structure", *Ger. Chem. Eng*., 2, 24-30

Hyland, R. W. (1975). "A correlation for the second interaction virial coefficients and enhancement factors for moist air." *J. Research NBS, A. Physics and Chemistry*, 79A, 551-560.

Jonson, M. F. L., and Stewart, W. E. (1965). "Pore structure and gaseous diffusion in solid catalyst." *Journal of Catalyst*, 4, 248-252.

Klecka, G., B. Boethling, J. Frankling, L. Grady, D. Graham, Ph. H. Howard, K. Kannan, R. J. Larson, D. Mackay, D. Muir, D. van de Meent. (2000). *Evaluation of Persistence and Long-Range Transport of Organic Chemicals in the Environment*, SETAC,

Knox, J., and McLaren. (1964). "A New Gas Chromatographic Method for Measuring Gaseous Diffusion Coefficients and Obstructive Factors." *L. Anal. Chem.*, 36, 1477 -

1482.

Krüger, H.-U. (2005). "Personal Communication, uli.krueger@uni-bayreuth.de." Bayreuth.

Krüger, H.-U., and Zetzsch, C. (2001). „Entwicklung eines Persistenz-Screeningverfahrens für den troposphärischen Abbau von mittelflüchtigen Pflanzenschutzmitteln durch OH-Radikale.“, *Report on the project UFOPLAN 200 67 406/03 to the Umweltbundesamt*

Leonard, C. (1989). Entwicklung eines UV-laserspektroskopischen Nachweisverfahrens für OH-Radikale und spektroskopische Untersuchungn an Spurengasen unter troposphärischen Bedingungen. Dissertation, Universität Hannover.

Lyman, W. J. (1990). *Chemical Property Estimation Methods*, American Chemical Society.

Meylan, W. M., and Howard, P. H. (1993). "Computer estimation of the atmospheric gas-phase reaction rate of organic compounds with hydroxyl radicals and ozone." *Chemosphere* 26, 2293-2299.

Molina, L. T., and Molina, M. J. (1981). "UV absorption cross section of HO_2NO_2 Vapor." *J. Photochem*, 15, 97-108.

Nicovich, J. M., and Wine, P. H. (1988). "Temperature-dependent absorption cross sections for hydrogen peroxide vapor." *J. Geophys. Res.*, 93, 2417–2421.

Nolting, F., Behnke, W., and Zetzsch, C. (1988). "A smog chamber for studies of the reactions of terpens and alkanes with ozone and OH." *J. Atmos. Chem.*, 6, 47-59.

Onuska, F. I., and Comba, M. E. (1975a). "Isolation and characterization of some methanonaphtalene photoproducts." *Biomedical Mass Spectrometry*, 2, 169-175.

Palm, W.-U., Millet, M., and Zetzsch, C. (1998) “OH Radical Reactivity of Pesticides Adsorbed on Aerosol Materials: First Results of Experiments with Filter Samples.” *Ecotoxicology and Environmental Safety*, 41, 36-43

Parlar, H., and Korte, F. (1977). "Photoreactions of cyclodiene insecticides under simulated environmental conditions, Review." *Chemosphere*, 10, 665-705.

European Parliament (2004). "Regulation (EC) No 850/2004."

Pharma Algorithms (2005). ADME Boxes

Pitts, J. N. J., Tuazon, E. C., Carter, W. P. L., Winer, A. M., Harris, G. W., Atkinson, R., and Graham, R. A. (1980). "Atmospheric chemistry of hydrazines: gas phase kinetics and mechanistic studies." Air Force Engineering Services Center, Tyndall AFB, FL.

Propp, W. A. (1998). "Graphite oxidation thermodynamics/reactions." Idaho National Engineering and Environmental Laboratory, Idaho.

Schiesser, W. E. (1991). *The Numerical Method of Lines*, Academic Press, New York, London.

Schittkowski, K. (2002). *Numerical data fitting in dynamical systems*, Kluwer Academic Publishers.

Schlosser, E., Bohn, B., Brauers, T., Dorn, H.-P., Fuchs, H., Häseler, R., Holzumahaus, A., Holland, F., Rohrer, F., Rupp, L. O., Siese, M., Tillmann, R., and Wahner, A. (2006). "Intercomparison of two hydroxyl radical measurement techniques at the atmosphere simulation chamber SAPHIR." *J. Atmos. Chem.*

Sircar, S., and Rao, M. B. (1990). "Estimation of Surface Diffusion Through Porous Media." *ALChE Journal*, 36(8), 1246 - 1254.

Sonntag, D. (1990). "Important new values of physical constants of 1986, vapour pressure formulations based on the ITS-90 and psychrometer formulas." *Z. Meteorol.*, 70(5), 340-344.

Takahashi, K., Takeuchi, Y., and Matsumi, Y. (2005). "Rate constants of the $O(^1D)$ reactions with N_2, O_2, N_2O and H_2O at 295 K." *Chemical Physics Letters*, 410, 196-200.

Tuazon, E. C., Carter, W. P. L., Atkinson, R., and Pitts, J. N. J. (1983). "The gas-phase reaction of hydrazine and ozone: a nonphotolytic source of OH radicals for measurements of relative OH radical rate constants." *International Journal of Chemical Kinetics*, 15, 619-629.

Tuazon, E. C., Carter, W. P. L., Brown, R. V., Atkinson, R., Winer, A. M., and Pitts, J. N. (1982). "Atmospheric reaction mechanisms for amine fuels." *Rep. ESL-TR-82-17*, Air Force Engineering and Service Center, Tyndall AFB, FL.

Tuazon, E. C., Carter, W. P. L., Winer, A. M., and Pitts, J. N. (1981). “Interactions between diesel emissions and gaseous copollutants in photochemical air pollution: Some health implications.” *Environ. Sci. Technol.*, 15, 823.

U.S. Environmetal Protection Agency (2000). AOPWIN (see Meylan and Howard (1993)

UNEP (2005). “Ridding the world of POPs: A guide to the Stockholm convention on persistent organic pollutants.” *United Nations Environment Programme (UNEP) Chemicals*.

Ung, A. Y.-M. (1974). "The photolysis of water vapor at 1470 A. H_2 production in the primary process." *Chemical Physics Letters*, 28, 603-607.

Vaghjiani, G. L., and Ravishankara, A. R. (1989). "Adsorption cross section of CH_3OOH, H_2O_2 and D_2O_2 vapors between 210 and 365 nm at 297 K." *J. Geophys. Res.*, 94, 3487-3492.

Wheeler, A. (1950). "Reaction Rates and Selectivity in Catalyst Pores" *Advanced in Catalyst, Vol. 3*. Academic Press, New York.

Zetzsch, C. (1991a). "Experimental simulation of the influence of aerosols on atmospheric chemistry." *Pollution Atmospherique*, 33S, 89-105.

17. Appendix 1

LIST OF IMPORTANT ABBREVIATIONS

Latin Symbols

Symbol	**Meaning**	**Unit**
a_v	dilution factor	L L^{-1}
C	concentration	mol L^{-1}
C_0	concentration of the outside medium	mol L^{-1}
C_s	surface concentration	mol L^{-1}
d	diameter	m
D_{air}	diffusion coefficient in air	$cm^2 s^{-1}$
D_{eff}	effective diffusion coefficient	$cm^2 s^{-1}$
D_k	diffusion coefficient	$cm^2 s^{-1}$
h	evaporation constant	cm s^{-1}
$[HC]$	hydrocarbon peak area	mVs
k	reaction rate	s^{-1}
K^{abs}	solid/air partition constant	kg kg^{-1}
k_{app}	apparent OH rate constant	cm^{-3} s^{-1}
k_B	Bolzmann constant	J K^{-1}
k_{OH}	OH rate constant	cm^{-3} s^{-1}
L	length	m
m	weight	kg
n	normal direction	-
N_A	Avogadro's number	mol^{-1}
$[OH]$	concentration of OH radicals	cm^{-3}
$\overline{[OH]}$	average concentration of OH radicals	cm^{-3}
$[Ozone]$	ozone concentration	cm^{-3}
P	pressure	Pa
$[PFH]$	perfluorhexane peak area	mVs
R	gas constant	Pa m^3 mol^{-1} K^{-1}
r	radius or radial distance	m
R_0	penetration depth of the hydroxyl radicals in the	m

	agglomerate	
R_f	retardation factor	-
t	time	s
T	temperature	K
$t_{1/2}$	half-life	s
V	volume	L
V_{dil}	dilution volume	L
x	distance	m

Greek symbols

Symbol	**Meaning**	**Unit**
α	evaporation constant	cm s^{-1}
Δ	diference	-
ε	porosity	m^3 m^{-3}
λ	free mean path	m
ρ_{bulk}	carrier density	kg m^{-3}
σ	absorption cross section	cm^{-2}
τ	tortousity	-
τ^{-1}	reciprocal lifetime	s^{-1}
$\bar{\upsilon}$	mean molecular speed	m s^{-1}
v	wind velocity	m s^{-1}

Superscripts

′	interpolated value

Subscripts

a	outer diameter
Ae	aerosol
f	filter
i	inner diameter or time point
j	species
norm	normalized value
p	particle or compound
0	value at the experiment start

st	standard value

18. Appendix 2

Aldrin 11

Filter	Time, h	[Aldrin]	[Mirex]	$C_{Aldrin,norm}$	av	∫[OH] dt	V_{de}, L	V_f, L	$C_{Aldrin,Ae}$	m_f, µg	c_{Ae}, mg/m^3
0	-0.18	691.60	4782.00	691.60	1.02	0.00	75.00	50.00	17.41	39.72	0.79
1	0.58	410.50	5462.00	359.39	1.04		125.00	50.00	10.27	35.00	0.70
2	1.55	189.90	5823.00	155.95	1.06		200.00	50.00	5.26	29.67	0.59
3	2.18	282.20	5296.00	254.81	1.08		235.00	70.00	6.80	37.48	0.54
4	3.05	423.60	5370.00	377.22	1.11		325.00	110.00	7.48	50.43	0.46
5	3.90	483.50	4900.00	471.86	1.13		385.00	120.00	9.89	47.69	0.40
W0	-0.38				1.01	0.00	25.00	50.00		37.80	0.76
W1	0.85				1.06		175.00	50.00		37.50	0.75
W2	2.62				1.09		270.00	70.00		34.90	0.50
W3	4.30				1.15		440.00	110.00		39.00	0.35
0	-0.18	691.20	4782.00	691.20	1.02	0.00	75.00	50.00	17.40	39.72	0.79
1	0.58	418.40	5460.00	366.44	1.04		125.00	50.00	10.47	35.00	0.70
2	1.55	260.80	5567.00	224.02	1.06		200.00	50.00	7.55	29.67	0.59
3	2.18	271.40	5055.00	256.74	1.08		235.00	70.00	6.85	37.48	0.54
4	3.05	468.10	4893.00	457.48	1.11		325.00	110.00	9.07	50.43	0.46
5	3.90	501.00	5629.00	425.61	1.13		385.00	120.00	8.92	47.69	0.40

Aldrin 12

Filter	Time, h	[Aldrin]	[Dieldrin]	[Mirex]	$C_{Aldrin,norm}$	$C_{Dieldr,norm}$	a_V	$\int[OH]\,dt$	V_{del}, L	V_f, L	$C_{Aldrin,Ae}$	$C_{Dieldrin,Ae}$	m_f, µg	c_{Ae}, mg/m^3
W0	-0.4						1.01	0.00E+00	25.00	50.00			46.20	0.92
W1	1.32						1.06	1.32E+00	175.00	50.00			27.20	0.54
W2	3.35						1.12	1.24E+10	355.00	70.00			41.60	0.59
W3	5.23						1.22	1.94E+10	630.00	100.00			43.70	0.44
0	-0.2	845	124.5	5629	845	124.5	1.02	0.00E+00	75.00	50.00	18.8	2.8	44.93	0.90
1	0.84	130	372	6004	130	372	1.04	3.11E+09	125.00	50.00	3.3	9.3	39.95	0.80
2	1.82	8.1	299	5900	8.1	299	1.07	6.73E+09	225.00	50.00	0.2	8.5	35.17	0.70
3	2.82	7	323	5658	7	323	1.09	1.04E+10	285.00	70.00	0.2	7.4	43.81	0.63
4	3.88	1.7	280	5668	1.7	280	1.14	1.44E+10	430.00	80.00	0.0	6.5	43.12	0.54
5	4.88	0.0	0.0	0.0	0.0	0.0	1.18	1.81E+10	525.00	110.00	0.0	0.0	52.18	0.47
0	-0.2	773	123.1	5198	773	123.1	1.02	0.00E+00	75.00	50.00	17.2	2.7	44.93	0.90
1	0.84	128	329	5228	128	329	1.04	3.11E+09	125.00	50.00	3.2	8.2	39.95	0.80
2	1.82	9.1	334	6284	9.1	334	1.07	6.73E+09	225.00	50.00	0.3	9.5	35.17	0.70
3	2.82	10.8	335	6083	10.8	335	1.09	1.04E+10	285.00	70.00	0.2	7.6	43.81	0.63
4	3.88	3.8	281	5631	3.8	281	1.14	1.44E+10	430.00	80.00	0.1	6.5	43.12	0.54
5	4.88	0.00	0.00	0.00	0.00	0.00	1.18	1.81E+10	525.00	110.00	0.0	0.0	52.18	0.47

Aldrin 12 OH

Time hh:mm	t, h	[PFH]	[DMB]	[Hexan]	$[PFH]_{norm}$	$[DMB]_{norm}$	$[Hexan]_{norm}$	dt, h	$[OH]_{DMB}$	$[OH]_{Hexan}$
11.58	0.00	136.00	62.20	54.00	136.00	62.20	54.00	0.50	2.65E+10	4.03E+09
12.31	0.50	141.00	62.90	55.40	136.00	60.67	53.44	0.45	-8.33E+09	1.11E+10
12.58	0.95	134.00	60.20	51.30	136.00	61.10	52.07	0.52	-5.45E+09	9.48E+09
13.29	1.47	131.30	59.30	49.00	136.00	61.42	50.75	0.62	1.16E+10	-5.24E+09
14.06	2.08	124.10	55.30	47.10	136.00	60.60	51.62	0.53	2.14E+10	3.72E+09
14.38	2.62	119.00	51.90	44.70	136.00	59.31	51.09	0.65	5.69E+09	1.67E+08
15.17	3.27	119.60	51.80	44.90	136.00	58.90	51.06	0.48	-8.53E+09	1.34E+10
15.46	3.75	110.20	48.10	40.00	136.00	59.36	49.36	0.73	-2.43E+07	-2.69E+09
16.30	4.48	111.80	48.80	41.00	136.00	59.36	49.87	0.43	-8.93E+09	-2.09E+08
16.56	4.92	100.30	44.10	36.80	136.00	59.80	49.90	0.48	7.31E+09	6.55E+09
17.25	5.40	102.80	44.90	37.10	136.00	59.40	49.08			

Time hh:mm	t, h	$\int[OH]dt_{DMB}$	$\int[OH]dt_{Hexan}$	$\overline{\int OHdt}$	$\overline{[OH]}$
11.58	0.00	1.33E+10	2.02E+09	7.63E+09	4.24E+06
12.31	0.50	9.50E+09	7.00E+09	8.25E+09	3.82E+05
12.58	0.95	6.69E+09	1.19E+10	9.29E+09	5.60E+05
13.29	1.47	1.38E+10	8.66E+09	1.13E+10	8.82E+05
14.06	2.08	2.53E+10	1.06E+10	1.80E+10	3.49E+06
14.38	2.62	2.90E+10	1.08E+10	1.99E+10	8.14E+05
15.17	3.27	2.48E+10	1.72E+10	2.10E+10	6.75E+05
15.46	3.75	2.48E+10	1.53E+10	2.00E+10	-3.77E+05
16.30	4.48	2.10E+10	1.52E+10	1.81E+10	-1.27E+06
16.56	4.92	2.45E+10	1.83E+10	2.14E+10	1.93E+06

Aldrin 13

Filter	Time, h	[Aldrin]	[Dieldrin]	[Mirex]	$C_{Aldrin,norm}$	$C_{Dieldr,norm}$	a_V	$\int[OH]\,dt$	V_{del}, L	V_f, L	$C_{Aldrin,Ae}$	$C_{Dieldrin,Ae}$	m_f, µg	c_{Ae}, mg/m^3
W0	-0.33						1.01	0.00E+00	25.00	50.00			62.10	1.24
W1	0.92						1.06	4.39E+09	175.00	50.00			55.60	1.11
W2	2.62						1.12	1.25E+10	365.00	70.00			62.70	0.90
W3	4.20						1.22	2.00E+10	635.00	110.00			75.60	0.69
0	-0.12	438.10	152.70	4676.00	438.10	152.70	1.02	0.00E+00	75.00	50.00	7.13	2.48	61.46	1.23
1	0.72	246.50	259.30	5336.00	216.01	227.23	1.04	3.43E+09	125.00	50.00	3.85	4.05	56.12	1.12
2	1.46	74.30	384.70	5240.00	66.30	343.29	1.07	6.96E+09	230.00	60.00	1.09	5.63	60.99	1.02
3	2.25	79.10	476.10	5168.00	71.57	430.77	1.10	1.07E+10	295.00	70.00	1.10	6.63	64.96	0.93
4	3.02	41.00	620.10	5176.00	37.04	560.20	1.15	1.44E+10	440.00	80.00	0.56	8.46	66.22	0.83
5	3.80	63.80	663.30	5382.00	55.43	576.29	1.18	1.81E+10	530.00	100.00	0.74	7.68	75.04	0.75
0	-0.12	468.20	164.70	5074.00	431.47	151.78	1.02	0.00E+00	75.00	50.00	7.02	2.47	61.46	1.23
1	0.72	243.40	261.00	5226.00	217.78	233.53	1.04	3.43E+09	125.00	50.00	3.88	4.16	56.12	1.12
2	1.46	79.20	413.80	5256.00	70.46	368.14	1.07	6.96E+09	230.00	60.00	1.16	6.04	60.99	1.02
3	2.25	91.60	495.20	5381.00	79.60	430.32	1.10	1.07E+10	295.00	70.00	1.23	6.62	64.96	0.93
4	3.02	37.00	568.20	5249.00	32.96	506.17	1.15	1.44E+10	440.00	80.00	0.50	7.64	66.22	0.83
5	3.80	62.00	597.40	4601.00	63.01	607.14	1.18	1.81E+10	530.00	100.00	0.84	8.09	75.04	0.75

Aldrin 13 OH

Time hh:mm	t, h	[PFH]	[DMB]	[Hexan]	$[PFH]_{norm}$	$[DMB]_{norm}$	$[Hexan]_{norm}$	dt, h	$[OH]_{DMB}$	$[OH]_{Hexan}$	$\int[OH]dt_{Hexan}$
13.09	0.00	104.80	44.60	35.70	104.80	44.60	35.70	0.30	1.77E+10	1.22E+10	5.24E+09
13.29	0.30	105.60	44.50	35.30	104.80	44.16	35.03	0.47	-1.67E+10	5.44E+09	-2.57E+09
13.57	0.76	106.40	45.50	35.10	104.80	44.82	34.57	1.63	1.26E+10	6.00E+09	1.80E+10
15.35	2.40	117.40	48.30	36.80	104.80	43.12	32.85	0.53	-3.90E+09	-8.72E+09	1.59E+10
16.07	2.93	112.10	46.30	36.00	104.80	43.28	33.66	0.37	1.34E+10	1.12E+10	2.08E+10
16.29	3.30	110.70	45.30	34.80	104.80	42.89	32.95	0.42	1.60E+10	1.51E+10	2.75E+10
16.54	3.71	112.10	45.30	34.10	104.80	42.35	31.88	0.33	-6.75E+10	-2.67E+10	5.03E+09
17.14	4.05	102.00	43.00	32.50	104.80	44.18	33.39	0.33	4.39E+10	2.35E+10	1.97E+10
17.34	4.38	100.70	41.30	30.80	104.80	42.98	32.05				

Time hh:mm	t, h	$\overline{\int OHdt}$	$\overline{[OH]}$
13.09	0.00	4.43E+09	4.15E+06
13.29	0.30	1.80E+09	-1.57E+06
13.57	0.76	1.70E+10	2.58E+06
15.35	2.40	1.36E+10	-1.75E+06
16.07	2.93	1.81E+10	3.42E+06
16.29	3.30	2.46E+10	4.33E+06
16.54	3.71	8.93E+09	-1.31E+07
17.14	4.05	2.02E+10	9.37E+06
17.34	4.38		

Aldrin 14

Filter	Time, h	[Aldrin]	[Dieldrin]	[Photoaldrin]	[Mirex]	$C_{Aldrin,norm}$	$C_{Dieldr,norm}$	$C_{Photoaldrin,norm}$	avy	∫[OH] dt
W0	-0.32								1.01	0.00E+00
W1	1.22								1.06	1.01E+10
W2	3.22								1.12	2.66E+10
W3	5.02								1.21	4.14E+10
0	-0.12	595.10	63.30	82.90	4333.00	595.10	63.30	82.90	1.02	0.00E+00
1	0.76	339.20	192.70	123.90	4582.00	320.77	182.23	117.17	1.04	6.27E+09
2	1.72	240.30	279.90	175.30	4398.00	236.75	275.76	172.71	1.08	1.42E+10
3	2.72	169.00	351.10	261.50	5089.00	143.89	298.94	222.65	1.10	2.24E+10
4	3.78	150.10	283.60	366.00	5025.00	129.43	244.55	315.60	1.15	3.12E+10
5	4.58	107.60	323.30	517.10	5117.00	91.11	273.77	437.87	1.18	3.78E+10
0	-0.12	771.10	49.40	116.40	5419.00	616.57	39.50	93.07	1.02	0.00E+00
1	0.76	383.40	130.60	128.10	4860.00	341.83	116.44	114.21	1.04	6.27E+09
2	1.72	254.50	271.40	186.70	4554.00	242.15	258.23	177.64	1.08	1.42E+10
3	2.72	173.70	323.30	253.00	4925.00	152.82	284.44	222.59	1.10	2.24E+10
4	3.78	107.80	252.20	302.90	4308.00	108.43	253.66	304.66	1.15	3.12E+10
5	4.58	120.30	285.70	434.60	4441.00	117.37	278.75	424.03	1.18	3.78E+10

Aldrin 14 OH

Time hh:mm	t, h	[PFH]	[DMB]	[Hexan]	$[PFH]_{norm}$	$[DMB]_{norm}$	$[Hexan]_{norm}$	dt, h	$[OH]_{DMB}$	$[OH]_{Hexan}$	$\int[OH]dt_{DMB}$
13.05	0.00	125.50	52.90	39.80	125.50	52.90	39.80	0.33	-1.81E+10	5.91E+09	1187.99
13.31	0.33	124.50	53.00	39.10	125.50	53.43	39.41	0.68	9.80E+08	2.29E+09	3647.99
14.12	1.01	119.70	50.90	37.30	125.50	53.37	39.11	0.65	1.50E+10	-6.12E+09	5987.99
14.51	1.66	116.40	48.70	37.00	125.50	52.51	39.89	0.55	6.77E+10	2.11E+10	7967.99
15.24	2.21	116.70	45.90	35.00	125.50	49.36	37.64	0.50	-2.03E+10	6.40E+09	9767.99
15.54	2.71	113.50	45.40	33.50	125.50	50.20	37.04	0.62	-4.01E+09	6.07E+08	11987.99
16.31	3.33	109.30	43.90	32.20	125.50	50.41	36.97	0.43	1.99E+10	1.24E+10	13547.99
16.57	3.76	108.10	42.80	31.00	125.50	49.69	35.99	0.53	7.83E+09	-5.64E+09	15467.99
17.29	4.30	105.80	41.60	30.80	125.50	49.35	36.53	0.43	-6.33E+09	7.98E+09	17027.99
17.55	4.73	103.80	41.00	29.70	125.50	49.57	35.91				

Time hh:mm	t, h	$\int[OH]dt_{Hexan}$	$\int[OH]dt_{TMB}$	$\overline{\int OHdt}$	$\overline{[OH]}$
13.05	0.00	-5.96E+09	1.95E+09	-2.00E+09	-1.69E+06
13.31	0.33	-5.29E+09	3.51E+09	-8.88E+08	4.54E+05
14.12	1.01	4.49E+09	-4.65E+08	2.01E+09	1.24E+06
14.51	1.66	4.17E+10	1.12E+10	2.64E+10	1.23E+07
15.24	2.21	3.16E+10	1.44E+10	2.30E+10	-1.93E+06
15.54	2.71	2.91E+10	1.47E+10	2.19E+10	-4.73E+05
16.31	3.33	3.77E+10	2.01E+10	2.89E+10	4.49E+06
16.57	3.76	4.19E+10	1.71E+10	2.95E+10	3.04E+05
17.29	4.30	3.92E+10	2.06E+10	2.99E+10	2.28E+05
17.55	4.73				

Aldrin 15

Filter	Time, h	[Aldrin]	[Mirex]	$C_{Aldrin,norm}$	a_V	∫[OH] dt	V_{del}, L	V_f, L	$C_{Aldrin,Ae}$	m_f, µg	c_{Ae}, mg/m3
W0	-0.18				1.01	0.00	25.00	50.00		77.60	1.55
W1	0.90				1.06	0.00	190.00	60.00		80.40	1.34
W2	2.23				1.12	0.00	360.00	60.00		69.50	1.16
W3	3.88				1.22	0.00	645.00	110.00		100.40	0.91
0	0.00	1034.10	5061.90	1034.10	1.03	0.00	80.00	60.00	11.47	90.14	1.50
1	0.68	510.60	4463.10	510.60	1.04	0.00	135.00	50.00	7.31	69.84	1.40
2	1.28	494.90	4712.80	494.90	1.08	0.00	245.00	50.00	7.70	64.25	1.28
3	1.98	543.00	4725.30	543.00	1.10	0.00	300.00	60.00	7.59	71.57	1.19
4	2.72	1142.50	5245.30	1142.50	1.15	0.00	440.00	100.00	10.63	107.47	1.07
5	3.72	788.30	5096.40	788.30	1.18	0.00	540.00	100.00	8.21	95.98	0.96
0	0.00	1095.10	4357.00	1095.10	1.02	0.00	55.00	60.00	12.05	90.85	1.51
1	0.68	502.50	4708.70	502.50	1.04	0.00	135.00	50.00	7.19	69.84	1.40
2	1.28	518.50	5240.70	518.50	1.08	0.00	245.00	50.00	8.07	64.25	1.28
3	1.98	582.30	4980.00	582.30	1.10	0.00	300.00	60.00	8.14	71.57	1.19
4	2.72	1125.20	4908.20	1125.20	1.15	0.00	440.00	100.00	10.47	107.47	1.07
5	3.72	780.80	5026.80	780.80	1.18	0.00	540.00	100.00	8.14	95.98	0.96

Aldrin 15 OH

Time hh:mm	t, h	[PFH]	[DMB]	[Hexan]	$[PFH]_{norm}$	$[DMB]_{norm}$	$[Hexan]_{norm}$
13.27	0.00	16.00	82.30	79.40	16.00	82.30	79.40
13.59	0.31	15.50	76.60	76.10	16.00	79.07	78.55
14.28	0.79	15.90	74.80	73.90	16.00	75.27	74.36
14.55	1.24	14.60	69.70	71.00	16.00	76.38	77.81
15.38	1.96	15.60	74.30	71.20	16.00	76.21	73.03
16.06	2.42	14.90	71.40	68.70	16.00	76.67	73.77
16.40	2.99	14.10	68.10	67.20	16.00	77.28	76.26
17.09	3.47	14.70	73.50	70.50	16.00	80.00	76.73
17.29	3.81	13.70	65.20	62.70	16.00	76.15	73.23
Time hh:mm	t, h	$[OH]_{DMB}$	$[OH]_{Hexan}$	$\int[OH]dt_{DMB}$	$\int[OH]dt_{Hexan}$	$\overline{\int OHdt}$	$\overline{[OH]}$
13.27	0.00	7.86E+10	6.98E+09	2.41E+10	2.14E+09	1.31E+10	1.19E+07
13.59	0.31	6.14E+10	2.27E+10	5.38E+10	1.31E+10	3.34E+10	1.17E+07
14.28	0.79	-1.97E+10	-2.01E+10	4.49E+10	4.05E+09	2.45E+10	-5.52E+06
14.55	1.24	1.97E+09	1.77E+10	4.64E+10	1.67E+10	3.15E+10	2.73E+06
15.38	1.96	-7.87E+09	-4.36E+09	4.27E+10	1.47E+10	2.87E+10	-1.70E+06
16.06	2.42	-8.36E+09	-1.17E+10	3.79E+10	8.08E+09	2.30E+10	-2.78E+06
16.40	2.99	-4.32E+10	-2.59E+09	1.71E+10	6.83E+09	1.20E+10	-6.36E+06
17.09	3.47	8.92E+10	2.81E+10	4.68E+10	1.62E+10	3.15E+10	1.63E+07
17.29	3.81						

Aldrin 19

Filter	Time, h	[Aldrin]	$C_{Aldrin, norm}$	a_V	∫[OH] dt	V_{del}, L	V_f, L	$C_{Aldrin, Ae}$	m_f, µg	c_{Ae}, mg/m3
W0	-0.47			1.01	0.00	25.00	50.00		43.10	0.86
W1	1.60			1.06	0.00	175.00	50.00		33.50	0.67
W2	3.10			1.13	0.00	380.00	80.00		42.70	0.53
W3	4.75			1.20	0.00	595.00	90.00		37.50	0.42
0	-0.27	165.80	165.80	1.02	0.00	75.00	50.00	3.97	41.76	0.84
1	1.37	104.90	104.90	1.04	0.00	125.00	50.00	3.03	34.61	0.69
2	2.15	94.00	94.00	1.07	0.00	230.00	60.00	2.54	37.03	0.62
3	2.85	210.70	210.70	1.10	0.00	300.00	80.00	4.69	44.88	0.56
4	3.58	171.70	171.70	1.15	0.00	445.00	50.00	6.91	24.83	0.50
5	4.38	268.80	268.80	1.17	0.00	510.00	80.00	7.51	35.79	0.45
0	-0.27	199.50	199.50	1.02	0.00	75.00	50.00	4.78	41.76	0.84
1	1.37	118.00	118.00	1.04	0.00	125.00	50.00	3.41	34.61	0.69
2	2.15	130.90	130.90	1.07	0.00	230.00	60.00	3.54	37.03	0.62
3	2.85	271.20	271.20	1.10	0.00	300.00	80.00	6.04	44.88	0.56
4	3.58	193.10	193.10	1.15	0.00	445.00	50.00	7.78	24.83	0.50
5	4.38	230.00	230.00	1.17	0.00	510.00	80.00	6.43	35.79	0.45

Aldrin 19 OH

Time hh:mm	t, h	[PFH]	[DMB]	[Hexan]	[TMB]	$[PFH]_{norm}$	$[DMB]_{norm}$	$[Hexan]_{norm}$	$[TMB]_{norm}$	dt, h
12.47	0.00	166.00	86.00	78.90	95.00	166.00	86.00	78.90	95.00	0.08
13.21	0.08	161.80	84.20	77.40	93.90	166.00	86.39	79.41	96.34	0.53
13.53	0.62	159.90	82.90	76.60	91.90	166.00	86.06	79.52	95.41	0.55
14.26	1.17	159.40	82.40	76.40	91.40	166.00	85.81	79.56	95.18	0.55
14.59	1.72	156.80	81.70	74.20	90.00	166.00	86.49	78.55	95.28	0.55
15.32	2.27	149.80	77.70	71.10	85.60	166.00	86.10	78.79	94.86	0.48
16.01	2.75	147.00	76.20	70.50	85.90	166.00	86.05	79.61	97.00	0.77
16.47	3.52	140.30	72.30	67.10	80.60	166.00	85.54	79.39	95.36	0.57
17.21	4.08	136.40	70.80	65.40	78.60	166.00	86.16	79.59	95.66	0.53
17.53	4.62	135.00	71.00	63.40	76.30	166.00	87.30	77.96	93.82	
Time hh:mm	t, h	$[OH]_{DMB}$	$[OH]_{Hexan}$	$[OH]_{TMB}$	$\int[OH]dt_{DMB}$	$\int[OH]dt_{Hexan}$	$\int[OH]dt_{TMB}$	$\overline{\int OHdt}$	$\overline{[OH]}$	
12.47	0.00	-3.23E+10	-1.54E+10	-4.09E+10	-2.70E+09	-1.29E+09	-3.41E+09	-2.46E+09	-4.74E+06	
13.21	0.08	4.23E+09	-5.34E+08	4.44E+09	-4.38E+08	-1.57E+09	-1.04E+09	-1.02E+09	7.54E+05	
13.53	0.62	3.20E+09	-1.88E+08	1.03E+09	1.32E+09	-1.67E+09	-4.73E+08	-2.76E+08	3.74E+05	
14.26	1.17	-8.67E+09	4.64E+09	-4.48E+08	-3.45E+09	8.80E+08	-7.19E+08	-1.10E+09	-4.14E+05	
14.59	1.72	4.96E+09	-1.09E+09	1.98E+09	-7.20E+08	2.81E+08	3.67E+08	-2.37E+07	5.41E+05	
15.32	2.27	7.79E+08	-4.30E+09	-1.13E+10	-3.43E+08	-1.80E+09	-5.09E+09	-2.41E+09	-1.37E+06	
16.01	2.75	4.63E+09	7.25E+08	5.42E+09	3.20E+09	-1.24E+09	-9.33E+08	3.43E+08	9.97E+05	
16.47	3.52	-7.68E+09	-8.93E+08	-1.32E+09	-1.15E+09	-1.75E+09	-1.68E+09	-1.53E+09	-9.16E+05	
17.21	4.08	-1.48E+10	7.78E+09	8.86E+09	-9.06E+09	2.40E+09	3.05E+09	-1.21E+09	1.67E+05	
17.53	4.62									

Aldrin 21

Filter	Time, h	[Aldrin]	[Dieldrin]	$C_{Aldrin, norm}$	$C_{Dieldr, norm}$	a_V	$\int[OH]\,dt$	V_{del}, L	V_f, L
W0	-0.25					1.01	0.00E+00	25.00	50.00
W1	0.90					1.06	1.64E+09	185.00	70.00
W2	1.93					1.12	3.51E+09	365.00	90.00
W3	2.95					1.19	5.37E+09	560.00	100.00
0	-0.07	1035.00	212.00	1035.00	212.00	1.02	0.00E+00	75.00	50.00
1	0.65	681.00	577.00	681.00	577.00	1.04	1.18E+09	125.00	50.00
2	1.28	291.00	656.00	291.00	656.00	1.08	2.33E+09	245.00	50.00
3	1.68	198.00	972.00	198.00	972.00	1.10	3.06E+09	295.00	50.00
4	2.28	17.50	900.00	17.50	900.00	1.15	4.15E+09	435.00	50.00
5	2.70	43.30	796.00	43.30	796.00	1.16	4.91E+09	485.00	50.00
0	-0.07	1294.00	249.50	1294.00	249.50	1.02	0.00E+00	75.00	50.00
1	0.65	895.00	566.00	895.00	566.00	1.04	1.18E+09	125.00	50.00
2	1.28	234.00	703.00	234.00	703.00	1.08	2.33E+09	245.00	50.00
3	1.68	203.00	999.00	203.00	999.00	1.10	3.06E+09	295.00	50.00
4	2.28	101.00	978.00	101.00	978.00	1.15	4.15E+09	435.00	50.00
5	2.70	41.30	746.00	41.30	746.00	1.16	4.91E+09	485.00	50.00

Aldrin 21

Filter	Time, h	$C_{Aldrin, Ae}$	$C_{Dieldrin, Ae}$	m_f, µg	c_{Ae}, mg/m³
W0	-0.25			25.30	0.51
W1	0.90			21.50	0.31
W2	1.93			34.40	0.38
W3	2.95			29.60	0.30
0	-0.07	41.72	8.54	24.81	0.50
1	0.65	30.18	25.57	22.57	0.45
2	1.28	14.35	32.35	20.28	0.41
3	1.68	10.36	50.87	19.11	0.38
4	2.28	1.02	52.57	17.12	0.34
5	2.70	2.69	49.46	16.09	0.32
0	-0.07	52.15	10.06	24.81	0.50
1	0.65	39.66	25.08	22.57	0.45
2	1.28	11.54	34.66	20.28	0.41
3	1.68	10.62	52.29	19.11	0.38
4	2.28	5.90	57.12	17.12	0.34
5	2.70	2.57	46.35	16.09	0.32

Aldrin 21 OH

Time hh:mm	t, h	[PFH]	[DMB]	[Hexan]	[TMB]	$[PFH]_{norm}$	$[DMB]_{norm}$	$[Hexan]_{norm}$	$[TMB]_{norm}$	dt, h
13.53	0.00	93.10	44.40	38.30	47.40	93.10	44.40	38.30	47.40	0.04
14.26	0.04	89.50	42.60	37.00	45.90	93.10	44.31	38.49	47.75	0.55
14.59	0.59	88.50	41.90	36.30	44.80	93.10	44.08	38.19	47.13	0.55
15.32	1.14	84.00	40.20	34.50	43.10	93.10	44.56	38.24	47.77	0.42
15.57	1.55	83.30	39.50	33.90	42.40	93.10	44.15	37.89	47.39	0.58
16.32	2.14	80.80	37.90	31.60	41.10	93.10	43.67	36.41	47.36	0.52
17.03	2.65	76.30	36.20	30.70	38.30	93.10	44.17	37.46	46.73	0.65
17.42	3.30	69.20	32.80	27.90	34.40	93.10	44.13	37.54	46.28	0.32
18.01	3.62	68.50	32.00	27.50	33.80	93.10	43.49	37.38	45.94	

Time hh:mm	t, h	$[OH]_{DMB}$	$[OH]_{Hexan}$	$[OH]_{TMB}$	$\int[OH]dt_{DMB}$	$\int[OH]dt_{Hexan}$	$\int[OH]dt_{TMB}$	$\overline{\int OHdt}$	$\overline{[OH]}$	
13.53	0.00	3.20E+10	-2.67E+10	-4.84E+10	1.17E+09	-9.81E+08	-1.78E+09	-5.27E+08	3.25E+05	
14.26	0.04	5.84E+09	2.86E+09	5.77E+09	4.39E+09	5.92E+08	1.40E+09	2.13E+09	1.34E+06	
14.59	0.59	-1.18E+10	-4.83E+08	-5.99E+09	-2.10E+09	3.27E+08	-1.89E+09	-1.22E+09	-1.69E+06	
15.32	1.14	1.33E+10	4.40E+09	4.69E+09	3.44E+09	2.16E+09	6.05E+07	1.89E+09	2.07E+06	
15.57	1.55	1.12E+10	1.36E+10	2.80E+08	9.99E+09	1.01E+10	2.24E+08	6.78E+09	2.33E+06	
16.32	2.14	-1.33E+10	-1.10E+10	6.26E+09	3.12E+09	4.44E+09	3.46E+09	3.67E+09	-1.67E+06	
17.03	2.65	8.88E+08	-6.26E+08	3.65E+09	3.70E+09	4.03E+09	5.83E+09	4.52E+09	3.62E+05	
17.42	3.30	2.76E+10	2.70E+09	5.72E+09	1.24E+10	4.88E+09	7.64E+09	8.32E+09	3.34E+06	
18.01	3.62									

Aldrin 23

Filter	Time, h	[Aldrin]	[Dieldrin]	[Mirex]	$C_{Aldrin, norm}$	$C_{Dieldr, norm}$	a_V	∫[OH] dt
W0	-1.20						1.01	0.00E+00
W1	0.60						1.18	7.44E+09
W2	1.98						1.27	2.46E+10
W3	5.42						1.63	6.72E+10
0	-1.02	1537.00	143.80	1226.00	1537.00	143.80	1.03	0.00E+00
1	0.30	956.30	100.50	1059.00	956.30	100.50	1.15	3.72E+09
2	1.05	1073.40	518.80	1181.00	1073.40	518.80	1.21	1.30E+10
3	1.75	679.80	1117.00	1378.00	679.80	1117.00	1.24	2.17E+10
4	2.83	274.10	1266.00	1676.00	274.10	1266.00	1.30	3.51E+10
5	3.75	104.60	3261.00	1091.00	104.60	3261.00	1.34	4.65E+10
6	4.05	62.50	1546.00	883.60	62.50	1546.00	1.39	5.02E+10
0	-1.02	1578.00	127.40	1644.00	1578.00	127.40	1.03	0.00E+00
1	0.30	1396.40	141.80	1339.00	1396.40	141.80	1.15	3.72E+09
2	1.05	1074.00	527.40	1282.00	1074.00	527.40	1.21	1.30E+10
3	1.75	673.50	1112.00	1396.00	673.50	1112.00	1.24	2.17E+10
4	2.83	266.40	1328.00	1671.00	266.40	1328.00	1.30	3.51E+10
5	3.75	56.60	1679.00	1173.00	56.60	1679.00	1.34	4.65E+10
6	4.05	26.80	1947.00	931.60	26.80	1947.00	1.39	5.02E+10

Filter	Time, h	V_{del}, L	V_f, L	$C_{Aldrin, Ae}$	$C_{Dieldrin, Ae}$	m_f, µg	c_{Ae}, mg/m3	
W0	-1.20	35.00	70.00			36.00	0.51	
W1	0.60	525.00	90.00			27.50	0.31	
W2	1.98	765.00	90.00			23.40	0.26	
W3	5.42	1555.00	270.00			32.50	0.12	
0	-1.02	95.00	50.00	64.74	6.06	23.74	0.47	
1	0.30	450.00	60.00	45.30	4.76	21.11	0.35	
2	1.05	605.00	70.00	50.92	24.61	21.08	0.30	
3	1.75	680.00	80.00	31.93	52.46	21.29	0.27	
4	2.83	850.00	80.00	15.84	73.18	17.30	0.22	
5	3.75	945.00	110.00	5.17	161.08	20.25	0.18	
6	4.05	1060.00	120.00	3.06	75.74	20.41	0.17	
0	-1.02	95.00	50.00	66.47	5.37	23.74	0.47	
1	0.30	450.00	60.00	66.14	6.72	21.11	0.35	
2	1.05	605.00	70.00	50.95	25.02	21.08	0.30	
3	1.75	680.00	80.00	31.63	52.23	21.29	0.27	
4	2.83	850.00	80.00	15.40	76.76	17.30	0.22	
5	3.75	945.00	110.00	2.80	82.93	20.25	0.18	
6	4.05	1060.00	120.00	1.31	95.39	20.41	0.17	

Aldrin 23 OH

Time hh:mm	t, h	[PFH]	[DMB]	[Hexan]	[TMB]	$[PFH]_{norm}$	$[DMB]_{norm}$	$[Hexan]_{norm}$	$[TMB]_{norm}$	dt, h
11.11	0.00	122.00	61.00	62.90	53.00	122.00	61.00	62.90	53.00	0.13
11.39	0.13	115.60	57.40	59.40	51.20	122.00	60.58	62.69	54.03	0.40
12.03	0.53	111.10	55.60	57.40	49.00	122.00	61.05	63.03	53.81	0.42
12.28	0.95	105.70	52.70	54.30	46.00	122.00	60.83	62.67	53.09	0.40
12.52	1.35	102.40	50.70	52.30	44.50	122.00	60.40	62.31	53.02	0.35
13.13	1.70	97.70	48.30	49.80	42.90	122.00	60.31	62.19	53.57	0.48
13.42	2.18	93.30	46.00	47.60	41.60	122.00	60.15	62.24	54.40	0.52
14.13	2.70	87.60	43.00	44.00	39.60	122.00	59.89	61.28	55.15	0.48
14.42	3.18	83.20	40.80	41.90	36.40	122.00	59.83	61.44	53.38	0.45
15.09	3.63	80.40	38.30	37.90	34.70	122.00	58.12	57.51	52.65	0.38
15.32	4.02	75.30	36.50	37.50	32.60	122.00	59.14	60.76	52.82	0.43
15.58	4.45	69.30	33.60	34.70	30.50	122.00	59.15	61.09	53.69	0.75
16.43	5.20	62.80	30.30	30.30	27.10	122.00	58.86	58.86	52.65	
Time hh:mm	t, h	$[OH]_{DMB}$	$[OH]_{Hexan}$	$[OH]_{TMB}$	$\int[OH]dt_{DMB}$	$\int[OH]dt_{Hexan}$	$\int[OH]dt_{TMB}$	$\overline{\int OHdt}$	$\overline{[OH]}$	
11.11	0.00	3.14E+10	5.05E+09	-3.54E+10	4.18E+09	6.73E+08	-4.72E+09	4.72E+07	2.94E+06	
11.39	0.13	-1.18E+10	-2.73E+09	2.57E+09	-5.42E+08	-4.18E+08	-3.69E+09	-1.55E+09	-1.11E+06	
12.03	0.53	5.41E+09	2.73E+09	7.82E+09	1.71E+09	7.21E+08	-4.31E+08	6.68E+08	1.48E+06	
12.28	0.95	1.05E+10	2.90E+09	8.74E+08	5.91E+09	1.88E+09	-8.09E+07	2.57E+09	1.32E+06	
12.52	1.35	2.60E+09	1.14E+09	-7.22E+09	6.82E+09	2.28E+09	-2.61E+09	2.16E+09	-3.23E+05	
13.13	1.70	3.38E+09	-3.72E+08	-7.73E+09	8.45E+09	2.10E+09	-6.34E+09	1.40E+09	-4.37E+05	
13.42	2.18	5.13E+09	6.04E+09	-6.50E+09	1.11E+10	5.22E+09	-9.70E+09	2.21E+09	4.33E+05	
14.13	2.70	1.23E+09	-1.09E+09	1.65E+10	1.17E+10	4.70E+09	-1.72E+09	4.89E+09	1.54E+06	
14.42	3.18	3.88E+10	2.94E+10	7.37E+09	2.92E+10	1.79E+10	1.60E+09	1.62E+10	7.00E+06	
15.09	3.63	-2.73E+10	-2.87E+10	-1.98E+09	1.87E+10	6.93E+09	8.39E+08	8.82E+09	-5.37E+06	
15.32	4.02	-3.46E+08	-2.51E+09	-9.26E+09	1.85E+10	5.85E+09	-3.17E+09	7.07E+09	-1.12E+06	
15.58	4.45	3.93E+09	9.89E+09	6.41E+09	2.15E+10	1.33E+10	1.63E+09	1.21E+10	1.87E+06	
16.43	5.20									

Aldrin 25

Filter	Time, h	[Aldrin]	[Dieldrin]	[Mirex]	$C_{Aldrin, norm}$	$C_{Dieldr, norm}$	a_V	∫[OH] dt
W0	-0.37						1.02	0.00E+00
W1	0.73						1.08	7.30E+09
W2	1.82						1.15	1.82E+10
W3	3.18						1.27	3.18E+10
0	-0.18	2627.00	122.20	1580.00	2627.00	122.20	1.04	0.00E+00
1	0.33	2763.00	325.80	1686.00	2589.29	305.32	1.05	3.30E+09
2	1.12	2733.00	1258.00	1900.00	2272.71	1046.13	1.10	1.12E+10
3	1.42	2139.00	2668.00	2497.00	1353.47	1688.20	1.12	1.42E+10
4	2.15	1336.00	7339.00	2642.00	798.97	4388.96	1.19	2.15E+10
5	2.68	761.20	9211.00	2689.00	447.27	5412.19	1.22	2.68E+10
0	-0.18	3209.00	98.20	1885.00	2689.77	82.31	1.04	0.00E+00
1	0.33	2749.00	271.80	1869.00	2323.93	229.77	1.05	3.30E+09
2	1.12	2728.00	1269.00	1907.00	2260.22	1051.40	1.10	1.12E+10
3	1.42	2193.00	2518.00	2160.00	1604.14	1841.87	1.12	1.42E+10
4	2.15	1238.00	6956.00	2722.00	718.60	4037.65	1.19	2.15E+10
5	2.68	578.60	9383.00	2783.00	328.49	5327.04	1.22	2.68E+10

Filter	Time, h	V_{del}, L	V_f, L	$C_{Aldrin, Ae}$	$C_{Dieldrin, Ae}$	m_f, µg	c_{Ae}, mg/m3
W0	-0.37	50.00	100.00			89.50	0.90
W1	0.73	240.00	100.00			68.40	0.68
W2	1.82	445.00	110.00			65.00	0.59
W3	3.18	760.00	120.00			56.70	0.47
0	-0.18	120.00	40.00	79.51	3.70	33.04	0.83
1	0.33	165.00	50.00	67.35	7.94	38.44	0.77
2	1.12	315.00	50.00	67.74	31.18	33.55	0.67
3	1.42	365.00	50.00	42.39	52.87	31.93	0.64
4	2.15	545.00	90.00	15.97	87.73	50.03	0.56
5	2.68	645.00	110.00	8.01	96.96	55.82	0.51
0	-0.18	120.00	40.00	81.41	2.49	33.04	0.83
1	0.33	165.00	50.00	60.45	5.98	38.44	0.77
2	1.12	315.00	50.00	67.37	31.34	33.55	0.67
3	1.42	365.00	50.00	50.24	57.69	31.93	0.64
4	2.15	545.00	90.00	14.36	80.71	50.03	0.56
5	2.68	645.00	110.00	5.89	95.44	55.82	0.51

Aldrin 25 OH

Time hh:mm	t, h	[PFH]	[DMB]	[Hexan]	[TMB]	$[PFH]_{norm}$	$[DMB]_{norm}$	$[Hexan]_{norm}$	$[TMB]_{norm}$	dt, h
11.25	0.00	84.20	39.60	39.10	35.40	84.20	39.60	39.10	35.40	0.22
11.44	0.22	82.30	38.70	38.20	33.90	84.20	39.59	39.08	34.68	0.28
12.01	0.50	80.90	37.90	37.10	33.20	84.20	39.45	38.61	34.55	0.30
12.19	0.80	77.90	36.20	34.70	31.40	84.20	39.13	37.51	33.94	0.30
12.37	1.10	74.30	34.40	34.30	30.30	84.20	38.98	38.87	34.34	0.33
12.57	1.43	75.10	34.30	32.60	29.40	84.20	38.46	36.55	32.96	0.38
13.20	1.82	72.50	32.90	31.30	29.00	84.20	38.21	36.35	33.68	0.33
13.40	2.15	70.70	32.20	29.50	26.10	84.20	38.35	35.13	31.08	0.48
14.09	2.63	67.40	30.50	27.70	25.10	84.20	38.10	34.60	31.36	0.32
14.28	2.95	66.70	29.80	27.00	24.40	84.20	37.62	34.08	30.80	

Time hh:mm	t, h	$[OH]_{DMB}$	$[OH]_{Hexan}$	$[OH]_{TMB}$	$\int[OH]dt_{DMB}$	$\int[OH]dt_{Hexan}$	$\int[OH]dt_{TMB}$	$\overline{\int OHdt}$	$\overline{[OH]}$	
11.25	0.00	4.61E+08	4.28E+08	2.30E+10	9.98E+07	9.26E+07	4.99E+09	1.73E+09	5.45E+05	
11.44	0.22	7.93E+09	8.51E+09	3.19E+09	2.35E+09	2.50E+09	5.90E+09	3.58E+09	1.82E+06	
12.01	0.50	1.63E+10	1.94E+10	1.46E+10	7.23E+09	8.32E+09	1.03E+10	8.61E+09	4.65E+06	
12.19	0.80	7.40E+09	-2.38E+10	-9.48E+09	9.45E+09	1.18E+09	7.43E+09	6.02E+09	-2.40E+06	
12.37	1.10	2.46E+10	3.69E+10	2.99E+10	1.77E+10	1.35E+10	1.74E+10	1.62E+10	8.47E+06	
12.57	1.43	1.01E+10	2.85E+09	-1.37E+10	2.15E+10	1.46E+10	1.21E+10	1.61E+10	-6.80E+04	
13.20	1.82	-6.57E+09	2.05E+10	5.87E+10	1.93E+10	2.14E+10	3.17E+10	2.42E+10	6.72E+06	
13.40	2.15	8.03E+09	6.27E+09	-4.41E+09	2.32E+10	2.44E+10	2.96E+10	2.57E+10	9.16E+05	
14.09	2.63	2.43E+10	9.57E+09	1.37E+10	3.09E+10	2.75E+10	3.39E+10	3.08E+10	4.41E+06	

Aldrin 26

Filter	Time, h	[Aldrin]	[Dieldrin]	[Photoaldrin]	[Mirex]	$C_{Aldrin,norm}$	$C_{Dieldr,norm}$	$C_{Photoaldrin,norm}$	ay	∫[OH] dt
W0	-0.27								1.01	0.00E+00
W1	0.63								1.06	4.64E+09
W2	2.32								1.13	2.41E+10
W3	4.25								1.25	5.89E+10
0	-0.05	551.97	111.30	89.10	843.10	551.97	111.30	89.10	1.03	0.00E+00
1	0.33	85.00	19.70	30.00	360.50	198.79	46.07	70.16	1.05	2.25E+09
2	1.07	183.20	125.90	439.80	683.00	226.14	155.41	542.89	1.09	8.73E+09
3	2.00	47.60	275.90	1347.50	1083.40	37.04	214.70	1048.62	1.11	1.96E+10
4	2.98	59.60	752.50	2379.50	1582.00	31.76	401.03	1268.11	1.17	3.45E+10
5	3.75	42.90	319.30	1028.40	883.00	40.96	304.87	981.93	1.20	4.86E+10
0	-0.05	439.70	111.10	125.60	886.70	418.08	105.64	119.42	1.03	0.00E+00
1	0.33	417.50	80.50	207.30	1114.90	315.72	60.88	156.76	1.05	2.25E+09
2	1.07	165.70	79.50	488.70	723.60	193.06	92.63	569.41	1.09	8.73E+09
3	2.00	52.30	272.30	1369.00	1173.70	37.57	195.60	983.39	1.11	1.96E+10
4	2.98	47.60	414.70	1480.80	1170.90	34.27	298.60	1066.24	1.17	3.45E+10
5	3.75	35.60	529.50	1451.10	1046.30	28.69	426.67	1169.28	1.20	4.86E+10

Aldrin 26

Filter	Time, h	V_{del}, L	V_f, L	$C_{Aldrin,Ae}$	$C_{Dieldrin,Ae}$	$C_{Photoaldrin,Ae}$	m_f, µg	c_{Ae}, mg/m^3
W0	-0.27	40	80				42.00	0.53
W1	0.63	200	80				36.50	0.46
W2	2.32	400	100				42.30	0.42
W3	4.25	705	130				39.30	0.30
0	-0.05	105	50	21.69	4.37	3.50	25.45	0.51
1	0.33	145	30	13.54	3.14	4.78	14.69	0.49
2	1.07	265	50	10.10	6.94	24.24	22.40	0.45
3	2.00	320	60	1.50	8.67	42.35	24.76	0.41
4	2.98	490	80	1.09	13.71	43.36	29.25	0.37
5	3.75	585	110	1.11	8.24	26.54	37.00	0.34
0	-0.05	105	50	16.43	4.15	4.69	25.45	0.51
1	0.33	145	30	21.50	4.14	10.67	14.69	0.49
2	1.07	265	50	8.62	4.14	25.43	22.40	0.45
3	2.00	320	60	1.52	7.90	39.71	24.76	0.41
4	2.98	490	80	1.17	10.21	36.46	29.25	0.37
5	3.75	585	110	0.78	11.53	31.60	37.00	0.34

Aldrin 26 OH

Time hh:mm	t, h	[PFH]	[DMB]	[Hexan]	[TMB]	$[PFH]_{norm}$	$[DMB]_{norm}$	$[Hexan]_{norm}$	$[TMB]_{norm}$	dt, h
11.21	0.00	80.70	36.40	34.30	31.50	80.70	36.40	34.30	31.50	0.16
11.54	0.16	77.60	34.80	33.20	31.00	80.70	36.19	34.53	32.24	0.38
12.17	0.55	77.90	34.60	32.80	30.30	80.70	35.84	33.98	31.39	0.33
12.37	0.88	76.00	33.60	31.50	29.20	80.70	35.68	33.45	31.01	0.38
13.00	1.26	73.80	32.70	30.00	27.80	80.70	35.76	32.80	30.40	0.37
13.22	1.63	73.40	32.20	29.50	26.60	80.70	35.40	32.43	29.25	0.38
13.45	2.01	72.30	31.00	28.60	27.30	80.70	34.60	31.92	30.47	0.38
14.08	2.40	69.80	30.00	26.10	24.60	80.70	34.68	30.18	28.44	0.53
14.40	2.93	67.30	28.60	24.20	22.90	80.70	34.29	29.02	27.46	0.48
15.09	3.41	65.30	27.10	22.80	21.90	80.70	33.49	28.18	27.06	0.43
15.35	3.85	63.80	26.00	21.20	20.30	80.70	32.89	26.82	25.68	0.52
16.06	4.36	58.50	23.90	18.90	17.70	80.70	32.97	26.07	24.42	

Time hh:mm	t, h	$[OH]_{DMB}$	$[OH]_{Hexan}$	$[OH]_{TMB}$	$\int[OH]dt_{DMB}$	$\int[OH]dt_{Hexan}$	$\int[OH]dt_{TMB}$	$\overline{\int OHdt}$	$\overline{[OH]}$	
11.21	0.00	2.13E+10	-8.05E+09	-3.46E+10	3.48E+09	-1.32E+09	-5.65E+09	-1.16E+09	7.05E+05	
11.54	0.16	1.51E+10	8.34E+09	1.70E+10	9.28E+09	1.88E+09	8.60E+08	4.01E+09	3.74E+06	
12.17	0.55	8.38E+09	9.45E+09	8.99E+09	1.2071E+10	5.03E+09	3.86E+09	6.99E+09	2.48E+06	
12.37	0.88	-3.49E+09	1.01E+10	1.26E+10	1.0731E+10	8.91E+09	8.68E+09	9.44E+09	1.78E+06	
13.00	1.26	1.64E+10	6.20E+09	2.57E+10	1.674E+10	1.12E+10	1.81E+10	1.53E+10	4.47E+06	
13.22	1.63	3.60E+10	8.29E+09	-2.61E+10	3.0522E+10	1.44E+10	8.09E+09	1.77E+10	1.68E+06	
13.45	2.01	-3.77E+09	2.94E+10	4.39E+10	2.9076E+10	2.56E+10	2.49E+10	2.65E+10	6.43E+06	
14.08	2.40	1.28E+10	1.47E+10	1.61E+10	3.5894E+10	3.34E+10	3.35E+10	3.43E+10	4.03E+06	
14.40	2.93	2.95E+10	1.22E+10	7.31E+09	5.0174E+10	3.93E+10	3.70E+10	4.22E+10	4.54E+06	
15.09	3.41	2.53E+10	2.29E+10	2.96E+10	6.1137E+10	4.92E+10	4.98E+10	5.34E+10	7.20E+06	
15.35	3.85	-2.92E+09	1.09E+10	2.38E+10	5.9626E+10	5.49E+10	6.21E+10	5.89E+10	2.94E+06	
16.06	4.36									

Aldrin 27

Filter	Time, h	[Aldrin]	[Dieldrin]	[Photoaldrin]	[Mirex]	$C_{Aldrin, norm}$	$C_{Dieldr, norm}$	$C_{Photoaldrin, norm}$	a_V	∫[OH] dt
W0	-0.27								1.01	0.00E+00
W1	1.02								1.06	2.24E+09
W2	3.25								1.13	1.66E+10
W3	5.03								1.23	3.73E+10
0	-0.07	2463.60	179.50	200.40	1045.00	2463.60	179.50	200.40	1.03	0.00E+00
1	0.72	2041.80	504.00	1314.30	404.00	2041.80	504.00	1314.30	1.04	1.30E+09
2	1.80	1030.00	848.00	2766.00	315.00	1030.00	848.00	2766.00	1.08	5.78E+09
3	2.83	339.80	1097.40	0.00	246.00	339.80	1097.40	0.00	1.11	1.29E+10
4	3.77	281.90	0.00	0.00	1421.00	281.90	0.00	0.00	1.16	2.18E+10
5	4.73	218.60	0.00	0.00	1260.00	218.60	0.00	0.00	1.19	3.32E+10
0	-0.07	2463.60	274.80	302.40	1645.30	2463.60	274.80	302.40	1.03	0.00E+00
1	0.72	2041.80	542.40	1637.70	1465.00	2041.80	542.40	1637.70	1.04	1.30E+09
2	1.80	1350.00	3645.00	4500.00	357.00	1350.00	3645.00	4500.00	1.08	5.78E+09
3	2.83	367.50	945.00	3216.00	1105.00	367.50	945.00	3216.00	1.11	1.29E+10
4	3.77	116.40	969.00	1800.00	746.00	116.40	969.00	1800.00	1.16	2.18E+10
5	4.73	213.90	1392.00	2844.00	575.00	213.90	1392.00	2844.00	1.19	3.32E+10

Aldrin 27

Filter	Time, h	V_{del}, L	V_f, L	$C_{Aldrin, Ae}$	$C_{Dieldrin, Ae}$	$C_{Photoaldrin, Ae}$	m_f, µg	c_{Ae}, mg/m³
W0	-0.27	35.00	70.00				119.00	1.70
W1	1.02	190.00	80.00				112.00	1.40
W2	3.25	395.00	90.00				99.40	1.10
W3	5.03	665.00	110.00				87.80	0.80
0	-0.07	85.00	30.00	0.00	3.65	4.07	49.24	1.64
1	0.72	125.00	50.00	0.00	6.74	17.58	74.78	1.50
2	1.80	260.00	60.00	13.37	11.01	35.90	77.05	1.28
3	2.83	320.00	60.00	4.99	16.12	0.00	68.08	1.13
4	3.77	480.00	80.00	3.59	0.00	0.00	78.45	0.98
5	4.73	565.00	90.00	2.81	0.00	0.00	77.93	0.87
0	-0.07	85.00	30.00	50.03	5.58	6.14	49.24	1.64
1	0.72	125.00	50.00	27.30	7.25	21.90	74.78	1.50
2	1.80	260.00	60.00	17.52	47.31	58.40	77.05	1.28
3	2.83	320.00	60.00	5.40	13.88	47.24	68.08	1.13
4	3.77	480.00	80.00	1.48	12.35	22.94	78.45	0.98
5	4.73	565.00	90.00	2.74	17.86	36.50	77.93	0.87

Aldrin 27 OH

Time hh:mm	t, h	[PFH]	[DMB]	[Hexan]	[TMB]	$[PFH]_{norm}$	$[DMB]_{norm}$	$[Hexan]_{norm}$	$[TMB]_{norm}$	dt, h
12.08	0.00	80.40	35.30	33.10	30.70	80.40	35.30	33.10	30.70	0.42
12.35	0.42	80.10	35.10	33.00	30.50	80.40	35.23	33.12	30.61	0.48
13.04	0.90	79.90	35.20	32.80	31.30	80.40	35.42	33.01	31.50	0.37
13.26	1.27	79.00	34.70	31.60	30.10	80.40	35.31	32.16	30.63	0.37
13.48	1.63	79.20	34.30	31.50	29.60	80.40	34.82	31.98	30.05	0.38
14.11	2.02	81.00	35.10	32.00	30.70	80.40	34.84	31.76	30.47	0.37
14.33	2.38	82.20	35.50	32.40	31.00	80.40	34.72	31.69	30.32	0.38
14.56	2.77	83.50	35.90	31.40	31.20	80.40	34.57	30.23	30.04	0.38
15.19	3.15	83.50	35.30	31.00	29.30	80.40	33.99	29.85	28.21	0.42
15.44	3.57	82.10	34.90	29.90	29.40	80.40	34.18	29.28	28.79	0.45
16.11	4.02	80.40	33.90	29.00	27.50	80.40	33.90	29.00	27.50	0.58
16.46	4.60	80.20	33.80	28.50	26.60	80.40	33.88	28.57	26.67	0.42
17.11	5.02	77.60	32.20	27.10	24.80	80.40	33.36	28.08	25.69	

Time hh:mm	t, h	$[OH]_{DMB}$	$[OH]_{Hexan}$	$[OH]_{TMB}$	$\int[OH]dt_{DMB}$	$\int[OH]dt_{Hexan}$	$\int[OH]dt_{TMB}$	$\overline{\int OHdt}$	$\overline{[OH]}$	
12.08	0.00	2.81E+09	-3.42E+08	1.64E+09	1.17E+09	-1.43E+08	6.82E+08	5.70E+08	2.92E+05	
12.35	0.42	-6.66E+09	1.48E+09	-1.43E+10	-2.05E+09	5.73E+08	-6.24E+09	-2.57E+09	-1.81E+06	
13.04	0.90	4.89E+09	1.42E+10	1.85E+10	-2.55E+08	5.76E+09	5.30E+08	2.01E+09	3.47E+06	
13.26	1.27	2.32E+10	3.11E+09	1.28E+10	8.25E+09	6.90E+09	5.23E+09	6.80E+09	3.62E+06	
13.48	1.63	-9.16E+08	3.51E+09	-8.92E+09	7.90E+09	8.25E+09	1.81E+09	5.99E+09	-5.86E+05	
14.11	2.02	5.54E+09	1.25E+09	3.31E+09	9.93E+09	8.70E+09	3.03E+09	7.22E+09	9.36E+05	
14.33	2.38	7.05E+09	2.45E+10	5.89E+09	1.26E+10	1.81E+10	5.29E+09	1.20E+10	3.47E+06	
14.56	2.77	2.65E+10	6.69E+09	4.00E+10	2.28E+10	2.07E+10	2.06E+10	2.14E+10	6.77E+06	
15.19	3.15	-7.97E+09	9.23E+09	-1.19E+10	1.95E+10	2.45E+10	1.57E+10	1.99E+10	-9.85E+05	
15.44	3.57	1.09E+10	4.28E+09	2.49E+10	2.44E+10	2.64E+10	2.68E+10	2.59E+10	3.71E+06	
16.11	4.02	4.79E+08	5.11E+09	1.29E+10	2.47E+10	2.94E+10	3.44E+10	2.95E+10	1.71E+06	
16.46	4.60	2.25E+10	8.36E+09	2.17E+10	3.40E+10	3.29E+10	4.34E+10	3.68E+10	4.87E+06	
17.11	5.02									

Aldrin 28

Filter	Time, h	[Aldrin]	[Dieldrin]	[Photoaldrin]	[Mirex]	$C_{Aldrin,\ norm}$	$C_{Dieldr,\ norm}$	$C_{Photoaldrin,\ norm}$	a_V	∫[OH] dt	V_{deb} L
W0	-0.30								1.01	0.00E+00	30.00
W1	0.67								1.04	7.06E+09	130.00
W2	2.27								1.09	1.62E+10	285.00
W3	5.47								1.24	3.20E+10	680.00
0	-0.12	1286.70	83.90	17.30	361.10	1286.70	83.90	17.30	1.02	0.00E+00	70.00
1	0.33	617.70	86.60	164.50	533.50	418.09	58.62	111.34	1.03	3.79E+09	90.00
2	1.17	265.40	164.70	645.40	661.30	144.92	89.93	352.42	1.06	1.08E+10	175.00
3	1.97	64.40	334.50	1156.30	708.30	32.83	170.53	589.50	1.07	1.50E+10	215.00
4	2.98	38.66	426.60	1366.20	616.70	22.64	249.79	799.96	1.12	1.85E+10	360.00
5	4.07	39.10	860.60	1838.70	597.80	23.62	519.84	1110.66	1.15	2.24E+10	445.00
6	5.08	121.50	1193.90	1523.90	876.50	50.06	491.86	627.82	1.19	2.85E+10	555.00
0	-0.12	2097.37	118.50	23.60	1024.10	739.54	41.78	8.32	1.02	0.00E+00	70.00
1	0.33	1066.80	126.40	240.00	1101.30	349.79	41.44	78.69	1.03	3.79E+09	90.00
2	1.17	389.70	223.60	835.30	1065.40	132.08	75.79	283.11	1.06	1.08E+10	175.00
3	1.97	112.30	332.90	1180.40	832.00	48.74	144.48	512.31	1.07	1.50E+10	215.00
4	2.98	115.30	618.10	1699.40	994.40	41.87	224.45	617.11	1.12	1.85E+10	360.00
5	4.07	102.70	818.40	1329.90	630.70	58.80	468.57	761.42	1.15	2.24E+10	445.00
6	5.08	85.70	739.00	886.80	577.40	53.60	462.16	554.60	1.19	2.85E+10	555.00

Aldrin 28

Filter	Time, h	V_f L	$C_{Aldrin,\ Ae}$	$C_{Dieldrin,\ Ae}$	$C_{Photoaldrin,\ Ae}$	m_f µg	c_{Ae}, mg/m³
W0	-0.30	60.00				56.00	0.93
W1	0.67	60.00				48.40	0.81
W2	2.27	90.00				54.60	0.61
W3	5.47	140.00				52.50	0.38
0	-0.12	20.00	71.82	4.68	0.97	17.92	0.90
1	0.33	20.00	24.83	3.48	6.61	16.84	0.84
2	1.17	30.00	6.54	4.06	15.90	22.16	0.74
3	1.97	50.00	0.99	5.16	17.84	33.03	0.66
4	2.98	60.00	0.68	7.47	23.93	33.43	0.56
5	4.07	110.00	0.45	9.97	21.31	52.13	0.47
6	5.08	110.00	1.13	11.07	14.13	44.44	0.40
0	-0.12	20.00	41.28	2.33	0.46	17.92	0.90
1	0.33	20.00	20.77	2.46	4.67	16.84	0.84
2	1.17	30.00	5.96	3.42	12.77	22.16	0.74
3	1.97	50.00	1.48	4.37	15.51	33.03	0.66
4	2.98	60.00	1.25	6.71	18.46	33.43	0.56
5	4.07	110.00	1.13	8.99	14.61	52.13	0.47
6	5.08	110.00	1.21	10.40	12.48	44.44	0.40

Aldrin 28 OH

Time hh:mm	t, h	[PFH]	[DMB]	[Hexan]	[TMB]	$[PFH]_{norm}$	$[DMB]_{norm}$	$[Hexan]_{norm}$	$[TMB]_{norm}$	dt, h
11.32	0.00	97.80	40.70	36.60	34.60	97.80	40.70	36.60	34.60	0.02
11.55	0.02	93.00	39.50	34.80	32.90	97.80	41.54	36.60	34.60	0.43
12.21	0.45	91.30	37.90	33.20	31.60	97.80	40.60	35.56	33.85	0.58
12.56	1.04	88.30	36.40	31.40	30.00	97.80	40.32	34.78	33.23	0.48
13.25	1.52	86.40	35.20	30.20	29.40	97.80	39.84	34.18	33.28	0.42
13.50	1.94	85.20	34.70	29.20	27.70	97.80	39.83	33.52	31.80	0.42
14.15	2.35	81.90	33.40	28.00	26.90	97.80	39.88	33.44	32.12	0.40
14.39	2.75	80.20	32.40	27.00	25.90	97.80	39.51	32.93	31.58	0.35
15.00	3.10	78.30	31.80	26.60	25.90	97.80	39.72	33.22	32.35	0.37
15.22	3.47	77.70	31.20	25.70	25.90	97.80	39.27	32.35	32.60	0.53
15.54	4.00	75.70	30.60	25.30	24.30	97.80	39.53	32.69	31.39	0.45
16.21	4.45	73.20	29.30	24.00	23.70	97.80	39.15	32.07	31.66	0.42
16.46	4.87	72.80	29.10	23.80	22.60	97.80	39.09	31.97	30.36	0.45
17.13	5.32	69.40	27.70	22.10	21.60	97.80	39.04	31.14	30.44	0.35
17.34	5.67	66.40	26.30	21.00	19.90	97.80	38.74	30.93	29.31	

Time hh:mm	t, h	$[OH]_{DMB}$	$[OH]_{Hexan}$	$[OH]_{TMB}$	$\int[OH]dt_{DMB}$	$\int[OH]dt_{Hexan}$	$\int[OH]dt_{TMB}$	$\overline{\int OHdt}$	$\overline{[OH]}$	
11.32	0.00	-6.14E+11	1.06E+09	6.82E+08	-1.23E+10	2.12E+07	1.36E+07	-4.08E+09	-5.68E+07	
11.55	0.02	3.18E+10	1.32E+10	1.23E+10	1.51E+09	5.74E+09	5.35E+09	4.20E+09	5.31E+06	
12.21	0.45	7.20E+09	7.66E+09	7.76E+09	5.71E+09	1.02E+10	9.87E+09	8.60E+09	2.09E+06	
12.56	1.04	1.47E+10	7.12E+09	-7.82E+08	1.28E+10	1.37E+10	9.49E+09	1.20E+10	1.95E+06	
13.25	1.52	4.63E+08	9.45E+09	2.67E+10	1.30E+10	1.76E+10	2.06E+10	1.71E+10	3.39E+06	
13.50	1.94	-1.91E+09	1.18E+09	-5.97E+09	1.22E+10	1.81E+10	1.81E+10	1.61E+10	-6.20E+05	
14.15	2.35	1.42E+10	7.70E+09	1.03E+10	1.79E+10	2.12E+10	2.22E+10	2.04E+10	2.98E+06	
14.39	2.75	-9.09E+09	-5.17E+09	-1.67E+10	1.47E+10	1.94E+10	1.64E+10	1.68E+10	-2.87E+06	
15.00	3.10	1.87E+10	1.46E+10	-5.12E+09	2.15E+10	2.47E+10	1.45E+10	2.03E+10	2.60E+06	
15.22	3.47	-7.52E+09	-3.90E+09	1.72E+10	1.75E+10	2.26E+10	2.37E+10	2.13E+10	5.39E+05	
15.54	4.00	1.32E+10	8.52E+09	-4.65E+09	2.34E+10	2.65E+10	2.16E+10	2.38E+10	1.58E+06	
16.21	4.45	1.98E+09	1.39E+09	2.46E+10	2.43E+10	2.70E+10	3.19E+10	2.77E+10	2.59E+06	
16.46	4.87	1.98E+09	1.17E+10	-1.39E+09	2.52E+10	3.23E+10	3.12E+10	2.96E+10	1.14E+06	
17.13	5.32	1.32E+10	3.92E+09	2.63E+10	2.98E+10	3.37E+10	4.05E+10	3.46E+10	4.02E+06	

Aldrin 32

Filter	Time, h	[Aldrin]	[Dieldrin]	[Photoaldrin]	$C_{Aldrin, norm}$	$C_{Dieldr, norm}$	$C_{Photoaldrin, norm}$	a_V	∫[OH] dt	V_{del}, L
W0	-0.56							1.01	0.00E+00	30.00
W1	1.32							1.06	1.88E+11	185.00
W2	2.97							1.13	2.70E+11	380.00
W3	4.37							1.25	2.04E+11	725.00
0	-0.16	1815.00	0.00	0.00	1815.00	0.00	0.00	1.03	0.00E+00	80.00
1	0.05	1482.00	0.00	0.00	1482.00	0.00	0.00	1.04	9.12E+09	125.00
2	1.58	251.00	624.00	0.00	251.00	624.00	0.00	1.08	2.12E+11	245.00
3	2.23	87.00	441.00	2256.00	87.00	441.00	2256.00	1.10	2.54E+11	295.00
4	3.35	63.00	520.00	1526.00	63.00	520.00	1526.00	1.16	2.64E+11	485.00
5	3.78	126.00	637.00	1398.00	126.00	637.00	1398.00	1.20	2.47E+11	585.00
0	-0.16	2068.00	78.00	90.00	2068.00	78.00	90.00	1.03	0.00E+00	80.00
1	0.05	1704.00	570.00	1674.00	1704.00	570.00	1674.00	1.04	9.12E+09	125.00
2	1.58	252.00	618.00	2052.00	252.00	618.00	2052.00	1.08	2.12E+11	245.00
3	2.23	111.00	432.00	2239.00	111.00	432.00	2239.00	1.10	2.54E+11	295.00
4	3.35	65.00	625.00	1580.00	65.00	625.00	1580.00	1.16	2.64E+11	485.00
5	3.78	124.00	638.00	1493.00	124.00	638.00	1493.00	1.20	2.47E+11	585.00

Aldrin 32

Filter	Time, h	V_f, L	$C_{Aldrin, Ae}$	$C_{Dieldrin, Ae}$	$C_{Photoaldrin, Ae}$	m_f, µg	c_{Ae}, mg/m³
W0	-0.56	60.00				33.80	0.56
W1	1.32	70.00				28.70	0.41
W2	2.97	120.00				33.20	0.28
W3	4.37	170.00				37.60	0.22
0	-0.16	40.00	86.18	0.00	0.00	21.06	0.53
1	0.05	50.00	58.88	0.00	0.00	25.17	0.50
2	1.58	50.00	12.96	32.23	0.00	19.36	0.39
3	2.23	50.00	5.02	25.46	130.23	17.32	0.35
4	3.35	90.00	2.53	20.86	61.23	24.92	0.28
5	3.78	110.00	4.55	22.98	50.44	27.72	0.25
0	-0.16	40.00	98.19	3.70	4.27	21.06	0.53
1	0.05	50.00	67.70	22.65	66.51	25.17	0.50
2	1.58	50.00	13.02	31.92	105.99	19.36	0.39
3	2.23	50.00	6.41	24.94	129.25	17.32	0.35
4	3.35	90.00	2.61	25.08	63.39	24.92	0.28
5	3.78	110.00	4.47	23.02	53.87	27.72	0.25

Aldrin 34

Filter	Time, h	[Aldrin]	[Mirex]	$C_{Aldrin, norm}$	a_V	∫[OH] dt	V_{del}, L	V_f, L	$C_{Aldrin, Ae}$	m_f, µg	c_{Ae}, mg/m³
W0	-0.75				1.01	0.00E+00	30.00	60.00		30,9	30,9
W1	0.50				1.06	1.30E+11	195.00	70.00		76.90	1.10
W2	1.38				1.13	3.59E+11	380.00	100.00		119.00	1.19
W3	2.53				1.22	6.58E+11	630.00	100.00		122.50	1.23
0	-0.23	12272.00	1838.30	12272.00	1.03	0.00E+00	85.00	50.00	235.48	52.12	1.04
1	0.22	8759.40	1692.20	9515.66	1.04	5.72E+10	135.00	50.00	181.16	52.53	1.05
2	0.76	7529.60	1843.90	7506.73	1.08	1.98E+11	255.00	50.00	144.25	52.04	1.04
3	1.05	6453.20	1836.50	6459.52	1.10	2.73E+11	305.00	50.00	124.19	52.01	1.04
4	1.78	6099.60	1729.20	6484.44	1.16	4.63E+11	465.00	70.00	90.11	71.96	1.03
5	2.12	6032.00	1926.60	5755.54	1.18	5.51E+11	540.00	80.00	70.38	81.77	1.02
0	-0.23	13431.60	1822.70	13546.56	1.03	0.00E+00	85.00	50.00	259.94	52.12	1.04
1	0.22	8827.00	1777.50	9128.93	1.04	5.72E+10	135.00	50.00	173.80	52.53	1.05
2	0.76	7545.20	1660.10	8355.12	1.08	1.98E+11	255.00	50.00	160.55	52.04	1.04
3	1.05	6510.40	1660.00	7209.68	1.10	2.73E+11	305.00	50.00	138.61	52.01	1.04
4	1.78	7339.80	1870.10	7214.99	1.16	4.63E+11	465.00	70.00	100.27	71.96	1.03
5	2.12	6832.80	2329.50	5392.03	1.18	5.51E+11	540.00	80.00	65.94	81.77	1.02

Aldrin 34 OH

Time hh:mm	t, h	[PFH]	[DMB]	[Hexan]	[TMB]	$[PFH]_{norm}$	$[DMB]_{norm}$	$[Hexan]_{norm}$	$[TMB]_{norm}$	dt, h	$[OH]_{DMB}$
14.02	0.00	155.80	68.10	72.60	68.60	155.80	68.10	72.60	68.60	0.16	4.22E+10
14.17	0.16	125.60	54.30	56.60	52.70	155.80	67.36	70.21	65.37	0.85	6.96E+10
15.08	1.01	105.90	41.50	31.20	35.60	155.80	61.05	45.90	52.37	0.20	9.97E+11
15.20	1.21	108.00	30.40	18.20	18.50	155.80	43.85	26.26	26.69	0.25	1.78E+11
15.35	1.46	102.50	26.80	11.90	9.10	155.80	40.74	18.09	13.83	0.23	3.99E+11
15.49	1.69	100.00	22.40	7.50	8.70	155.80	34.90	11.69	13.55	0.25	3.24E+11
16.04	1.94	99.60	19.50	5.10	6.00	155.80	30.50	7.98	9.39	0.27	2.48E+11
16.20	2.21	95.20	16.70	3.60	4.60	155.80	27.33	5.89	7.53	0.32	1.32E+10
16.39	2.52	88.40	15.40	2.60	3.40	155.80	27.14	4.58	5.99	0.28	5.08E+11
16.56	2.81	88.20	12.10	1.70	2.40	155.80	21.37	3.00	4.24	0.32	2.82E+11
17.15	3.12	85.40	10.10	1.20	2.00	155.80	18.43	2.19	3.65	0.35	2.39E+11
17.36	3.47	81.60	8.40	1.10	1.70	155.80	16.04	2.10	3.25		

Time hh:mm	t, h	$[OH]_{Hexan}$	$[OH]_{TMB}$	$\int[OH]dt_{DMB}$	$\int[OH]dt_{Hexan}$	$\int[OH]dt_{TMB}$	$\overline{\int OHdt}$	$\overline{[OH]}$
14.02	0.00	4.27E+10	6.76E+10	6.62E+09	6.70E+09	1.06E+10	6.66E+09	1.18E+07
14.17	0.16	1.00E+11	5.73E+10	6.58E+10	9.17E+10	5.93E+10	7.87E+10	2.36E+07
15.08	1.01	5.59E+11	7.41E+11	2.65E+11	2.03E+11	2.07E+11	2.34E+11	2.16E+08
15.20	1.21	2.98E+11	5.78E+11	3.10E+11	2.78E+11	3.52E+11	2.94E+11	6.61E+07
15.35	1.46	3.75E+11	1.91E+10	4.03E+11	3.65E+11	3.56E+11	3.84E+11	1.07E+08
15.49	1.69	3.05E+11	3.23E+11	4.84E+11	4.42E+11	4.37E+11	4.63E+11	8.75E+07
16.04	1.94	2.27E+11	1.82E+11	5.50E+11	5.02E+11	4.86E+11	5.26E+11	6.60E+07
16.20	2.21	1.59E+11	1.58E+11	5.54E+11	5.53E+11	5.36E+11	5.53E+11	2.39E+07
16.39	2.52	2.98E+11	2.68E+11	6.98E+11	6.37E+11	6.12E+11	6.68E+11	1.12E+08
16.56	2.81	2.00E+11	1.04E+11	7.87E+11	7.00E+11	6.45E+11	7.44E+11	6.69E+07
17.15	3.12	2.37E+10	7.35E+10	8.71E+11	7.09E+11	6.71E+11	7.90E+11	3.65E+07

Aldrin 37

Filter	Time, h	[Aldrin]	[Mirex]	$C_{Aldrin, norm}$	a_V	∫[OH] dt	V_{del}, L	V_f, L	$C_{Aldrin, Ae}$	m_f, µg	c_{Ae}, mg/m^3
W0	-1.80				1.01	0.00E+00	35.00	70.00		40.10	0.57
W1	0.56				1.08	2.88E+10	240.00	80.00		36.50	0.46
W2	1.67				1.17	1.34E+11	495.00	90.00		36.30	0.40
W3	3.00				1.29	1.80E+11	815.00	150.00		50.80	0.34
0	-1.40	2821.00	2027.70	2821.00	1.03	0.00E+00	105.00	70.00	74.29	37.97	0.54
1	0.20	1077.30	1645.80	1327.28	1.05	6.62E+09	170.00	60.00	45.66	29.07	0.48
2	0.96	359.20	1666.00	437.18	1.11	6.41E+10	330.00	100.00	9.91	44.10	0.44
3	1.33	304.50	1209.80	510.36	1.14	1.01E+11	415.00	70.00	17.35	29.42	0.42
4	2.06	352.40	2215.40	322.54	1.20	1.66E+11	590.00	100.00	8.46	38.14	0.38
5	2.48	198.40	1953.00	205.99	1.24	1.86E+11	690.00	100.00	5.71	36.08	0.36

Aldrin 37 OH

Time hh:mm	t, h	[PFH]	[DMB]	[Hexan]	[TMB]	$[PFH]_{norm}$	$[DMB]_{norm}$	$[Hexan]_{norm}$	$[TMB]_{norm}$	dt, h
11.26	0.00	51.90	26.70	22.40	23.50	51.90	26.70	22.40	23.50	0.12
13.13	0.12	46.70	23.50	20.10	23.20	51.90	26.12	22.34	25.78	0.23
13.27	0.35	44.00	23.20	19.50	22.20	51.90	27.37	23.00	26.19	0.28
13.44	0.64	42.50	21.10	17.50	20.60	51.90	25.77	21.37	25.16	0.23
13.58	0.87	41.60	20.40	15.90	19.00	51.90	25.45	19.84	23.70	0.23
14.12	1.10	40.20	19.30	14.00	17.10	51.90	24.92	18.07	22.08	0.30
14.30	1.40	39.20	17.80	12.00	15.30	51.90	23.57	15.89	20.26	0.47
14.58	1.87	37.00	15.00	9.40	12.20	51.90	21.04	13.19	17.11	0.30
15.16	2.17	35.90	14.90	8.30	11.10	51.90	21.54	12.00	16.05	0.25
15.31	2.42	35.40	14.10	7.50	10.30	51.90	20.67	11.00	15.10	0.28
15.48	2.70	34.20	12.80	6.60	8.10	51.90	19.42	10.02	12.29	0.60
16.24	3.30	31.70	11.90	5.80	8.10	51.90	19.48	9.50	13.26	

Time hh:mm	t, h	$[OH]_{DMB}$	$[OH]_{Hexan}$	$[OH]_{TMB}$	$\int[OH]dt_{DMB}$	$\int[OH]dt_{Hexan}$	$\int[OH]dt_{TMB}$	$\overline{\int OHdt}$	$\overline{[OH]}$	
11.26	0.00	1.24E+11	4.80E+09	-1.88E+11	1.49E+10	5.76E+08	-2.26E+10	7.75E+09	1.79E+07	
13.13	0.12	-1.35E+11	-2.61E+10	-1.62E+10	-1.66E+10	-5.52E+09	-2.64E+10	-1.11E+10	-2.24E+07	
13.27	0.35	1.44E+11	5.41E+10	3.45E+10	2.40E+10	9.80E+09	-1.66E+10	1.69E+10	2.74E+07	
13.44	0.64	3.57E+10	6.65E+10	6.21E+10	3.24E+10	2.53E+10	-2.11E+09	2.88E+10	1.42E+07	
13.58	0.87	6.14E+10	8.31E+10	7.43E+10	4.67E+10	4.47E+10	1.52E+10	4.57E+10	2.01E+07	
14.12	1.10	1.25E+11	8.96E+10	6.99E+10	8.43E+10	7.16E+10	3.62E+10	7.80E+10	2.99E+07	
14.30	1.40	1.64E+11	8.32E+10	8.81E+10	1.61E+11	1.10E+11	7.74E+10	1.36E+11	3.44E+07	
14.58	1.87	-5.29E+10	6.55E+10	5.23E+10	1.45E+11	1.30E+11	9.30E+10	1.38E+11	1.74E+06	
15.16	2.17	1.11E+11	7.28E+10	5.93E+10	1.73E+11	1.48E+11	1.08E+11	1.61E+11	2.56E+07	
15.31	2.42	1.48E+11	6.86E+10	1.77E+11	2.15E+11	1.68E+11	1.58E+11	1.91E+11	3.01E+07	
15.48	2.70	-3.38E+09	1.85E+10	-3.09E+10	2.13E+11	1.79E+11	1.40E+11	1.96E+11	2.10E+06	

Aldrin 41

Filter	Time, h	[Aldrin]	[Mirex]	$C_{Aldrin, norm}$	a_V	∫[OH] dt	V_{del}, L	V_f, L	$C_{Aldrin, Ae}$	m_f, µg	c_{Ae}, mg/m^3
W0	-0.48				1.02	0	50.00	100.00		62.50	0.63
W1	1.00				1.10	1.74E+11	305.00	90.00			
W2	2.82				1.20	2.5192E+11	590.00	140.00		111.30	0.80
W3	4.55				1.35	4.315E+11	970.00	180.00		96.60	0.54
0	-0.13	1607.50	3002.00	1607.50	1.04	0	130.00	60.00	44.92	35.79	0.60
1	1.28	288.20	2885.50	299.84	1.12	1.9832E+11	375.00	70.00	8.09	37.07	0.53
2	1.82	142.20	2487.20	171.63	1.14	2.2636E+11	430.00	60.00	5.58	30.73	0.51
3	3.95	136.20	2343.00	174.51	1.29	3.2957E+11	820.00	120.00	3.42	51.05	0.43
0	-0.13	1701.00	2496.00	2045.83	1.04	0	130.00	60.00	57.16	35.79	0.60
1	1.28	118.50	2192.00	162.29	1.12	1.9832E+11	375.00	70.00	4.38	37.07	0.53
2	1.82	108.00	2505.00	129.43	1.14	2.2636E+11	430.00	60.00	4.21	30.73	0.51
3	3.95	277.00	2850.00	291.77	1.29	3.2957E+11	820.00	120.00	5.72	51.05	0.43

Aldrin 41 OH

Time hh:mm	t, h	[PFH]	[DMB]	[Hexan]	[TMB]	$[PFH]_{norm}$	$[DMB]_{norm}$	$[Hexan]_{norm}$	$[TMB]_{norm}$	dt, h
12.27	0.00	1219.60	438.60	250.30	401.10	1219.60	438.60	250.30	401.10	0.35
13.12	0.35	1263.10	391.80	168.20	380.00	1219.60	378.31	162.41	366.91	0.32
13.31	0.67	1271.00	371.20	129.30	359.00	1219.60	356.19	124.07	344.48	0.28
13.48	0.95	1246.00	357.50	116.50	352.20	1219.60	349.93	114.03	344.74	0.32
14.07	1.27	1170.90	342.50	119.50	308.50	1219.60	356.75	124.47	321.33	0.25
14.22	1.52	1160.70	337.70	109.50	325.00	1219.60	354.84	115.06	341.49	0.30
14.40	1.82	1202.00	340.30	104.20	331.00	1219.60	345.28	105.73	335.85	0.23
14.54	2.05	1180.00	332.00	100.20	319.60	1219.60	343.14	103.56	330.33	0.38
15.17	2.44	1186.90	316.40	88.20	314.96	1219.60	325.12	90.63	323.64	0.38
15.40	2.82	1136.90	312.30	86.90	300.30	1219.60	335.02	93.22	322.14	0.38
16.03	3.20	945.40	247.50	69.10	248.90	1219.60	319.28	89.14	321.09	0.37
16.25	3.57	1019.00	253.70	68.50	265.90	1219.60	303.64	81.98	318.24	0.38
16.48	3.95	1014.30	244.00	63.60	261.30	1219.60	293.39	76.47	314.19	0.38
17.11	4.34	1006.00	240.60	58.60	253.40	1219.60	291.69	71.04	307.20	0.38
17.34	4.72	991.00	232.40	54.80	246.00	1219.60	286.01	67.44	302.75	

Time hh:mm	t, h	$[OH]_{DMB}$	$[OH]_{Hexan}$	$[OH]_{TMB}$	$\int[OH]dt_{DMB}$	$\int[OH]dt_{Hexan}$	$\int[OH]dt_{TMB}$	$\overline{\int OHdt}$	$\overline{[OH]}$	
12.27	0.00	2.36E+11	2.64E+11	3.20E+11	8.35E+10	9.32E+10	1.13E+11	9.67E+10	5.68E+07	
13.12	0.35	1.07E+11	1.83E+11	2.53E+11	1.18E+11	1.51E+11	1.93E+11	1.54E+11	5.04E+07	
13.31	0.67	3.54E+10	6.42E+10	-3.33E+09	1.28E+11	1.69E+11	1.92E+11	1.63E+11	8.91E+06	
13.48	0.95	-3.44E+10	-5.96E+10	2.82E+11	1.17E+11	1.51E+11	2.82E+11	1.83E+11	1.74E+07	
14.07	1.27	1.21E+10	6.78E+10	-3.09E+11	1.20E+11	1.68E+11	2.04E+11	1.64E+11	-2.12E+07	
14.22	1.52	5.14E+10	6.08E+10	7.06E+10	1.35E+11	1.86E+11	2.26E+11	1.82E+11	1.69E+07	
14.40	1.82	1.51E+10	1.91E+10	9.03E+10	1.39E+11	1.90E+11	2.47E+11	1.92E+11	1.15E+07	
14.54	2.05	7.95E+10	7.50E+10	6.78E+10	1.69E+11	2.19E+11	2.73E+11	2.20E+11	2.06E+07	
15.17	2.44	-4.42E+10	-1.58E+10	1.53E+10	1.52E+11	2.13E+11	2.79E+11	2.15E+11	-4.14E+06	
15.40	2.82	7.09E+10	2.52E+10	1.09E+10	1.79E+11	2.23E+11	2.83E+11	2.28E+11	9.90E+06	
16.03	3.20	7.74E+10	4.92E+10	3.08E+10	2.08E+11	2.41E+11	2.94E+11	2.47E+11	1.46E+07	
16.25	3.57	5.06E+10	3.91E+10	4.25E+10	2.27E+11	2.56E+11	3.10E+11	2.64E+11	1.22E+07	
16.48	3.95	8.57E+09	4.14E+10	7.45E+10	2.30E+11	2.71E+11	3.39E+11	2.80E+11	1.15E+07	
17.11	4.34	2.90E+10	2.92E+10	4.84E+10	2.42E+11	2.83E+11	3.57E+11	2.94E+11	9.88E+06	

Calculated Abraham salvation parameters for Aldrin

A	0.00
B	0.43
Bo	0.43
L	9.476
S	1.20
E	2.01
V	2.0134

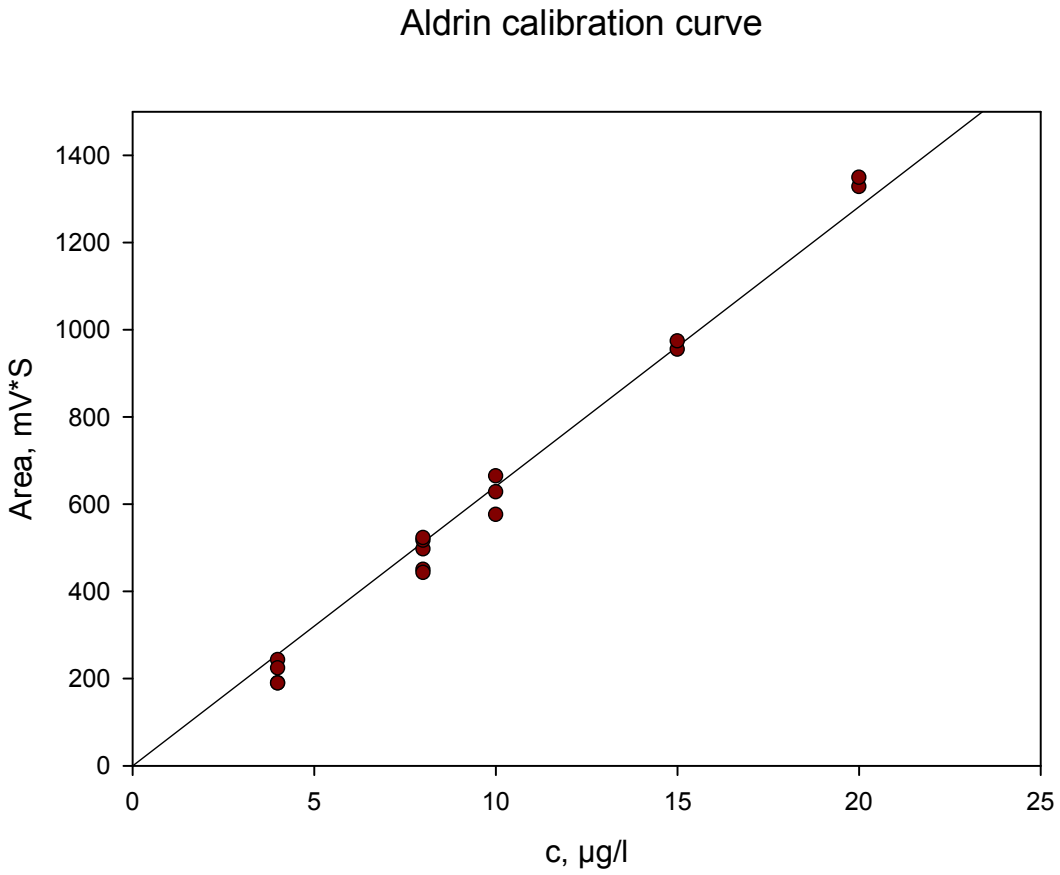

Sympatec GmbH
System-Partikel-Technik

HELOS-Partikelgrößenanalyse

WINDOX 4

HELOS (H1269) & SPRAYER, R3: 0.5/0.9...175µm 29.10.04, 11:21:18,4600

x_{10} = 15.31 µm	**x_{50} = 46.20 µm**	**x_{90} = 98.58 µm**	**SMD = 30.42 µm**	**VMD = 52.24 µm**	
x_{16} = 19.83 µm	x_{84} = 86.09 µm	x_{99} = 138.92 µm	S_V = 0.20 m²/cm³	S_m = 727.78 cm²/g	

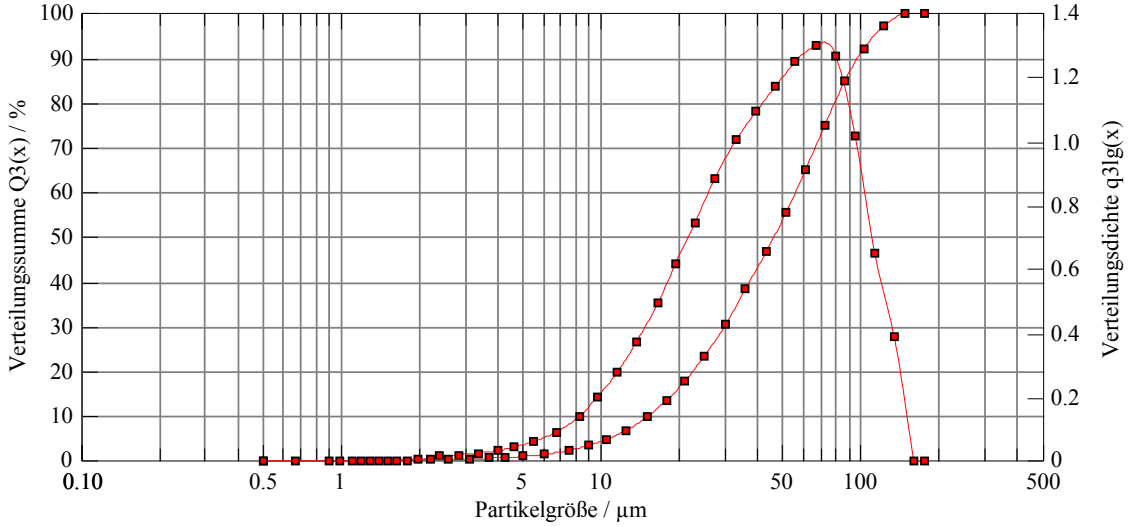

Hohle Glaskugeln von U. Krüger

Auswertung: WINDOX 4.1.2.0, *HRLD*	
Revalidierung:	
Referenzmessung:	29.10 11:20:55
Kontamination:	0.00 %

Produkt: Glaskugeln U. Krüger
Dichte: 2.71 g/cm³, Formfaktor: 1.00
Disp.-Meth.: Dispergierdüse 2,5 bar
C_{opt}= 1.20 %

Meßbedingung: 5s opt. Konz. v> 1%	
Zeitbasis:	1000.00 ms
Start:	c.opt >= 1.00%
Gültigkeit:	immer
Stopp:	5.00s Echtzeit

Benutzerparameter:
Bediener: Oliver Nolte
Probenkennung: Glaskugeln (GeFA)
Probennummer: 13.00
Parameter 4:

Methylnitrite production

10 g $NaNO_2$, 100 ml Methanol and a magnetic still bar are put in a 500 ml three-neck-flask. At the first 0.5 l/min nitrogen are piped with a glass tube in the solution. The flask was placed in a water quench on a magnetic stirrer. On the second flask neck are connected with a pipe and one after another 50 ml – NaOH – impinger, 100 ml – $CaCl_2$ – impinger and 100 ml – coldtrap with liquid nitrogen quenching bath. A dropping funnel with 50 g 50 % sulphuric acids is connected. The acid was mixed with the solution in drops. The solution reacts app. 60 min. The yield is about 60%. The product was stored in 1.3 ml vails in container with liquid nitrogen.

EASY-FIT **A02_1** *25-Apr-07*

Partial Differential Equation

General Information:

Information	Diffusion with chemical Reaction
Model Name	PDE
Project Number	Aldrin 02
Measurement Set	...
User Name	Gavrilov
Date	10/14/2006
Memo	

Model Data:

Number of Variables	3
Number of Constraints	0
Number of Equality Constraints	0
Number of Differential Equations	1
Number of Measurement Sets	1
Number of Time Values	6
Number of Integration Areas	1
Residual Norm	L2

Optimization Variables:

name	lower	init	upper	final
R05	0	2	5	4.996897058
k0	0	0.0002	0.005	0.002851116
alfa	1E-07	0.000001	0.0001	8.9415E-5

Parameter Estimation Data ([y]):

EASY-FIT *A02_1* *25-Apr-07*

time	conc	meas data	function value	error (%)	weight
0	0	1.01313841	1	-1.3	1
270	0	0.02201257	0.021970416	-0.19	1
828	0	0.00436507	8.262594768	-99.81	1
1872	0	0.00375744	2.043343279	-100	1
3420	0	6.95054945	4.685257381	-100	1
6912	0	3.87409200	1.875916898	-100	1

User-Defined Parameters:

Parameter Estimation Method	DFNLP
Maximum Number of Iterations	100
Maximum Number of Function Calls	20
Print Flag (0/1/2/3/...)	2
Termination Accuracy	1.00E-08
First Optimization Tolerance	1.00E-02
Second Optimization Tolerance	2.00E+00
Spatial Discretization Method	5-pt difference formula for 1st and 2nd derivatives
Spatial Upwind Formula	no upwind, standard approximation
ODE-Solver	implicit
Order of Derivative Approximation	7
Accuracy for Gradient Approximation	0
Bandwidth for Jacobian of Right-Hand Side	0
Absolute Error Tolerance for ODE-Solver	1.00E-07
Relative Error Tolerance for ODE-Solver	1.00E-07
Initial Stepsize	1.00E-04
Scaling Method	0

Integration Area Information:

name	i	j	size	disc-pnts	status L	status R	discretization
u(x,t)	1	1	5	61	2	2	0

EASY-FIT *A02_1* *25-Apr-07*

Fitting Positions:

position	line
0.01	1

Numerical Results:

Termination Reason	0
Number of Function Evaluations	24
Number of Gradient Evaluations	18
Number of PDE-Function Calls	44882
Number of PDE-Gradient Calls	0
Final Residual Value (scaled)	2.0600E-04
Sum of Constraint Violations	0.0000E+00
Calculation Time	0 h : 0 min : 4 sec

EASY-FIT **A03_1** *14-May-07*

Partial Differential Equation

General Information:

Information	Diffusion with chemical Reaction
Model Name	PDE
Project Number	Aldrin 03
Measurement Set	...
User Name	Gavrilov
Date	10/14/2006
Memo	

Model Data:

Number of Variables	3
Number of Constraints	0
Number of Equality Constraints	0
Number of Differential Equations	1
Number of Measurement Sets	1
Number of Time Values	7
Number of Integration Areas	1
Residual Norm	L2

Optimization Variables:

name	lower	init	upper	final
R	0	2.3	5	3.113456554
alfa	0.000005	0.00005	0.0005	2.64445E-05
k	0	0.0011	0.0015	0.001493779

Parameter Estimation Data ([y]):

EASY-FIT *A03_1* *14-May-07*

time	conc	meas data	function value	error (%)	weight
0	0	1.00029178	1	-0.03	1
270	0	0.22510427	0.225431413	0.15	1
1170	0	0.00893054	0.001581881	-82.29	1
3060	0	4.3593E-04	4.74263E-04	-99.99	1
5220	0	1.7243E-04	-2.95994E-04	-100	1
7380	0	2.1013E-04	4.70587E-04	-100	1
9972	0	6.0667E-5	8.69794E-04	-100	1

User-Defined Parameters:

Parameter Estimation Method	DFNLP
Maximum Number of Iterations	100
Maximum Number of Function Calls	20
Print Flag (0/1/2/3/...)	2
Termination Accuracy	1.00E-08
First Optimization Tolerance	1.00E-02
Second Optimization Tolerance	2.00E+00
Spatial Discretization Method	5-pt difference formula for 1st and 2nd derivatives
Spatial Upwind Formula	no upwind, standard approximation
ODE-Solver	implicit
Order of Derivative Approximation	7
Accuracy for Gradient Approximation	0
Bandwidth for Jacobian of Right-Hand Side	0
Absolute Error Tolerance for ODE-Solver	1.00E-07
Relative Error Tolerance for ODE-Solver	1.00E-07
Initial Stepsize	1.00E-04
Scaling Method	0

Integration Area Information:

name	i	j	size	disc-pnts	status L	status R	discretization
u(x,t)	1	1	5	61	2	2	0

EASY-FIT *A03_1* *14-May-07*

Fitting Positions:

position	line
0.001	1

Numerical Results:

Termination Reason	0
Number of Function Evaluations	56
Number of Gradient Evaluations	16
Number of PDE-Function Calls	57342
Number of PDE-Gradient Calls	0
Final Residual Value (scaled)	5.4500E-05
Sum of Constraint Violations	0.0000E+00
Calculation Time	0 h : 0 min : 5 sec

EASY-FIT **A04_1** *25-Apr-07*

Partial Differential Equation

General Information:

Information	Diffusion with chemical Reaction
Model Name	PDE
Project Number	Aldrin 04
Measurement Set	...
User Name	Gavrilov
Date	10/14/2006
Memo	

Model Data:

Number of Variables	3
Number of Constraints	0
Number of Equality Constraints	0
Number of Differential Equations	1
Number of Measurement Sets	1
Number of Time Values	7
Number of Integration Areas	1
Residual Norm	L2

Optimization Variables:

name	lower	init	upper	final
R	0	2	5	3.324423940
alfa	0.000001	0.00009	0.008	3.40E-5
k	0.000001	0.00005	0.0001	9.599E-5

Parameter Estimation Data ([y]):

EASY-FIT *A04_1* *25-Apr-07*

time	conc	meas data	function value	error (%)	weight
0	0	1.00330796	1	-0.33	1
331.2	0	1.04435934	0.906131941	-13.24	1
1368	0	0.79513623	0.665870102	-16.26	1
4212	0	0.20073424	0.285998287	42.48	1
8172	0	0.01888344	0.088168686	366.91	1
13032	0	0.00106371	0.020802605	1855.65	1
16848	0	0.00065825	0.006693487	916.86	1

User-Defined Parameters:

Parameter Estimation Method	DFNLP
Maximum Number of Iterations	100
Maximum Number of Function Calls	20
Print Flag (0/1/2/3/...)	2
Termination Accuracy	1.00E-08
First Optimization Tolerance	1.00E-02
Second Optimization Tolerance	2.00E+00
Spatial Discretization Method	5-pt difference formula for 1st and 2nd derivatives
Spatial Upwind Formula	no upwind, standard approximation
ODE-Solver	implicit
Order of Derivative Approximation	7
Accuracy for Gradient Approximation	0
Bandwidth for Jacobian of Right-Hand Side	0
Absolute Error Tolerance for ODE-Solver	1.00E-07
Relative Error Tolerance for ODE-Solver	1.00E-07
Initial Stepsize	1.00E-04
Scaling Method	0

Integration Area Information:

name	i	j	size	disc-pnts	status L	status R	discretization
u(x,t)	1	1	5	61	2	2	0

EASY-FIT *A04_1* *25-Apr-07*

Fitting Positions:

position	line
0.001	1

Numerical Results:

Termination Reason	0
Number of Function Evaluations	126
Number of Gradient Evaluations	32
Number of PDE-Function Calls	88291
Number of PDE-Gradient Calls	0
Final Residual Value (scaled)	4.8300E-02
Sum of Constraint Violations	0.0000E+00
Calculation Time	0 h : 0 min : 8 sec

EASY-FIT **A12_1** *25-Apr-07*

Partial Differential Equation

General Information:

Information	Diffusion with chemical Reaction
Model Name	PDE
Project Number	Aldrin 12
Measurement Set	...
User Name	Gavrilov
Date	10/14/2006
Memo	

Model Data:

Number of Variables	3
Number of Constraints	0
Number of Equality Constraints	0
Number of Differential Equations	1
Number of Measurement Sets	1
Number of Time Values	10
Number of Integration Areas	1
Residual Norm	L2

Optimization Variables:

name	lower	init	upper	final
R	0	0.9	2	1.973263761
alfa	0.000001	0.00008	0.001	5.049805E-5
k	0.000001	0.00008	0.0003	0.000294480

Parameter Estimation Data ([C]):

EASY-FIT *A12_1* *25-Apr-07*

time	conc	meas data	function value	error (%)	weight
0	0	0.91504381	1	9.28	1
0	0	1.00027428	1	-0.03	1
3024	0	0.17043809	0.169300575	-0.67	1
3024	0	0.17310119	0.169300575	-2.2	1
6552	0	0.01225083	0.021329556	74.11	1
6552	0	0.01376328	0.021329556	54.97	1
10152	0	0.00849958	0.002575984	-69.69	1
10152	0	0.01311365	0.002575984	-80.36	1
13968	0	0.00209699	0.000274046	-86.93	1
13968	0	0.00468738	0.000274046	-94.15	1

User-Defined Parameters:

Parameter Estimation Method	DFNLP
Maximum Number of Iterations	100
Maximum Number of Function Calls	20
Print Flag (0/1/2/3/...)	2
Termination Accuracy	1.00E-08
First Optimization Tolerance	1.00E-02
Second Optimization Tolerance	2.00E+00
Spatial Discretization Method	5-pt difference formula for 1st and 2nd derivatives
Spatial Upwind Formula	no upwind, standard approximation
ODE-Solver	implicit
Order of Derivative Approximation	7
Accuracy for Gradient Approximation	0
Bandwidth for Jacobian of Right-Hand Side	0
Absolute Error Tolerance for ODE-Solver	1.00E-07
Relative Error Tolerance for ODE-Solver	1.00E-07
Initial Stepsize	1.00E-04
Scaling Method	0

EASY-FIT *A12_1* *25-Apr-07*

Integration Area Information:

name	i	j	size	disc-pnts	status L	status R	discretization
u(x,t)	1	1	5	61	2	2	0

Fitting Positions:

position	line
0.001	1

Numerical Results:

Termination Reason	0
Number of Function Evaluations	112
Number of Gradient Evaluations	24
Number of PDE-Function Calls	86046
Number of PDE-Gradient Calls	0
Final Residual Value (scaled)	7.5400E-03
Sum of Constraint Violations	0.0000E+00
Calculation Time	0 h : 0 min : 8 sec

EASY-FIT **A13_1** *25-Apr-07*

Partial Differential Equation

General Information:

Information	Diffusion with chemical Reaction
Model Name	PDE
Project Number	Aldrin 13
Measurement Set	...
User Name	Gavrilov
Date	10/14/2006
Memo	

Model Data:

Number of Variables	3
Number of Constraints	0
Number of Equality Constraints	0
Number of Differential Equations	1
Number of Measurement Sets	1
Number of Time Values	12
Number of Integration Areas	1
Residual Norm	L2

Optimization Variables:

name	lower	init	upper	final
R	0	1	2.5	2.283142552
alfa	0.00001	0.00007	100	1.3172E-05
k	0.00000	0.00008	0.0001	9.9503E-05

Parameter Estimation Data ([y]):

EASY-FIT *A13_1* *25-Apr-07*

time	conc	meas data	function value	error (%)	weight
0	0	0.94746114	1	5.55	1
0	0	1.00051071	1	-0.05	1
2592	0	0.49392205	0.523991355	6.09	1
2592	0	0.50004660	0.523991355	4.79	1
5256	0	0.18332242	0.269720400	47.13	1
5256	0	0.19713371	0.269720400	36.82	1
8100	0	0.19548757	0.132744424	-32.1	1
8100	0	0.20935259	0.132744424	-36.59	1
10872	0	0.07712895	0.066514086	-13.76	1
10872	0	0.12004822	0.066514086	-44.59	1
13680	0	0.13296240	0.033030374	-75.16	1
13680	0	0.15721998	0.033030374	-78.99	1

User-Defined Parameters:

Parameter Estimation Method	DFNLP
Maximum Number of Iterations	100
Maximum Number of Function Calls	20
Print Flag (0/1/2/3/...)	2
Termination Accuracy	1.00E-08
First Optimization Tolerance	1.00E-02
Second Optimization Tolerance	2.00E+00
Spatial Discretization Method	5-pt difference formula for 1st and 2nd derivatives
Spatial Upwind Formula	no upwind, standard approximation
ODE-Solver	implicit
Order of Derivative Approximation	7
Accuracy for Gradient Approximation	0
Bandwidth for Jacobian of Right-Hand Side	0
Absolute Error Tolerance for ODE-Solver	1.00E-07
Relative Error Tolerance for ODE-Solver	1.00E-07
Initial Stepsize	1.00E-04
Scaling Method	0

EASY-FIT *A13_1* *25-Apr-07*

Integration Area Information:

name	i	j	size	disc-pnts	status L	status R	discretization
u(x,t)	1	1	5	61	2	2	0

Fitting Positions:

position	line
0.001	1

Numerical Results:

Termination Reason	0
Number of Function Evaluations	176
Number of Gradient Evaluations	34
Number of PDE-Function Calls	95072
Number of PDE-Gradient Calls	0
Final Residual Value (scaled)	5.5200E-02
Sum of Constraint Violations	0.0000E+00
Calculation Time	0 h : 0 min : 9 sec

EASY-FIT **A14_1** *25-Apr-07*

Partial Differential Equation

General Information:

Information	Diffusion with chemical Reaction
Model Name	PDE
Project Number	Aldrin 14
Measurement Set	...
User Name	Gavrilov
Date	10/14/2006
Memo	

Model Data:

Number of Variables	3
Number of Constraints	0
Number of Equality Constraints	0
Number of Differential Equations	1
Number of Measurement Sets	1
Number of Time Values	12
Number of Integration Areas	1
Residual Norm	L2

Optimization Variables:

name	lower	init	upper	final
k0	0.000001	0.0001	0.0002	0.000190023
R05	0	0.8	2	0.980996053
alfa	0	0.00000	0.000007	6.34603E-06

Parameter Estimation Data ([y]):

EASY-FIT *A14_1* *25-Apr-07*

time	conc	meas data	function value	error (%)	weight
0	0	0.96681189	1	3.43	1
0	0	1.00168755	1	-0.17	1
2736	0	0.57736229	0.694021444	20.21	1
2736	0	0.61526682	0.694021444	12.8	1
6192	0	0.40469019	0.437639440	8.14	1
6192	0	0.41392237	0.437639440	5.73	1
9792	0	0.27662172	0.270717290	-2.13	1
9792	0	0.29378228	0.270717290	-7.85	1
13608	0	0.20691256	0.162704471	-21.37	1
13608	0	0.24699514	0.162704471	-34.13	1
16488	0	0.13525911	0.110794728	-18.09	1
16488	0	0.17424267	0.110794728	-36.41	1

User-Defined Parameters:

Parameter Estimation Method	DFNLP
Maximum Number of Iterations	100
Maximum Number of Function Calls	20
Print Flag (0/1/2/3/...)	2
Termination Accuracy	1.00E-08
First Optimization Tolerance	1.00E-02
Second Optimization Tolerance	2.00E+00
Spatial Discretization Method	5-pt difference formula for 1st and 2nd derivatives
Spatial Upwind Formula	no upwind, standard approximation
ODE-Solver	implicit
Order of Derivative Approximation	7
Accuracy for Gradient Approximation	0
Bandwidth for Jacobian of Right-Hand Side	0
Absolute Error Tolerance for ODE-Solver	1.00E-07
Relative Error Tolerance for ODE-Solver	1.00E-07
Initial Stepsize	1.00E-04
Scaling Method	0

EASY-FIT *A14_1* *25-Apr-07*

Integration Area Information:

name	i	j	size	disc-pnts	status L	status R	discretization
u(x,t)	1	1	5	61	2	2	0

Fitting Positions:

position	line
0.001	1

Numerical Results:

Termination Reason	0
Number of Function Evaluations	175
Number of Gradient Evaluations	29
Number of PDE-Function Calls	77439
Number of PDE-Gradient Calls	0
Final Residual Value (scaled)	3.6800E-02
Sum of Constraint Violations	0.0000E+00
Calculation Time	0 h : 0 min : 7 sec

EASY-FIT **A21_1** *25-Apr-07*

Partial Differential Equation

General Information:

Information	Diffusion with chemical Reaction
Model Name	PDE
Project Number	Aldrin 21
Measurement Set	...
User Name	Gavrilov
Date	10/14/2006
Memo	

Model Data:

Number of Variables	3
Number of Constraints	0
Number of Equality Constraints	0
Number of Differential Equations	1
Number of Measurement Sets	1
Number of Time Values	12
Number of Integration Areas	1
Residual Norm	L2

Optimization Variables:

name	lower	init	upper	final
R	0	0.6	2.5	2.16879787
k	0.000001	0.00008	0.0001	9.7497E-05
alfa	0	0.000005	0.00001	2.6998E-07

EASY-FIT *A21_1* *25-Apr-07*

Parameter Estimation Data ([y]):

time	conc	meas data	function value	error (%)	weight
0	0	0.80221990	1	24.65	1
0	0	1.00296864	1	-0.3	1
2340	0	0.58033954	0.545623515	-5.98	1
2340	0	0.76270763	0.545623515	-28.46	1
4608	0	0.22188787	0.303341382	36.71	1
4608	0	0.27593748	0.303341382	9.93	1
6048	0	0.19928641	0.208954330	4.85	1
6048	0	0.20431890	0.208954330	2.27	1
8208	0	0.01965687	0.119462325	507.74	1
8208	0	0.11344822	0.119462325	5.3	1
9720	0	0.04934880	0.080771226	63.67	1
9720	0	0.05173857	0.080771226	56.11	1

User-Defined Parameters:

Parameter Estimation Method	DFNLP
Maximum Number of Iterations	100
Maximum Number of Function Calls	20
Print Flag (0/1/2/3/...)	2
Termination Accuracy	1.00E-08
First Optimization Tolerance	1.00E-02
Second Optimization Tolerance	2.00E+00
Spatial Discretization Method	5-pt difference formula for 1st and 2nd derivatives
Spatial Upwind Formula	no upwind, standard approximation
ODE-Solver	implicit
Order of Derivative Approximation	7
Accuracy for Gradient Approximation	0
Bandwidth for Jacobian of Right-Hand Side	0
Absolute Error Tolerance for ODE-Solver	1.00E-07
Relative Error Tolerance for ODE-Solver	1.00E-07
Initial Stepsize	1.00E-04
Scaling Method	0

EASY-FIT *A21_1* *25-Apr-07*

Integration Area Information:

name	i	j	size	disc-pnts	status L	status R	discretization
u(x,t)	1	1	5	61	2	2	0

Fitting Positions:

position	line
0.001	1

Numerical Results:

Termination Reason	0
Number of Function Evaluations	70
Number of Gradient Evaluations	29
Number of PDE-Function Calls	49207
Number of PDE-Gradient Calls	0
Final Residual Value (scaled)	1.0700E-01
Sum of Constraint Violations	0.0000E+00
Calculation Time	0 h : 0 min : 4 sec

EASY-FIT **A23_1** *14-May-07*

Partial Differential Equation

General Information:

Information	Diffusion with chemical Reaction
Model Name	PDE
Project Number	Aldrin 23
Measurement Set	...
User Name	Gavrilov
Date	10/14/2006
Memo	

Model Data:

Number of Variables	3
Number of Constraints	0
Number of Equality Constraints	0
Number of Differential Equations	1
Number of Measurement Sets	1
Number of Time Values	14
Number of Integration Areas	1
Residual Norm	L2

Optimization Variables:

name	lower	init	upper	final
R	0	0.4	2	1.930510780
k	1E-07	0.000001	0.00006	0.000059686
alfa	1E-07	0.000001	0.00001	4.61180E-07

Parameter Estimation Data ([y]):

EASY-FIT *A23_1* *14-May-07*

time	conc	meas data	function value	error (%)	weight
0	0	0.774496875	1	29.12	1
0	0	1.011575625	1	-1.14	1
1080	0	0.81938656	0.861568147	5.15	1
1080	0	0.946280625	0.861568147	-8.95	1
3780	0	0.76133251	0.593734917	-22.01	1
3780	0	0.82598053	0.593734917	-28.12	1
6300	0	0.43408023	0.419445305	-3.37	1
6300	0	0.44386384	0.419445305	-5.5	1
10188	0	0.17653057	0.245375708	39	1
10188	0	0.18109113	0.245375708	35.5	1
13500	0	0.04565693	0.155411515	240.39	1
13500	0	0.09071838	0.155411515	71.31	1
14580	0	0.02699875	0.133907336	395.98	1
14580	0	0.06638390	0.133907336	101.72	1

User-Defined Parameters:

Parameter Estimation Method	DFNLP
Maximum Number of Iterations	100
Maximum Number of Function Calls	20
Print Flag (0/1/2/3/...)	2
Termination Accuracy	1.00E-08
First Optimization Tolerance	1.00E-02
Second Optimization Tolerance	2.00E+00
Spatial Discretization Method	5-pt difference formula for 1st and 2nd derivatives
Spatial Upwind Formula	no upwind, standard approximation

EASY-FIT *A23_1* *14-May-07*

ODE-Solver	implicit
Order of Derivative Approximation	7
Accuracy for Gradient Approximation	0
Bandwidth for Jacobian of Right-Hand Side	0
Absolute Error Tolerance for ODE-Solver	1.00E-07
Relative Error Tolerance for ODE-Solver	1.00E-07
Initial Stepsize	1.00E-04
Scaling Method	0

Integration Area Information:

name	i	j	size	disc-pnts	status L	status R	discretization
u(x,t)	1	1	5	61	2	2	0

Fitting Positions:

position	line
0.001	1

Numerical Results:

Termination Reason	0
Number of Function Evaluations	96
Number of Gradient Evaluations	27
Number of PDE-Function Calls	47824
Number of PDE-Gradient Calls	0
Final Residual Value (scaled)	1.8400E-01
Sum of Constraint Violations	0.0000E+00
Calculation Time	0 h : 0 min : 5 sec

EASY-FIT **A25_1** *14-May-07*

Partial Differential Equation

General Information:

Information	Diffusion with chemical Reaction
Model Name	PDE
Project Number	Aldrin 25
Measurement Set	...
User Name	Gavrilov
Date	10/14/2006
Memo	

Model Data:

Number of Variables	3
Number of Constraints	0
Number of Equality Constraints	0
Number of Differential Equations	1
Number of Measurement Sets	1
Number of Time Values	12
Number of Integration Areas	1
Residual Norm	L2

Optimization Variables:

name	lower	init	upper	final
R	0	0.8	1.5	1.156494220
k	0.000001	0.00008	0.00015	0.000149906
alfa	0	0.000001	0.00001	7.96569E-06

Parameter Estimation Data ([y]):

EASY-FIT *A25_1* *14-May-07*

time	conc	meas data	function value	error (%)	weight
0	0	0.98160055	1	1.87	1
0	0	1.00505579	1	-0.5	1
1188	0	0.74631624	0.844150195	13.11	1
1188	0	0.83153544	0.844150195	1.52	1
4032	0	0.83172192	0.562939424	-32.32	1
4032	0	0.83631619	0.562939424	-32.69	1
5112	0	0.52334147	0.482660949	-7.77	1
5112	0	0.62026573	0.482660949	-22.18	1
7740	0	0.17734009	0.331931158	87.17	1
7740	0	0.19717328	0.331931158	68.34	1
9648	0	0.07265593	0.252929915	248.12	1
9648	0	0.09892676	0.252929915	155.67	1

User-Defined Parameters:

Parameter Estimation Method	DFNLP
Maximum Number of Iterations	100
Maximum Number of Function Calls	20
Print Flag (0/1/2/3/...)	2
Termination Accuracy	1.00E-08
First Optimization Tolerance	1.00E-02
Second Optimization Tolerance	2.00E+00
Spatial Discretization Method	5-pt difference formula for 1st and 2nd derivatives
Spatial Upwind Formula	no upwind, standard approximation
ODE-Solver	implicit
Order of Derivative Approximation	7
Accuracy for Gradient Approximation	0
Bandwidth for Jacobian of Right-Hand Side	0
Absolute Error Tolerance for ODE-Solver	1.00E-07
Relative Error Tolerance for ODE-Solver	1.00E-07
Initial Stepsize	1.00E-04
Scaling Method	0

EASY-FIT *A25_1* *14-May-07*

Integration Area Information:

name	i	j	size	disc-pnts	status L	status R	discretization
u(x,t)	1	1	5	51	2	2	0

Fitting Positions:

position	line
0.001	1

Numerical Results:

Termination Reason	0
Number of Function Evaluations	179
Number of Gradient Evaluations	55
Number of PDE-Function Calls	83543
Number of PDE-Gradient Calls	0
Final Residual Value (scaled)	2.7600E-01
Sum of Constraint Violations	0.0000E+00
Calculation Time	0 h : 0 min : 7 sec

EASY-FIT **A26_1** *14-May-07*

Partial Differential Equation

General Information:

Information	Diffusion with chemical Reaction
Model Name	PDE
Project Number	Aldrin 26
Measurement Set	...
User Name	Gavrilov
Date	11/21/2006
Memo	

Model Data:

Number of Variables	3
Number of Constraints	0
Number of Equality Constraints	0
Number of Differential Equations	1
Number of Measurement Sets	1
Number of Time Values	12
Number of Integration Areas	1
Residual Norm	L2

Optimization Variables:

name	lower	init	upper	final
R	0	1	3	1.580353018
k	1E-07	0.0001	0.0003	0.000134613
alfa	1E-08	0.000005	0.00001	1.450462E-07

Parameter Estimation Data ([y]):

EASY-FIT *A26_1* *14-May-07*

time	conc	meas data	function value	error (%)	weight
0	0	0.78228480	1	27.83	1
0	0	1.03280510	1	-3.18	1
1188	0	0.64453416	0.751389588	16.58	1
1188	0	1.02365320	0.751389588	-26.6	1
3852	0	0.41051525	0.395971844	-3.54	1
3852	0	0.48085054	0.395971844	-17.65	1
7200	0	0.07123235	0.177024530	148.52	1
7200	0	0.07224432	0.177024530	145.04	1
10728	0	0.05171428	0.075788856	46.55	1
10728	0	0.05580285	0.075788856	35.82	1
13500	0	0.03691428	0.038915805	5.42	1
13500	0	0.05270952	0.038915805	-26.17	1

User-Defined Parameters:

Parameter Estimation Method	DFNLP
Maximum Number of Iterations	100
Maximum Number of Function Calls	20
Print Flag (0/1/2/3/...)	2
Termination Accuracy	1.00E-08
First Optimization Tolerance	1.00E-02
Second Optimization Tolerance	2.00E+00
Spatial Discretization Method	5-pt difference formula for 1st and 2nd derivatives
Spatial Upwind Formula	no upwind, standard approximation
ODE-Solver	implicit
Order of Derivative Approximation	7
Accuracy for Gradient Approximation	0
Bandwidth for Jacobian of Right-Hand Side	0
Absolute Error Tolerance for ODE-Solver	1.00E-07
Relative Error Tolerance for ODE-Solver	1.00E-07
Initial Stepsize	1.00E-04
Scaling Method	0

EASY-FIT *A26_1* *14-May-07*

Integration Area Information:

name	i	j	size	disc-pnts	status L	status R	discretization
u(x,t)	1	1	5	61	2	2	0

Fitting Positions:

position	line
0.001	1

Numerical Results:

Termination Reason	0
Number of Function Evaluations	76
Number of Gradient Evaluations	23
Number of PDE-Function Calls	49402
Number of PDE-Gradient Calls	0
Final Residual Value (scaled)	1.6500E-01
Sum of Constraint Violations	0.0000E+00
Calculation Time	0 h : 0 min : 5 sec

EASY-FIT **A27_1** *14-May-07*

Partial Differential Equation

General Information:

Information	Diffusion with chemical Reaction
Model Name	PDE
Project Number	Aldrin 27
Measurement Set	...
User Name	Gavrilov
Date	11/21/2006
Memo	

Model Data:

Number of Variables	3
Number of Constraints	0
Number of Equality Constraints	0
Number of Differential Equations	1
Number of Measurement Sets	1
Number of Time Values	12
Number of Integration Areas	1
Residual Norm	L2

Optimization Variables:

name	lower	init	upper	final
alfa	0	0.00000	0.00001	3.73198E-06
k0	0.000008	0.0002	0.0005	0.000119238
R05	0	1.6	5	1.589403834

Parameter Estimation Data ([y]):

EASY-FIT *A27_1* *14-May-07*

time	conc	meas data	function value	error (%)	weight
0	0	1.00058125	1	-0.06	1
2592	0	0.54609820	0.585564720	7.23	1
6480	0	0.26734816	0.262444122	-1.83	1
6480	0	0.35040778	0.262444122	-25.1	1
10188	0	0.09982362	0.122077284	22.29	1
10188	0	0.10796110	0.122077284	13.08	1
13572	0	0.02967420	0.060712422	104.6	1
13572	0	0.07186562	0.060712422	-15.52	1
17028	0	0.05489672	0.029748563	-45.81	1
17028	0	0.05610296	0.029748563	-46.98	1

User-Defined Parameters:

Parameter Estimation Method	DFNLP
Maximum Number of Iterations	100
Maximum Number of Function Calls	20
Print Flag (0/1/2/3/...)	2
Termination Accuracy	1.00E-08
First Optimization Tolerance	1.00E-02
Second Optimization Tolerance	2.00E+00
Spatial Discretization Method	5-pt difference formula for 1st and 2nd derivatives
Spatial Upwind Formula	no upwind, standard approximation
ODE-Solver	implicit
Order of Derivative Approximation	7
Accuracy for Gradient Approximation	0
Bandwidth for Jacobian of Right-Hand Side	0
Absolute Error Tolerance for ODE-Solver	1.00E-07
Relative Error Tolerance for ODE-Solver	1.00E-07
Initial Stepsize	1.00E-04
Scaling Method	0

EASY-FIT *A27_1* *14-May-07*

Integration Area Information:

name	i	j	size	disc-pnts	status L	status R	discretization
u(x,t)	1	1	5	61	2	2	0

Fitting Positions:

position	line
0.001	1

Numerical Results:

Termination Reason	0
Number of Function Evaluations	119
Number of Gradient Evaluations	40
Number of PDE-Function Calls	87882
Number of PDE-Gradient Calls	0
Final Residual Value (scaled)	1.4000E-02
Sum of Constraint Violations	0.0000E+00
Calculation Time	0 h : 0 min : 8 sec

EASY-FIT **A28_1** *14-May-07*

Partial Differential Equation

General Information:

Information	Diffusion with chemical Reaction
Model Name	PDE
Project Number	Aldrin 28
Measurement Set	...
User Name	Gavrilov
Date	11/21/2006
Memo	

Model Data:

Number of Variables	3
Number of Constraints	0
Number of Equality Constraints	0
Number of Differential Equations	1
Number of Measurement Sets	1
Number of Time Values	13
Number of Integration Areas	1
Residual Norm	L2

Optimization Variables:

name	lower	init	upper	final
alfa	0	0.000001	0.00001	9.92082E-06
k0	1E-07	2E-06	0.0004	0.000386956
R05	0	0.5	2	1.999994585

Parameter Estimation Data ([y]):

EASY-FIT *A28_1* *14-May-07*

time	conc	meas data	function value	error (%)	weight
0	0	1.01148437	1	-1.14	1
1188	0	0.29257331	0.336364525	14.97	1
1188	0	0.34970393	0.336364525	-3.81	1
4212	0	0.08393746	0.021027168	-74.95	1
4212	0	0.09209595	0.021027168	-77.17	1
7092	0	0.01399808	0.001499975	-89.28	1
7092	0	0.02078042	0.001499975	-92.78	1
10728	0	0.00953830	5.34972 E-04	-99.44	1
10728	0	0.01764225	5.34972 E-04	-99.7	1
14652	0	0.00638112	1.46262 E-04	-99.98	1
14652	0	0.01588647	1.46262 E-04	-99.99	1
18288	0	0.01586450	5.25494E-04	-100	1

User-Defined Parameters:

Parameter Estimation Method	DFNLP
Maximum Number of Iterations	100
Maximum Number of Function Calls	20
Print Flag (0/1/2/3/...)	2
Termination Accuracy	1.00E-08
First Optimization Tolerance	1.00E-02
Second Optimization Tolerance	2.00E+00
Spatial Discretization Method	5-pt difference formula for 1st and 2nd derivatives
Spatial Upwind Formula	no upwind, standard approximation
ODE-Solver	implicit
Order of Derivative Approximation	7
Accuracy for Gradient Approximation	0
Bandwidth for Jacobian of Right-Hand Side	0
Absolute Error Tolerance for ODE-Solver	1.00E-07
Relative Error Tolerance for ODE-Solver	1.00E-07
Initial Stepsize	1.00E-04
Scaling Method	0

EASY-FIT *A28_1* *14-May-07*

Integration Area Information:

name	i	j	size	disc-pnts	status L	status R	discretization
u(x,t)	1	1	5	61	2	2	0

Fitting Positions:

position	line
1	13

Numerical Results:

Termination Reason	0
Number of Function Evaluations	71
Number of Gradient Evaluations	19
Number of PDE-Function Calls	64915
Number of PDE-Gradient Calls	0
Final Residual Value (scaled)	1.2700E-02
Sum of Constraint Violations	0.0000E+00
Calculation Time	0 h : 0 min : 6 sec

EASY-FIT **A_32** *30-Nov-06*

Partial Differential Equation

General Information:

Information	Diffusion with chemical Reaction
Model Name	PDE
Project Number	Aldrin 32
Measurement Set	Aldr32
User Name	Gavrilov
Date	11/30/2006
Memo	

Model Data:

Number of Variables	3
Number of Constraints	0
Number of Equality Constraints	0
Number of Differential Equations	1
Number of Measurement Sets	1
Number of Time Values	12
Number of Integration Areas	1
Residual Norm	L2

Optimization Variables:

name	lower	init	upper	final
R	0	2.39532	100	2.34
alfa	0	0.00000	100	0.00012
k	0	0.00067	100	0.000894

Parameter Estimation Data ([y]):

EASY-FIT *A_32* *30-Nov-06*

time	conc	meas data	function value	error (%)	weight
0	0	0.87939053	1	13.72	1
0	0	1.00197224	1	-0.2	1
180	0	0.60083785	0.654373306213	8.91	1
180	0	0.69084190	0.654373306213	-5.28	1
5688	0	0.13229578	1.5785200E-04	-100	1
5688	0	0.13282286	1.5785200E-04	-100	1
8028	0	0.05124768	6.9971178E-04	-100	1
8028	0	0.06538497	6.9971177E-04	-100	1
12060	0	0.02579357	-9.624286E-04	-100	1
12060	0	0.02661241	-9.624286E-04	-100	1
13608	0	0.04565264	6.1571029E-04	-100	1
13608	0	0.04638897	6.1571029E-04	-100	1

User-Defined Parameters:

Parameter Estimation Method	DFNLP
Maximum Number of Iterations	100
Maximum Number of Function Calls	20
Print Flag (0/1/2/3/...)	2
Termination Accuracy	1.00E-08
First Optimization Tolerance	1.00E-02
Second Optimization Tolerance	2.00E+00
Spatial Discretization Method	5-pt difference formula for 1st and 2nd derivatives
Spatial Upwind Formula	no upwind, standard approximation
ODE-Solver	implicit
Order of Derivative Approximation	7
Accuracy for Gradient Approximation	0
Bandwidth for Jacobian of Right-Hand Side	0
Absolute Error Tolerance for ODE-Solver	1.00E-07
Relative Error Tolerance for ODE-Solver	1.00E-07
Initial Stepsize	1.00E-04
Scaling Method	0

EASY-FIT *A_32* *30-Nov-06*

Integration Area Information:

name	i	j	size	disc-pnts	status L	status R	discretization
u(x,t)	1	1	5	61	2	2	0

Fitting Positions:

position	line
0.001	1

Numerical Results:

Termination Reason	0
Number of Function Evaluations	216
Number of Gradient Evaluations	28
Number of PDE-Function Calls	157107
Number of PDE-Gradient Calls	0
Final Residual Value (scaled)	6.6400E-02
Sum of Constraint Violations	0.0000E+00
Calculation Time	0 h : 0 min : 15 sec

EASY-FIT **A_34** *11-Dec-06*

Partial Differential Equation

General Information:

Information	Diffusion with chemical Reaction
Model Name	PDE
Project Number	Aldrin 34
Measurement Set	Aldr34
User Name	Gavrilov
Date	11/30/2006
Memo	sniatam bez izporenie

Model Data:

Number of Variables	3
Number of Constraints	0
Number of Equality Constraints	0
Number of Differential Equations	1
Number of Measurement Sets	1
Number of Time Values	12
Number of Integration Areas	1
Residual Norm	L2

Optimization Variables:

name	lower	init	upper	final
R	0	4.5	100	4.78
k0	0	0.00008	100	3.71E-3
D_{eff}	0	0.45	1000	0.32

Parameter Estimation Data ([y]):

EASY-FIT *A_34* *11-Dec-06*

time	conc	meas data	function value	error (%)	weight
0	0	0.90918467	1	9.99	1
0	0	1	1	0	1
792	0	0.67102	0.865280817	28.95	1
792	0	0.69945549	0.865280817	23.71	1
2736	0	0.55694987	0.606675215	8.93	1
2736	0	0.61989	0.606675215	-2.13	1
3780	0	0.47948747	0.501354263	4.56	1
3780	0	0.5351	0.501354263	-6.31	1
6408	0	0.34792582	0.310233026	-10.83	1
6408	0	0.3871	0.310233026	-19.86	1
7632	0	0.2545	0.248083925	-2.52	1
7632	0	0.27175608	0.248083925	-8.71	1

User-Defined Parameters:

Parameter Estimation Method	DFNLP
Maximum Number of Iterations	100
Maximum Number of Function Calls	20
Print Flag (0/1/2/3/...)	2
Termination Accuracy	1.00E-08
First Optimization Tolerance	1.00E-02
Second Optimization Tolerance	2.00E+00
Spatial Discretization Method	5-pt difference formula for 1st and 2nd derivatives
Spatial Upwind Formula	no upwind, standard approximation
ODE-Solver	implicit
Order of Derivative Approximation	7
Accuracy for Gradient Approximation	0
Bandwidth for Jacobian of Right-Hand Side	0
Absolute Error Tolerance for ODE-Solver	1.00E-07
Relative Error Tolerance for ODE-Solver	1.00E-07
Initial Stepsize	1.00E-04
Scaling Method	0

EASY-FIT *A_34* *11-Dec-06*

Integration Area Information:

name	i	j	size	disc-pnts	status L	status R	discretization
u(x,t)	1	1	5	61	2	2	0

Fitting Positions:

position	line
0.001	1

Numerical Results:

Termination Reason	0
Number of Function Evaluations	73
Number of Gradient Evaluations	17
Number of PDE-Function Calls	29425
Number of PDE-Gradient Calls	0
Final Residual Value (scaled)	8.5700E-02
Sum of Constraint Violations	0.0000E+00
Calculation Time	0 h : 0 min : 2 sec

EASY-FIT **A37_1** *14-May-07*

Partial Differential Equation

General Information:

Information	Diffusion with chemical Reaction
Model Name	PDE
Project Number	Aldrin 37
Measurement Set	...
User Name	Gavrilov
Date	12/11/2006
Memo	

Model Data:

Number of Variables	3
Number of Constraints	0
Number of Equality Constraints	0
Number of Differential Equations	1
Number of Measurement Sets	1
Number of Time Values	7
Number of Integration Areas	1
Residual Norm	L2

Optimization Variables:

name	lower	init	upper	final
R	2.6	3.5	5	2.699442656
alfa	0	0.0001	0.001	0.000958862
k	0.0008	0.001	0.003	0.000813043

Parameter Estimation Data ([y]):

EASY-FIT *A37_1* *14-May-07*

time	conc	meas data	function value	error (%)	weight
0	0	1.00390648	1	-0.39	1
720	0	0.61705574	0.712863543	15.53	1
3456	0	0.13397871	0.198135644	47.89	1
4788	0	0.23442615	0.106232438	-54.68	1
7416	0	0.11427537	0.031057208	-72.82	1
8928	0	0.07715417	0.015306470	-80.16	1

User-Defined Parameters:

Parameter Estimation Method	DFNLP
Maximum Number of Iterations	100
Maximum Number of Function Calls	20
Print Flag (0/1/2/3/...)	2
Termination Accuracy	1.00E-08
First Optimization Tolerance	1.00E-02
Second Optimization Tolerance	2.00E+00
Spatial Discretization Method	5-pt difference formula for 1st and 2nd derivatives
Spatial Upwind Formula	no upwind, standard approximation
ODE-Solver	implicit
Order of Derivative Approximation	7
Accuracy for Gradient Approximation	0
Bandwidth for Jacobian of Right-Hand Side	0
Absolute Error Tolerance for ODE-Solver	1.00E-07
Relative Error Tolerance for ODE-Solver	1.00E-07
Initial Stepsize	1.00E-04
Scaling Method	0

Integration Area Information:

name	i	j	size	disc-pnts	status L	status R	discretization
u(x,t)	1	1	5	61	2	2	0

EASY-FIT *A37_1* *14-May-07*

Fitting Positions:

position	line
2	25

Numerical Results:

Termination Reason	0
Number of Function Evaluations	100
Number of Gradient Evaluations	27
Number of PDE-Function Calls	80095
Number of PDE-Gradient Calls	0
Final Residual Value (scaled)	4.0500E-02
Sum of Constraint Violations	0.0000E+00
Calculation Time	0 h : 0 min : 8 sec

EASY-FIT **A_38** *25-Nov-06*

Partial Differential Equation

General Information:

Information	Diffusion with chemical Reaction
Model Name	PDE
Project Number	Aldrin 38
Measurement Set	Aldr38
User Name	Gavrilov
Date	11/25/2006
Memo	

Model Data:

Number of Variables	3
Number of Constraints	0
Number of Equality Constraints	0
Number of Differential Equations	1
Number of Measurement Sets	1
Number of Time Values	10
Number of Integration Areas	1
Residual Norm	L2

Optimization Variables:

name	lower	init	upper	final
k	0	2.79E-03	100	0.00205
R	0	3.30855	100	3.16
alfa	0	4.36E-03	100	0.00289

Parameter Estimation Data ([y]):

EASY-FIT *A_38* *25-Nov-06*

time	conc	meas data	function value	error (%)	weight
0	0	0.84052988	1	18.97	1
0	0	1.00000128	1	0	1
900	0	0.21582698	0.228576697208	5.91	1
900	0	0.23162819	0.228576697208	-1.32	1
3456	0	0.07023586	0.00352407084	-94.98	1
3456	0	0.09675116	0.00352407084	-96.36	1
4536	0	0.04043877	0.00060452187	-98.51	1
4536	0	0.05651464	0.00060452187	-98.93	1
5832	0	0.04318512	7.28891104553	-99.81	1
5832	0	0.03785680	7.28891104553	-99.83	1

User-Defined Parameters:

Parameter Estimation Method	DFNLP
Maximum Number of Iterations	100
Maximum Number of Function Calls	20
Print Flag (0/1/2/3/...)	2
Termination Accuracy	1.00E-08
First Optimization Tolerance	1.00E-02
Second Optimization Tolerance	2.00E+00
Spatial Discretization Method	5-pt difference formula for 1st and 2nd derivatives
Spatial Upwind Formula	no upwind, standard approximation
ODE-Solver	implicit
Order of Derivative Approximation	7
Accuracy for Gradient Approximation	0
Bandwidth for Jacobian of Right-Hand Side	0
Absolute Error Tolerance for ODE-Solver	1.00E-07
Relative Error Tolerance for ODE-Solver	1.00E-07
Initial Stepsize	1.00E-04
Scaling Method	0

EASY-FIT *A_38* *25-Nov-06*

Integration Area Information:

name	i	j	size	disc-pnts	status L	status R	discretization
u(x,t)	1	1	5	61	2	2	0

Fitting Positions:

position	line
0.001	1

Numerical Results:

Termination Reason	0
Number of Function Evaluations	100
Number of Gradient Evaluations	21
Number of PDE-Function Calls	92087
Number of PDE-Gradient Calls	0
Final Residual Value (scaled)	4.6700E-02
Sum of Constraint Violations	0.0000E+00
Calculation Time	0 h : 0 min : 9 sec

EASY-FIT **A41** *14-May-07*

Partial Differential Equation

General Information:

Information	Diffusion with chemical Reaction
Model Name	PDE
Project Number	Aldrin 41
Measurement Set	...
User Name	Gavrilov
Date	5/9/2007
Memo	

Model Data:

Number of Variables	3
Number of Constraints	0
Number of Equality Constraints	0
Number of Differential Equations	1
Number of Measurement Sets	1
Number of Time Values	10
Number of Integration Areas	1
Residual Norm	L2

Optimization Variables:

name	lower	init	upper	final
R	0	2	5	2.059248898
alfa	0.00E-8	0.0007	0.008	0.000941378
k	0.0009	0.001	0.002	0.001043037

Parameter Estimation Data ([C]):

EASY-FIT *A41* *14-May-07*

time	conc	meas data	function value	error (%)	weight
0	0	0.78574307	1	27.27	1
0	0	1	1	0	1
4608	0	7.65759875	0.130727320	70.72	1
4608	0	0.14147760	0.130727320	-7.6	1
6552	0	7.3667E-04	0.055465185	-24.71	1
6552	0	9.7690E-04	0.055465185	-43.22	1
14220	0	5.9802E-04	0.001885050	-96.85	1
14220	0	9.9987E-04	0.001885050	-98.11	1

User-Defined Parameters:

Parameter Estimation Method	DFNLP
Maximum Number of Iterations	100
Maximum Number of Function Calls	20
Print Flag (0/1/2/3/...)	2
Termination Accuracy	1.00E-08
First Optimization Tolerance	1.00E-02
Second Optimization Tolerance	2.00E+00
Spatial Discretization Method	5-pt difference formula for 1st and 2nd derivatives
Spatial Upwind Formula	no upwind, standard approximation
ODE-Solver	implicit
Order of Derivative Approximation	7
Accuracy for Gradient Approximation	0
Bandwidth for Jacobian of Right-Hand Side	0
Absolute Error Tolerance for ODE-Solver	1.00E-07
Relative Error Tolerance for ODE-Solver	1.00E-07
Initial Stepsize	1.00E-04
Scaling Method	0

Integration Area Information:

name	i	j	size	disc-pnts	status L	status R	discretization
u(x,t)	1	1	5	61	2	2	0

EASY-FIT *A41* *14-May-07*

Fitting Positions:

position	line
1	13

Numerical Results:

Termination Reason	0
Number of Function Evaluations	27
Number of Gradient Evaluations	12
Number of PDE-Function Calls	32418
Number of PDE-Gradient Calls	0
Final Residual Value (scaled)	6.4000E-02
Sum of Constraint Violations	0.0000E+00
Calculation Time	0 h : 0 min : 3 sec

DANKSAGUNG

Ich möchte mich ganz herzlich bei Herrn Prof. Dr. Cornelius Zetzsch für die Aufnahme in seine Arbeitsgruppe und die Überlassung dieses interessanten Themas sowie für seine konstruktive Hilfe und die motivierenden Diskussionen bedanken. Ich bedanke mich auch für die ausgezeichneten Arbeitsbedingungen und die Möglichkeit, verschiedene Orte und Länder zu bereisen.
Ich bedanke mich auch bei Prof. Dr. Klaus Schittkowski für die Gestattung sein Programm "EasyFit" zu benutzen.
Bei Heinz-Ulrich Krüger, der immer Unerklärbares erklärbar machen konnte und Antworten auf alle Fragen parat hatte, bedanke ich mich für die zahlreichen konstruktiven Kommentare, Diskussionen und die Hilfe.
Ich möchte mich auch bedanken bei:
Frank Siekmann, Ana-Maria Geller und Ayhan Sen für die Hilfe,
speziell Olimpia Kolcun für die Unterstützung und
meiner Familie für Glauben, Hoffnung und Liebe.

ERKLÄRUNG

Hiermit erkläre ich, dass ich die Arbeit selbstständig verfasst und keine anderen als die von mir angegebenen Quellen und Hilfsmittel benutzt habe.
Ferner erkläre ich, dass ich anderweitig mit oder ohne Erfolg nicht versucht habe, diese Dissertation einzureichen. Ich habe keine gleichartige Doktorprüfung an einer anderen Hochschule endgültig nicht bestanden.
Bayreuth, den 23. September 2007

(Radostin Gavrilov)